UNIVERSITY OF CALIFORNIA, SAN DIEGO

Investigation of the sources and composition of submicron organic aerosol particles in marine environments through artificial generation and atmospheric measurements

A dissertation submitted in partial satisfaction of the
requirements for the degree
Doctor of Philosophy

in

Oceanography

by

Amanda A. Frossard

Committee in charge:

Professor Lynn M. Russell, Chair
Professor Lihini I. Aluwihare
Professor Timothy H. Bertram
Professor Kimberly A. Prather
Professor Jeffrey P. Severinghaus
Professor Richard C. J. Somerville

2014

The Dissertation of Amanda A. Frossard is approved, and it is acceptable in quality and form for publication on microfilm and electronically:

_____

_____

_____

_____

_____

_____
Chair

University of California, San Diego

2014

DEDICATION

This doctoral dissertation is dedicated to my parents, Doreen and Tony, for their continuous encouragement and support.

TABLE OF CONTENTS

LIST OF FIGURES

LIST OF TABLES

ACKNOWLEDGEMENTS

First, I would like to thank Professor Lynn Russell for her guidance as my graduate adviser and thesis chair. I appreciate the time she spent editing the many drafts of my papers and all of the knowledge she has passed on to me which will be valuable throughout my career. Second, I thank the current and former members of the Russell Group as well as our many collaborators at different institutions for their support, teamwork, assistance, and guidance in all aspects of my graduate career. These collaborations have all helped shape my work and have greatly contributed to my dissertation as a whole. Last, I thank my family and friends without whose support this dissertation would not have been possible.

Chapter 1, in full, is a reprint of the material as it appears in the *Journal of Geophysical Research-Atmospheres* 2011 with slight modifications. Frossard, A.A., P.M. Shaw, L.M. Russell, J.H. Kroll, M. Canagaratna, D. Worsnop, P.K. Quinn, and T.S. Bates (2011), "Springtime Arctic Haze Contributions of Submicron Organic Particles from European and Asian Combustion Sources." *Journal of Geophysical Research-Atmospheres.* 116, D05205, doi:10.1029/2010JD015178. The dissertation author was the primary investigator and author of this paper.

Chapter 2, in full, is a reprint of the material as it appears in *Environmental Science and Technology* 2012 with slight modifications. Frossard, A.A. and L.M. Russell (2012), "Removal of Sea Salt Hydrate Water from Seawater-Derived Samples by Dehydration." *Environmental Science and Technology.* 46, 13326-13333, doi:

10.1021/es3032083. The dissertation author was the primary investigator and author of this paper.

Chapter 3, in full, is a reprint of the material as it appears in *Aerosol Science and Technology* 2014 with slight modifications. Frossard, A.A., L.M. Russell, P. Massoli, T.S. Bates, and P.K. Quinn (2014), "Side-by-Side Comparison of Four Techniques Explains the Apparent Differences in the Organic Composition of Generated and Ambient Marine Aerosol Particles." *Aerosol Science and Technology* 48:3, v-x, doi: 10.1080/02786826.2013.879979. The dissertation author was the primary investigator and author of this paper.

Chapter 4, in full, has been submitted for publication to the *Journal of Geophysical Research – Atmospheres*. Frossard, A.A., L.M. Russell, M.S. Long, S.M. Burrows, S.M. Elliot, T.S. Bates, P.K. Quinn (2014), "Sources and Composition of Submicron Organic Mass in Marine Aerosol Particles." The dissertation author was the primary investigator and author of this paper.

VITA

2008 B. S. in Chemistry, University of California, Berkeley

2011 Graduate Teaching Assistant, University of California, San Diego

2012 M. S. in Oceanography, University of California, San Diego

2014 Ph. D. in Oceanography, University of California, San Diego

PUBLICATIONS

Frossard, A.A., L.M. Russell, M.S. Long, S.M. Burrows, S.M. Elliot, T.S. Bates, P.K. Quinn (submitted). "Sources and Composition of Submicron Organic Mass in Marine Aerosol Particles." *Journal of Geophysical Research – Atmospheres*.

Frossard, A.A., L.M. Russell, P. Massoli, T.S. Bates, and P.K. Quinn (2014). "Side-by-Side Comparison of Four Techniques Explains the Apparent Differences in the Organic Composition of Generated and Ambient Marine Aerosol Particles." *Aerosol Science and Technology*. 48(3), v-x, doi: 10.1080/02786826.2013.879979.

Frossard, A.A. and L.M. Russell (2012). "Removal of Sea Salt Hydrate Water from Seawater-Derived Samples by Dehydration." *Environmental Science and Technology.* 46, 13326-13333, doi: 10.1021/es3032083.

Frossard, A.A., P.M. Shaw, L.M. Russell, J.H. Kroll, M. Canagaratna, D. Worsnop, P.K. Quinn, and T.S. Bates (2011). "Springtime Arctic Haze Contributions of Submicron Organic Particles from European and Asian Combustion Sources." *Journal of Geophysical Research- Atmospheres.* 116, D05205, doi:10.1029/2010JD015178.

Long, M.S., W.C. Keene, D.J. Kieber, **A.A. Frossard**, L.M. Russell, J.R. Maben, J. D. Kinsey, P.K. Quinn, and T. S. Bates (2014). "Light-Enhanced Primary Marine Aerosol Production from Biologically Productive Seawater." *Geophysical Research Letters*. doi: 10.1002/2014GL059436.

Quinn, P.K., T.S. Bates, K.S. Schultz, D.C. Coffman, **A.A. Frossard**, L.M. Russell, W.C. Keene, and D.J. Kieber (Accepted). "Empirical Constraints on Modeling the Organic Matter Enrichment in Nascent Sea Spray Aerosol." *Nature Geoscience.*

Burrows, S.M., O. Ogunro, **A.A. Frossard**, L.M. Russell, P.J. Rasch, and S. Elliott (2014). "A Physically-based Framework for Modelling the Organic Fractionation of Sea

Spray Aerosol from Bubble Film Langmuir Equilibria." *Atmospheric Chemistry and Physics Discussions*.

Guzman-Morales, J., **A.A. Frossard**, A.L. Corrigan, L.M. Russell, S. Liu, S. Takahama; J.W. Taylor, J. Allan, H. Coe, Y. Zhao, and A.H. Goldstein (2013). "Estimated Contributions of Primary and Secondary Organic Aerosol from Fossil Fuel Combustion during the CalNex and Cal-Mex Campaigns." *Atmospheric Environment.* doi: http://dx.doi.org/10.1016/j.atmosenv.2013.08.047

Russell, L.M., A. Sorooshian, J.H. Seinfeld, B.A. Albrecht, A. Nenes, L. Ahlm, Y.-C. Chen, M. Coggon, J.S. Craven, R.C. Flagan, **A.A. Frossard**, H. Jonsson, E. Jung, Jack J. Lin, A.R. Metcalf, R.L. Modini, J. Mülmenstädt, G.C. Roberts, T. Shingler, S. Song, Z. Wang, A. Wonaschütz (2013). "Eastern Pacific Emitted Aerosol Cloud Experiment (E-PEACE)." *Bulletin of the American Meteorological Society*. doi: http://dx.doi.org/10.1175/BAMS-D-12-00015.1.

Wonaschütz, A., M. Coggon, A. Sorooshian, R. Modini, **A. A. Frossard**, L. Ahlm, J. Muelmenstaedt, G. C. Roberts, L. M. Russell, S. Dey, F. J. Brechtel, and J. H. Seinfeld (2013). "Aerosol Hygroscopic Properties of Organic Particles Emitted in the Marine Atmosphere." *Atmospheric Chemistry and Physics.* 13, 9819-9835, doi:10.5194/acp-13-0819-2013.

Worton, D.R.; J., Surratt, B. LaFranchi, A. Chan, Y. Zhao, R. Weber, J.-H. Park, J. Gilman, J. de Gouw, C. Park, G. Schade, M. Beaver, J. StClair, J. Crounse, P. Wennberg, G. Wolfe, S. Harrold, J. Thornton, D. Farmer, K. Docherty, M. Cubison, J. Jimenez, **A.A. Frossard**, L.M. Russell, K. Kristensen, M. Glasius, J. Mao, X. Ren, B. Brune, E. Browne, S. Pusede, R. Cohen, J. Seinfeld, A.H. Goldstein (2013). "Observational Constraints on High- and Low-NOx Aerosol Formation from Isoprene. *Environmental Science and Technology.* 47(20), 11403–11413, doi: 10.1021/es4011064.

Bates, T.S., P.K. Quinn, **A.A. Frossard**, L.M. Russell, J. Hakala, T. Petäjä, M. Kulmala, D.S. Covert, C.D. Cappa, S.-M. Li, K.L. Hayden, I. Nuaaman, R. McLaren, P. Massoli, M.R. Canagaratna, T.B. Onasch, D. Sueper, D.R. Worsnop, and W.C. Keene (2012). "Measurements of Ocean Derived Aerosol off the Coast of California." *Journal of Geophysical Research- Atmospheres.* 117, D00V15, doi:10.1029/2012JD017588.

Coggon, M.M., A. Sorooshian, Z. Wang, A.R. Metcalf, **A.A. Frossard**, J.J. Lin, J.S. Craven, A. Nenes, H.H. Jonsson, L.M. Russell, R.C. Flagan, and J.H. Seinfeld (2012). "Ship Impacts on the Marine Atmosphere: Insights into the Contribution of Shipping Emissions to the Properties of Marine Aerosol and Clouds." *Atmospheric Chemistry and Physics.* 12, 8439-8458, doi: 10.5194/acp-12-8439-2012.

Ebben, C.J., M. Shrestha, I.S. Martinez, A.L. Corrigan, **A.A. Frossard**, W.W. Song, D.R. Worton, T. Petäjä, J. Williams, L.M. Russell, M. Kulmala, A.H. Goldstein, P. Artaxo, S.T. Martin, R.J. Thomson, and F.M. Geiger (2012). "Organic Constituents on the

Surfaces of Aerosol Particles from Southern Finland, Amazonia, and California Studied by Vibration Sum Frequency." *Journal of Physical Chemistry*. 116, 8271-8290, doi: 10.1021/jp302631z.

Zhang, H., D.R. Worton, M. Lewandowski, J. Ortega, C.L. Rubitschun, J-H. Park, K. Kristensen, P. Campusano-Jost, D.A. Day, J.L. Jimenez, M. Jaoui, J.H. Offenberg, T.E. Kleindienst, J. Gilman, W.C. Kuster, J. de Gouw, C. Park, G.W. Schade, **A.A. Frossard**, L.M. Russell, et al. (2012). "Organosulfates as Tracers for Secondary Organic Aerosol (SOA) Formation from 2‐Methyl-3-Buten-2-ol (MBO) in the Atmosphere." *Environmental Science and Technology*. 46, 9437-9446, doi: 10.1021/es301648z.

Russell, L.M., L.N. Hawkins, **A.A. Frossard**, P.K. Quinn, and T.S. Bates (2010). "Carbohydrate-Like Composition of Submicron Atmospheric Particles and their Production from Ocean Bubble Bursting." *Proceedings of the National Academy of Sciences of the United States of America.* 107, 6652-6647.

ABSTRACT OF THE DISSERTATION

Investigation of the sources and composition of submicron organic aerosol particles in marine environments through artificial generation and atmospheric measurements

by

Amanda A. Frossard

Doctor of Philosophy in Oceanography

University of California, San Diego, 2014

Professor Lynn M. Russell, Chair

Atmospheric aerosol particles in the marine boundary layer (MBL) play an important role in the Earth's radiative balance, and recent studies have proposed a variety of interpretations of their sources and compositions. This dissertation improves the characterization of the sources and organic composition of aerosol particles in the MBL. Atmospheric aerosol particles were collected in the MBL of five ocean regions and analyzed using Fourier transform infrared (FTIR) spectroscopy, high resolution time of flight aerosol mass spectrometry (HR-ToF-AMS), HR-ToF-AMS with a light scattering module HR-ToF-AMS (LS-ToF-AMS), and scanning transmission X-ray microscopy with near-edge X-ray absorption fine structure (STXM-NEXAFS) to determine their

organic functional group and mass fragment composition. Model ocean systems were used to generate ocean-derived primary marine aerosol particles (gPMA), which include particles resulting from seawater bubble bursting. The methods for measuring the organic composition of gPMA are compared, and the discrepancy between high resolution time of flight aerosol mass spectrometry (HR-ToF-AMS) and Fourier transform infrared (FTIR) spectroscopy measurements is attributed to the refractory nature of organics on sea salt in the HR-ToF-AMS. A method for dehydrating samples prior to analysis by FTIR spectroscopy is also presented. Both ocean-derived and anthropogenic emissions contribute to the organic mass (OM) in the MBL. Primary marine aerosol particles (PMA) were found to have similar compositions to marine saccharides and amino sugars, with 65% hydroxyl, 21% alkane, 6% amine, and 7% carboxylic acid functional groups. Contributions from photochemical reactions add carboxylic acid groups (15%-25%) to the PMA OM. Non-ocean-derived sources include shipping and other anthropogenic combustion emissions that together contribute more than half of the OM in the MBL. Seawater and gPMA have very similar compositions to the ocean-derived marine aerosol (mainly PMA). But there is a slightly larger fraction of alkane functional groups in gPMA from biologically productive seawater (35%) compared to oligotrophic seawater (16%). Surfactants in productive seawater may stabilize bubbles at the sea surface, enhancing drainage of soluble organics from their films before bursting and emitting particles. gPMA has a hydroxyl group absorption peak location characteristic of monosaccharides and disaccharides, while the seawater hydroxyl group peak location is more consistent with polysaccharides. This may result from the polysaccharides preferentially remaining in the seawater during PMA production.

Introduction

Atmospheric aerosol particles influence both air quality and climate change, but the extent of their impacts remains largely unconstrained. Aerosol particles can directly influence the radiation balance of the atmosphere with surface cooling due to scattering and warming due to absorbing incoming solar radiation [*Stocker et al.*, 2013; *Yu et al.*, 2006]. They also contribute to planetary albedo indirectly by altering cloud microphysical properties and acting as cloud condensation nuclei (CCN), which influence both cloud droplet formation and cloud lifetime [*Albrecht*, 1989; *Twomey*, 1974]. The magnitude of these impacts, or forcings, remains a focus of current research [*Stocker et al.*, 2013].

Different regions of the Earth can contribute to the climate as a whole. The ocean covers over two thirds of the Earth's surface, and aerosol particles in the marine boundary layer (MBL) over the ocean play an important role in regulating climate. Sea salt particles, measured in the MBL, are strongly reflective, contributing to direct scattering of solar radiation, and are highly CCN active, contributing to cloud formation, both of which lead to surface cooling. However, it was observed as early as 1964 that aerosol particles in the MBL contain organic components, in addition to sea salt [*Blanchard*, 1964]. The organic constituents mixed with sea salt can reduce the cooling effect observed with pure sea salt particles [*Randles et al.*, 2004]. The sources,

composition, and concentration of the organic fraction of aerosol in the MBL, as well as the production mechanisms leading to organic enrichment of the aerosol particles relative to seawater, have not been well characterized [*Gantt and Meskhidze*, 2013]. Because climate models estimate anthropogenic forcings relative to initial concentrations of natural aerosols, understanding the properties of the organic fraction of ocean-derived marine aerosol is necessary in order to predict the degree to which aerosol particles in the MBL contribute to the current and future climate forcing [*Randles et al.*, 2004].

The composition of submicron particles in the MBL is controlled by the sources and atmospheric processing of the aerosol. Aerosol particles in the MBL originate from transported biogenic and anthropogenic continental emissions as well as natural processes in the ocean [*Hawkins et al.*, 2010; *Quinn et al.*, 2006]. The transported aerosol particles contribute non-sea salt (nss) sulfate, nitrate, ammonium, and organic and elemental carbon to the otherwise clean MBL [*Hawkins et al.*, 2010; *Quinn et al.*, 2006]. There are two established production mechanisms of seawater-derived aerosol in the MBL that contribute to the concentration and composition of "clean marine aerosol" (which refers to specifically ocean-derived): direct emission, which produces primary marine aerosol particles (PMA), also referred to as nascent sea spray aerosol particles (SSA), and secondary formation of marine aerosol particles produced from the reaction of emitted gases [*Quinn and Bates*, 2011]. PMA is produced when wind stress over the sea surface causes breaking waves that trap air in the form of bubbles. The bubbles rise and burst at the sea surface, and their films produce submicron aerosol particles [*Blanchard and Woodcock*, 1980]. PMA contain both sea salt and organic components [*Blanchard*, 1964], and the relative fraction of organics has been observed to be inversely related to particle

size [*Facchini et al.*, 2008; *Keene et al.*, 2007]. Oxidation of phytoplankton-emitted volatile organic compounds (VOCs) can form secondary organic aerosol [*Bates et al.*, 1992; *Gantt et al.*, 2009; *Meskhidze and Nenes*, 2006].

One MBL region that is thought to be isolated from direct sources of anthropogenic emissions is the Arctic. However, in the spring, meridional transport from the midlatitudes to the Arctic intensifies and brings emissions from Eurasia northward [*Carlson*, 1981; *Iversen*, 1984; *Iversen and Joranger*, 1985]. It has been observed that in the springtime, organic mass (OM) contributes up to 30% of the particle mass (PM) in the Arctic region [*Shaw et al.*, 2010]. While contributions of anthropogenic emissions to PM in the Arctic have been studied, little is known about the sources and composition of the organic fraction.

The OM fraction of clean marine aerosol particles has been investigated in a number of studies. Some have focused on measuring only the water soluble organic carbon (WSOC) or water insoluble organic carbon (WIOC) content. An enrichment in WIOC relative to WSOC has been associated with PMA OM at a coastal ground site in Ireland [*Ceburnis et al.*, 2008; *O'Dowd et al.*, 2004]. At that same site, *Ovadnevaite et al.* [2011] used mass spectral signatures to classify the hydrocarbon-like components of marine aerosol particles as PMA, based on their similarity to WIOM [*O'Dowd et al.*, 2004]. In addition, collection and extraction of filter samples has enabled quantification of low molecular weight (LMW) saturated fatty acids associated with PMA in the North Pacific [*Mochida et al.*, 2002]. In the North Atlantic and Arctic oceans, submicron marine aerosol particles identified as largely PMA were observed to contain carbohydrate-like (saccharide) content [*Hawkins and Russell*, 2010; *Russell et al.*, 2010]

based on functional group analysis. Measurements of WSOC in the northeastern Atlantic has identified WSOC as marine secondary organic aerosol (SOA) with oxidized fragments [*Ovadnevaite et al.*, 2011], in addition to diethyl and dimethyl amine salts [*Facchini et al.*, 2010].

Model ocean systems are used to mimic the bubble bursting process from wave breaking to produce generated primary marine aerosol particles (gPMA) [*Bates et al.*, 2012; *Collins et al.*, 2013; *Facchini et al.*, 2008; *Fuentes et al.*, 2010a; *Hultin et al.*, 2010; *Keene et al.*, 2007; *King et al.*, 2012; *Martensson et al.*, 2003; *Sellegri et al.*, 2006]. The advantage of this approach is that the composition of PMA can be studied before mixing with shipping or continental emissions or accumulating secondary components. These model ocean systems have been used to study the organic composition of gPMA for different ocean regions. In the northeastern Atlantic, gPMA were observed to contain WIOC with lipo-polysaccharides [*Facchini et al.*, 2008; *Facchini et al.*, 2010], while gPMA from the Sargasso Sea were found to have a significant WSOC fraction [Keene et al., 2007]. The organic fraction of gPMA generated from the northeastern Pacific was identified to be similar to polysaccharides and also contain a hydrocarbon-like component [Bates et al., 2012]. Using seawater from the Scripps pier, Ault et al. [2013] observed a change in the hydrocarbon structure in the gPMA from the addition of bacteria and phytoplankton.

The OM in PMA may be related to the organic constituents in seawater. *Aluwihare et al.* [1997] and *Benner et al.* [1992] found that up to 80% of dissolved organic carbon (DOC) in the surface ocean is carbohydrates (50% polysaccharides), which can be produced, in addition to other WSOC, from marine algae in the euphotic

zone [*Druffel et al.*, 1992; *Williams and Gordon*, 1970]. Amine functional groups in marine OM are found in Chitosan, which is derived from the deacetylation of Chitin in seawater [*Aluwihare et al.*, 2005]. Additional amino sugars such as Glucosamine and Galactosamine have been observed in both seawater particulate organic mass (POM) and ultra-filtered seawater dissolved organic mass (DOM) [*Benner and Kaiser*, 2003]. *Aminot and Kerouel* [2006] also measured dissolved free primary amines and amino acids in seawater.

The organic fraction of primary marine aerosol is a result of the organic matter in the seawater. Phytoplankton exude DOM that is rich in polysaccharides [*Aluwihare and Repeta*, 1999]. Studies of seawater POM collected in the euphotic zone found that 82% of the total organic carbon in plankton is comprised of amino acids (originally proteins), carbohydrates (originally polysaccharides), and lipids, with amino acids contributing 67% of the total organic carbon [*Wakeham et al.*, 1997]. Phytoplankton in the surface ocean contain chlorophyll-*a* for photosynthesis, but chlorophyll-*a* represents less that 0.2% of the total organic carbon in phytoplankton [*Wakeham et al.*, 1997]. Several parameterizations used to predict marine aerosol emissions rely on empirical relationships with ocean chlorophyll-*a* concentrations [*Fuentes et al.*, 2010b; *Gantt et al.*, 2011; *Long et al.*, 2011; *O'Dowd et al.*, 2008; *Vignati et al.*, 2010]. However, chlorophyll-*a* concentrations have been found to be only moderately predictive of [*Sciare et al.*, 2009] or even unrelated to the organic fraction of marine aerosol [*Bates et al.*, 2012]. However, chlorophyll-*a* has been associated with surface active compounds in seawater [*Wurl et al.*, 2011] which can alter the persistence time of bubbles at the sea surface [*Modini et al.*, 2013; *Sellegri et al.*, 2006].

In this dissertation, multiple analytical techniques were used to create a complete picture of the organic composition of aerosol in the MBL and are discussed here. Fourier transform infrared (FTIR) spectroscopy measures the organic functional group composition and total OM of particles collected on filters [*Maria et al.*, 2002; *Russell et al.*; *Russell et al.*, 2009; *Takahama et al.*, 2013]. High resolution time of flight mass spectrometry (HR-ToF-AMS) has been widely used to measure the mass spectral composition and concentration of aerosol in real time [*DeCarlo et al.*, 2006; *Jayne et al.*, 2000]. The high mass resolution of the HR-ToF-AMS allows for improved organic characterization through the separation of different ions and ion groups. A modification of the HR-ToF-AMS includes a light scattering module (LS-ToF-AMS) which optically detects single particles before vaporization [*Cross et al.*, 2007]. This technique can provide an individual mass spectrum for each optically detected particle. Scanning transmission X-ray microscopy with near edge X-ray absorption fine structure (STXM-NEXAFS) is a highly sensitive, single particle analysis technique that is used to non-destructively determine the organic composition and morphology of individual particles impacted on a silicon nitride window [*Kilcoyne et al.*, 2003; *Takahama et al.*, 2010]. The STXM-NEXAFS technique provides image scans at varying energies of individual particles to determine the X-ray absorption spectra with characteristic peaks at different energy transitions of the bound carbon atoms, from which functional groups and organic composition can be identified.

The reported organic compositions of both ambient and generated marine aerosol particles differ substantially in recent results [*Bates et al.*, 2012; *Rinaldi et al.*, 2010]. No studies have been able to distinguish whether the observed organic composition is

controlled by seawater composition or by partitioning during particle formation processes. Additionally, the cause of the difference, attributed to either the use of different OM measurement approaches or differences in seawater properties that produce the marine particles, is still unresolved [*Rinaldi et al.*, 2010]. Side by side measurements of generated marine aerosol particles from the Sea Sweep in seawater off the coast of California found the OM to be oxygenated and saccharide-like using FTIR spectroscopy and minimally oxidized and hydrocarbon-like using HR-ToF-AMS [*Bates et al.*, 2012]. This discrepancy in organic composition of the same generated marine aerosol measured by different techniques needs to be resolved.

Sea salt is a large fraction of the mass of marine aerosol particles, especially in generated marine aerosol. Unlike NaCl, other components in evaporated seawater, such as $MgSO_4$, $MgKCl_3$, and $MgCl_2$ can bind hydrate water as they dry in their crystal structure [*Harvie et al.*, 1980]. Hydrate water absorbs in the same infrared region as hydroxyl functional groups [*Weis and Ewing*, 1999; *Cziczo et al.*, 1997; *Hoffman et al.*, 2004; *Zhao et al.*, 2006]. This causes interference in quantifying the organic hydroxyl functional group absorption. In order to use FTIR spectroscopy to measure the organic composition of seawater derived particles, which contain a large fraction of sea salt and thus hydrate water, a method needs to be developed to remove the hydrate water from these samples.

This dissertation uses measurements of ambient atmospheric and generated marine aerosol particles from numerous analytical techniques in multiple ocean regions to create a more complete picture of the organic composition of aerosol in the MBL. The aims of this dissertation are to (i) characterize the sources and organic composition of

aerosol particles in the MBL and (ii) determine the contribution of ocean-derived primary marine aerosol particles to the organic composition of aerosol particles in the MBL. In this work several techniques were compared, and analysis procedures developed, to more accurately and completely characterize the organic fraction of marine aerosol particles.

Chapter 1 presents measurements of atmospheric aerosol particles in the MBL of the North Atlantic and Arctic oceans and in Barrow, Alaska. Positive matrix factorization (PMF) of FTIR spectroscopy and HR-ToF-AMS measurements, as well as HYSPLIT back trajectories and a potential source contribution function (PSCF), identified the contribution of European and Asian combustion sources to the organic fraction of aerosol in the MBL of the two Arctic regions relative to the natural, ocean-derived aerosol.

Chapter 2 defines a new method for preparing seawater-derived samples to measure their organic functional group composition. Samples of seawater-derived particles need to be dehydrated before analysis by FTIR spectroscopy in order to remove the interference of sea salt hydrate bound water with the quantification of hydroxyl group absorbance.

Chapter 3 compares measurements of the organic fraction of ambient atmospheric and generated marine aerosol to resolve the apparent discrepancy in the organic composition measured with multiple techniques. FTIR spectroscopy, HR-ToF-AMS, LS-ToF-AMS, and STXM-NEXAFS measurements are combined to provide a complete description of the organic fraction.

Chapter 4 presents measurements of ambient atmospheric and generated marine aerosol particles from five research cruises, including two distinct seawater types (biologically productive and oligotrophic). The measured organic mass of atmospheric

marine aerosol particles is comprised of primary, carboxylic acid containing, shipping influenced, and mixed marine aerosol particles. The organic composition of generated marine aerosol particles shows the influence of seawater organics on the organic composition of primary marine aerosol.

Together, this work investigates the extent to which organic mass in the MBL is influenced by anthropogenic emissions and the fraction of clean marine organic aerosol that is directly emitted from the sea surface. The following questions are answered in the dissertation and summarized in the Conclusions: (i) What are the sources and composition of the OM in the springtime Arctic MBL?; (ii) How can seawater-derived particle samples be prepared for analysis by FTIR spectroscopy to avoid interference of sea salt hydrate bound water?; (iii) What causes the discrepancy between the organic composition of generated primary marine aerosol particles measured with different techniques?; (iv) What is the organic composition of ocean-derived atmospheric marine aerosol particles?; (v) How much of the atmospheric marine aerosol particle organic composition can be explained by generating primary marine aerosol (gPMA) from bubbled seawater?; and (vi) What are the differences between gPMA and seawater? Future work is also suggested to expand upon these studies and improve the understanding of organic mass in the MBL.

References

Albrecht, B. A. (1989), Aerosols, cloud microphyics, and fractional cloudiness, *Science*, *245*(4923), 1227-1230, doi:10.1126/science.245.4923.1227.

Aluwihare, L. I., and D. J. Repeta (1999), A comparison of the chemical characteristics of oceanic DOM and extracellular DOM produced by marine algae, *Marine Ecology-Progress Series*, *186*, 105-117.

Aluwihare, L. I., D. J. Repeta, and R. F. Chen (1997), A major biopolymeric component to dissolved organic carbon in surface sea water, *Nature*, *387*(6629), 166-169.

Aluwihare, L. I., D. J. Repeta, S. Pantoja, and C. G. Johnson (2005), Two chemically distinct pools of organic nitrogen accumulate in the ocean, *Science*, *308*(5724), 1007-1010, doi:10.1126/science.1108925.

Aminot, A., and R. Kerouel (2006), The determination of total dissolved free primary amines in seawater: Critical factors, optimized procedure and artefact correction, *Marine Chemistry*, *98*(2-4), 223-240, doi:10.1016/j.marchem.2005.07.005.

Ault, A. P., D. F. Zhao, C. J. Ebben, M. J. Tauber, F. M. Geiger, K. A. Prather, and V. H. Grassian (2013), Raman microspectroscopy and vibrational sum frequency generation spectroscopy as probes of the bulk and surface compositions of size-resolved sea spray particles, *Physical Chemistry - Chemical Physics*, *15*(17), 6206-6214.

Bates, T. S., J. A. Calhoun, and P. K. Quinn (1992), Variations in the methansulfonate to sulfate moldar ratio in submicrometer marine aerosol-particles over the South-Pacific, *Journal of Geophysical Research-Atmospheres*, *97*(D9), 9859-9865, doi:10.1029/92jd00411.

Bates, T. S., P.K. Quinn, A.A. Frossard, L.M. Russell, J. Hakala, T. Petäjä, M. Kulmala, D.S. Covert, C.D. Cappa, S.-M. Li, K.L. Hayden, I. Nuaaman, R. McLaren, P. Massoli, M.R. Canagaratna, T.B. Onasch, D. Sueper, D.R. Worsnop, and W.C. Keene (2012), Measurements of ocean derived aerosol off the coast of California, *Journal of Geophysical Research - Atmospheres*, *117*(D00V15), doi:10.1029/2012JD017588.

Benner, R., and K. Kaiser (2003), Abundance of amino sugars and peptidoglycan in marine particulate and dissolved organic matter, *Limnology and Oceanography*, *48*(1), 118-128.

Benner, R., J. D. Pakulski, M. McCarthy, J. I. Hedges, and P. G. Hatcher (1992), Bulk chemical characteristics of dissolved organic-matter in the ocean, *Science*, *255*(5051), 1561-1564.

Blanchard, D. C. (1964), Sea-to-air transport of surface active material, *Science*, *146*(364), 396-397.

Blanchard, D. C., and A. H. Woodcock (1980), The production, concentration, and vertical distribution of the sea-salt aerosol, *Annals of the New York Academy of Sciences*, *338*(1), 330-347.

Carlson, T. N. (1981), Speculations on the movement of polluted air to the Arctic, *Atmospheric Environment*, *15*(8), 1473-1477.

Ceburnis, D., C. D. O'Dowd, G. S. Jennings, M. C. Facchini, L. Emblico, S. Decesari, S. Fuzzi, and J. Sakalys (2008), Marine aerosol chemistry gradients: Elucidating primary and secondary processes and fluxes, *Geophysical Research Letters*, *35*(7), doi:10.1029/2008gl033462.

Cziczo, D. J., J. B. Nowak, J. H. Hu, and J. P. D. Abbatt (1997), Infrared spectroscopy of model tropospheric aerosols as a function of relative humidity: Observation of deliquescence and crystallization, *Journal of Geophysical Research-Atmospheres*, *102*(D15), 18843-18850, doi:10.1029/97jd01361.

Collins, D. B., D. Zhao, M. J. Ruppel, G. B. Deane, M. D. Stokes, P. J. DeMott, C. Lee, R. L. Modini, L. M. Russell, and K. A. Prather (2013), Evaluating the properties of sea spray aerosols produced in the laboratory: Comparisons with controlled breaking waves, *AIP Conference Proceedings*, *1527*, 551-554, doi:10.1063/1.4803330.

Cross, E. S., J. G. Slowik, P. Davidovits, J. D. Allan, D. R. Worsnop, J. T. Jayne, D. K. Lewis, M. Canagaratna, and T. B. Onasch (2007), Laboratory and ambient particle density determinations using light scattering in conjunction with aerosol mass spectrometry, *Aerosol Science and Technology*, *41*(4), 343-359.

DeCarlo, P. F., J. R. Kimmel, A. Trimborn, M. J. Northway, J. T. Jayne, A. C. Aiken, M. Gonin, K. Fuhrer, T. Horvath, K. S. Docherty, D. R. Worsnop and J. L. Jimenez (2006), Field-deployable, high-resolution, time-of-flight aerosol mass spectrometer, *Analytical Chemistry*, *78*(24), 8281-8289, doi:10.1021/ac061249n.

Druffel, E. R. M., P. M. Williams, J. E. Bauer, and J. R. Ertel (1992), Cycling of dissolved and particulate organic-matter in the open ocean, *Journal of Geophysical Research-Oceans*, *97*(C10), 15639-15659.

Facchini, M. C., M. Rinaldi, S. Decesari, C. Carbone, E. Finessi, M. Mircea, S. Fuzzi, D. Ceburnis, R. Flanagan, E. D. Nilsson, G. de Leeuw, M. Martino, J. Woeltjen, C. D. O'Dowd (2008), Primary submicron marine aerosol dominated by insoluble organic colloids and aggregates, *Geophysical Research Letters*, L17814 (17815 pp.), doi:10.1029/2008gl034210.

Facchini, M. C., M. Rinaldi, S. Decesari, and S. Fuzzi (2010), Marine organic aerosol and biological oceanic activity, *Chemical Engineering*, *22*.

Fuentes, E., H. Coe, D. Green, G. de Leeuw, and G. McFiggans (2010a), Laboratory-generated primary marine aerosol via bubble-bursting and atomization, *Atmospheric Measurement Techniques*, *3*(1), 141-162.

Fuentes, E., H. Coe, D. Green, G. de Leeuw, and G. McFiggans (2010b), On the impacts of phytoplankton-derived organic matter on the properties of the primary marine aerosol - Part 1: Source fluxes, *Atmospheric Chemistry and Physics*, *10*(19), 9295-9317, doi:10.5194/acp-10-9295-2010.

Gantt, B., and N. Meskhidze (2013), The physical and chemical characteristics of marine primary organic aerosol: a review, *Atmospheric Chemistry and Physics*, *13*(8), 3979-3996, doi:10.5194/acp-13-3979-2013.

Gantt, B., N. Meskhidze, M. C. Facchini, M. Rinaldi, D. Ceburnis, and C. D. O'Dowd (2011), Wind speed dependent size-resolved parameterization for the organic mass fraction of sea spray aerosol, *Atmospheric Chemistry and Physics*, *11*(16), 8777-8790.

Gantt, B., N. Meskhidze, and D. Kamykowski (2009), A new physically-based quantification of marine isoprene and primary organic aerosol emissions, *Atmospheric Chemistry and Physics*, *9*(14), 4915-4927.

Harvie, C. E., J. H. Weare, L. A. Hardie, and H. P. Eugster (1980), Evaporation of seawater - calculated mineral sequences, *Science*, *208*(4443), 498-500.

Hawkins, L. N., and L. M. Russell (2010), Polysaccharides, proteins, and phytoplankton fragments: Four chemically distinct types of marine primary organic aerosol classified by single particle spectromicroscopy, *Advances in Meteorology*, *2010*(Article ID 612132), 14, doi:10.1155/2010/612132.

Hawkins, L. N., L. M. Russell, D. S. Covert, P. K. Quinn, and T. S. Bates (2010), Carboxylic acids, sulfates, and organosulfates in processed continental organic aerosol over the southeast Pacific Ocean during VOCALS-REx 2008, *Journal of Geophysical Research-Atmospheres*, *115*(D13201), doi:10.1029/2009jd013276.

Hoffman, R. C., A. Laskin, and B. J. Finlayson-Pitts (2004), Sodium nitrate particles: physical and chemical properties during hydration and dehydration, and implications for aged sea salt aerosols, *Journal of Aerosol Science*, *35*(7), 869-887, doi:10.1016/j.jaerosci.2004.02.003.

Hultin, K. A. H., E. D. Nilsson, R. Krejci, E. M. Martensson, M. Ehn, A. Hagstrom, and G. de Leeuw (2010), In situ laboratory sea spray production during the Marine Aerosol Production 2006 cruise on the northeastern Atlantic Ocean, *Journal of Geophysical Research-Atmospheres*, *115*(D06201), doi:10.1029/2009jd012522.

Iversen, T. (1984), On the atmospheric transport of pollution to the Arctic, *Geophysical Research Letters*, *11*(5), 457-460.

Iversen, T., and E. Joranger (1985), Arctic air-pollution and large-scale atmospheric flows, *Atmospheric Environment*, *19*(12), 2099-2108.

Jayne, J. T., D. C. Leard, X. F. Zhang, P. Davidovits, K. A. Smith, C. E. Kolb, and D. R. Worsnop (2000), Development of an aerosol mass spectrometer for size and composition analysis of submicron particles, *Aerosol Science and Technology*, *33*(1-2), 49-70.

Keene, W. C., H. Maring, J. R. Maben, D. J. Kieber, A. A. P. Pszenny, E. E. Dahl, M. A. Izaguirre, A. J. Davis, M. S. Long, X. L. Zhou, L. Smoydzin, R. Sander (2007), Chemical and physical characteristics of nascent aerosols produced by bursting bubbles at a model air-sea interface, *Journal of Geophysical Research-Atmospheres*, *112*(D21), doi:10.1029/2007jd008464.

Kilcoyne, A. L. D., T. Tyliszczak, W. F. Steele, S. Fakra, P. Hitchcock, K. Franck, E. Anderson, B. Harteneck, E. G. Rightor, G. E. Mitchell, A. P. Hitchcock, L. Yang, T. Warwick, and H. Ade (2003), Interferometer-controlled scanning transmission X-ray microscopes at the Advanced Light Source, *Journal of Synchrotron Radiation*, *10*, 125.

King, S. M., A. C. Butcher, T. Rosenoern, E. Coz, K. I. Lieke, G. de Leeuw, E. D. Nilsson, and M. Bilde (2012), Investigating primary marine aerosol properties: ccn activity of sea salt and mixed inorganic-organic particles, *Environmental Science & Technology*, *46*(19), doi:10.1021/es300574u.

Long, M. S., W. C. Keene, D. J. Kieber, D. J. Erickson, and H. Marine (2011), A sea-state based source function for size- and composition-resolved marine aerosol production, *Atmospheric Chemistry and Physics*, *11*(3), 1203-1216.

Maria, S. F., L. M. Russell, B. J. Turpin, and R. J. Porcja (2002), FTIR measurements of functional groups and organic mass in aerosol samples over the Caribbean, *Atmospheric Environment*, *36*(33), 5185-5196.

Martensson, E. M., E. D. Nilsson, G. de Leeuw, L. H. Cohen, and H. C. Hansson (2003), Laboratory simulations and parameterization of the primary marine aerosol production, *Journal of Geophysical Research-Atmospheres*, *108*(D9), doi:10.1029/2002jd002263.

Meskhidze, N., and A. Nenes (2006), Phytoplankton and cloudiness in the Southern Ocean, *Science*, *314*(5804), 1419-1423, doi:10.1126/science.1131779.

Mochida, M., Y. Kitamori, K. Kawamura, Y. Nojiri, and K. Suzuki (2002), Fatty acids in the marine atmosphere: Factors governing their concentrations and evaluation of organic films on sea-salt particles, *Journal of Geophysical Research-Atmospheres*, *107*(D17).

Modini, R. L., L. M. Russell, G. B. Deane, and M. D. Stokes (2013), Effect of soluble surfactant on bubble persistence and bubble-produced aerosol particles, *Journal of Geophysical Research-Atmospheres*, *118*(3), 1388-1400, doi:10.1002/jgrd.50186.

O'Dowd, C. D., M. C. Facchini, F. Cavalli, D. Ceburnis, M. Mircea, S. Decesari, S. Fuzzi, Y. J. Yoon, and J. P. Putaud (2004), Biogenically driven organic contribution to marine aerosol, *Nature*, *431*(7009), 676-680, doi:10.1038/nature02959.

O'Dowd, C. D., B. Langmann, S. Varghese, C. Scannell, D. Ceburnis, and M. C. Facchini (2008), A combined organic-inorganic sea-spray source function, *Geophysical Research Letters*, *35*(1), doi:10.1029/2007gl030331.

Ovadnevaite, J., C. O'Dowd, M. Dall'Osto, D. Ceburnis, D. R. Worsnop, and H. Berresheim (2011), Detecting high contributions of primary organic matter to marine aerosol: A case study, *Geophysical Research Letters*, *38*, doi:10.1029/2010gl046083.

Quinn, P. K., and T. S. Bates (2011), The case against climate regulation via oceanic phytoplankton sulphur emissions, *Nature*, *480*(7375), 51-56, doi:10.1038/nature10580.

Quinn, P. K., T. S. Bates, D. Coffman, T. B. Onasch, D. Worsnop, T. Baynard, J. A. de Gouw, P. D. Goldan, W. C. Kuster, E. Williams, J. M. Roberts, B. Lerner, A. Stohl, A. Pettersson and E. R. Lovejoy (2006), Impacts of sources and aging on submicrometer aerosol properties in the marine boundary layer across the Gulf of Maine, *Journal of Geophysical Research-Part D-Atmospheres*, 1-20, doi:10.1029/2006jd007582.

Randles, C. A., L. M. Russell, and V. Ramaswamy (2004), Hygroscopic and optical properties of organic sea salt aerosol and consequences for climate forcing, *Geophysical Research Letters*, *31*(L16108), doi:10.1029/2004gl020628.

Rinaldi, M., S. Decesari, E. Finessi, L. Giulianelli, C. Carbone, S. Fuzzi, C. D. O'Dowd, D. Ceburnis, and M. C. Facchini (2010), Primary and secondary organic marine aerosol and oceanic biological activity: recent results and new perspectives for future studies, *Advances in Meteorology*, *2010*(Arctic ID 310682), 10.

Russell, L. M., R. Bahadur, and P. J. Ziemann (2011), Identifying organic aerosol sources by comparing functional group composition in chamber and atmospheric particles, *Proceedings of the National Academy of Sciences of the United States of America*, *108*(9), 3516-3521, doi:10.1073/pnas.1006461108.

Russell, L. M., L. N. Hawkins, A. A. Frossard, P. K. Quinn, and T. S. Bates (2010), Carbohydrate-like composition of submicron atmospheric particles and their production from ocean bubble bursting, *Proceedings of the National Academy of Sciences of the United States of America*, *107*(15), 6652-6657, doi:10.1073/pnas.0908905107.

Russell, L. M., S. Takahama, S. Liu, L. N. Hawkins, D. S. Covert, P. K. Quinn, and T. S. Bates (2009), Oxygenated fraction and mass of organic aerosol from direct emission and atmospheric processing measured on the R/V Ronald Brown during TEXAQS/GoMACCS 2006, *Journal of Geophysical Research-Atmospheres*, *114*, doi:10.1029/2008jd011275.

Sciare, J., O. Favez, R. Sarda-Esteve, K. Oikonomou, H. Cachier, and V. Kazan (2009), Long-term observations of carbonaceous aerosols in the Austral Ocean atmosphere: Evidence of a biogenic marine organic source, *Journal of Geophysical Research-Atmospheres*, *114*, doi:10.1029/2009jd011998.

Sellegri, K., C. D. O'Dowd, Y. J. Yoon, S. G. Jennings, and G. de Leeuw (2006), Surfactants and submicron sea spray generation, *Journal of Geophysical Research-Atmospheres*, *111*(D22), doi:10.1029/2005jd006658.

Shaw, P. M., L. M. Russell, A. Jefferson, and P. K. Quinn (2010), Arctic organic aerosol measurements show particles from mixed combustion in spring haze and from frost flowers in winter, *Geophysical Research Letters*, *37*.

Stocker, T. F., D. Qin, G.-K. Plattner, M. Tignor, S. K. Allen, J. Boschung, A. Nauels, Y. Xia, V. Bex, and P. M. Midgley (eds.) (2013), Climate change 2013: The physical science basis. Contribution of Working Group I to the Fifth Assessment Report of the Intergovernmental Panel on Climate Change, edited, Cambridge Univ. Press, Cambridge, UK and New York, NY, USA.

Takahama, S., A. Johnson, and L. M. Russell (2013), Quantification of carboxylic and carbonyl functional groups in organic aerosol infrared absorbance spectra, *Aerosol Science and Technology*, doi:10.1080/02786826.2012.752065.

Takahama, S., S. Liu, and L. M. Russell (2010), Coatings and clusters of carboxylic acids in carbon-containing atmospheric particles from spectromicroscopy and their implications for cloud-nucleating and optical properties, *Journal of Geophysical Research-Atmospheres*, *115*, 21, doi:10.1029/2009jd012622.

Twomey, S. (1974), Pollution and planetary albedo, *Atmospheric Environment*, *8*(12), 1251-1256, doi:10.1016/0004-6981(74)90004-3.

Vignati, E., M. C. Facchini, M. Rinaldi, C. Scannell, D. Ceburnis, J. Sciare, M. Kanakidou, S. Myriokefalitakis, F. Dentener, and C. D. O'Dowd (2010), Global scale emission and distribution of sea-spray aerosol: Sea-salt and organic enrichment, *Atmospheric Environment*, *44*(5), 670-677, doi:10.1016/j.atmosenv.2009.11.013.

Wakeham, S. G., C. Lee, J. I. Hedges, P. J. Hernes, and M. L. Peterson (1997), Molecular indicators of diagenetic status in marine organic matter, *Geochimica Et Cosmochimica Acta*, *61*(24), 5363-5369, doi:10.1016/s0016-7037(97)00312-8.

Williams, P. M., and L. I. Gordon (1970), C-13-C-12 ratios in dissolved and particulate organic matter in sea, *Deep-Sea Research*, *17*(1), 19-&.

Weis, D. D., and G. E. Ewing (1999), Water content and morphology of sodium chloride aerosol particles, *Journal of Geophysical Research-Atmospheres*, *104*(D17), doi:10.1029/1999jd900286.

Wurl, O., E. Wurl, L. Miller, K. Johnson, and S. Vagle (2011), Formation and global distribution of sea-surface microlayers, *Biogeosciences*, *8*(1), 121-134, doi:10.5194/bg-8-121-2011.

Yu, H., Y. J. Kaufman, M. Chin, G. Feingold, L. A. Remer, T. L. Anderson, Y. Balkanski, N. Bellouin, O. Boucher, S. Christopher, P. DeCola, R. Kahn, D. Koch, N. Loeb, M. S. Reddy, M. Schulz, T. Takemura, M. Zhou (2006), A review of measurement-based assessments of the aerosol direct radiative effect and forcing, *Atmospheric Chemistry and Physics*, *6*, 613-666.

Zhao, L. J., Y. H. Zhang, Z. F. Wei, H. Cheng, and X. H. Li (2006), Magnesium sulfate aerosols studied by FTIR spectroscopy: Hygroscopic properties, supersaturated structures, and implications for seawater aerosols, *Journal of Physical Chemistry A*, *110*(3), doi:10.1021/jp055291i.

Chapter 1

Springtime Arctic Haze Contributions of Submicron Organic Particles from European and Asian Combustion Sources

The composition of Arctic aerosol, especially during the springtime Arctic haze, may play an important role in the radiative balance of the Arctic. The contribution of organic components to Arctic haze has only recently been investigated. Because measurements in this region are sparse, little is known about organic particle composition, sources, and concentrations. This study compares springtime measurements in the Arctic regions north of the Atlantic (ICEALOT, 2008) and Pacific (Barrow, Alaska, 2008 and 2009) oceans. The aerosol organic functional group composition from Fourier transform infrared spectroscopy combined with positive matrix factorization (PMF) and elemental tracer analysis indicate that mixed combustion sources account for

more than 60% (>0.3 μg m^{-3}) of the submicron organic mass (OM_1) for springtime haze conditions in both regions. Correlations with typical combustion tracers (S, Zn, K, Br, V) provide evidence for the contribution of combustion sources to the Arctic OM_1. However, the two regions are influenced by different urban and industrial centers with different fuel usage. High-sulfur coal burning in northeastern Europe impacts the northern Atlantic Arctic region, while oil burning and forest fires in northeastern Asia and Alaska impact the northern Pacific Arctic region. Quadrupole and High Resolution Aerosol Mass Spectrometry measurements confirm the highly oxygenated nature of the OM_1, with an oxygenated organic aerosol (OOA) spectrum from PMF. High co-emissions of sulfate and organics from coal-burning in northeastern Europe produce significant concentrations of organosulfate functional groups that account for 10% of OM_1 measured by FTIR spectroscopy during ICEALOT. These observations provide preliminary support for a heterogeneous mechanism of organosulfate formation on acidic sulfate particles.

1.1 Background

Arctic haze has been studied since it was reported by pilots over 50 years ago [*Greenway*, 1950; *Mitchell*, 1956]. This haze is comprised mostly of sulfate aerosol, primarily from anthropogenic sources, with small amounts of ammonium, nitrate, dust, organics, and black carbon [*Li and Barrie*, 1993; *Quinn et al.*, 2002]. Significant anthropogenic sulfur (S) emissions exist within the Arctic region [*Hole et al.*, 2009]. On time scales of a few days to weeks, the polar dome isolates the Arctic lower troposphere from warmer regions to the south making northern Europe and northern Russia major contributors to Arctic haze [*Law and Stohl*, 2007]. However, emissions from populated sub-Arctic regions are the most likely cause of the high aerosol particle concentrations in the springtime Arctic, when meridional transport from the mid-latitudes to the Arctic intensifies and brings emissions from Eurasia northward [*Carlson*, 1981; *Iversen*, 1984; *Iversen and Joranger*, 1985]. There is more rapid transport from Europe and northern Asia to the Arctic [*Stohl*, 2006] than from more southern regions [*Hole et al.*, 2009] or North America. Measurements of trace metals from combustion (Mn, V) have been used to confirm the contributions of European sources to aerosol in the Arctic [*Rahn*, 1981]. Subsequent studies of the springtime Arctic haze have also linked contributions of sulfate aerosol to these metal tracers [*Quinn et al.*, 2009; *Rahn and McCaffrey*, 1980].

Emissions from fuel-burning activities, including industry, electricity production, and domestic heating, have been identified as contributors to Arctic haze by chemical analyses of Arctic aerosol particles [*Ottar et al.*, 1986; *Rahn and McCaffrey*, 1979; *Rahn et al.*, 1977; *Rahn et al.*, 1989]. Chemical tracers for these types of anthropogenic

emissions, such as sulfate, black carbon, Pb, Cd, Cu, and Zn, were found in Greenland snow [*Candelone et al.*, 1996; *Davidson et al.*, 1993; *Masclet et al.*, 2000], suggesting similar types of emission sources for these species and the constituents of Arctic haze. During the winter and early spring, fossil fuel combustion is the main source of sulfate to the Arctic since there is minimal biological activity [*Ferek et al.*, 1995]. Anthropogenic emissions from conurbations, such as Murmansk on the Kola peninsula, industrial emissions from the northern part of Russia, oil industry, and shipping all contribute to haze particles [*Hole et al.*, 2006a]. The Kola peninsula, in addition to other parts of northern Russia, has many Ni, Cu, and other non-ferrous metal producing industries, which also contribute to anthropogenic emissions [*Hole et al.*, 2006b; *Weiler et al.*, 2005].

Recent evidence has shown that organic compounds comprise more than 30% of the submicron PM (PM_1) in Arctic Haze [*Shaw et al.*, 2010]. Aerosol haze particles are thought to be chemically-aged, very efficient at scattering solar radiation, and possibly weakly absorbing of solar radiation [*Law and Stohl*, 2007]. Identifying the sources of the haze and determining its chemical composition is necessary to define and mitigate its climate impact on both the shortwave and longwave radiation balance in the Arctic [*Quinn et al.*, 2007]. Here, we use springtime measurements from the International Chemistry Experiment in the Arctic Lower Troposphere (ICEALOT) and from Barrow, Alaska, to characterize and contrast the composition and identify the sources of organic components that contribute to haze from the Atlantic and Pacific sides of the Arctic.

1.2 Methods

As part of the 2008-2009 International Polar Year, submicron particles were measured aboard the R/V *Knorr* during ICEALOT (19 March 2008 to 24 April 2008) over the North Atlantic and Arctic Oceans and the Greenland, Norwegian, and Barents Seas (20°-30°W and 41°-81°N). Submicron particles were collected from an isokinetic sampling inlet 18 m above sea level that extended 5 m above the aerosol measurement container. The inlet was heated to dry the aerosol to a relative humidity (RH) of 25% or less, during sampling. Sector control for the flow was used to prevent sampling emissions directly from R/V *Knorr*. From 1 March 2008 to 1 March 2010, similar measurements were made at the National Oceanic and Atmospheric Administration Earth System Research Laboratory (NOAA ESRL) observatory at Barrow, Alaska, with an analogous collection method described by *Shaw et al.* [2010] for the 2008 samples. The Barrow sampling site is at a coastal location (156.6°W, 71.5°N) in the northern Pacific side of the Arctic. Sector control is used at Barrow to avoid emissions from the local town. This stops the sample collection when the wind direction is between 0 and 130 degrees, which reduced the sampling time by 35% for the 221 collected filters in this study.

1.2.1 Filter-based Particle Collection

During ICEALOT, submicron particles were collected on 37 mm Teflon filters for 12 and 24 hour periods using the previously described isokinetic inlet. At Barrow, two years of near-continuous submicron particle measurements were collected using an automated rotating filter holder that exposed 47 mm Teflon filters to ambient air drawn

into the warmed inlet at 30 L min^{-1} [*Quinn et al.*, 2002; *Shaw et al.*, 2010]. Filters at Barrow were exposed for different durations depending on season to accommodate changes in overall mass loadings: spring and winter filters were exposed for 24 hours and summer filters for 96 hours. After collection, the filters from both Barrow and the ICEALOT cruise were frozen, to prevent losses due to desorption or reaction, and transported back to San Diego for analysis by Fourier transform infrared spectroscopy (FTIR). The FTIR spectra were analyzed using an automated algorithm that includes baselining, peak-fitting, and integrating at specific peak locations to quantify organic functional group mass associated with major carbon bond types based on the method outlined by *Maria et al.* [2002] and revised by *Russell et al.* [2009a]. Filters with detectable absorption at 876 cm^{-1} were rinsed with 2 mL of hexane, which removes the organosulfate containing compound without removing bisulfate or carbonate that also absorb in this region [*Blando et al.*, 1998; *Maria et al.*, 2003]. After the rinse, there was no absorbance remaining at 876 cm^{-1}, indicating efficient removal of organosulfate. Concentrations were calculated by dividing the mass of each functional group measured for each filter by the total volume of air sampled through the corresponding filters. Functional groups that were quantified include: hydroxyl (including alcohol, C-OH), alkane (C-CH), amine ($C\text{-}NH_2$), carbonyl (C=O), carboxylic acid (COOH), and organosulfate ($COSO_3$). Aromatic, alkene (C=CH), and organonitrate functional groups were below the detection limit for all filters discussed here.

Prior to rinsing with hexane, X-ray Fluorescence (XRF; Chester LabNet, Tigard, Oregon) was performed on the FTIR analyzed filters to quantify the elemental mass concentrations of elements Na and heavier [*Maria et al.*, 2003]. For ICEALOT, S, K, Br,

Ca, and Zn were measured above detection limit for 75% of the samples, Fe, Na, and Cl were above detection limit for 50% to 70%, and V and Si were above detection limit for between 35% and 40% of the samples. The remaining measured elements were above the detection limit for less than 15% of the samples and are not used in this analysis. Of the 221 filters collected from Barrow, a subset of 47 was analyzed by XRF for which Na, Cl, Fe, S, Br, K and Zn were consistently above detection limits [*Shaw et al.*, 2010]. The concentration of inorganic oxidized material (IOM – dust and fly ash) was calculated from the mass concentrations of Al, Si, Ca, Fe, and Ti assuming that each element was present in the aerosol in its most common oxide form [*Bates et al.*, 2008]. Because Al was below detection limit for all but one of the samples where V was above detection limit, the measured V was identified as non-crustal.

Submicron particles (RH < 25%) were also collected with a Berner-type cascade impactor on Millipore Fluoropore filters downstream of a jet plate with a 50% aerodynamic cutoff diameter of 1 μm on the R/V *Knorr.* 1 mL of spectral grade methanol was added to the filters followed by 5 mL of distilled, deionized water. The substrates were extracted by sonicating for 30 min. They were then analyzed by ion chromatography (IC) to quantify inorganic ions including sodium (Na^+), chloride (Cl^-), sulfate, nitrate, and ammonium [*Quinn et al.*, 1998]. Non-sea salt SO_4^{2-} concentrations were calculated from Na^+ concentrations and the ratio of SO_4^{2-} to Na^+ in seawater [*Quinn et al.*, 2000]. Sea salt concentrations were calculated from the measured concentrations of Na^+ and Cl^-, in order to take into account Cl^- depletion in the atmosphere [*Bates et al.*, 2008].

1.2.2 Aerosol Mass Spectrometry

A quadrupole aerosol mass spectrometer (Q-AMS) was used to measure submicron particle composition averaged over 5-min intervals aboard the R/V *Knorr*. Non-refractory ions (chemical components that vaporize at 600°C) including sulfate (SO_4^{2-}), nitrate (NO_3^-), and ammonium (NH_4^+), were measured by Q-AMS, in addition to OM [*Allan et al.*, 2003; *Jayne et al.*, 2000]. A collection efficiency of 1 was used for all species described here based on the high acidity (low molar ratio of ammonium to sulfate) of measured particles and high relative humidity during measurements [*Matthew et al.*, 2008; *Quinn et al.*, 2006]. Comparisons of sulfate and ammonium concentrations measured by the Q-AMS and separately by IC of filter extracts were used to confirm the collection efficiency [*Hawkins et al.*, 2010; *Russell et al.*, 2010]. Sulfate measured by the Q-AMS was higher than that measured by IC (slope = 1.42, r = 0.82) suggesting sufficient collection by the Q-AMS. Ammonium measured by both instruments compared well (slope = 0.99, r = 0.75) further supporting a collection efficiency of 1. The total submicron OM (OM_1) measured by FTIR exceeds the OM_1 measured by the Q-AMS (slope = 0.91, r = 0.57) but is within the 20% uncertainty reported for either technique and is consistent with a reduced collection efficiency of organic mass on sea salt or other non-refractory particles [*Russell et al.*, 2010; *Russell et al.*, 2009b].

Submicron particle composition was also measured aboard the R/V *Knorr* using a high resolution time of flight aerosol mass spectrometer (HR-ToF-AMS, Aerodyne Research Inc., Billerica, MA) [*Canagaratna et al.*, 2007; *DeCarlo et al.*, 2006]. Measurements were made every minute alternating automatically between V and W mode, with and without a thermal denuder, and in combination with particle time of flight

(PToF) mode. The HR-ToF-AMS data were analyzed using SQUIRREL and PIKA software (described at http://tinyurl.com/tofams-analysis) to determine the concentrations of mass fragments and common aerosol species [*Canagaratna et al.*, 2007; *DeCarlo et al.*, 2006]. The speciated HR-ToF-AMS mass concentrations correlated well with those obtained from the Q-AMS. An unknown problem caused the absolute concentrations determined by the HR-ToF-AMS to be unusually and systematically low throughout this campaign, so only the Q-AMS was used for quantitative mass concentrations of the major aerosol components. The high resolution mass spectra obtained from the HR-ToF-AMS were used to investigate the normalized oxygen to carbon (O/C) ratios of the observed organic aerosol. The organic aerosol was further characterized by positive matrix factorization (PMF) of HR-ToF-AMS organic mass spectra.

1.2.3 Potential Source Contribution Function

A potential source contribution function (PSCF) was used to determine the regions that have higher probabilities of being sources for the input of aerosol mass [*Pekney et al.*, 2006]. This algorithm uses the calculated 5-day isentropic Hybrid Single Particle Lagrangian Integrated Trajectory (HYSPLIT) model to generate air mass back trajectories [*Draxler and Rolph*, 2003] with gridded frequencies of co-occurrence with high concentration samples. Back trajectories were calculated arriving at 500 m above the sampling platform every hour for ICEALOT and every 4 hours for Barrow. PSCF analysis was calculated individually on the time series of concentrations and mass fractions of organic functional groups, total OM, PMF derived factors, and Q-AMS mass fragments.

1.3 Results

Five aerosol source regions were identified along the ICEALOT cruise track based on HYSPLIT 5-day isentropic back trajectories [*Draxler and Rolph*, 2003]. The five regions, including three continental (Long Island, North American, and European) and two marine (North Atlantic and Arctic), are shown along the shiptrack in Figure 1.1. Particles from the marine source regions had carbohydrate-like OM_1 signatures mixed with sea salt and are described by *Russell et al.* [2010]. The continental regions differ from the marine regions in that they have higher OM_1, PM_1, and combustion tracer concentrations in addition to higher radon concentrations (European source region: 540 mBq m^{-3}) relative to the marine source regions (190 mBq m^{-3} for the Arctic and 340 mBq m^{-3} for the North Atlantic).

1.3.1 Particle Mass

Average non-sea salt PM_1 concentrations from European, Long Island, and North American source regions were 2.75 ± 0.80, 3.40 ± 1.10, and 2.26 ± 0.76 μg m^{-3}, respectively. The European and Arctic regions have similar relative particle compositions (Figure 1.1). Overall during ICEALOT, non-sea salt sulfate was the dominant anthropogenic aerosol component and had the highest measured concentration levels with an overall mean of 1.06±0.70 μg m^{-3}, which was 53% of the total PM_1 (Figure 1.2). The highest fractions of sulfate were measured from the European and Arctic source regions (58 and 64% of PM_1, respectively). Nitrate and ammonium levels were relatively low, accounting for less than 2% and 8% of the overall PM_1, respectively. At Barrow, the

submicron particle composition had a larger fraction of OM_1 (35%, Figure 1.1) and a comparable fraction of sea salt (13%) and IOM (8%).

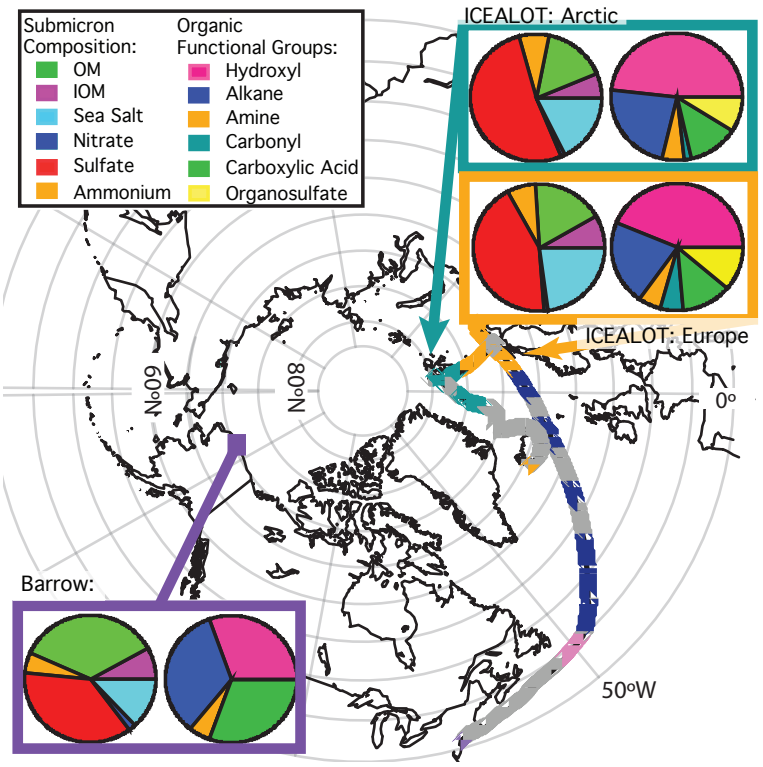

Figure 1.1: Track of the R/V *Knorr* during the ICEALOT cruise colored by regions of air mass origin including Long Island (purple), North America (pink), North Atlantic (dark blue), Europe (bronze), and Arctic (teal). The pies represent the submicron particle composition (left) and organic functional group composition (right) for the European and Arctic source regions during ICEALOT and Barrow (dark purple). The submicron particle composition excludes the elemental carbon (estimated on average less than 3% during ICEALOT and at Barrow).

During ICEALOT, the ratio of non-sea salt sulfate to non-crustal V was 2.15±1.39, overall. Previously reported values at Barrow, 3 [*Rahn and McCaffrey*, 1980] and 2.9 - 4.2 [*Quinn et al.*, 2009], are within the standard deviation of this average suggesting that similar source regions were being measured, specifically European. *Rahn and McCaffrey* [1980] state that the ratio measured at Barrow in 1976 and 1977 is an

order of magnitude greater than ratios measured at mid-latitudes. This suggests that the aerosol measured during ICEALOT also has contributions of secondary aerosol, like that measured previously at Barrow. The higher ratio (2.44) measured from the European source region suggests that resulting aerosol from the European source region are more secondary and oxidized during transport.

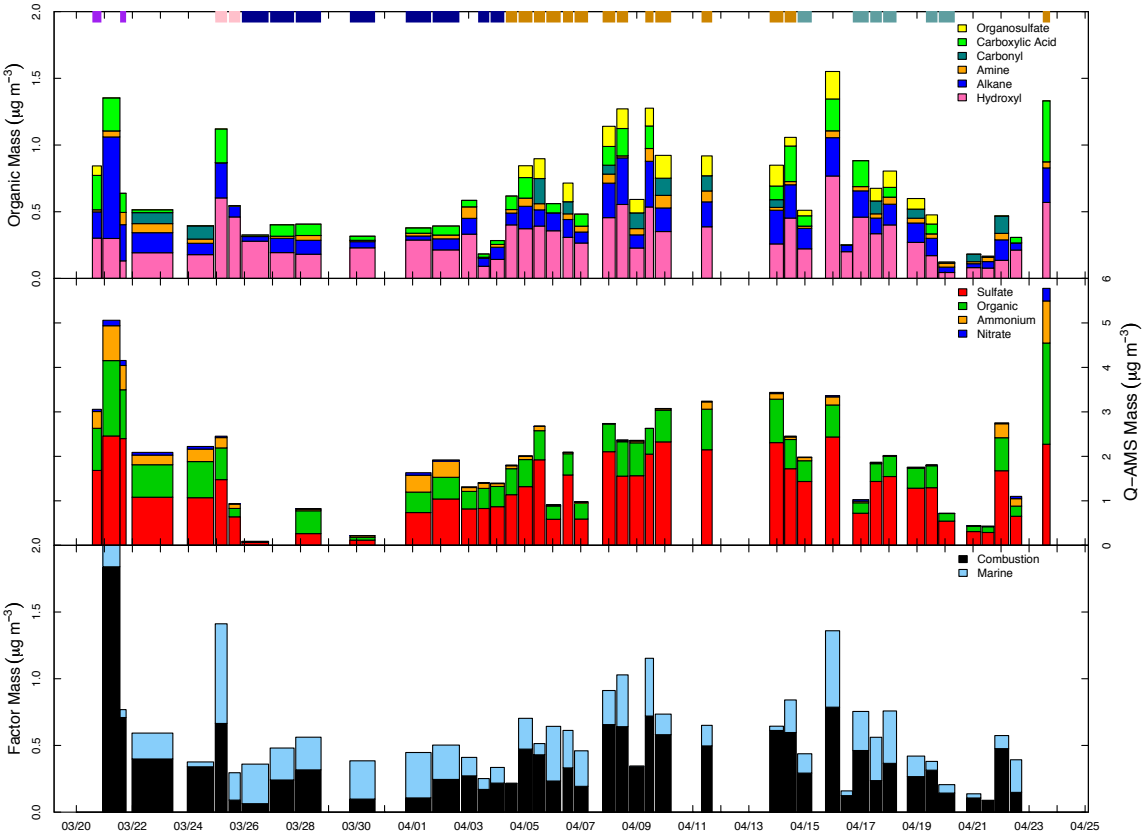

Figure 1.2: Time series and average composition of aerosol mass. Horizontal color bar: regions of air mass origin colored according to the shiptrack in Figure 1.1. Top panel: Functional group concentrations contributing to the total OM_1 measured by FTIR. Middle panel: Mass fragment contribution to total PM_1 measured by Q-AMS. Bottom panel: Factors contributing to organic mass derived from PMF on FTIR spectra.

1.3.2 Organic Mass

Total OM_1 measured by FTIR was calculated by summing the concentrations of the functional groups on each filter. The average OM_1 concentration for ICEALOT

(Figure 1.2) was 0.61 ± 0.36 μg m^{-3}. The highest concentrations (average: 0.89 ± 0.27 μg m^{-3}) were observed when sampling was from the European source region. For two years at Barrow, the average springtime OM_1 was 0.41 ± 0.36 μg m^{-3}. The organic functional group composition measured at Barrow had a larger fraction of alkane (34%) and carboxylic acid (30%) than the Arctic (23%, 13%) and European (21%, 12%) source regions measured during ICEALOT. In addition, organosulfate and non-acid carbonyl functional groups were measured in the Arctic and European source regions (on average 10% and 4%, respectively) and not observed at Barrow.

1.3.3 Ratio of Oxygen to Carbon

The oxygenated fraction of organic aerosol has been used as an indicator of atmospheric processing and photochemical age [*Maria et al.*, 2004; *Zhang et al.*, 2005a]. The O/C ratio is sometimes an indicator of acid groups, which are a result of photochemical aging in the atmosphere. However, some oxygenated groups such as hydroxyl may also increase O/C, although they can originate from primary sources such as ocean-derive marine aerosol [*Russell et al.*, 2010].

For ICEALOT, the O/C ratio was calculated by two methods. Oxygen-containing functional groups (hydroxyl, carboxylic acid, carbonyl, and organosulfate) from FTIR measurements were summed to give the contribution of oxygen atoms to the FTIR O/C ratio and normalized by the total number of carbon atoms from each measured functional group [*Hawkins et al.*, 2010; *Russell et al.*, 2009a]. Because hydroxyl was a large fraction of the OM_1 measured by FTIR, it had the largest contribution to the total O/C ratio, contributing on average 70% (0.66) of the total O/C. The O/C ratio calculated from the

functional groups measured with FTIR spectroscopy was high (0.94) during ICEALOT indicating a highly oxygenated aerosol [*Russell et al.*, 2010]. The O/C from the European source region was 1.0, while the O/C in the Arctic source region was slightly lower (0.87) but still highly oxygenated.

The HR-ToF-AMS O/C ratio was calculated from the individual abundances of O and C for each mass fragment using the Analytical Procedure for Elemental Separation (APES) included in the PIKA analysis software (described at http://tinyurl.com/tofams-analysis) [*Aiken et al.*, 2007; *Aiken et al.*, 2008]. In ambient environments, observed O/C values for oxidized secondary organic aerosol species range from ~0.2 to ~0.9 [*Jimenez et al.*, 2009]. Primary urban vehicle emissions have very low AMS O/C ratios from 0.06 - 0.1 [*Aiken et al.*, 2008], and an O/C ratio greater than 0.40 is considered highly oxygenated [*DeCarlo et al.*, 2008]. The calculated O/C ratio for ICEALOT correlates well (r = 0.91) with the ratio of particulate CO_2 (at nominal *m/z* 44) to total OM_1 consistent with the relationship proposed by *Aiken et al.* [2008]. The ICEALOT campaign averaged HR-ToF-AMS based O/C ratio is 0.41. Aerosol measured from the European source region has an O/C of 0.44, while the Arctic source region aerosol has a larger O/C (0.60). Taken together, these results indicate that the ICEALOT aerosol was highly oxidized. The increase in O/C in the Arctic region is likely indicative of continued processing and aging of aerosols as they are transported from sources to the Arctic.

In general, the HR-ToF-AMS O/C values are systematically lower than those measured by the FTIR. The mild correlation (r = 0.68) of the percent difference in the FTIR and HR-ToF-AMS O/C with the hydroxyl fraction of OM_1 suggests that this difference in the O/C of the two methods is likely due to the lower O/C observed for

hydroxyl groups by the HR-ToF-AMS [*Aiken et al.*, 2007; *Hawkins et al.*, 2010]. The HR-ToF-AMS O/C correlates weakly with O/C calculated from only the FTIR carboxylic acid groups (r = 0.45 in the European source region, but r = 0.27 overall), which is consistent with the HR-ToF-AMS O/C correlation with the ratio of particulate CO_2 (at nominal *m/z* 44) to total OM_1, much of which is often attributed to acid mass fragments.

1.3.4 FTIR PMF

Positive matrix factorization (PMF) was calculated for the FTIR spectra [*Paatero*, 1997; *Paatero and Tapper*, 1994] from the ICEALOT cruise and (separately) from the two-year Barrow data. A four-factor solution, which was recombined into two factors that were less correlated to each other in time, was found to best recreate the original ICEALOT time series (Figure 1.2), as previously discussed by *Russell et al.* [2010] (in the Supporting Information). The two factors were determined to be a mixed combustion factor and a marine-derived factor (the latter of which is discussed in detail by *Russell et al.* [2010]). The mixed combustion factor was determined from correlations ($0.5 < r < 1$) with typical combustion tracers (S, Zn, K, Br) [*Qureshi et al.*, 2006; *Russell et al.*, 2009a; *Sharma and Maloo*, 2005] and large fractions of alkane and carboxylic acid functional groups consistent with combustion factors, containing both primary and secondary aerosol, from previous studies [*Hawkins et al.*, 2010; *Russell et al.*, 2011; *Russell et al.*, 2009a]; see also Section 1.4.1 of Discussion. The time series reconstructed from the factors of OM_1 correlates well with the original FTIR OM_1 time series (r = 0.86). The correlation improves when the organosulfate functional group, which is not included in the wavelength range used for PMF, is removed from the FTIR OM_1 correlation (r =

0.89). The slope of the line (Factor OM_1 = 1.01*FTIR OM_1) shows that the factors provide a good representation of the OM_1 and its variations.

For the Barrow time series, PMF was performed on the 221 spectra resulting in a two-factor solution with FPEAK = 0. The FPEAK = 0 rotation of the PMF solution was selected since there was little sensitivity to rotations with higher or lower FPEAK values. Furthermore, the first half of the time series (from 2008) had measurements of inorganic ions by IC and trace elements by XRF on the same filters that correlated strongly with signatures for each factor. The spectra of the factors from the updated PMF analysis for the full 221 filters at Barrow are indistinguishable from those obtained from the original 118 spectra from 2008-2009, so we applied the same source-based definitions. The first factor was determined to be a mixed combustion factor because it exhibits strong spectral signatures in the alkane and carboxylic acid regions of the IR spectrum and correlates with combustion and industrial tracers (V, K, Fe, Zn, Br, etc.). The other factor was defined as an ocean derived factor because it exhibits strong spectral signatures of marine hydroxyl groups similar to those of ICEALOT described by *Russell et al.* [2010], correlated strongly with Na^+ and Cl^- associated with sea salt, and corresponded to air masses that originated from open ocean in summer [*Shaw et al.*, 2010].

1.3.5 AMS PMF

PMF was used for the organic portion of the HR-ToF-AMS mass spectrum calculated at unit mass resolution [*Allan et al.*, 2004b; *Ulbrich et al.*, 2009]. All analysis for HR-ToF-AMS PMF was done using PMF2 in robust mode [*Paatero*, 1997; *Paatero and Tapper*, 1994]. The PMF Evaluation Tool (PET) developed in Igor Pro

(Wavemetrics, Inc., Portland, Oregon), described by *Ulbrich et al.* [2009], was used to evaluate the PMF output for HR-ToF-AMS spectra, with additional details provided in the Appendix.

The three factors of the solution that best reconstructs the OM time series are: (1) an oxygenated organic aerosol (OOA) factor, with intense *m/z* 44 signal; (2) a hydrocarbon-like organic aerosol (HOA) factor, characterized by hydrocarbon ion fragments (*m/z* 41, 43, 55, 57, 67, 69, 71, etc.); and (3) a third factor (F3) with unique ion fragments (*m/z* 50-55, 65, 67, 77, 79, 91). The time series and spectra of the factors are shown in Figure 1.3a and b.

The OOA factor contributes 33% to the ICEALOT project average OM_1 and 31% in the European source region. The OOA factor spectrum correlates strongly with the reference spectra of oxalic, glyoxcylic, and fulvic acids (r = 0.94, r = 0.93, r = 0.84, respectively) [*Alfarra*, 2004; *Takegawa et al.*, 2007] from the AMS spectral database (Ulbrich, I.M., Lechner, M., and Jimenez, J.L., URL: http://cires.colorado.edu/jimenez-group/AMSsd/) described by *Ulbrich et al.* [2009], providing an indication that this highly oxygenated factor is representative of acid-containing organic aerosol. The OOA factor correlates mildly in time with the FTIR measured carboxylic acid functional group (r = 0.49 overall, r = 0.71 in the European source region) consistent with the interpretation of the OOA factor as an acid-containing, secondary, aged, organic component. The time series of the OOA factor also correlates (r = 0.67) with sulfate, consistent with other measurements in eastern Europe [*Lanz et al.*, 2007].

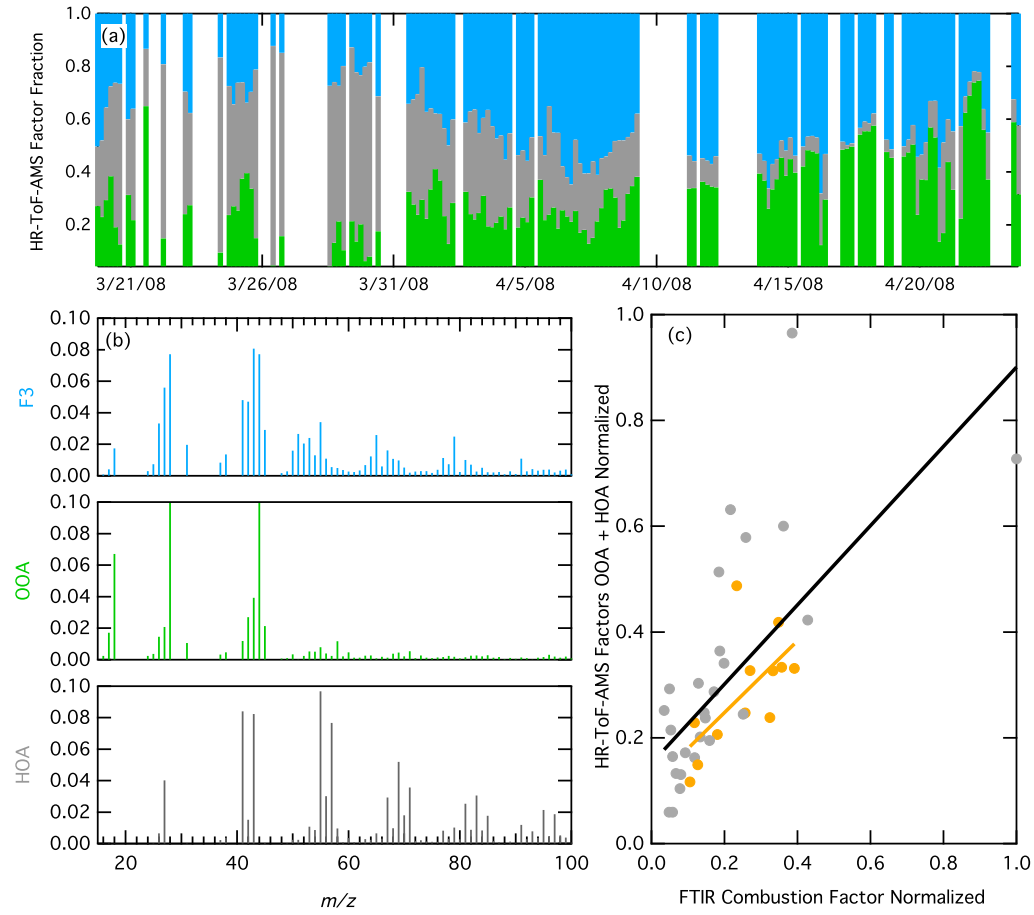

Figure 1.3: (a) Time series of HR-ToF-AMS factor fractions of total OM including HOA (dark grey), OOA (green), and F3 (light blue). (b) The mass spectra of the three distinct factors: HOA, OOA, and F3. (c) Comparison between the HR-ToF-AMS factors OOA + HOA (normalized by the maximum value) and the FTIR combustion factor (normalized by the maximum value), r = 0.64 overall (black) and r = 0.64 in the European source region (orange).

The HOA factor is present mainly at the start of the cruise in the Long Island and North American source regions. HOA contributes 28% to the total OM_1 and 29% and 41% in the Long Island and North American source regions, respectively. The HOA factor spectrum correlates strongly with HOA spectra measured in other campaigns (r = 0.99 and r = 0.98) [*Lanz et al.*, 2009; *Zhang et al.*, 2005b] and also diesel bus exhaust (r = 0.98) [*Canagaratna et al.*, 2004; *Ulbrich et al.*, 2009]. In addition, the HOA factor correlates (r = 0.68) with NO_X (measured on board the R/V *Knorr* using the method

described by *Lerner et al.* [2009]), consistent with less processed emissions [*Lanz et al.*, 2007]. HOA is lower in the European source region (20%) where there is a longer distance between emissions and sampling, suggesting that the emissions measured in the European source region had been processed more or longer in the atmosphere.

The OOA factor and the FTIR combustion factor show a correlation of r = 0.42 overall and r = 0.74 for the European source region, which is consistent with the large contribution of carboxylic acid functional groups to the FTIR combustion factor. The HOA factor has a moderate correlation with the FTIR combustion factor (r = 0.51), but the correlation to the FTIR combustion factor is higher for the sum of OOA and HOA (r = 0.67 overall and r = 0.64 for the European source region, Figure 1.3c). This suggests that the FTIR combustion factor includes both hydrogenated and oxygenated carbon mass fragments, likely including a range of recent and more processed components of combustion emissions. In the European source region, the stronger correlation of the FTIR combustion factor with OOA than with OOA+HOA suggests that the FTIR combustion factor OM_1 from that region is more processed.

1.4 Discussion

1.4.1 Combustion Sources of Organic Mass in Arctic Haze

Emissions from combustion sources provide a large fraction of the aerosol mass in the Arctic that makes up the springtime Arctic haze. Recent measurements at Barrow and during ICEALOT show that the combustion sources typically contribute more than half of OM_1 and over a quarter of PM_1, based on FTIR, AMS, and IC analyses. A comparison of aerosol measured during the spring in these two regions of the Arctic

provides insight into the differences in emission sources and regions contributing to the springtime Arctic haze. The large fraction of oxygenated functional groups measured in the Arctic indicates a high O/C fraction close to 1 (discussed in Section 1.3.3), which is consistent with an aged combustion source and indicates one oxygen for every carbon in an organic particle [*Jimenez et al.*, 2009; *Russell et al.*, 2010; *Russell et al.*, 2009a]. Emissions from coal combustion in northeastern Europe contribute to the OM_1 measured in the northern Atlantic region of the Arctic, while biomass burning, shipping, and industrial emissions contribute to the OM_1 measured in the northern Pacific region of the Arctic.

1.4.1.1 Combustion Factor Contribution to OM_1

PMF of both ICEALOT and Barrow FTIR spectra provide evidence for combustion factors that constitute more than 60% of the OM_1 measured at both sites. The combustion factors show significant fractions of alkane, hydroxyl, and carboxylic acid functional groups. During ICEALOT, the combustion factor was 63% of the total OM_1 and contributed 0.36 ± 0.31 μg m^{-3} to the total organic mass (Figure 1.2). When the aerosol originated from the European source region, the combustion factor was 68% of the total OM_1 and contributed 0.47 ± 0.18 μg m^{-3}. Since OM_1 was approximately 33% of the overall PM_1 and 43% in the European air mass source region, this large contribution of combustion sources from Europe provided a substantial part of the Arctic haze aerosol concentrations in the Barents and Greenland Sea regions during the ICEALOT cruise.

Measurements taken in Barrow, Alaska, span two years and three different seasons (spring, summer and winter). The Barrow spring season was defined to represent

the high OM_1 concentrations that prevail in March through June [*Shaw et al.*, 2010] and includes the ICEALOT sampling period. The OM_1 measured during spring in both 2008 and 2009 at Barrow was higher (0.41 ± 0.36 μg m^{-3}) than the average OM_1 measured both years (0.32 ± 0.36 μg m^{-3}). Most (80% or 0.32 ± 0.22 μg m^{-3}) of the OM_1 measured in the spring was attributed to combustion sources based on correlations with trace metals in spring 2008 [*Shaw et al.*, 2010]. The OM_1 concentration and fraction of the combustion factor were significantly higher than the annual average combustion OM_1 (0.19 ± 0.21 μg m^{-3}), indicating that combustion sources also had a substantial impact at Barrow on the OM_1 fraction of springtime Arctic haze.

1.4.1.2 Combustion Factor Composition

The spectra of the combustion factors for aerosol measured in the northern Pacific and northern Atlantic regions of the Arctic are similar (Figure 1.4a). The differences between the two combustion factor spectra may result both from differences in their source emissions (i.e. between the mixture of combustion sources in Siberia and those in eastern Europe) and in their atmospheric oxidation processes. The ICEALOT combustion factor OM_1 includes large mass fractions of hydroxyl (36%), alkane (35%), and carboxylic acid (27%) functional groups, with a minor fraction (3%) of amine groups (Figure 1.4a). The large fraction of carboxylic acid functional groups suggests that particles aged from combustion emissions contribute to this factor [*Maria et al.*, 2004; *Zhang et al.*, 2005a]. The Barrow combustion factor for the full 2-year study consists of alkane (60%) and carboxylic acid (31%) groups and smaller fractions of amine (5%) and hydroxyl (4%) groups (Figure 1.4a). The large fraction of alkane groups suggests that the

combustion emissions contributing to this factor may have undergone less atmospheric processing than those measured during ICEALOT.

The combustion factors retrieved from the organic FTIR spectra for both ICEALOT and Barrow have large contributions from both carboxylic acid and hydroxyl functional groups. These oxygenated groups are characteristic of the products expected from photochemical oxidation [*Huebert and Charlson*, 2000; *Lim and Ziemann*, 2005; 2009; *Putaud et al.*, 2000] indicating that the measured particles are due in part to secondary organic aerosol. The weakness of the correlations during ICEALOT to elemental tracers (Fe and V) indicates that the variability in the combustion factor OM may lag the primary combustion products, which is expected for secondary rather than primary OM.

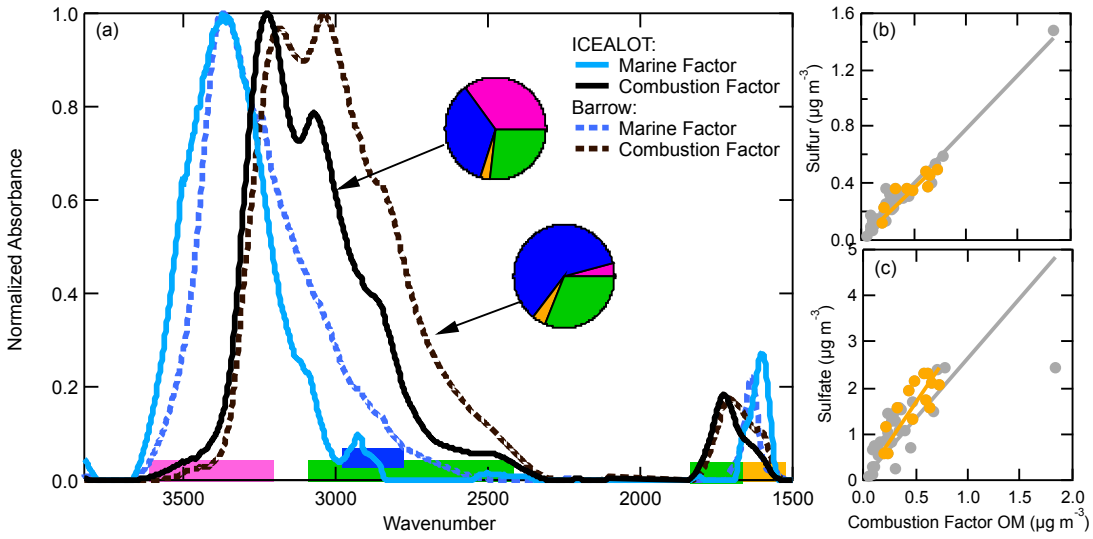

Figure 1.4: (a) Factor spectra from PMF of FTIR sample spectra for ICEALOT (solid) and Barrow (dashed). The pie charts show the average composition of the combustion factor, using the colors described in Figure 1.1, for both ICEALOT and Barrow. Comparisons of the ICEALOT combustion factor with (b) S (r = 0.97, r = 0.9) and (c) sulfate (r = 0.75, r = 0.8) for all air masses (grey) and the European source region (orange), respectively.

1.4.1.3 Sources of Combustion in Northeastern Europe and Asia

The combustion factor derived from measurements in the north Atlantic and adjacent regions of the Arctic Ocean during ICEALOT reflects aerosol influenced by emissions from northeastern Europe and Russia. Coal burning is one of the main sources of heating, and there are also numerous coal burning smelters in that area [*Hole et al.*, 2006a; *Kubica*, 2003; *Weiler et al.*, 2005]. The Kola Peninsula, northeast of Finland, has Cu and Ni producing industry which emits high levels of SO_2 and NO_2 [*Weiler et al.*, 2005]. In the Kola Peninsula, the conurbation of Murmansk is a highly populated metropolitan area and sea port, which contributes to the polluted air from that area [*Law and Stohl*, 2007]. The combustion factor concentration correlates strongly with S concentrations for both overall (r = 0.97) and the European source region (r = 0.90, Figure 1.4b) indicating that coal burning is likely collocated or co-emitted with the organic combustion sources. This strong correlation of the combustion factor OM_1 with sulfur likely is a consequence of S being primarily sulfate, a typical secondary aerosol product of coal combustion emissions, which also correlates strongly with r = 0.75 overall (and r = 0.80 in the European source region, Figure 1.4c) suggesting that the sources of the organic combustion factor and those of the sulfate are collocated. Correlations with Zn (total r = 0.74; European source region r = 0.57) are consistent with emissions from non-ferrous metal producing industries, such as copper smelting in northeastern Europe [*Polissar et al.*, 1998; *Polissar et al.*, 2001; *Shaw*, 1982]. The combustion factor weakly correlates with V (r = 0.24 overall, r = 0.44 in the European source region), suggesting that the combustion factor may also have some contributions from oil burning. The ratio of non-sea salt sulfate to non-crustal V mildly correlates (r =

0.55) in the European source region with the combustion factor fraction of OM. In addition to the correlations with the combustion and pollution tracers (Zn, Ca, Fe, S, and V), the concentrations of these metals were 5-65% higher in the European source region than the ICEALOT average.

About 50% of Europe's electricity is produced from fossil fuel combustion [*Kubica*, 2003], and high alkane concentrations are found in petroleum combustion emissions from Europe [*Blake et al.*, 1994; *Blake et al.*, 2003]. In eastern Europe, combustion of fuels such as coal and lignite lead to high levels of SOx, NOx, PM, and CO_2 emissions [*Ross et al.*, 2002]. The mixture of high SOx emissions from coal and alkane emissions from petroleum could explain the correlation of the organic combustion factor and the sulfate observed during the European source region of the ICEALOT cruise, making emissions from northeastern Europe the main source of OM_1 in the Arctic haze on the northern Atlantic side.

At Barrow, the combustion factor also correlates strongly to S but, in addition, is correlated to non-dust K, characteristic of a biomass burning source, where [non-dust K] = [K] – 0.62*[Al] [*Cachier et al.*, 1995; *Gilardoni et al.*, 2009]. Alaskan and Siberian wildfires were observed in spring 2008 and 2009 [*Forest Service*, 2010; *Shaw et al.*, 2010; *Warneke et al.*, 2009], which provide evidence for the influence of biomass burning in the combustion factor. V, which is characteristic of processed emissions from oil burning, is mildly correlated with the combustion factor. V is a tracer for the combustion of heavy residual oil only used in the sub-Arctic since it is too viscous to use at low temperature and is hence a tracer of the long range transport of emissions from oil combustion [*Isakson et al.*, 2001].

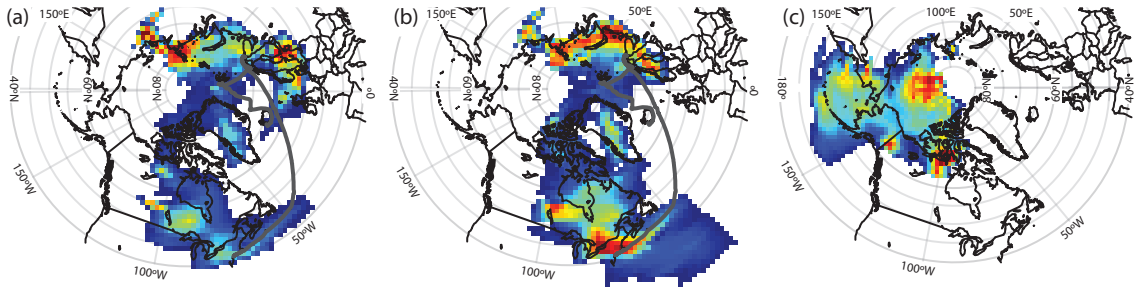

Figure 1.5: PSCF of (a) the total OM1 measured during ICEALOT, (b) the ICEALOT combustion factor, and (c) the Barrow combustion factor. The higher potential source regions are indicated by red and the lower potential source regions are indicated with blue.

To investigate the probability that these two different urban and industrial centers were the emission sources that were responsible for the observed high OM_1 from combustion factors, PSCF were calculated for Barrow and ICEALOT [*Pekney et al.*, 2006]. The region with high potential of being a source of the ICEALOT combustion factor is northeastern Europe, with the highest potential sources shown in Figure 1.5b as Scandinavia and the Kola Peninsula, as well as the northwestern edge of Russia. These areas of northeastern Europe have significant industrial activity, including non-ferrous metal producing plants that contribute to the organic emissions [*Blake et al.*, 2003; *Hole et al.*, 2006a; *Mira-Salama et al.*, 2008; *Weiler et al.*, 2005]. The PSCF of sulfate measured during ICEALOT shows a trend similar to the potential source of the organic combustion factor (see Figure 1.6a and 1.5b for comparison), supporting the suggestion that the organic and sulfate sources are collocated. In addition, PSCF for OM_1 measured during ICEALOT also shows potential sources in northeastern Europe (Figure 1.5a). PSCF of the Barrow combustion factor shows potential sources from northeastern Asia, shipping lanes in the Bering Strait, and along the Canadian-Alaskan border (Figure 1.5c), which are similar to the potential sources observed in 2008. The differences in the

potential source regions shown in Figure 1.5 highlight the importance of northeastern Asian sources for Arctic haze at Barrow in contrast to the northeastern European sources of the Arctic haze during ICEALOT.

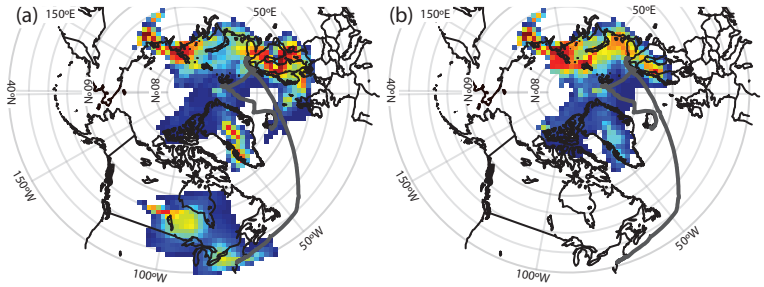

Figure 1.6: PSCF of (a) sulfate and (b) organosulfate functional group concentrations. The higher potential source regions are indicated by red and the lower potential source regions are indicated with blue.

In summary, the functional group composition indicates that the majority of the organic aerosol in Arctic haze is produced from combustion emissions, and back trajectories from both regions suggest that the combustion sources are in northeastern Europe and Asia. The two different sources of measured Arctic aerosol are demonstrated in the differences between the composition of their combustion factors and the potential source regions determined from PSCF.

1.4.2 Organosulfate Formation from Combustion Emissions

One interesting chemical consequence of the co-emissions of sulfate from coal burning and volatile organic compound (VOC) emissions in northeastern Europe is the production of organosulfate functional groups. In air masses sampled from both the European and Arctic source regions of the ICEALOT campaign, organosulfate groups contributed 9% and 11% of the organic mass, respectively, whereas no organosulfate groups were measured at Barrow. The organosulfate functional group fraction of PM_1

has a strong correlation (r = 0.84) with the sulfate fraction of PM_1 for the European region and a moderate correlation (r = 0.50) for the entire ICEALOT cruise (Figure 1.7b) and was only detected in samples with sulfate concentrations greater than 1.25 μg m^{-3}. This observed increase in organosulfate group fraction of PM_1 with increased sulfate fraction of PM_1 is consistent with organosulfate formation on sulfate particles, many of which are likely acidic in this region [*Surratt et al.*, 2007a]. The molar ratio of ammonium to sulfate was 1.13 for the whole project and 1.22 during the periods of filter sampling. The lower average molar ratio of ammonium to sulfate (0.96) of particles measured from the European and Arctic source regions and their implied higher acidity provides conditions consistent with the acid-catalyzed particle-phase formation of organosulfate in air masses from those source regions [*Iinuma et al.*, 2009; *Iinuma et al.*, 2007; *Liggio et al.*, 2005; *Perri et al.*, 2010; *Surratt et al.*, 2007a; *Surratt et al.*, 2010; *Surratt et al.*, 2007b; *Surratt et al.*, 2008]. Organosulfate group fraction of PM_1 has a mild negative correlation (r = -0.50) with relative humidity for the European source region (Figure 1.7c). In addition, organosulfate group concentration is mildly negatively correlated (r = -0.64) with absolute humidity in the European source region. These relationships suggest that organosulfate formation decreases with higher aerosol water concentrations, which may be due in part to the decrease in aerosol acidity with an increase in relative humidity (r = 0.52 overall, r = 0.51 for the European source region), consistent with the findings of a previous study in the southeastern Pacific [*Hawkins et al.*, 2010; *Liggio et al.*, 2005]. In summary, four conditions coincide with organosulfate group formation in the European and Arctic source regions, relative to the ICEALOT measurement period: high organic mass (> 0.75 μg m^{-3}), high sulfate (> 1.25 μg m^{-3}), low

ammonium to sulfate ratio (< 1.0), and high overall relative humidity (> 50%). These observations are consistent with sulfate particles providing acidic aqueous conditions that enhance organosulfate formation from organic precursors. The correlation of the sulfate and the organosulfate fractions of PM_1 also suggests both similar sources and similar processing times in the atmosphere (given the time resolution of the filter sampling, namely 12 hour).

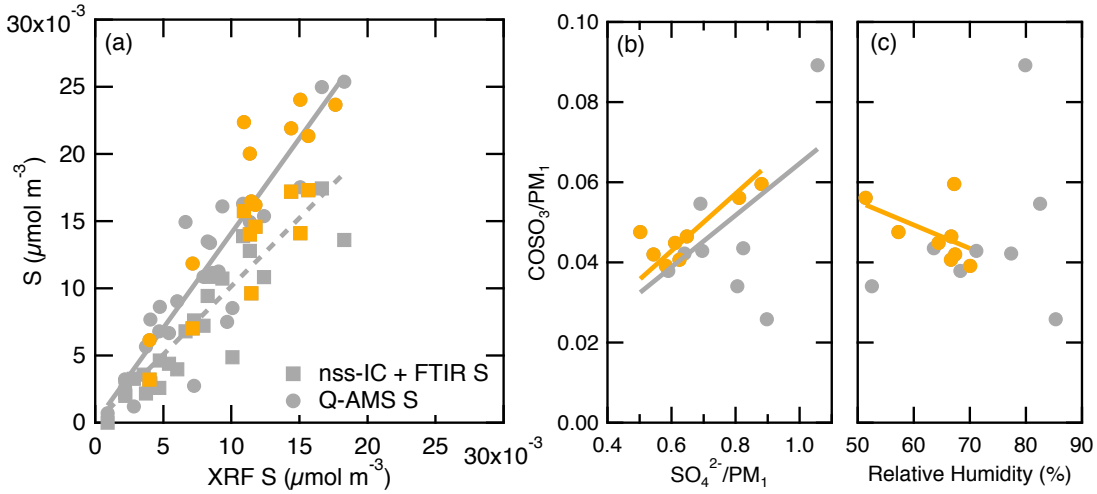

Figure 1.7: (a) Comparison of S measured by XRF with IC + FTIR derived S (slope = 1.02, r = 0.92) and Q-AMS derived S (y = 1.41, r = 0.91) for the total project (grey) and the European source region (orange). (b) Correlation of organosulfate group fraction of PM1 with sulfate fraction of PM1 (r = 0.84 for the European source region). (c) Negative correlation of organosulfate group fraction of PM1 and relative humidity (r = -0.50 for the European source region).

The four conditions for organosulfate formation observed during ICEALOT did not all occur at Barrow, which could explain the lack of organosulfate formation there. During the spring seasons, the average sulfate concentration measured at Barrow was 0.64 μg m^{-3}, which is less than observed during ICEALOT but consistent with the range reported by *Quinn et al.* [2002] for the spring seasons of 1998-2000. On the other hand, the average molar ratio of ammonium to sulfate (0.75) was consistent with the acidic

ratio measured during ICEALOT. Average OM_1 concentration (0.70 μg m^{-3}) measured during the spring season is slightly less than was observed for periods with organosulfate functional groups during ICEALOT. The process of acid-catalyzed particle haze formation of organosulfate likely does not occur during the spring seasons at Barrow.

The sum of S (μmol m^{-3}) from inorganic sulfate measured by IC and organosulfate groups measured by FTIR correlates well (r = 0.92) with the total S measured by XRF (Figure 1.7a). Without the organosulfate group component, there is still a strong correlation (r = 0.92) to elemental (XRF) S, but the slope of the line (0.94) suggests that there is a missing source of S. When organosulfate is added to the IC measured sulfate, the total S is better represented, with a slope of 1.02. This suggests that the majority (94%) of the S concentration measured during ICEALOT is inorganic sulfate, with the remaining 6%, on average, coming from organic sulfate. The S from Q-AMS measurements of sulfate also correlates well (r = 0.91) with XRF measurements of S, consistent with the expectation that the Q-AMS detects both organic and inorganic sulfate [*Allan et al.*, 2004a; *Farmer et al.*, 2010].

Using PSCF, the highest potential source contributions of the ICEALOT sulfate concentrations were found in northeastern Europe, similar to the locations of potential sources for the combustion factor, as is evident by comparing Figures 1.5b and 1.6a. In addition, the potential source of organosulfate groups is collocated with sulfate, as shown in Figure 1.6b.

Other studies have shown organosulfate formation from biogenic precursors [*Gomez-Gonzalez et al.*, 2008; *Iinuma et al.*, 2009; *Surratt et al.*, 2007a; *Surratt et al.*, 2010; *Surratt et al.*, 2008]. Because there were no large sources of terrestrial biogenic

emissions measured during ICEALOT, biogenic precursors during ICEALOT were not identified as a likely source of organosulfate functional groups. While the emissions from the European source region measured during ICEALOT have been attributed to fossil fuel burning, due to the absence of biogenic volatile organic compounds (BVOCs) in the air measured at the ship, it remains possible that co-located BVOCs did contribute to OM and to subsequent reactions with sulfate in particles to form organosulfate. *Claeys et al.* [2010] found evidence that organosulfate functional groups can occur with acidic particles produced from oxidation productions of dimethyl sulfide (DMS) and bacteria sources in a clean marine environment. The organosulfate measured during ICEALOT was unlikely to be the result of marine emissions since organosulfate functional groups were only observed when air masses were from European and Arctic source regions. Organosulfate group concentrations or fractions did not correlate with the marine factor, as would be expected for marine sources.

1.5 Conclusions

Emissions from combustion sources greatly impact the concentrations of submicron aerosol particles in the Arctic and contribute to Arctic haze in both the Atlantic and Pacific sides of the Arctic region. Complementary measurement techniques show higher OM_1 in air masses sampled from the European source regions than from the marine source regions, both measured on the Atlantic side of the Arctic during ICEALOT. A large fraction (74%) of the OM_1 was attributed to eastern European combustion sources (industrial and other petroleum burning) based on PMF-derived factors from FTIR measurements. Measurements from Barrow, Alaska, on the Pacific

side of the Arctic show the largest percent of OM_1 from mixed combustion sources (biomass burning and shipping) in the spring season. The organic functional group compositions indicate that mixed combustion sources account for more than 60% (>0.3 μg m^{-3}) of the total organic mass measured in air masses influenced from both the European and Arctic source regions during ICEALOT and the spring season at Barrow.

Carboxylic acid and hydroxyl groups account for more than 35% of the combustion factor organic functional groups in the Atlantic and Pacific sides of the Arctic, reflecting the products of oxidation of emissions from fuel burning. The ICEALOT combustion factor, dominated by carboxylic acid, alkane, and hydroxyl functional groups, correlates well with sulfate suggesting that their sources are collocated. The large fraction of the carboxylic acid functional group is consistent with the secondary products expected from oxidation of VOCs. Q-AMS and HR-ToF-AMS measurements confirm the highly oxygenated nature of the OM_1 from combustion, with an OOA spectrum similar to that of oxygenated acid groups. Aerosol measured in the Pacific side of the Arctic at Barrow has a larger fraction of alkane suggesting that the aerosol is less aged. The differences in the combustion-derived spectra from the two regions result from the mixtures of sources in each region, although more specific contributions could not be resolved in these campaigns.

On the Atlantic side of the Arctic, high levels of sulfate and OM_1 were typically associated with back trajectories that originated in northeastern Europe. The correlations between the combustion factor for ICEALOT and S and sulfate suggest emissions from the high coal burning regions of northeastern Europe. On the other hand, the correlations between the Barrow combustion factor and V and non-dust K are characteristic of

emissions from northern Asia, Siberia, and, to a lesser extent, interior regions of Alaska and Canada.

The high emissions of sulfate from coal-burning in northeastern Europe produce significant concentrations of the organosulfate functional groups that account for as much as 10% of OM_1 measured by FTIR over the Barents and Greenland seas during ICEALOT. There is some evidence suggesting that organosulfate formation occurs heterogeneously when compounds react in acidic (aqueous) sulfate particles. Organosulfate functional groups were measured in air masses from both the European and Arctic source regions, when high concentrations (1.25-2.40 μg m^{-3}) of sulfate were present but not at Barrow, which had lower sulfate concentrations (0.64 μg m^{-3}, average). The potential source region of organosulfate groups is collocated with the potential source region of sulfate during ICEALOT, where there are high S emissions from abundant sources of coal combustion. The high correlation between the organosulfate fraction of PM_1 and sulfate fraction of PM_1 and the low molar ratio of ammonium to sulfate (high acidity) suggests that organosulfate functional groups are formed on sulfate particles through acid-catalyzed aqueous reactions.

Our findings suggest that pan-Arctic air quality is not uniform in composition but rather regionally dependent on different transport mechanisms and source regions. Since these unique aerosol contributions produce different chemical and microphysical consequences, climate models that are able to simulate direct and indirect aerosol effects must be able to treat the specific areas differently in order to make predictions of radiative forcing in the Arctic.

1.6 Appendix: PMF of HR-ToF-AMS

Unit mass resolution PMF analysis was performed on the HR-ToF-AMS data. The PET software and analysis methods outlined *by Ulbrich et al.* [2009] were used to perform the PMF analysis. The data and error matrices input into the PMF analysis were obtained with the SQUIRREL analysis program (described at http://tinyurl.com/tofams-analysis) [*Allan et al.*, 2003; *Allan et al.*, 2004b]. The error matrices account for Poisson statistics in ion counting. A minimum error constraint was additionally placed on the error matrix according to *Ulbrich et al.* [2009]. Due to low signal to noise (S/N), ion fragments with masses above *m/z* 200 were removed from the analysis. The remaining ion fragments with 0.2 <S/N<2 were downweighted by a factor of 3 [*Ulbrich et al.*, 2009]. PMF analysis results were compared for solutions with 1 through 10 factors. The largest drop in Q/Qexpected occurred going from 1 to 2 factors, showing that at least two factors are needed to accurately represent the organic mass and explain the variance. The three factor solution, which had a minimum Q value and did not show any evidence of factor splitting, was chosen as the optimum solution for this analysis. The three factors together account for 97% of the observed OM. The effect of rotation on the PMF solution was examined by changing the Fpeak parameter from -1 to 1 with 0.2 intervals. Solutions with -0.22< Fpeak< 0 yielded component spectra and time series that did not contain unreasonable zeros. The chosen solution is supported by the strongest correlations with reference spectra posted at http://cires.colorado.edu/jimenez-group/AMSsd/ [*Ulbrich et al.*, 2009].

1.7 Acknowledgements

This study was funded by the National Science Foundation (ATM-0744636; ARC-0714052) as part of the International Polar Year. We would like to thank John Ogren, Pat Sheridan, Anne Jefferson, and the staff of the NOAA ESRL Barrow station for guidance and assistance in the collection of the particle measurements discussed here. The authors would also like to acknowledge Brian Lerner at NOAA ERSL for the collection and interpretation of NO_X data during ICEALOT.

Chapter 1, in full, is a reprint of the material as it appears in the *Journal of Geophysical Research-Atmospheres* 2011 with slight modifications. Frossard, A.A., P.M. Shaw, L.M. Russell, J.H. Kroll, M. Canagaratna, D. Worsnop, P.K. Quinn, and T.S. Bates (2011), "Springtime Arctic Haze Contributions of Submicron Organic Particles from European and Asian Combustion Sources." *Journal of Geophysical Research-Atmospheres.* 116, D05205, doi:10.1029/2010JD015178. The dissertation author was the primary investigator and author of this paper.

References

Aiken, A. C., P. F. DeCarlo, and J. L. Jimenez (2007), Elemental analysis of organic species with electron ionization high-resolution mass spectrometry, *Analytical Chemistry*, *79*(21), 8350-8358.

Aiken, A. C., P. F. Decarlo, J. H. Kroll, D. R. Worsnop, J. A. Huffman, K. S. Docherty, I. M. Ulbrich, C. Mohr, J. R. Kimmel, D. Sueper, Y. Sun, Q. Zhang, A. Trimborn, M. Northway, P. J. Ziemann, M. R. Canagaratna, T. B. Onasch, M. R. Alfarra, A. S. H. Prevot, J. Dommen, J. Duplissy, A. Metzger, U. Baltensperger and J. L. Jimenez (2008), O/C and OM/OC ratios of primary, secondary, and ambient organic aerosols with high-resolution time-of-flight aerosol mass spectrometry, *Environmental Science and Technology*, *42*(12), 4478-4485.

Alfarra, M. R. (2004), Insights into atmospheric organic aerosols using an aerosol mass spectrometer, University of Manchester, Institute of Science and Technology.

Allan, J. D., J. L. Jimenez, P. I. Williams, M. R. Alfarra, K. N. Bower, J. T. Jayne, H. Coe, and D. R. Worsnop (2003), Quantitative sampling using an Aerodyne aerosol mass spectrometer - 1. Techniques of data interpretation and error analysis, *Journal of Geophysical Research - Atmospheres*, *108*(D3).

Allan, J. D., K. N. Bower, H. Coe, H. Boudries, J. T. Jayne, M. R. Canagaratna, D. B. Millet, A. H. Goldstein, P. K. Quinn, R. J. Weber, D. R. Worsnop (2004a), Submicron aerosol composition at Trinidad Head, California, during ITCT 2K2: Its relationship with gas phase volatile organic carbon and assessment of instrument performance, *Journal of Geophysical Research - Atmospheres*, *109*(D23).

Allan, J. D., A. E. Delia, H. Coe, K. N. Bower, M. R. Alfarra, J. L. Jimenez, A. M. Middlebrook, F. Drewnick, T. B. Onasch, M. R. Canagaratna, J. T. Jayne and D. R. Worsnop (2004b), A generalised method for the extraction of chemically resolved mass spectra from aerodyne aerosol mass spectrometer data, *Journal of Aerosol Science*, *35*(7), 909-922.

Bates, T. S., P. K. Quinn, D. Coffman, K. Schulz, D. S. Covert, J. E. Johnson, E. J. Williams, B. M. Lerner, W. M. Angevine, S. C. Tucker, W. A. Brewer and A. Stohl (2008), Boundary layer aerosol chemistry during TexAQS/GoMACCS 2006: Insights into aerosol sources and transformation processes, *Journal of Geophysical Research - Atmospheres*, *113*.

Blake, D. R., T. W. Smith, T. Y. Chen, W. J. Whipple, and F. S. Rowland (1994), Effects of biomass burning on summertime nonmethane hydrocarbon concentrations in Canadian wetlands, *Journal of Geophysical Research - Atmospheres*, *99*(D1), 1699-1719.

Blake, N. J., D. R. Blake, B. C. Sive, A. S. Katsenstein, S. Meinardi, O. W. Wingenter, E. L. Atlas, F. Flocke, B. A. Ridley, and F. S. Rowland (2003), The seasonal evolution of NMHCs and light alkyl nitrates at middle to high northern latitudes during TOPSE, *Journal of Geophysical Research*, *108*(D4), TOP7-1-16.

Blando, J. D., R. J. Porcja, T. H. Li, D. Bowman, P. J. Lioy, and B. J. Turpin (1998), Secondary formation and the Smoky Mountain organic aerosol: An examination of aerosol polarity and functional group composition during SEAVS, *Environmental Science and Technology*, *32*(5), 604-613.

Cachier, H., C. Liousse, P. Buatmenard, and A. Gaudichet (1995), Particulate content of savanna fire emissions, *Journal of Atmospheric Chemistry*, *22*(1-2), 123-148.

Canagaratna, M. R., J. T. Jayne, D. A. Ghertner, S. Herndon, Q. Shi, J. L. Jimenez, P. J. Silva, P. Williams, T. Lanni, F. Drewnick, K. L. Demerjian, C. E. Kolb, D. R. Worsnop (2004), Case studies of particulate emissions from in-use New York City vehicles, *Aerosol Science and Technology*, *38*(6), 555-573.

Canagaratna, M. R., J. T. Jayne, D. A. Ghertner, S. Herndon, Q. Shi, J. L. Jimenez, P. J. Silva, P. Williams, T. Lanni, F. Drewnick, K. L. Demerjian, C. E. Kolb and D. R. Worsnop (2007), Chemical and microphysical characterization of ambient aerosols with the aerodyne aerosol mass spectrometer, *Mass Spectrometry Reviews*, *26*(2), 185-222.

Candelone, J. P., J. L. Jaffrezo, S. M. Hong, C. I. Davidson, and C. F. Boutron (1996), Seasonal variations in heavy metals concentrations in present day Greenland snow, *Science of the Total Environment*, *193*(2), 101-110.

Carlson, T. N. (1981), Speculations on the movement of polluted air to the Arctic, *Atmospheric Environment*, *15*(8), 1473-1477.

Claeys, M., W. Wang, R. Vermeylen, I. Kourtchev, X. G. Chi, Y. Farhat, J. D. Surratt, Y. Gomez-Gonzalez, J. Sciare, and W. Maenhaut (2010), Chemical characterisation of marine aerosol at Amsterdam Island during the austral summer of 2006-2007, *Journal of Aerosol Science*, *41*(1), 13-22.

Davidson, C. I., J. L. Jaffrezo, B. W. Mosher, J. E. Dibb, R. D. Borys, B. A. Bodhaine, R. A. Rasmussen, C. F. Boutron, U. Gorlach, H. Cachier, J. Ducret, J. L. Colin, N. Z. Heidam, K. Kemp and R. Hillamo (1993), Chemical-constituents in the air and snow at dye-3, Greenland. 1. Seasonal-variations, *Atmospheric Environment Part a-General Topics*, *27*(17-18), 2709-2722.

DeCarlo, P. F., J. R. Kimmel, A. Trimborn, M. J. Northway, J. T. Jayne, A. C. Aiken, M. Gonin, K. Fuhrer, T. Horvath, K. S. Docherty, D. R. Worsnop and J. L. Jimenez (2006), Field-deployable, high-resolution, time-of-flight aerosol mass spectrometer, *Analytical Chemistry*, *78*(24), 8281-8289.

DeCarlo, P. F., E. J. Dunlea, J. R. Kimmel, A. C. Aiken, D. Sueper, J. Crounse, P. O. Wennberg, L. Emmons, Y. Shinozuka, A. Clarke, J. Zhou, J. Tomlinson, D. R. Collins, D. Knapp, A. J. Weinheimer, D. D. Montzka, T. Campos and J. L. Jimenez (2008), Fast airborne aerosol size and chemistry measurements above Mexico City and Central Mexico during the MILAGRO campaign, *Atmospheric Chemistry and Physics*, *8*(14), 4027-4048.

Draxler, R. R., and G. D. Rolph (2003), HYSPLIT (HYbrid Single-Particle Lagrangian Integrated Trajectory), Air Resources Laboratory, NOAA, Silver Spring, MD, (Model access via NOAA ARL READY Website http://www.arl.noaa.gov/readyhysplit4.html).

Farmer, D. K., A. Matsunaga, K. S. Docherty, J. D. Surratt, J. H. Seinfeld, P. J. Ziemann, and J. L. Jimenez (2010), Response of an aerosol mass spectrometer to organonitrates and organosulfates and implications for atmospheric chemistry, *Proceedings of the National Academy of Sciences of the United States of America*, *107*(15), 6670-6675.

Ferek, R. J., P. V. Hobbs, L. F. Radke, J. A. Herring, W. T. Sturges, and G. F. Cota (1995), Dimethyl sulfide in the arctic atmosphere, *Journal of Geophysical Research - Atmospheres*, *100*(D12), 26093-26104.

Gilardoni, S., S. Liu, S. Takahama, L. M. Russell, J. D. Allan, R. Steinbrecher, J. L. Jimenez, P. F. De Carlo, E. J. Dunlea, and D. Baumgardner (2009), Characterization of organic ambient aerosol during MIRAGE 2006 on three platforms, *Atmospheric Chemistry and Physics*, *9*(15), 5417-5432.

Gomez-Gonzalez, Y., J. D. Surratt, F. Cuyckens, R. Szmigielski, R. Vermeylen, M. Jaoui, M. Lewandowski, J. H. Offenberg, T. E. Kleindienst, E. O. Edney, F. Blockhuys, C. Van Alsenoy (2008), Characterization of organosulfates from the photooxidation of isoprene and unsaturated fatty acids in ambient aerosol using liquid chromatography/(-) electrospray ionization mass spectrometry, *Journal of Mass Spectrometry*, *43*(3), 371-382.

Greenaway, K. R. (1950), Experiences with Arctic flying weather, report, Canadian Branch, Royal Meteorological Society, Toronto, Ontario, Canada.

Hawkins, L. N., L. M. Russell, D. S. Covert, P. K. Quinn, and T. S. Bates (2010), Carboxylic acids, sulfates, and organosulfates in processed continental organic aerosol over the southeast Pacific Ocean during VOCALS-REx 2008, *Journal of Geophysical Research - Atmospheres*, *115*.

Hole, L. R., J. Christensen, M. Forsius, M. Nyman, A. Stohl, and S. Wilson (2006a), Sources of acidifying pollutants and Arctic haze precursors, in *AMAP Assessment Report: Acidifying Pollutants, Arctic Haze, and Acidification in the Arctic*, chap. 2, pp. 2–10, Arctic Monitoring and Assessment Programme, Oslo.

Hole, L. R., J. H. Christensen, T. Ruoho-Airola, K. Torseth, V. Ginzburg, and P. Glowacki (2009), Past and future trends in concentrations of sulphur and nitrogen compounds in the Arctic, *Atmospheric Environment*, *43*(4), 928-939.

Hole, L. R., J. Christensen, V. A. Ginzburg, V. Makarov, A. I. Polishok, T. Ruoho−Airola, and V. N. Vasilenko (2006b), Concentrations and deposition of acidifying air pollutants, in *AMAP Assessment Report: Acidifying Pollutants, Arctic Haze, and Acidification in the Arctic*, chap. 3, pp. 11–30, Arctic Monitoring and Assessment Programme, Oslo.

Huebert, B. J., and R. J. Charlson (2000), Uncertainties in data on organic aerosols, *Tellus Series B-Chemical and Physical Meteorology*, *52*(5), 1249-1255.

Iinuma, Y., O. Boge, A. Kahnt, and H. Herrmann (2009), Laboratory chamber studies on the formation of organosulfates from reactive uptake of monoterpene oxides, *Physical Chemistry Chemical Physics*, *11*(36), 7985-7997.

Iinuma, Y., C. Muller, T. Berndt, O. Boge, M. Claeys, and H. Herrmann (2007), Evidence for the existence of organosulfates from beta-pinene ozonolysis in ambient secondary organic aerosol, *Environmental Science and Technology*, *41*, 6678-6683.

Isakson, J., T. A. Persson, and E. S. Lindgren (2001), Identification and assessment of ship emissions and their effects in the harbour of Goteborg, Sweden, *Atmospheric Environment*, *35*(21), 3659-3666.

Iversen, T. (1984), On the atmospheric transport of pollution to the Arctic, *Geophysical Research Letters*, *11*(5), 457-460.

Iversen, T., and E. Joranger (1985), Arctic air-pollution and large-scale atmospheric flows, *Atmospheric Environment*, *19*(12), 2099-2108.

Jayne, J. T., D. C. Leard, X. F. Zhang, P. Davidovits, K. A. Smith, C. E. Kolb, and D. R. Worsnop (2000), Development of an aerosol mass spectrometer for size and composition analysis of submicron particles, *Aerosol Science and Technology*, *33*(1-2), 49-70.

Jimenez, J. L., M. R. Canagaratna, N. M. Donahue, A. S. H. Prevot, Q. Zhang, J. H. Kroll, P. F. DeCarlo, J. D. Allan, H. Coe, N. L. Ng, A. C. Aiken, K. S. Docherty, I. M. Ulbrich, A. P. Grieshop, A. L. Robinson, J. Duplissy, J. D. Smith, K. R. Wilson, V. A. Lanz, C. Hueglin, Y. L. Sun, J. Tian, A. Laaksonen, T. Raatikainen, J. Rautiainen, P. Vaattovaara, M. Ehn, M. Kulmala, J. M. Tomlinson, D. R. Collins, M. J. Cubison, E. J. Dunlea, J. A. Huffman, T. B. Onasch, M. R. Alfarra, P. I. Williams, K. Bower, Y. Kondo, J. Schneider, F. Drewnick, S. Borrmann, S. Weimer, K. Demerjian, D. Salcedo, L. Cottrell, R. Griffin, A. Takami, T. Miyoshi, S. Hatakeyama, A. Shimono, J. Y. Sun, Y. M. Zhang, K. Dzepina, J. R. Kimmel, D. Sueper, J. T. Jayne, S. C. Herndon, A. M. Trimborn, L. R. Williams, E. C. Wood, A. M. Middlebrook, C. E. Kolb, U. Baltensperger and D. R. Worsnop (2009), Evolution of Organic Aerosols in the Atmosphere, *Science*,

326(5959),1525-1529.

Lanz, V. A., M. R. Alfarra, U. Baltensperger, B. Buchmann, C. Hueglin, and A. S. H. Prevot (2007), Source apportionment of submicron organic aerosols at an urban site by factor analytical modelling of aerosol mass spectra, *Atmospheric Chemistry and Physics*, *7*(6), 1503-1522.

Lanz, V. A., S. Henne, J. Staehelin, C. Hueglin, M. K. Vollmer, M. Steinbacher, B. Buchmann, and S. Reimann (2009), Statistical analysis of anthropogenic non-methane VOC variability at a European background location (Jungfraujoch, Switzerland), *Atmospheric Chemistry and Physics*, *9*(10), 3445-3459.

Law, K. S., and A. Stohl (2007), Arctic air pollution: Origins and impacts, *Science*, *315*(5818), 1537-1540.

Lerner, B. M., P. C. Murphy, and E. J. Williams (2009), Field measurements of small marine craft gaseous emission factors during NEAQS 2004 and TexAQS 2006, *Environmental Science and Technology*, *43*(21), 8213-8219.

Li, S. M., and L. A. Barrie (1993), Biogenic sulfur aerosol in the Arctic troposphere. 1. Contributions to total sulfate, *Journal of Geophysical Research - Atmospheres*, *98*(D11), 20613-20622.

Liggio, J., S. M. Li, and R. McLaren (2005), Heterogeneous reactions of glyoxal on particulate matter: Identification of acetals and sulfate esters, *Environmental Science and Technology*, *39*(6), 1532-1541.

Lim, Y. B., and P. J. Ziemann (2005), Products and mechanism of secondary organic aerosol formation from reactions of n-alkanes with OH radicals in the presence of NOx, *Environmental Science and Technology*, *39*(23), 9229-9236.

Lim, Y. B., and P. J. Ziemann (2009), Chemistry of secondary organic aerosol formation from oh radical-initiated reactions of linear, branched, and cyclic alkanes in the presence of NOx, *Aerosol Science and Technology*, *43*(6), 604-619.

Maria, S. F., L. M. Russell, B. J. Turpin, and R. J. Porcja (2002), FTIR measurements of functional groups and organic mass in aerosol samples over the Caribbean, *Atmospheric Environment*, *36*(33), 5185-5196.

Maria, S. F., L. M. Russell, M. K. Gilles, and S. C. B. Myneni (2004), Organic aerosol growth mechanisms and their climate-forcing implications, *Science*, *306*(5703), 1921-1924.

Maria, S. F., L. M. Russell, B. J. Turpin, R. J. Porcja, T. L. Campos, R. J. Weber, and B. J. Huebert (2003), Source signatures of carbon monoxide and organic functional groups

in Asian Pacific Regional Aerosol Characterization Experiment (ACE-Asia) submicron aerosol types, *Journal of Geophysical Research - Atmospheres*, *108*(D23).

Masclet, P., V. Hoyau, J. L. Jaffrezo, and H. Cachier (2000), Polycyclic aromatic hydrocarbon deposition on the ice sheet of Greenland. Part I: Superficial snow, *Atmospheric Environment*, *34*(19), 3195-3207.

Matthew, B. M., A. M. Middlebrook, and T. B. Onasch (2008), Collection efficiencies in an Aerodyne Aerosol Mass Spectrometer as a function of particle phase for laboratory generated aerosols, *Aerosol Science and Technology*, *42*(11), 884-898.

Mira-Salama, D., C. Gruning, N. R. Jensen, P. Cavalli, J. P. Putaud, B. R. Larsen, F. Raes, and H. Coe (2008), Source attribution of urban smog episodes caused by coal combustion, *Atmospheric Research*, *88*(3-4), 294-304.

Mitchell, M. (1956), Visual range in the polar regions with particular reference to the Alaskan Arctic, *Atmospheric Terrestrial Physics* (Special Suppl.), 195-211.

Ottar, B., J. M. Pacyna, and T. C. Berg (1986), Aircraft measurements of air-pollution in the Norwegian Arctic, *Atmospheric Environment*, *20*(1), 87-100.

Paatero, P. (1997), Least squares formulation of robust non-negative factor analysis, *Chemometrics and Intelligent Laboratory Systems*, *37*(1), 23-35.

Paatero, P., and U. Tapper (1994), Positive matrix factorization- a nonnegative factor model with optimal utilization of error-estimates of data values, *Environmetrics*, *5*(2), 111-126.

Pekney, N. J., C. I. Davidson, L. M. Zhou, and P. K. Hopke (2006), Application of PSCF and CPF to PMF-modeled sources of PM2.5 in Pittsburgh, *Aerosol Science and Technology*, *40*(10), 952-961.

Perri, M. J., Y. B. Lim, S. P. Seitzinger, and B. J. Turpin (2010), Organosulfates from glycolaldehyde in aqueous aerosols and clouds: Laboratory studies, *Atmospheric Environment*, *44*(21-22), 2658-2664.

Polissar, A. V., P. K. Hopke, and P. Paatero (1998), Atmospheric aerosol over Alaska - 2. Elemental composition and sources, *Journal of Geophysical Research - Atmospheres*, *103*(D15), 19045-19057.

Polissar, A. V., P. K. Hopke, and J. M. Harris (2001), Source regions for atmospheric aerosol measured at Barrow, Alaska, *Environmental Science and Technology*, *35*(21), 4214-4226.

Putaud, J. P., R. Van Dingenen, M. Mangoni, A. Virkkula, F. Raes, H. Maring, J. M. Prospero, E. Swietlicki, O. H. Berg, R. Hillamo and T. Makela (2000), Chemical mass closure and assessment of the origin of the submicron aerosol in the marine boundary

layer and the free troposphere at Tenerife during ACE-2, *Tellus Series B-Chemical and Physical Meteorology*, *52*(2), 141-168.

Quinn, P. K., T. S. Bates, K. Schulz, and G. E. Shaw (2009), Decadal trends in aerosol chemical composition at Barrow, Alaska: 1976-2008, *Atmospheric Chemistry and Physics*, *9*(22), 8883-8888.

Quinn, P. K., D. J. Coffman, V. N. Kapustin, T. S. Bates, and D. S. Covert (1998), Aerosol optical properties in the marine boundary layer during the First Aerosol Characterization Experiment (ACE 1) and the underlying chemical and physical aerosol properties, *Journal of Geophysical Research - Atmospheres*, *103*(D13), 16547-16563.

Quinn, P. K., T. L. Miller, T. S. Bates, J. A. Ogren, E. Andrews, and G. E. Shaw (2002), A 3-year record of simultaneously measured aerosol chemical and optical properties at Barrow, Alaska, *Journal of Geophysical Research - Atmospheres*, *107*(D11).

Quinn, P. K., G. E. Shaw, E. Andrews, E. G. Dutton, T. Ruoho-Airola, and S. L. Gong (2007), Arctic haze: current trends and knowledge gaps, *Tellus Series B-Chemical and Physical Meteorology*, *59*(1), 99-114.

Quinn, P. K., T. S. Bates, T. L. Miller, D. J. Coffman, J. E. Johnson, J. M. Harris, J. A. Ogren, G. Forbes, T. L. Anderson, D. S. Covert and M. J. Rood (2000), Surface submicron aerosol chemical composition: What fraction is not sulfate?, *Journal of Geophysical Research - Atmospheres*, *105*(D5), 6785-6805.

Quinn, P. K., T. S. Bates, D. Coffman, T. B. Onasch, D. Worsnop, T. Baynard, J. A. de Gouw, P. D. Goldan, W. C. Kuster, E. Williams, J. M. Roberts, B. Lerner, A. Stohl, A. Pettersson and E. R. Lovejoy (2006), Impacts of sources and aging on submicrometer aerosol properties in the marine boundary layer across the Gulf of Maine, *Journal of Geophysical Research - Atmospheres*, 1-20.

Qureshi, S., V. A. Dutkiewicz, A. R. Khan, K. Swami, K. X. Yang, L. Husain, J. J. Schwab, and K. L. Demerjian (2006), Elemental composition of PM2.5 aerosols in Queens, New York: Solubility and temporal trends, *Atmospheric Environment*, *40*, S238-S251.

Rahn, K. A. (1981), The Mn-V ratio as a tracer of large-scale sources of pollution aerosol for the Arctic, *Atmospheric Environment*, *15*(8), 1457-1464.

Rahn, K. A., and R. J. McCaffrey (1979), Compositional differences between Arctic aerosol and snow, *Nature*, *280*(5722), 479-480.

Rahn, K. A., and R. J. McCaffrey (1980), On the origin and transport of the winter Arctic aerosol, *Annals of the New York Academy of Science*, *388*, 486-503.

Rahn, K. A., R. D. Borys, and G. E. Shaw (1977), Asian source of Arctic haze bands, *Nature*, *268*(5622), 713-715.

Rahn, K. A., D. H. Lowenthal, and J. M. Harris (1989), Long-range transport of pollution aerosol from Asia and the Arctic to Okushiri Island, Japan, *Atmospheric Environment*, *23*(11), 2597-2607.

Ross, A. B., J. M. Jones, S. Chaiklangmuang, M. Pourkashanian, A. Williams, K. Kubica, J. T. Andersson, M. Kerst, P. Danihelka, and K. D. Bartle (2002), Measurement and prediction of the emission of pollutants from the combustion of coal and biomass in a fixed bed furnace, *Fuel*, *81*(5), 571-582.

Russell, L. M., R. Bahadur, and P. J. Ziemann (2011), Identifying organic aerosol sources by comparing functional groups composition in chamber studies and atmospheric particles, *Proceedings of the National Academy of the Sciences of the United States of America*, *108*(9), 3516-3521, doi:10.1073/pnas.1006461108.

Russell, L. M., L. N. Hawkins, A. A. Frossard, P. K. Quinn, and T. S. Bates (2010), Carbohydrate-like composition of submicron atmospheric particles and their production from ocean bubble bursting, *Proceedings of the National Academy of Sciences of the United States of America*, *107*(15), 6652-6657.

Russell, L. M., S. Takahama, S. Liu, L. N. Hawkins, D. S. Covert, P. K. Quinn, and T. S. Bates (2009a), Oxygenated fraction and mass of organic aerosol from direct emission and atmospheric processing measured on the R/V Ronald Brown during TEXAQS/GoMACCS 2006, *Journal of Geophysical Research - Atmospheres*, *114*.

Russell, L. M., R. Bahadur, L. N. Hawkins, J. Allan, D. Baumgardner, P. K. Quinn, and T. S. Bates (2009b), Organic aerosol characterization by complementary measurements of chemical bonds and molecular fragments, *Atmospheric Environment*, *43*(38), 6100-6105.

Sharma, M., and S. Maloo (2005), Assessment of ambient air PM10 and PM2.5 and characterization of PM10 in the city of Kanpur, India, *Atmospheric Environment*, *39*(33), 6015-6026.

Shaw, G. E. (1982), Evidence for a central Eurasian source area of Arctic haze in Alaska, *Nature*, *299*(5886), 815-818.

Shaw, P. M., L. M. Russell, A. Jefferson, and P. K. Quinn (2010), Arctic organic aerosol measurements show particles from mixed combustion in spring haze and from frost flowers in winter, *Geophysical Research Letters*, *37*.

Stohl, A. (2006), Characteristics of atmospheric transport into the Arctic troposphere, *Journal of Geophysical Research - Atmospheres*, *111*(D11).

Surratt, J. D., M. Lewandowski, J. H. Offenberg, M. Jaoui, T. E. Kleindienst, E. O. Edney, and J. H. Seinfeld (2007a), Effect of acidity on secondary organic aerosol formation from isoprene, *Environmental Science and Technology*, *41*(15), 5363-5369.

Surratt, J. D., A. W. H. Chan, N. C. Eddingsaas, M. N. Chan, C. L. Loza, A. J. Kwan, S. P. Hersey, R. C. Flagan, P. O. Wennberg, and J. H. Seinfeld (2010), Reactive intermediates revealed in secondary organic aerosol formation from isoprene, *Proceedings of the National Academy of Sciences of the United States of America*, *107*(15), 6640-6645.

Surratt, J. D., J. H. Kroll, T. E. Kleindienst, E. O. Edney, M. Claeys, A. Sorooshian, N. L. Ng, J. H. Offenberg, M. Lewandowski, M. Jaoui, R. C. Flagan and J. H. Seinfeld (2007b), Evidence for organosulfates in secondary organic aerosol, *Environmental Science and Technology*, *41*(2), 517-527.

Surratt, J. D., Y. Gomez-Gonzalez, A. W. H. Chan, R. Vermeylen, M. Shahgholi, T. E. Kleindienst, E. O. Edney, J. H. Offenberg, M. Lewandowski, M. Jaoui, W. Maenhaut, M. Claeys, R. C. Flagan and J. H. Seinfeld (2008), Organosulfate formation in biogenic secondary organic aerosol, *Journal of Physical Chemistry A*, *112*(36), 8345-8378.

Takegawa, N., T. Miyakawa, K. Kawamura, and Y. Kondo (2007), Contribution of selected dicarboxylic and omega-oxocarboxylic acids in ambient aerosol to the m/z 44 signal of an aerodyne aerosol mass spectrometer, *Aerosol Science and Technology*, *41*, 418-437.

Ulbrich, I. M., M. R. Canagaratna, Q. Zhang, D. R. Worsnop, and J. L. Jimenez (2009), Interpretation of organic components from Positive Matrix Factorization of aerosol mass spectrometric data, *Atmospheric Chemistry and Physics*, *9*(9), 2891-2918.

U.S. Department of Agriculture (2010), Fire and aviation management fiscal year 2009 accountability report, 54 pp., U.S. Forest Service, Washington, D. C.

Warneke, C., R. Bahreini, J. Brioude, C. A. Brock, J. A. de Gouw, D. W. Fahey, K. D. Froyd, J. S. Holloway, A. Middlebrook, L. Miller, S. Montzka, D. M. Murphy, J. Peischl, T. B. Ryerson, J. P. Schwarz, J. R. Spackman and P. Veres (2009), Biomass burning in Siberia and Kazakhstan as an important source for haze over the Alaskan Arctic in April 2008, *Geophysical Research Letters*, *36*.

Weiler, K., H. Fischer, D. Fritzsche, U. Ruth, F. Wilhelms, and H. Miller (2005), Glaciochemical reconnissance of a new ice core from Severnya Zemlya, Eurasian Arctic, *Journal of Glaciology*, *51*(172), 64-74.

Zhang, Q., D. R. Worsnop, M. R. Canagaratna, and J. L. Jimenez (2005a), Hydrocarbon-like and oxygenated organic aerosols in Pittsburgh: insights into sources and processes of organic aerosols, *Atmospheric Chemistry and Physics*, *5*, 3289-3311.

Zhang, Q., M. R. Alfarra, D. R. Worsnop, J. D. Allan, H. Coe, M. R. Canagaratna, and J. L. Jimenez (2005b), Deconvolution and quantification of hydrocarbon-like and oxygenated organic aerosols based on aerosol mass spectrometry, *Environmental Science and Technology*, *39*(13), 4938-4952.

Chapter 2

Removal of Sea Salt Hydrate Water from Seawater-Derived Samples by Dehydration

Aerosol particles produced from bubble bursting of natural seawater contain both sea salts and organic components. Depending on the temperature, pressure, and speed of drying, the salt components can form hydrates that bind water, slowing evaporation of the water, particularly if large particles or thick layers of salts undergo drying that is non-uniform and incomplete. The water bound in these salt hydrates interferes with measuring organic hydroxyl and amine functional groups by Fourier transform infrared (FTIR) spectroscopy because it absorbs at the same infrared wavelengths. Here, a method for separating the hydrate water in sea salt hydrates using freezing and then heating in warm, dry air (70°C) is evaluated and compared to other methods, including spectral

subtraction. Laboratory-generated sea salt analogs show an efficient removal of 89% of the hydrate water absorption peak height by 24 h of heating at atmospheric pressure. The heating method was also applied to bubbled submicron (Sea Sweep), generated bulk (Bubbler), and atomized seawater samples, with efficient removal of 5, 22, and 39 μg of hydrate water from samples of initial masses of 11, 30, 58 μg, respectively. The strong spectral similarity between the difference of the initial and dehydrated spectra and the laboratory generated sea salt hydrate spectrum provided verification of the removal of hydrate water. In contrast, samples of submicron atmospheric particles from marine air masses did not have detectable signatures of sea salt hydrate absorbance, likely because their smaller particles and lower filter loadings provided higher surface area to volume ratios and allowed faster and more complete drying.

2.1 Introduction

Seawater and freshly-emitted sea spray particles are 97% water, by mass, but they also contain trace amounts of important organic components. A macroscopic sample of seawater dried to 0% RH can leave up to 15% of the mass of dry sea salt as bound water molecules in hydrates [*Lewis and Schwartz*, 2004], depending on the morphology of the salt mixture and the method of drying. The rationale for this study was to develop a method for characterizing the organic components of particles produced by seawater bubble bursting (and by other sources such as dust that retain substantial amounts of water bound as hydrates). FTIR spectroscopy has been shown effective for measuring the organic components of salt and dust-containing refractory particles, but the presence of hydrate water interferes with the measurement of organic hydroxyl groups.

Evaporated seawater can include halite (NaCl), kieserite ($MgSO_4 \bullet 1H_2O$), carnallite ($KMgCl_3 \bullet 6H_2O$), anhydrite ($CaSO_4$), and bischofite ($MgCl_2 \bullet 6H_2O$) [*Harvie et al.*, 1980]. The most abundant salt formed from standard seawater evaporation is NaCl (~90%) followed by $MgCl_2$ and $MgSO_4$ (~3-4% each) and $KMgCl_3$ and $CaSO_4$ (~2% each) [*Harvie et al.*, 1980]. Previous studies have shown absorbance in the infrared (IR) region of hydrate bound and liquid water in salt water mixtures using Fourier transform infrared (FTIR) spectroscopy at differing RH values [*Cziczo et al.*, 1997; *Hoffman et al.*, 2004; *Weis and Ewing*, 1999; *Zhao et al.*, 2006]. *Cziczo and Abbatt* [2000] observed that a low flow, directly into the sample chamber, of $MgCl_2$ aerosol (lognormal distribution with a mean radius of 0.18 μm and a standard deviation of 1.8 μm) at 1% RH had distinct

IR spectral absorbance signatures of $MgCl_2$ hydrates, including sharp peaks at about 3390 and 3210 cm^{-1} and a double peak at about 1650 and 1630 cm^{-1}. The low RH spectra did not change with increases or decreases in temperature, indicating that $MgCl_2$ hydrates have similar absorption spectra or only hexahydrate was formed [*Cziczo and Abbatt*, 2000]. The aerosol passed through a diffusion drier (with a residence time of 2 min to obtain 1% RH) that likely did not allow sufficient time to reach a stable equilibrium if the hydrate water was prevented from diffusing out.

FTIR spectroscopy has been used to identify the composition of ambient submicron marine particles collected and dried in thin layers on Teflon filters [*Hawkins et al.*, 2010; *Russell*, 2003; *Russell et al.*, 2011; *Russell et al.*, 2010]. This technique has not been used previously to quantify the organic composition of samples of artificially-generated submicron and supermicron sea spray particles formed from model ocean systems that may be deposited in thicker layers on filters. Because the evaporation of hydrate water at 0% RH can be slowed if diffusion is limited, these larger, thicker samples retain substantially higher quantities of hydrate water as they dry, which are more difficult to remove and may be part of salt hydrates that have formed into gels [*Chan et al.*, 2000]. Multiple techniques for extracting hydrate water from seawater derived sea salt hydrates, while retaining the organic components, have been proposed including: (i) freezing which causes the hydrate water to break apart from the salt hydrate to form solid water [*Wang et al.*, 2009]; (ii) heating which causes the hydrate water to evaporate directly [*Ni et al.*, 2011] but may alter the chemical composition of reactive or volatile organic components; (iii) vacuum drying after freezing which reduces the pressure then allows the frozen water to sublime without directly heating the sample

[*Popp et al.*, 1996]; and (iv) desiccating which pushes the equilibrium of the hydrate water and RH of the air towards water evaporation [*Weis and Ewing*, 1996].

Here we evaluate several approaches for removing hydrate water from seawater-derived samples while retaining intact the organic components for chemical characterization. The amount of hydrate water removed by each technique was measured for four types of seawater derived samples: standards of seawater components, generated submicron marine aerosol, generated bulk marine aerosol, and atomized seawater. IR spectroscopy was used here to assess the extent to which hydrate water mass was removed by each process. Spectral subtraction was also investigated to determine if it is a sufficient technique to isolate the hydrate water absorbance from the organic absorbance.

2.2 Methods

2.2.1 Particle Generation and Collection

The five types of seawater-related samples studied here are: standards of seawater components, generated submicron marine aerosol, generated bulk marine aerosol, atomized seawater, and ambient marine aerosol particles (Table 2.1). For all of the following sampling conditions, particles were collected by drawing air through 37 mm Teflon filters. Samples collected in the field were frozen and transported to San Diego for analysis. Prior to analysis, each sample was equilibrated in a temperature (20°C) and humidity controlled (< 55%) cleanroom for 24 hours. The FTIR spectrum of each sample was collected by transmission through the 1 cm diameter portion of the filter that was exposed during sampling, before and after collection of particles, using a Tensor 27 spectrometer with DTGS detector (Bruker Optics Inc., Billerica, MA; OPUS software).

Table 2.1: Conditions for particle generation and collection.

Name (Number of Samples)	Aerosol Source	Particle Size	Drying During Collection	Mass (μg m^{-3})			OC/ Na
				OM*	Hydrate Water*	Na	
Sea Sweep (6)	**Generated**	**Submicron**	**RH controlled**	**3.50**	**2.44**	**4.59**	**0.37**
				5.00	2.20	NA	NA
				4.62	3.10	5.74	0.42
				3.96	2.87	4.07	0.42
				2.16	1.53	2.33	0.39
				2.50	2.31	5.29	0.29
				2.74	2.62	5.49	0.26
Bubbler (12)	**Generated**	**Sub- and supermicron**	**None**	**16.6**	**47.7**	**53.2**	**0.15**
				14.0	11.3	30.8	0.24
				10.3	24.3	37.9	0.16
				9.8	26.7	NA	NA
				16.6	40.5	24.5	0.30
				13.0	33.9	NA	NA
				13.9	23.8	28.6	0.26
				10.4	16.3	NA	NA
				25.4	164.0	NA	NA
				36.4	173.2	170.7	0.07
				17.9	31.1	NA	NA
				16.0	16.7	NA	NA
				15.5	10.4	26.6	0.34
Atomized Seawater (6)	**Generated**	**Sub- and supermicron**	**Inline drier**	**487.5**	**995.9**	**NA**	**NA**
				285.2	952.0	NA	NA
				362.9	1231.8	NA	NA
				535.4	766.7	NA	NA
				494.6	970.3	NA	NA
				847.7	1388.8	NA	NA
				399.1	665.6	NA	NA
Ambient (6)	**Ambient**	**Submicron**	**RH controlled**	**1.15**	**NA**	**0.07**	**8.35**
				2.87	NA	0.05	30.9
				0.75	NA	0.03	9.9
				1.45	NA	0.04	20.0
				0.78	NA	0.12	3.6
				0.73	NA	0.16	1.9
				0.31	NA	0.04	3.3

*OM and hydrate water were determined using the dehydration procedures presented.

Quantification procedures are described in Section 2.4.1. After initial analysis, the filters were returned to the freezer before further dehydration. After all dehydration steps were completed, X-ray Fluorescence (XRF; Chester LabNet, Tigard, OR) was used to quantify the masses of elements Na, Mg, S, Cl, K, Ca, V, Fe, Br, and Sr [*Maria et al.*, 2003]. Ambient submicron particles were also collected on additional filters using two-stage multi-jet cascade impactors [*Berner et al.*, 1979] and analyzed with ion chromatography (IC) to quantify inorganic ions, including Na and Cl [*Bates et al.*, 2012; *Quinn et al.*, 1998].

2.2.1.1 Laboratory Generated Reference Standards of Seawater Components

Filter samples of seawater components were prepared by collecting atomized aqueous solutions of sea salt (Sigma Aldrich, S9883; 55% Cl, 31% Na, 8% SO_4^{2-}, 4% Mg, 1% K, 1% Ca, <1% other), $MgCl_2$ hexahydrate (Macron Chemicals, 5958), NaCl (EMD Chemicals, SX0425), and glucose (Sigma Aldrich, G5250). Mixtures of standards of glucose and sea salt, glucose and $MgCl_2$, and glucose and NaCl were created by first depositing glucose on the filters, scanning using FTIR spectroscopy, and then depositing the salt over the glucose (discussion in Section 2.4.2). Standards of sea salt were used to calculate the absorptivity of sea salt hydrate water (as described in Section 2.4.5).

2.2.1.2 Sea Sweep Sea Spray Particles (Submicron)

The Sea Sweep consisted of stainless steel frits attached to a small raft that was deployed alongside of the R/V *Atlantis* [*Bates et al.*, 2012]. Zero air was bubbled through the surface seawater, and the generated aerosol was separated by a cyclone so that submicron particles could be collected on filters. After the initial FTIR scan, the filters

were stored frozen for 8.3 months and re-analyzed before heating to 30, 40, 50, and 70°C for 20 min and re-analyzing after each 20 min heating period. The filters were frozen for an additional 5.4 months and then placed in a desiccator containing silica gel for 4.0 days, rescanned, and returned to the desiccator box for 7.0 more days. After scanning, the filters were placed in a dehydrator (Nesco/American Harvest FD-80) at 70°C in the cleanroom and re-scanned after 1.8 and 14.9 total days.

2.2.1.3 Bubbler Sea Spray Particles (Submicron and Supermicron)

The Bubbler consisted of a large glass cylinder filled with seawater, and bubbles were produced by flowing zero air through two sets of ceramic frits (fine and coarse) or by dropping jets of seawater on to the model seawater surface [*Keene et al.*, 2007]. The continuously regenerated seawater surface contained ambient seawater constantly pumped by the R/V *Atlantis*. The bubbles burst at the seawater surface, which lofted the resulting aerosol into a continuous air stream. Submicron and supermicron particles were collected on filters without drying. After the initial FTIR scan, the filters were stored frozen for 13.8 months and then re-scanned. They were then placed in a desiccator for and re-scanned after 2.0, 6.0, and 13.0 total days. Then, the filters were placed in a dehydrator at 70°C in the cleanroom and re-scanned after 2.7, 6.7, 22.4, and 28.0 total days.

2.2.1.4 Atomized Seawater

Ambient seawater was collected during the CalNex 2010 cruise and frozen. The seawater was thawed and atomized to produce a broad mode of submicron particles, dried by passing through a drier containing drierite (average residence times of 2 to 7 s), and

deposited on Teflon filters. After the initial FTIR scan, the filters were frozen for 15.9 months and then re-scanned. They were then placed in a desiccator for 15 days and rescanned. After, the filters were placed in a dehydrator at 70°C in the cleanroom and re-scanned after 1.8, 5.7, 14.4, 27.4, and 42.7 total days.

2.2.1.5 Submicron Atmospheric Marine Particles

Atmospheric aerosol particles were collected off the coast of California on board the R/V *Atlantis* at 18 m above sea level through a heated mast that controlled the RH of the air masses to 60% during CalNex 2010. Particles were collected on filters for 5 to 10 h durations. Hybrid Single Particle Lagrangian Integrated Trajectory (HYSPLIT) 3-day isentropic backtrajectories (arriving at 500 m) were used to identify air masses of marine origin [*Draxler and Rolph*, 2003].

2.3 Results and Discussion

2.3.1 Reference Standards and Hydrate Spectral Signatures

The initial spectra of the reference standards of dried NaCl particles had negligible IR absorption (Figure 2.1a), as expected [*Pavia et al.*, 2001; *Weis and Ewing*, 1999]. The laboratory generated standards of both sea salt and $MgCl_2$ contained double peaks in the hydroxyl absorption region at 3380 and 3235 cm^{-1} and 3340 and 3235 cm^{-1}, respectively. The sea salt hydrate water double peak signature is sharper and more defined than that of $MgCl_2$ but both contain a local minimum at 3260 cm^{-1} and an additional peak at 1640 cm^{-1} (Figure 2.1a). $MgCl_2$, sea salt, and NaCl are not vibrationally active at 3700-3100 cm^{-1} and 1640 cm^{-1}, but hydrate water is. For

comparison, liquid water absorbs at 3450 and 1650 cm^{-1} [*Cziczo and Abbatt*, 2000; *Weis and Ewing*, 1996], and water vapor absorbs at 4000-3500 and 1800-1350 cm^{-1}. Liquid water and water vapor were ruled out both by the peak positions as well as the analysis at 0% RH in a N_2 purge in the FTIR spectrometer sample chamber. This implies that the absorption for the sea salt and $MgCl_2$ standards is due to bound water in hydrates, which do not form with NaCl.

The spectra of NaCl deposited on glucose showed no discernible change in spectral shape or additional absorption from the original glucose spectra (Figure 2.1a). The standards with sea salt or $MgCl_2$ and glucose showed an increase in absorption from the original glucose sample at 3700-3100 cm^{-1} and 1640 cm^{-1} (Figure 2.1a). The spectra of the glucose and $MgCl_2$ and the glucose and sea salt were very similar to that of pure $MgCl_2$ and pure sea salt, respectively.

Spectra of $MgCl_2$ standards had little remaining IR absorption after 24 h in the dehydrator, and the maximum peak height of the spectra decreased by 89%. After freezing and heating, standards of glucose and sea salt mixtures had resulting spectra similar to the original deposited glucose spectra (cosine similarity of 0.93; defined in Section 2.4.3), with maximum peak heights within 13% of the initial glucose peak heights.

2.3.2 Dehydration of Seawater-Derived Samples

The initial spectra of the generated marine aerosol and atomized seawater samples had absorbance at 3700-3100 cm^{-1} and 1640 cm^{-1}, similar to the bound water in $MgCl_2$ and sea salt hydrates (Figure 2.1b). The different generation methods (Sea Sweep,

Bubbler, and atomized seawater) resulted in differences in the IR spectra, but all of the spectra showed the double peak at 3380 and 3235 cm^{-1} and a minimum at 3260 cm^{-1}.

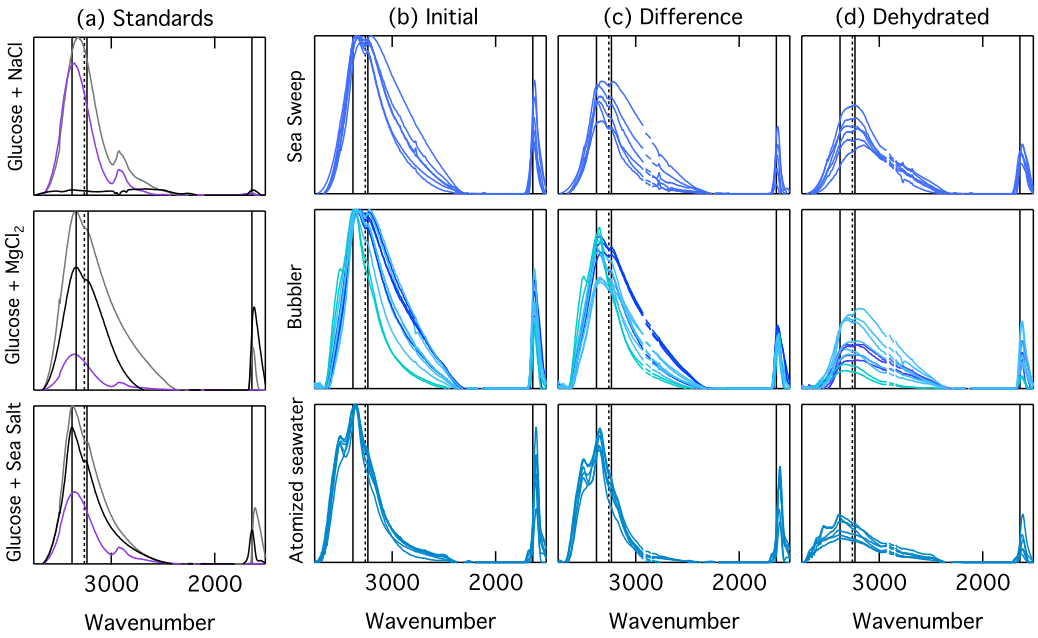

Figure 2.1: FTIR absorption spectra of standards, Sea Sweep, Bubbler, and atomized seawater samples. (a) Spectra of NaCl, $MgCl_2$, and sea salt (black), spectra of the respective salts added to glucose (grey), and the initial spectra of glucose (purple). These spectra were normalized by the maximum absorption of the glucose and salt mixtures. (b) Initial spectra for each sampling condition. (c) Difference spectra of the initial and dehydrated spectra. (d) Final spectra of the mass remaining in the dehydrated samples. The Initial, Difference, and Dehydrated spectra were all normalized by the maximum absorption of the initial spectrum of each sample to show the relative differences in absorption. Gaps in the spectra represent artifacts from the dehydrator at 2917±12 and 2850±6 cm^{-1} (Dehydrator and Difference). Vertical lines indicate sea salt hydrate signature peaks at 3380, 3235, and 1640 cm^{-1} (solid) and a signature local minimum at 3260 cm^{-1} (dashed). In the "Glucose + $MgCl_2$" plot, the vertical lines represent the $MgCl_2$ hydrate signature peaks at 3340, 3235, and 1640 cm^{-1} (solid).

Multiple drying techniques were used to remove the hydrate water from the sea salt hydrates while preserving the organic fraction for samples of the generated marine aerosol, atomized seawater, and reference standards, as summarized in Table 2.2. For the Sea Sweep, Bubbler, and atomized seawater samples, the first method employed for removing hydrate water was freezing, whereby the saturation vapor pressure was lowered

to enhance evaporation rates of remaining hydrate water. Freezing for multiple months removed an average of 1.2, 6.2, and 14.0 μg of hydrate water (26%, 28%, 36%) for the Sea Sweep, Bubbler, and atomized seawater samples, respectively. The difference between the initial spectra and the spectra after freezing were compared to the spectrum of sea salt hydrate using cosine similarities to give 0.92, 0.93, and 0.64, respectively (Table 2.2), showing that in the first two cases the absorbance that was removed was nearly identical to sea salt hydrate. However, the IR spectra after freezing still had sharp peaks at 3380 and 3225 cm^{-1} and 1640 cm^{-1}, similar to the sea salt hydrates, suggesting that some hydrate water remained.

The samples were then heated in a dehydrator at 70°C for varying lengths of time, and 4.7, 21.8, and 38.8 μg of hydrate water mass was removed from the Sea Seep, Bubbler, and atomized seawater samples, respectively, including the mass removed by freezing and desiccating (Table 2.2). The spectra after full dehydration (Figure 2.1d) showed a large reduction in the absorption at 3700-3100 cm^{-1} and 1640 cm^{-1}. The remaining spectra lack the signatures of the sea salt hydrates and are more similar to previous measurements of atmospheric particles from marine regions, identified as carbohydrates, rather than sea salt hydrates [*Russell et al.*, 2010]. The difference of the IR spectra from before and after complete dehydration look very similar to the sea salt hydrate spectrum (Figure 2.1c) for all three types of samples, with average cosine similarities of 0.98, 0.97, and 0.91 (Table 2.2), indicating that the only component removed was hydrate water.

Table 2.2: Hydrate water removed during dehydration and spectral subtraction for the different sampling conditions, and the cosine similarity between spectra removed and the hydrate water spectrum.

Sampling Condition (# of samples)	Step in Drying Procedure (Duration)*	Hydrate Water Removed		Cosine similarity of difference spectra and hydrate water spectra
		(μg)	(% of total)	
	Dehydration			
Sea Sweep (6)	Freezer (8.3 mo)	1.2 ± 0.5	26	0.92
	Heating to 70°C	2.2 ± 1.1	47	0.95
	Freezer (5.4 mo) + Des. (4.0 d)	3.2 ± 1.6	68	0.96
	Desiccator (7.0 d)	3.7 ± 1.1	79	0.97
	Dehydrator (1.8 d)	4.0 ± 1.2	85	0.98
	(+13.0 d)	4.7 ± 1.6	100	0.98
Bubbler (12)	Freezer (13.8 mo)	6.2 ± 5.7	28	0.93
	Desiccator (2.0 d)	9.0 ± 8.7	41	0.90
	(+4.0 d)	9.8 ± 10.7	45	0.94
	(+7.0 d)	8.1 ± 7.4	37	0.78
	Dehydrator (2.7 d)	15.3 ± 17.4	70	0.96
	(+4.0 d)	19.6 ± 18.6	90	0.97
	(+15.7 d)	20.9 ± 18.7	96	0.97
	(+5.7 d)	21.8 ± 19.0	100	0.97
Atomized seawater (6)	Freezer (15.9 mo)	14.0 ± 16.2	36	0.64
	Desiccator (15.0 d)	12.5 ± 19.1	32	0.62
	Dehydrator (1.8 d)	17.0 ± 21.5	44	0.61
	(+3.9 d)	35.2 ± 22.1	91	0.91
	(+8.8 d)	31.3 ± 17.9	81	0.90
	(+12.9 d)	36.9 ± 22.3	95	0.92
	(+15.3 d)	38.8 ± 23.8	100	0.91
	Spectral Subtraction			
Sea Sweep (6)	1	6.2 ± 1.7	NA	NA
	2a	4.7 ± 1.7	NA	NA
	2b	3.8 ± 1.3	NA	NA
	2c	6.8 ± 3.4	NA	NA
Bubbler (12)	1	18.3 ± 11.5	NA	NA
	2a	12.3 ± 8.7	NA	NA
	2b	10.0 ± 7.0	NA	NA
	2c	23.4 ± 16.8	NA	NA
Atomized seawater (6)	1	21.7 ± 12.5	NA	NA

*Durations are given in month (mo), day (d), and hour (h) for each drying procedure step. The "+" indicates that the duration listed is the incremental rather than cumulative amount of time for that step. Hydrate water is the total removed after each step in the drying procedure, including the mass removed in the previous drying procedure steps.

Since the Sea Sweep, Bubbler, and atomized seawater samples had different masses of sea salt and hence hydrate water, the drying process was carried out in a series of steps of different duration to identify the minimum time needed to remove the hydrate water (as listed in Table 2.2). For the Sea Sweep, the largest average removal of hydrate water (1.2 μg; 26%) was during the initial storage time in the freezer. The largest average removal of hydrate water from the Bubbler samples was 7.2 μg (in addition to the previous mass removed) after the first 2.7 days of drying in the dehydrator. The largest average removal of hydrate water from the atomized seawater samples was 18.2 μg, which occurred during the second drying step in the dehydrator of 3.9 days (5.7 days total). While dehydrating with mild heating is required to expedite removal of the hydrate water, substantial water was also removed during frozen storage (Figure 2.2). For Sea Sweep samples, an average of 85% of the hydrate water had been removed after 1.8 days in the dehydrator. The Bubbler and atomized seawater samples, which had more deposited mass, required additional time in the dehydrator to fully remove the hydrate water (Table 2.2).

In the end, 14.9, 28.0, and 42.7 days in the dehydrator were required to fully dehydrate the Sea Sweep, Bubbler, and atomized seawater samples, respectively. Multiple factors may have influenced the difference in the dehydration time required for the different sampling techniques: (i) Because the Sea Sweep particles were dried to 60% RH and the atomized seawater particles were passed through a drier before sampling, some of the liquid water was removed from these samples before the particles dried and the sea salt crystallized. This reduced the liquid water available to bind as hydrate water, compared to that of the Bubbler particles that were not dried prior to collection. Also,

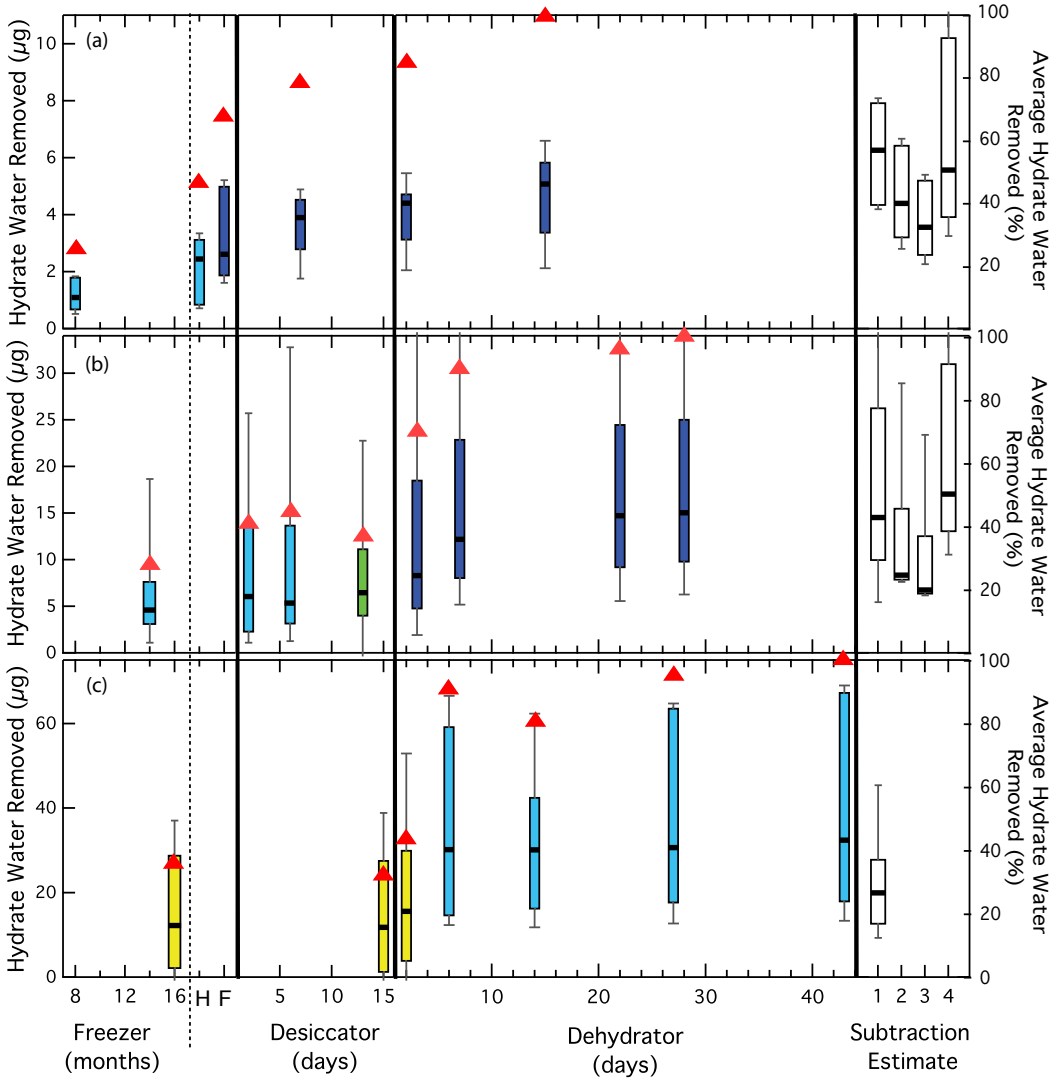

Figure 2.2: Total hydrate water mass (left axis) removed from the initial samples after each drying step and subtraction estimates for the (a) 6 Sea Sweep samples, (b) 12 Bubbler samples, and (c) 6 atomized seawater samples. The black lines are the median values of all of the samples, and the boxes represent the 25 to 75th percentiles with whiskers to the 10 and 90th percentiles, showing the differences among the individual samples of each type. Boxes are colored by the cosine similarity of the sea salt hydrate spectra with the difference of the spectra at each step from the initial spectra (yellow: 0.60-0.69; green: 0.70-0.79; light blue: 0.90-0.95; dark blue: 0.96-0.99). The red triangles represent the average percent hydrate water mass removed during each process (right axis). In the Freezer section, "H" is the first heating step for the Sea Sweep (to 30, 40, 50, and 70°C for 20 minutes each), and "F" is the second freezing step (5.4 months) and includes desiccating (4.0 days). The bars and points are plotted at the total number of days spent for each type of drying procedure with times in the freezer, desiccator, and dehydrator shown separately.

Woods et al. [2010] found that aerosol particles with mixtures of NaCl and $MgSO_4$ formed a NaCl core upon drying, with uneven $MgSO_4$ coatings. This allows the available chloride to be used in the NaCl crystallization and reduces the Cl available to bond with magnesium to form $MgCl_2$ and bind water as hydrates. (ii) The Bubbler particles dried on the filters rather than in the aerosol phase, which could potentially trap pockets of hydrate water or induce a different drying pattern in which NaCl does not first form as a core, leaving more chloride available for $MgCl_2$ formation. (iii) *Keene et al*. [2007] showed that the ratio of organic carbon to sodium in bulk generated marine aerosol particles is lower than in submicron generated marine particles. With a higher percentage of sea salt, there should be a larger fraction of sea salt hydrates in the Bubbler (bulk) than the Sea Sweep (submicron) marine aerosol. (iv) On average, the Sea Sweep samples contained less initial average absorption area at 3700-3100 cm^{-1} (5.6) due to less deposited mass on the filters than the Bubbler (19.2) and atomized seawater (37.9) samples. With more mass deposited on the filters, more water could be bound as hydrates or trapped in pockets. All of these factors contributed to a lower amount of hydrate water in the initial Sea Sweep spectra and reduced the necessary time for dehydration, compared to the Bubbler and atomized seawater samples.

In addition to the absorption at 3380, 3235, and 1640 cm^{-1}, some of the initial spectra of the Bubbler and atomized seawater samples have absorbance at 3500 cm^{-1} (Figure 2.1b). This peak was observed in samples with high deposited mass (initial 3700-3200 cm^{-1} absorption peak area > 19), which could indicate that liquid water was trapped in pockets or between layers of aerosol mass. Of the Bubbler samples, only one of the two jet configuration samples, which had the highest peak areas, had the additional

spectral peak. *Cziczo and Abbatt* [2000] observed an absorption peak at 3450 cm^{-1} for generated aerosol, which was attributed to OH stretch of liquid water. They also suggest that liquid water may be trapped within the aerosol particles and not yet formed as hydrate [*Cziczo and Abbatt*, 2000]. *Weis and Ewing* [1999] observed a liquid water absorption band at 3400 cm^{-1} for porous NaCl particles. This was compared to liquid water absorbed on to the faces of single NaCl crystals, which was found to absorb around 3525 cm^{-1} at RH < 40% and 30°C [*Foster and Ewing*, 1999]. The final dehydrated spectra lack the third peak absorbance at 3500 cm^{-1} (Figure 2.1d) showing that the trapped, liquid water was removed.

Spectra from all of the sampling conditions show little change between the post-freezer spectra and the post-desiccator spectra, and there is little hydrate water mass removed by the dessicator (Figure 2.2). This suggests that desiccation alone is not sufficient for removing hydrate water. The samples were kept in a desiccator between the steps of the drying procedure to prevent water from condensing on the samples.

Freeze-drying was tested as another dehydration technique, but it did not dehydrate the standards. To test this, the sea salt hydrate standards were frozen and then placed under vacuum. The initial freezing procedure step removed some hydrate water mass, as discussed earlier, but the spectra of the standards after being under vacuum for both 22 hours and 5 days showed little decrease in absorbance from the initial scan. The spectra also still displayed the signatures of bound water in sea salt hydrates, so the vacuum technique was not used to dehydrate the Sea Sweep, Bubbler, or atomized seawater samples.

2.3.3 Hydrate Water Removal using Spectral Subtraction

In some circumstances, it may not be possible to physically dehydrate samples – either because they are no longer available or because the water needs to be preserved. For this reason, four different methods were used to estimate the mass of hydrate water in a seawater-derived sample by subtracting hydrate water-related absorption from the measured spectrum. Each method uses a different approach to approximate the amount of hydrate water and the scaling for the spectrum to subtract.

In the first method, the measured sea salt hydrate spectrum was scaled to the maximum absorbance possible without exceeding the measured spectrum; the resulting scaled hydrate spectrum was subtracted from each of the initial sample spectra, as given by Equation 2.1:

$$S_{dehy1} = S_0 - \left(S_{SS} \times \min\left(\frac{S_0}{S_{SS}}[x1, x2] > 0 \right) \right) \qquad (2.1)$$

where S_{dehy1} is the final spectra with hydrate water removed, S_0 is the initial spectrum, S_{ss} is the sea salt hydrate spectrum, and $x1$ and $x2$ are the wavenumber bounds of the region of interest (described in Section 2.4.4). This method was applied to the Sea Sweep, Bubbler, and atomized seawater samples, and the resulting dehydrated spectra are shown in Figure 2.3b. The scaling of the sea salt spectrum was used to calculate the hydrate water mass removed (Section 2.4.6). With this method, an average of 6.2, 18.3, and 21.7 μg of hydrate water were removed for the Sea Sweep, Bubbler, and atomized seawater samples, respectively (Table 2.2). Equation 2.1 gives an upper bound of the hydrate water in the sample by assuming that all of the absorption at 3700-3100 cm^{-1} that fits the hydrate water spectral shape could be due to hydrate water. Because primary marine

aerosol particles have been found to contain significant fractions of hydroxyl functional groups [*Russell et al.*, 2010], this assumption provides an upper bound on, and likely an overestimate of, the hydrate water mass.

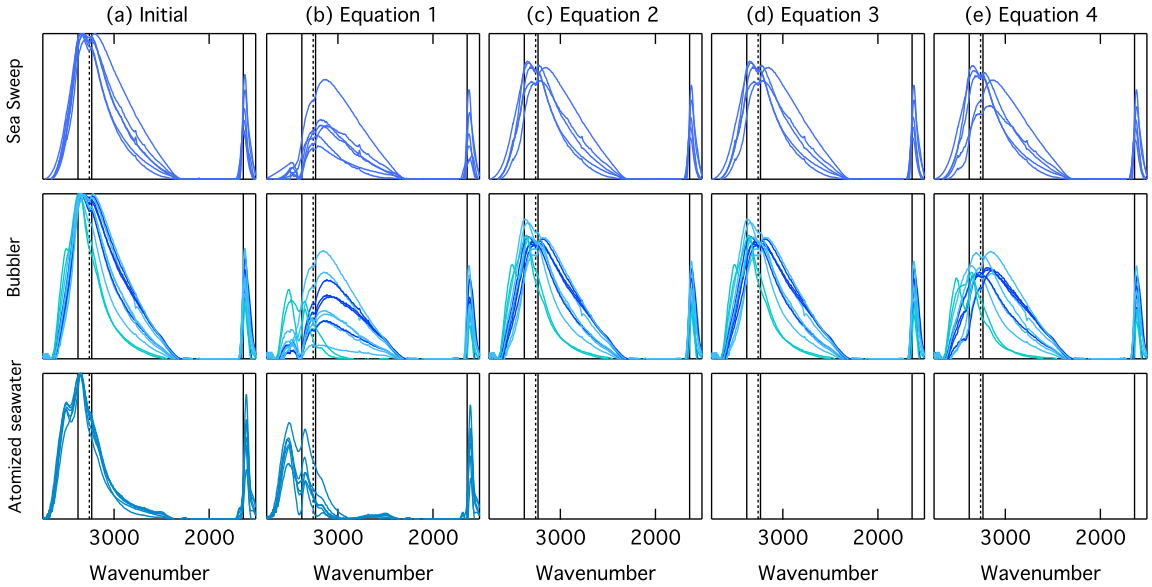

Figure 2.3: FTIR absorption spectra of Sea Sweep, Bubbler, and atomized seawater samples. (a) Initial spectra for each sampling condition repeated from Figure 2.1. Resulting spectra from (b) Equation 2.1, (c) Equation 2.2, (d) Equation 2.3, and (e) Equation 2.4 dehydration subtraction techniques. The spectra were all normalized by the maximum absorption of the initial spectrum of each sample to show the relative differences in absorption. Vertical lines indicate sea salt hydrate signature peaks at 3380, 3235, and 1640 cm^{-1} (solid) and a signature local minimum at 3260 cm^{-1} (dashed).

The spectra resulting from Equation 2.1 compare well in peak height and shape with the dehydrated spectra from freezing and heating for the Sea Sweep and frit configuration Bubbler samples (Figure 2.3; Figure 2.1d), although there is less remaining absorbance area, as is consistent with Equation 2.1 as an upper bound. The spectra resulting from Equation 2.1 for the atomized seawater and jet configuration Bubbler samples do not compare as well with the spectra from the dehydration because the peak at 3500 cm^{-1} was removed by dehydration but not by Equation 2.1. This spectral

subtraction does not remove the peak at 3500 cm^{-1} because that peak is associated with trapped liquid water rather than hydrate water.

The second type of estimate used Equations 2.2, 2.3, and 2.4 to calculate the dehydrated spectra for each sample by subtracting a scaled sea salt hydrate spectrum based on the XRF or IC-measured elemental masses. In Equation 2.2, the measured mass of Na (M_{Na}, μg) for each sample was used to calculate the dehydrated spectra:

$$S_{dehy2} = S_0 - \left(S_{SS} \times \frac{rM_{Na}F_{hw}Abs}{F_{Na}m_wP_{SS}} \right) \quad (2.2)$$

where r is the ratio of μmol OH per μmol of water (2 OH per H_2O), F_{hw} is the observed mass fraction of hydrate water in dried sea water (0.15) [*Lewis and Schwartz*, 2004], *Abs* is the sea salt hydrate absorptivity (Section 2.4.5), F_{Na} is the mass fraction of Na in sea salt (0.31), m_w is the molecular weight of water (18 μg μmol^{-1}), and P_{SS} is the total peak area of the standard sea salt hydrate spectra. In Equation 2.3, the ratio of Mg to Na (r_{Na}, 0.088) in seawater and M_{Na} were used to calculate the dehydrated spectra for each sample:

$$S_{dehy3} = S_0 - \left(S_{SS} \times \frac{rM_{Na}r_{Na}Abs}{r_{Mg}m_{Mg}P_{SS}} \right) \quad (2.3)$$

where r_{Mg} is the molar ratio of Mg to hydrate water in sea salt hydrates (1:6) and m_{Mg} is the molecular weight of Mg (24.3 μg μmol^{-1}). In Equation 2.4 the mass of Mg (M_{Mg}, μg) for each sample was used to calculate the dehydrated spectra:

$$S_{dehy4} = S_0 - \left(S_{SS} \times \frac{rM_{Mg}Abs}{r_{Mg}m_{Mg}P_{SS}} \right) \quad (2.4)$$

The resulting averages for the hydrate water removed with Equations 2.2, 2.3, and 2.4 are 5.7, 3.8, and 6.8 μg from the Sea Sweep samples and 12.3, 10.0, and 23.4 μg of hydrate water from the Bubbler samples (Table 2.2 and Figure 2.2). The dehydrated spectra from the different spectral subtraction equations compare well to each other in shape and magnitude (Figure 2.3). The atomized seawater samples were not analyzed by XRF or IC, so hydrate water was not calculated with Equations 2.2, 2.3, or 2.4. The quantification of the organic components remaining is discussed in Section 2.4.1.

2.3.4 Comparison to Atmospheric Particles from Seawater-Derived Spray

The submicron atmospheric aerosol particles collected during the CalNex cruise, in airmasses of marine origin, had FTIR spectra that lacked the signatures of sea salt hydrate absorption (Figure 2.4), even without the dehydration procedures described here. The characteristic double peak at 3380 and 3235 and the local minimum at 3260 cm^{-1} are absent. Using Equation 2.2 to calculate an upper bound on the amount of hydrate water present, hydrate water could contribute at most less than 5% of the organic mass.

There are two likely explanations for the absence of hydrate water in the submicron atmospheric aerosol particles collected. First, they were sampled through an RH-controlled (heated) inlet that dried particles to approximately 60% RH before collection on the filter, which is in contrast to the reference, bubbler, and atomized seawater samples that were not heated. This meant that there was less liquid water present when the salts dried. Second, the lower atmospheric concentrations of salt particles relative to the generated samples meant the mass of salt collected on filters was

lower (ambient Na: 0.07 μg m^{-3}; Sea Sweep Na: 4.59 μg m^{-3}), even though sampling times were longer. Hence the collected samples were thinner and collected more slowly, providing for uniform and complete drying of the sample. For the Sea Sweep, Bubbler, atomized seawater, and reference samples, rapid collection of a larger mass of salt may have inhibited drying by crystallization of salt layers on top of layers of undried water pockets [*Cziczo and Abbatt*, 2000]. A third possibility, if the particles were more aged, is that as ambient marine aerosol ages and reacts with sulfuric and nitric acids in the atmosphere, it becomes depleted in chlorine and enriched in sulfur [*McInnes et al.*, 1994]. The average ratio of Na to Cl in the CalNex ambient marine samples is 2.01, which is greater than the ratio in seawater (0.56) showing Cl depletion. Since Cl is needed to form $MgCl_2$ and $KMgCl_3$, less water is bound in Cl-containing hydrates.

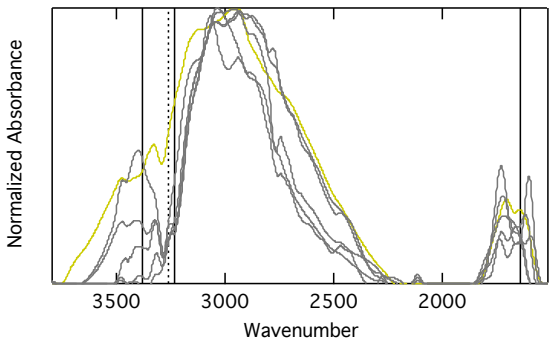

Figure 2.4: Normalized, FTIR spectra from atmospheric particles collected during CalNex in clean marine air masses (grey) and marine derived particle spectra from Scripps Pier 2008 (gold). Vertical lines indicate hydrate signatures that are present in spectra in Figure 2.1a but absent here: peaks (solid) and local minimum (dashed). Spectral noise for these spectra was smoothed using Savitzky-Golay with 31 points and second order.

In summary, low heating at atmospheric pressure enabled dehydration of metastable hydrate water from sea salts. Initial FTIR spectra of Sea Sweep, Bubbler, and atomized seawater samples showed absorbance signatures characteristic of sea salt

hydrates, which were removed by dehydration that included freezing and heating the samples. The dehydrated spectra resemble atmospheric particles from clean marine regions and have spectral shapes consistent with previously identified marine organic components. High cosine similarity values between the difference of the spectra before and after dehydration with the spectra of sea salt hydrates confirmed that the mass removed during dehydration was hydrate water and not volatile organic species. While not recommended for quantifying hydrate water or for recovering the non-water organic hydroxyl spectrum, spectral subtraction of scaled reference spectra of sea salt hydrate provides a useful indicator of the presence and potential contribution of hydrate water. Since minor artifacts from contamination were caused by the dehydrator, we recommend that future seawater derived aerosol sampling include drying particles by heating and dessication before collection on filters to reduce the need for dehydration after sampling. Another prudent sampling technique is limiting the mass of salt-containing particles that are deposited on the filters so that the thickness of the salt layer does not slow mass transfer by trapping bound water in hydrate pockets.

2.4 Appendix

2.4.1 Quantification of Organic Functional Groups

The spectra from each scan were analyzed using an automated algorithm that includes baselining, peak-fitting, and integrating at specific peak locations to identify the organic functional group mass associated with the major carbon bond types, based on the method outlined by *Maria et al.* [2002] and revised by *Russell et al.* [2009]. Concentrations were calculated by dividing the mass of each functional group measured

for each filter by the total volume of air sampled through the corresponding filters. Functional groups that were quantified in these samples include: hydroxyl (including alcohol, C-OH), alkane (C-CH), amine ($C\text{-}NH_2$), and carboxylic acid (COOH). Total organic mass (OM) was calculated by adding the functional group concentrations. Aromatic, alkene (C=CH), carbonyl (C=O), organosulfate ($COSO_3$), and organonitrate functional groups were below the detection limit for all filter samples discussed here. Dehydrated spectra calculated from Equations 2.1-2.4 were analyzed with the same procedure to determine the resulting functional group composition and OM.

2.4.2 Marine Organic Components

Past studies have shown that the organic fraction of ambient primary marine particles is carbohydrate-like [*Russell et al.*, 2010]. The carbohydrate glucose was chosen to represent the organic component of marine aerosol in the standards. The melting point of glucose is greater than 140°C, so it will not volatilize at 70°C. Past studies have also shown that ambient marine organic aerosol may contain volatile organic compounds (VOCs) due to particle formation from secondary reactions forming secondary organic aerosol (SOA) [*O'Dowd et al.*, 2004]. The focus of this paper is on generated, fresh, primary marine particles. These generated marine particles are produced directly from the seawater and are not formed as SOA. Since they do not contain VOCs, they are not volatile at 70°C. Using the measurements of particles from the Sea Sweep, *Bates et al.* [2012] found that the fresh, primary particles were not volatile even at temperatures as high as 230°C. *Modini et al.* [2010] found that generated marine aerosol had a minor organic component that evaporated over the temperature range of 170-200°C.

2.4.3 Cosine Similarity of FTIR Spectra

Cosine similarity is used to determine the similarity between two spectra, and it is defined as the cosine of the angle between two vectors [*Stein and Scott*, 1994]. The values range from 0 to 1, and values closer to 1 indicate higher cosine similarity. For the cosine similarity calculations, wavenumbers from 3800 to 1500 cm^{-1} were used with the following exclusions: (i) 2927 – 2908 cm^{-1}, (ii) 2856 – 2844 cm^{-1}, (iii) 2785 – 2766 cm^{-1}, and (iv) 2692 – 2673 cm^{-1}. The listed wavenumbers were excluded because there was evidence of artifacts in those regions of the sample spectra.

2.4.4 Bounds for Spectral Subtraction

The specific bounds used in the spectral subtraction for hydrate separation were 3616 to 2464 cm^{-1} for the Sea Sweep spectra, 3574 to 2848 cm^{-1} for the Bubbler spectra, and 3424 to 2848 cm^{-1} for the atomized seawater spectra, in order to scale the sea salt hydrate spectrum in the appropriate region.

2.4.5 Hydrate Absorptivity

Five filter sample standards of sea salt with varying deposited masses were used to determine the absorptivity of bound water in sea salt hydrates. Filters were weighed and scanned prior to depositing sea salt. The combined mass of the sea salt and bound hydrates (M_S; μg) was found by subtracting the original weight from the final weight of the filters. For Technique 1, this weight was used to calculate the μmol of OH (N_{OH1}) using:

$$N_{OH1} = \frac{M_S \times F_{Mg+hyd} \times r}{m_{Mg+hyd} \times r_{Mg}} \qquad (2.5)$$

where F_{Mg+hyd} is the fraction of Mg and hydrate mass in sea salt with hydrate water (0.17 μg Mg hydrate per μg sea salt and bound hydrates), r_{Mg} is the molar ratio of Mg to hydrates in sea salt (1 μmol Mg per 6 μmol hydrate), m_{Mg+hyd} is the molecular weight of Mg hydrate (132 μg μmol^{-1}), and r is the ratio of μmol OH per μmol of hydrate (2). For Technique 2, the μmol of OH (N_{OH2}) was calculated using:

$$N_{OH2} = \frac{M_S \times F_{hw} \times r}{m_w} \qquad (2.6)$$

where F_{hw} is the mass fraction of hydrate water in sea salt (0.15 μg bound water per μg sea salt) and m_w is the molecular weight of water (18 μg μmol^{-1}). The peak area due to OH bonds from hydrate water was found using the integral of the absorption in the 3200-3700 cm^{-1} region using FTIR spectroscopy of the filters. All of the area was attributed to hydrates because no other components in the sea salt standards absorb in this region. The sea salt hydrate absorptivity was calculated as the slope of the best fit line between the OH peak area and μmol of OH bond (Figure 2.5). Using Technique 1, the absorptivity was found to be 7.39 peak area per μmol bond, and using the Technique 2, it was found to be 7.00 peak area per μmol bond. Both techniques gave a strong correlation (r = 0.99) between OH peak area and μmol OH bond. Because the difference between the two absorptivity calculations is ~5%, the absorptivity from the first technique was used. The ratio of hydrate peak area in the hydroxyl region to hydrate peak area in the amine region remained constant for all of the sea salt standards. Hydrate peak area at 1640 cm^{-1} is 5% of the peak area at 3200-3700 cm^{-1}.

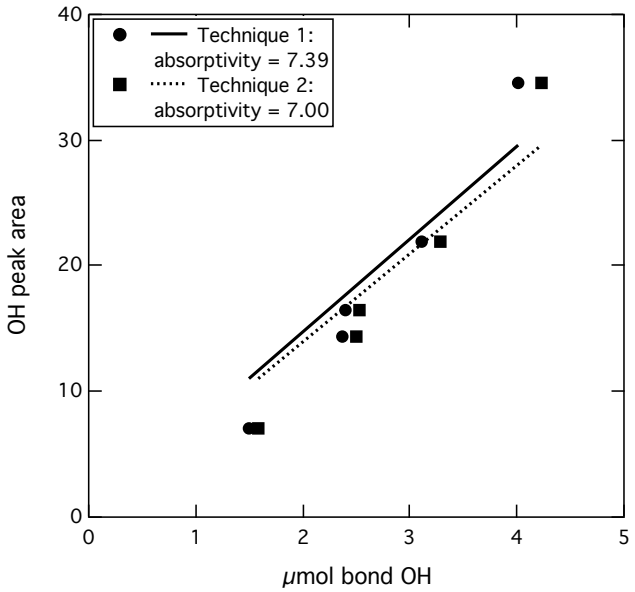

Figure 2.5: Calculation of sea salt absorptivity using Technique 1 and 2 to determine μmol of OH bonds.

2.4.6 Hydrate Water Mass Calculation

The hydrate water mass removed during dehydration was calculated for each sample using the difference between the final peak areas at each step and the initial peak areas. Because hydrate absorbs at 3200-3600 cm^{-1} and at 1640 cm^{-1}, the total equivalent hydrate peak area was calculated as the sum of the peak areas in those two regions. The mass of hydrate removed (M_{hw}; μg) was calculated using the following equation:

$$M_{hw} = \frac{P_{hw} \times m_w}{r \times Abs} \qquad (2.7)$$

where P_{hw} is the total difference hydrate peak area from the initial and final scans and *Abs* is the sea salt hydrate absorptivity.

2.5 Acknowledgements

This work was funded by NSF grants ATM-0744636, OCE-0948252, and OCE-1129580. The authors gratefully acknowledge Timothy Bates and Patricia Quinn for organizing the CalNex 2010 cruise and for the creation and deployment of the Sea Sweep and William Keene and John Maben for the design and deployment of the Bubbler. The authors acknowledge Shang Liu, Anita Johnson, and Robin Modini for assisting in the preparation of laboratory standards. The authors thank Derek Coffman and Drew Hamilton for their assistance in sample collection and the scientists, captain, and crew of the R/V *Atlantis* for their support in the field.

Chapter 2, in full, is a reprint of the material as it appears in *Environmental Science and Technology* 2012 with slight modifications. Frossard, A.A. and L.M. Russell (2012), "Removal of Sea Salt Hydrate Water from Seawater-Derived Samples by Dehydration." *Environmental Science and Technology*. 46, 13326-13333, doi: 10.1021/es3032083. The dissertation author was the primary investigator and author of this paper.

References

Bates, T. S., P.K. Quinn, A.A. Frossard, L.M. Russell, J. Hakala, T. Petäjä, M. Kulmala, D.S. Covert, C.D. Cappa, S.-M. Li, K.L. Hayden, I. Nuaaman, R. McLaren, P. Massoli, M.R. Canagaratna, T.B. Onasch, D. Sueper, D.R. Worsnop, and W.C. Keene (2012), Measurements of ocean derived aerosol off the coast of California, *Journal of Geophysical Research - Atmospheres*, *117*(D00V15), doi:10.1029/2012JD017588.

Berner, A., C. Lurzer, F. Pohl, O. Preining, and P. Wagner (1979), Size distribution of the urban aerosol in Vienna, *Science of the Total Environment*, *13*(3), 245-261, doi:10.1016/0048-9697(79)90105-0.

Chan, C. K., Z. Y. Ha, and M. Y. Choi (2000), Study of water activities of aerosols of mixtures of sodium and magnesium salts, *Atmospheric Environment*, *34*(28), 4795-4803, doi:10.1016/s1352-2310(00)00252-1.

Cziczo, D. J., and J. P. D. Abbatt (2000), Infrared observations of the response of NaCl, MgCl2, NH4HSO4, and NH4NO3 aerosols to changes in relative humidity from 298 to 238 K, *Journal of Physical Chemistry A*, *104*(10), 2038-2047, doi:10.1021/jp9931408.

Cziczo, D. J., J. B. Nowak, J. H. Hu, and J. P. D. Abbatt (1997), Infrared spectroscopy of model tropospheric aerosols as a function of relative humidity: Observation of deliquescence and crystallization, *Journal of Geophysical Research - Atmospheres*, *102*(D15), 18843-18850, doi:10.1029/97jd01361.

Draxler, R. R., and G. D. Rolph (2003), HYSPLIT (HYbrid Single-Particle Lagrangian Integrated Trajectory), Air Resources Laboratory, NOAA, Silver Spring, MD, (Model access via NOAA ARL READY Website http://www.arl.noaa.gov/readyhysplit4.html).

Foster, M., and G. E. Ewing (1999), An infrared spectroscopic study of water thin films on NaCl (100), *Surface Science*, *427-28*, doi:10.1016/s0039-6028(99)00242-3.

Harvie, C. E., J. H. Weare, L. A. Hardie, and H. P. Eugster (1980), Evaporation of seawater - Calculated mineral sequences, *Science*, *208*(4443), 498-500.

Hawkins, L. N., L. M. Russell, D. S. Covert, P. K. Quinn, and T. S. Bates (2010), Carboxylic acids, sulfates, and organosulfates in processed continental organic aerosol over the southeast Pacific Ocean during VOCALS-REx 2008, *Journal of Geophysical Research - Atmospheres*, *115*, doi:10.1029/2009jd013276.

Hoffman, R. C., A. Laskin, and B. J. Finlayson-Pitts (2004), Sodium nitrate particles: physical and chemical properties during hydration and dehydration, and implications for aged sea salt aerosols, *Journal of Aerosol Science*, *35*(7), 869-887, doi:10.1016/j.jaerosci.2004.02.003.

Keene, W. C., H. Maring, J. R. Maben, D. J. Kieber, A. A. P. Pszenny, E. E. Dahl, M. A. Izaguirre, A. J. Davis, M. S. Long, X. L. Zhou, L. Smoydzin, R. Sander (2007), Chemical and physical characteristics of nascent aerosols produced by bursting bubbles at a model air-sea interface, *Journal of Geophysical Research - Atmospheres*, *112*(D21), doi:10.1029/2007jd008464.

Lewis, E. R., and S. E. Schwartz (2004), *Sea salt aerosol production: mechanisms, methods, measurements, and models - a critical review*, American Geophysical Union, Washington.

Maria, S. F., L. M. Russell, B. J. Turpin, R. J. Porcja, T. L. Campos, R. J. Weber, and B. J. Huebert (2003), Source signatures of carbon monoxide and organic functional groups in Asian Pacific Regional Aerosol Characterization Experiment (ACE-Asia) submicron aerosol types, *Journal of Geophysical Research - Atmospheres*, *108*(D23), doi:10.1029/2003jd003703.

Maria, S. F., L. M. Russell, B. J. Turpin, and R. J. Porcja (2002), FTIR measurements of functional groups and organic mass in aerosol samples over the Caribbean, *Atmospheric Environment*, *36*(33), 5185-5196.

McInnes, L. M., D. S. Covert, P. K. Quinn, and M. S. Germani (1994), Measurements of chloride depletion and sulfur enrichment in individual sea-salt particles collected from the remote marine boundary-layer, *Journal of Geophysical Research - Atmospheres*, *99*(D4), 8257-8268, doi:10.1029/93jd03453.

Modini, R. L., B. Harris, and Z. D. Ristovski (2010), The organic fraction of bubble-generated, accumulation mode Sea Spray Aerosol (SSA), *Atmospheric Chemistry and Physics*, *10*(6), 2867-2877.

Ni, Q.-y., Y.-l. Wu, M.-d. Yang, H.-s. Hu, Y.-f. He, L.-j. Zhang, and J. Dang (2011), TG-FTIR analysis of thermal degradation of bischofite's crystals with aniline hydrochloride, *Spectroscopy and Spectral Analysis*, *31*(7), 1747-1751, doi:10.3964/j.issn.1000-0593(2011)07-1747-05.

O'Dowd, C. D., M. C. Facchini, F. Cavalli, D. Ceburnis, M. Mircea, S. Decesari, S. Fuzzi, Y. J. Yoon, and J. P. Putaud (2004), Biogenically driven organic contribution to marine aerosol, *Nature*, *431*(7009), 676-680, doi:10.1038/nature02959.

Pavia, D. L., G. M. Lapman, and G. S. Kriz (2001), *Introduction to spectroscopy*, Third ed., Brooks/Cole.

Popp, M., W. Lied, A. J. Meyer, A. Richter, P. Schiller, and H. Schwitte (1996), Sample preservation for determination of organic compounds: Microwave versus freeze-drying, *Journal of Experimental Botany*, *47*(303), 1469-1473, doi:10.1093/jxb/47.10.1469.

Quinn, P. K., D. J. Coffman, V. N. Kapustin, T. S. Bates, and D. S. Covert (1998), Aerosol optical properties in the marine boundary layer during the First Aerosol Characterization Experiment (ACE 1) and the underlying chemical and physical aerosol properties, *Journal of Geophysical Research - Atmospheres*, *103*(D13), 16547-16563.

Russell, L. M. (2003), Aerosol organic-mass-to-organic-carbon ratio measurements, *Environmental Science and Technology*, *37*(13), 2982-2987, doi:10.1021/es026123w.

Russell, L. M., R. Bahadur, and P. J. Ziemann (2011), Identifying organic aerosol sources by comparing functional group composition in chamber and atmospheric particles, *Proceedings of the National Academy of Sciences of the United States of America*, *108*(9), 3516-3521, doi:10.1073/pnas.1006461108.

Russell, L. M., L. N. Hawkins, A. A. Frossard, P. K. Quinn, and T. S. Bates (2010), Carbohydrate-like composition of submicron atmospheric particles and their production from ocean bubble bursting, *Proceedings of the National Academy of Sciences of the United States of America*, *107*(15), 6652-6657, doi:10.1073/pnas.0908905107.

Russell, L. M., S. Takahama, S. Liu, L. N. Hawkins, D. S. Covert, P. K. Quinn, and T. S. Bates (2009), Oxygenated fraction and mass of organic aerosol from direct emission and atmospheric processing measured on the R/V Ronald Brown during TEXAQS/GoMACCS 2006, *Journal of Geophysical Research - Atmospheres*, *114*, doi:10.1029/2008jd011275.

Stein, S. E., and D. R. Scott (1994), Optimization and testing of mass spectral library search algorithms for compound identification, *Journal of the American Society for Mass Spectrometry*, *5*(9), 859-866.

Wang, A., J. J. Freeman, and B. L. Jolliff (2009), Phase transition pathways of the hydrates of magnesium sulfate in the temperature range 50 degrees C to 5 degrees C: Implication for sulfates on Mars, *Journal of Geophysical Research - Planets*, *114*, doi: 10.1029/2008je003266.

Weis, D. D., and G. E. Ewing (1996), Infrared spectroscopic signatures of (NH4)(2)SO4 aerosols, *Journal of Geophysical Research - Atmospheres*, *101*(D13), 18709-18720, doi:10.1029/96jd01543.

Weis, D. D., and G. E. Ewing (1999), Water content and morphology of sodium chloride aerosol particles, *Journal of Geophysical Research - Atmospheres*, *104*(D17), doi:10.1029/1999jd900286.

Woods, E., D. Chung, H. M. Lanney, and B. A. Ashwell (2010), Surface morphology and phase transitions in mixed nacl/MgSO(4) aerosol particles, *Journal of Physical Chemistry A*, *114*(8), 2837-2844, doi:10.1021/jp911133j.

Zhao, L. J., Y. H. Zhang, Z. F. Wei, H. Cheng, and X. H. Li (2006), Magnesium sulfate aerosols studied by FTIR spectroscopy: Hygroscopic properties, supersaturated structures, and implications for seawater aerosols, *Journal of Physical Chemistry A*, *110*(3), doi:10.1021/jp055291i.

Chapter 3

Side-by-Side Comparison of Four Techniques Explains the Apparent Differences in the Organic Composition of Generated and Ambient Marine Aerosol Particles

3.1 Introduction

Characterizing the organic composition of marine aerosol particles is important for understanding the sources of marine aerosol and their impact on cloud microphysical properties [*de Leeuw et al.*, 2011]. A variety of measurement techniques have been used to measure the organic composition of both ambient atmospheric and freshly emitted sea spray aerosol (Table 3.2, Appendix). Using Fourier transform infrared (FTIR) spectroscopy, atmospheric aerosol particles collected in marine regions on multiple shipboard campaigns were shown to be saccharide-like based on their functional group composition, with a high ratio of oxygen to carbon (O/C) [*Russell et al.*, 2010]. Similarly, using scanning transmission X-ray microscopy with near-edge X-ray absorption fine structure (STXM-NEXAFS), *Russell et al.* [2010] and *Hawkins and Russell* [2010] found chemically distinct ambient marine particle types including saccharide-like components on sea salt particles and protein particles. Model ocean systems have been used to generate nascent sea spray aerosol (SSA) from seawater [*Bates et al.*, 2012; *Keene et al.*, 2007], to determine the organic composition of particles directly emitted from wave breaking and bubble bursting at the sea surface (Table 3.2). FTIR spectroscopy showed the organic composition of these generated nascent SSA, hereafter referred to as generated marine particles, also to be highly oxidized [*Bates et al.*, 2012]. In contrast, using high resolution time of flight aerosol mass spectrometry (HR-ToF-AMS) in the same study, *Bates et al.* [2012] found that generated marine aerosol particles were highly unsaturated and minimally oxidized (low O/C).

In this study, we resolve this apparent discrepancy by comparing the measured organic composition of ambient and generated marine aerosol particles using these three techniques as well as a light scattering module of the HR-ToF-AMS (LS-ToF-AMS). Each of these methods is used to calculate the level of oxidation of the organic mass (OM) and assess the differences in the composition of ambient and generated marine particles. Additionally, we consider the extent to which each method provides additional insight into the particle composition.

3.2 Measurements of the Organic Composition of Ambient and Generated Marine Particles

Ambient atmospheric, which frequently included non-marine particles from the U.S east coast and shipping sources, and generated marine aerosol particles were sampled aboard the research vessel *Ronald H. Brown* during the Western Atlantic Climate Study (WACS) August 19-28, 2012. Ambient particles were sampled through two side-by-side humidity and temperature controlled masts ~18 m above sea level [*Bates et al.*, 2002]. The Sea Sweep model ocean system [*Bates et al.*, 2012] was used to generate marine aerosol particles. Particles were characterized using four complementary techniques (Table 3.1): (i) FTIR spectroscopy [*Russell et al.*, 2010]; (ii) HR-ToF-AMS [*DeCarlo et al.*, 2006]; (iii) LS-ToF-AMS [*Liu et al.*, 2013]; and (iv) STXM-NEXAFS [*Hawkins and Russell*, 2010]. The Appendix (Section 3.5) has details for particle collection and OM analysis, as well as organic carbon (OC) measurements by evolved gas analysis (EGA) of quartz filters. The range of particle aerodynamic diameters (d_a) measured by each method is shown in Table 3.1 and Figure 3.3.

Table 3.1: Descriptions of the four techniques used to measure marine organic composition and the separation of the low and high O/C OM.

Technique, Resolution (Samples)	**Particle Size Range**[a]			**Low O/C**[b]	**High O/C**[b]
	d_a	**d_p** ρ = 1.1 g cm^{-3}	**d_p** ρ = 2.05 g cm^{-3}		
FTIR Spectroscopy, Bulk filter samples; 1-8 hours (5 ambient, 16 Sea Sweep)	< 750 nm (< 1 μm)[c]	< 682 nm (< 909 nm)[c]	< 366 nm (< 488 nm)[c]	Alkane and amine functional groups	Hydroxyl and carboxylic acid functional groups
HR-ToF-AMS, 2 minutes (Continuous)	90-700 nm (< 1 μm)[d]	82-636 nm (< 909 nm)[d]	44-341 nm (< 488 nm)[d]	Mass fragment group C_XH_Y	Mass fragment groups C_XH_YO and $C_XH_YO_{>1}$
LS-ToF-AMS, Single particles (384 ambient, 7319 generated)	180-700 nm (430 nm - 1 μm)[e]	164-636 nm (391-909 nm)[e]	88-341 nm (210-488 nm)[e]	Particles with CH mass fragment signature, m/z 41, 43, 55, 57	Particles with high m/z 44 mass fragments
STXM-NEXAFS, Single particles (18 ambient, 26 generated)	0.39-3.1 μm[f]	0.39-3.1 μm[f]		Particles spectra with alkyl and aromatic functional groups	Particle spectra with carboxylic carbonyl and alcohol functional groups

[a]Aerodynamic diameter (d_a) and physical diameter (d_p) particles sizes that have 100% transmission efficiency to the detector (HR-ToF-AMS and LS-ToF-AMS) and filters, with 50% transmission efficiency in parentheses. Physical diameters for FTIR, HR-ToF-AMS, and LS-ToF-AMS were calculated using densities of 1.1 and 2.05 g cm^{-3} to represent purely organic particles and particles with 11% organics and 89% sea salt, respectively.

[b]Low O/C OM also contains functional groups and fragment groups with calculated O/C values of 0. High O/C OM contains any oxidized OM.

[c](Gussman et al. 2002); particles less than 100 nm are not collected as efficiently.

[d](DeCarlo et al. 2006; Jayne et al. 2000; Williams et al. 2013); 30% transmission efficiency at 1 μm.

[e](Liu et al. 2013; Williams et al. 2013); 180 nm are the smallest particles that produce significant optical signals. 30% transmission efficiency at 1 μm.

[f]Diameter range of measured particles (physical). Aerodynamic diameters were calculated from physical diameters for individual particles.

Based on FTIR spectroscopy, the OM in generated marine particles contained on average 46% hydroxyl, 41% alkane, and 13% amine functional groups (Figure 3.1a). The average composition of the ambient OM was 18% hydroxyl, 45% alkane, 2% amine, and 35% carboxylic acid functional groups (Figure 3.1e). This corresponds to average O/C values of 0.55±0.17 and 0.51±0.22 for ambient and generated marine particles, respectively (Table 3.4). Carboxylic acid and hydroxyl functional groups have high O/C ratios, while alkane and amine functional groups contain no oxygen (O/C=0) and are grouped here as low O/C (Table 3.1; Figure 3.1i and 3.1m). Using this distinction, the generated OM was 46% high O/C and 54% low O/C organic components (±12%), while the ambient OM was 53% and 47% ±10%, respectively (Figure 3.2). This composition is similar to previous FTIR spectroscopy measurements of generated marine OM with 53% high O/C and 47% low O/C [*Bates et al.*, 2012] and ambient marine OM with 55% high O/C and 45% low O/C (including 4% organosulfate functional groups) [*Hawkins et al.*, 2010].

The organic composition measured by the HR-ToF-AMS was split into ion families based on high resolution data analysis (Section 3.5.2.2). The first group is C_XH_Y, which has the characteristic ion pattern from the alkane series $C_xH_{2y-1}^+$ and $C_xH_{2y+1}^+$, with $C_3H_5^+$ (m/z=41), $C_3H_7^+$ (m/z=43), $C_4H_7^+$ (m/z=55) and $C_4H_9^+$ (m/z=57) among the main peaks. The second group is represented by $C_xH_yO_1^+$, which is slightly oxidized and typically contains $C_2H_3O^+$ (m/z=43) and CHO^+ (m/z=29). The third group is $C_xH_yO_{>1}^+$, which contains the most oxidized ions and has the highest content of CO_2^+ (m/z=44).

The generated and ambient marine OM compositions were 22% $C_XH_YO_{>1}$, 13% $C_XH_YO_1$, and 65% C_XH_Y and 32% $C_XH_YO_{>1}$, 18% $C_XH_YO_1$, and 50% C_XH_Y, respectively

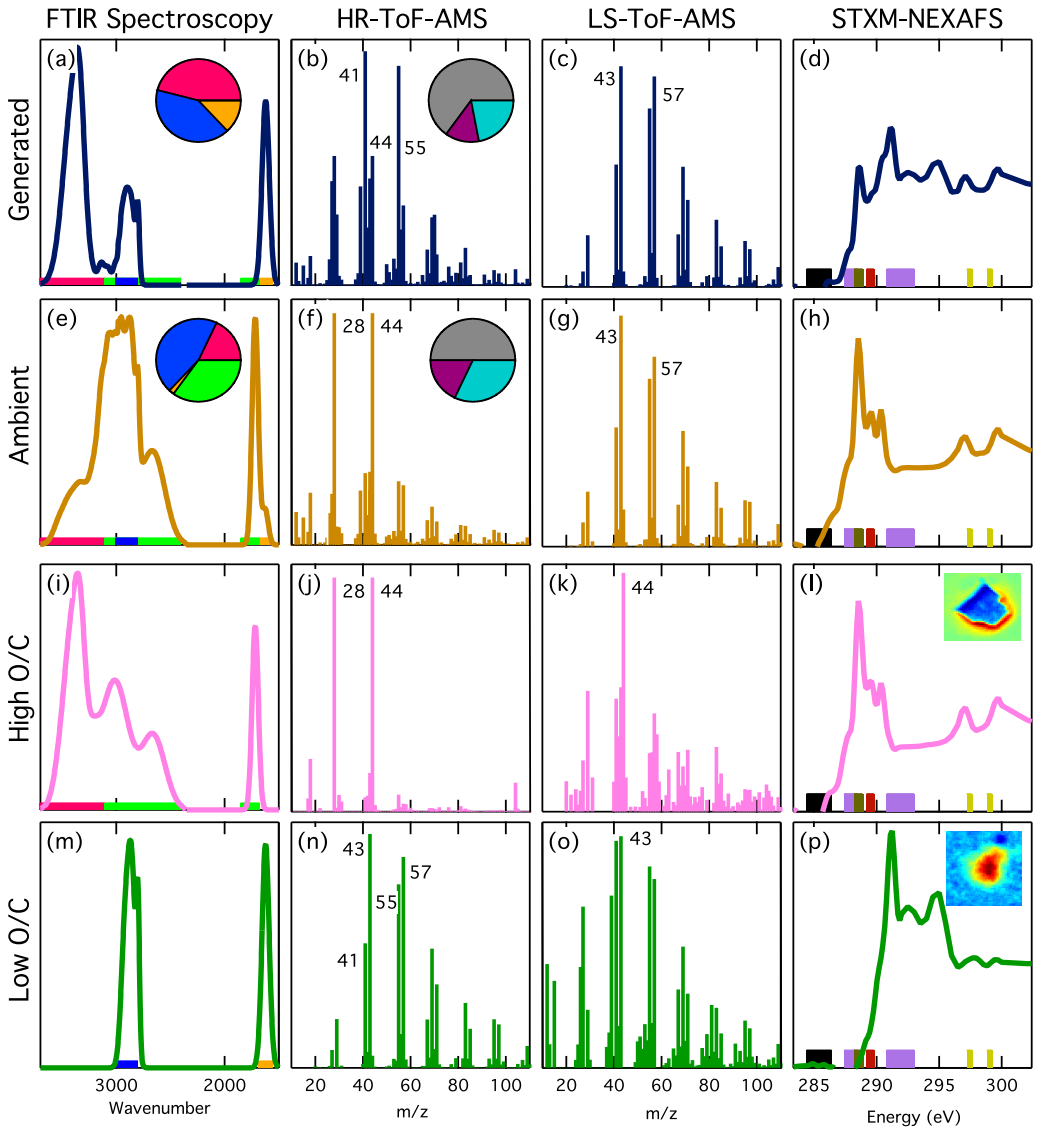

Figure 3.1: Normalized spectra of (a-d) generated and (e-h) ambient marine OM and (i-l) high O/C and (m-p) low O/C particle OM types, colored across the rows as dark blue, bronze, light pink, and dark green, respectively. Columns represent the four measurement techniques. FTIR spectroscopy pies show the average functional group composition including: carboxylic acid (lime green), hydroxyl (bright pink), amine (orange), and alkane (blue). The color bars show the functional group absorption regions, using the same colors. HR-ToF-AMS pies show the average OM mass fragment group composition with $C_XH_YO_{>1}$ (grey), $C_XH_YO_1$ (dark purple), and C_XH_Y (teal). Specific m/z values are labeled in the HR-ToF-AMS and LS-ToF-AMS panels. In the STXM-NEXAFS panel, density maps (inset in l and p) illustrate the typical particle morphology and are colored as low (blue) to high (red) probability of carbon. Color bars (left to right) represent aromatic (black), alkyl (purple), carboxylic carbonyl (brown), and alcohol (red) functional group and potassium (yellow) absorption regions for the STXM-NEXAFS spectra.

(Figure 3.1b and 3.1f). This composition is consistent with previous HR-ToF-AMS results from similar measurements [*Bates et al.*, 2012]. Other organic fragment groups, including $C_XH_YO_{>1}N$, $C_XH_YO_1N$, and C_XH_YN, contribute less than 2% to the total OM and are excluded from this analysis. When grouping $C_XH_YO_1$ and $C_XH_YO_{>1}$ as high O/C and C_XH_Y as low O/C (Figure 3.1j and 3.1n), the composition of the generated OM is 35% high O/C and 65% low O/C, while the ambient OM is 50% high O/C and 50% low O/C (Figure 3.2). This corresponds to average O/C values of 0.63±0.11 for ambient aerosol particles and 0.20±0.08 for generated marine particles, respectively (Table 3.4).

The HR-ToF-AMS collection efficiency (which includes lens transmission efficiency, detector efficiency, and losses due to particle bounce) was calculated by comparing HR-ToF-AMS sulfate to IC sulfate (CE_{IC}, see Section 3.5.6). The ambient CE_{IC} is 0.35, and the generated CE_{IC} is 0.17 (lighter shading in Figure 3.2). After the CE_{IC} was applied to the HR-ToF-AMS measurements, the FTIR OM and HR-ToF-AMS OM agreed within the instrument uncertainties with an overall average percent difference of 12%. Correlations are shown in Figure 3.4. Because the CE_{IC} may be size dependent, the composition of the unmeasured OM may not be the same as the measured OM. Comparisons of the FTIR and HR-ToF-AMS OM with EGA OC are shown in Section 3.5.3. The HR-ToF-AMS measurements were also used to calculate the mass of sea salt and the CE_{total}, which includes sea salt (CE_{SS}), described in Section 3.5.4.

The LS-ToF-AMS optically detected 7,300 generated and 360 ambient single particles, and their average spectra are shown in Figure 3.1c and 3.1g, respectively. Of the ambient single particles that were optically detected, 47% of the particles had corresponding mass spectra that had total signal to noise (S/N) exceeding 3 (LS+MS)

(see Section 3.5.2.3). This result is consistent with previously measured LS+MS fractions of 0.52 [*Liu et al.*, 2013]. This corresponds to a total ambient LS-ToF-AMS CE (CE_{LSA}) of 0.47 (grey area of Figure 3.2b), which is consistent with the HR-ToF-AMS CE_{totalA} of 0.49 (which includes sea salt, see Section 3.5.6). For the generated particle sampling, only 7% of the particles had corresponding mass spectra with total S/N exceeding 3 (LS+MS), which corresponds to a generated marine CE_{LSG} of 0.07 (grey area of Figure 3.2b) and is consistent with CE_{totalG} of 0.07 (see Section 3.5.6).

The LS+MS particle mass spectra were clustered based on their organic signal using the method outlined by *Liu et al.* [2013]. To identify organic types, only signals at selected organic m/z values were used (m/z 20, 22, 24-27, 29, 31, 40-45, 47, 49-59, 61-63, 65-79, 82-90, 92-97, 98-110). Particles with spectra that contained less than 6 organic ions (~50% of the LS+MS particles) were not included in the clustering. The cluster analysis separated the particles with C_XH_Y hydrocarbon-like signatures (low O/C), including m/z 41, 43, 55, 57 (Figure 3.1o), from those with m/z 44 (high O/C, due to the oxidized CO_2^+ fragment) (Figure 3.1k). The organic fraction of ambient particles is 9% high O/C and 91% low O/C, while the generated particles is 8% high O/C and 92% low O/C (Figure 3.2).

The average STXM-NEXAFS spectra of the generated and ambient marine particles are shown in Figure 3.1d and 3.1h, respectively. The particle spectra were grouped using Ward cluster analysis, resulting in two types: high O/C and low O/C organics, based on functional group peaks. The high O/C group (Figure 3.1l) contains particle spectra with high absorbance in the carboxylic carbonyl region (288.2 – 288.9 eV) and varying absorption in the alcohol region (289.5 eV), which are both oxidized and

considered high O/C. The second type of particle spectra, low O/C group (Figure 3.1p), did not contain oxidized functional groups but instead showed absorbance only in the two alkyl regions (287.4 – 288.5 eV for C-H bonds and 290.8 – 293 eV for C-C bonds). One spectrum in this type also had absorbance from 284.4 – 286.4 eV, indicative of aromatic or alkene functional groups. Of the 26 generated particles, 13 had high O/C spectra. For the ambient particles, 17 of 18 particles had high O/C spectra (Figure 3.2). The particle morphologies provided by STXM-NEXAFS are discussed in Section 3.5.7. All of the generated high O/C particles were identified as similar to saccharides on sea salt, indicating that high O/C OM in the generated particles is associated with sea salt.

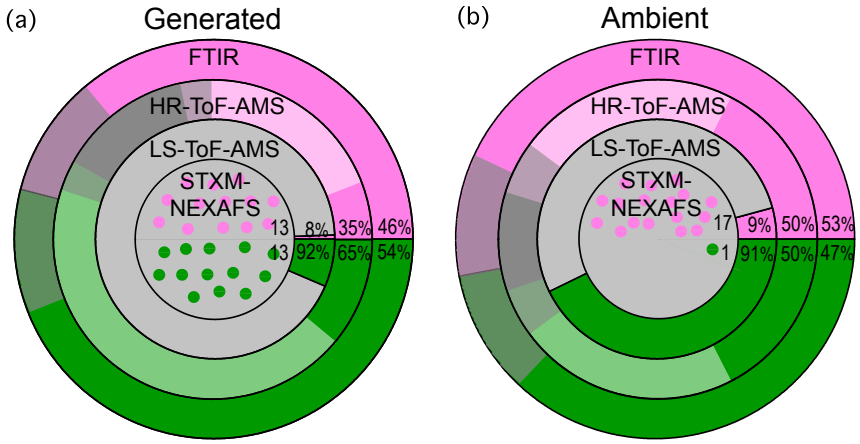

Figure 3.2: Comparison of the OM composition for the (a) generated marine and (b) ambient atmospheric marine particles. The OM is separated into high O/C (pink) and low O/C (green). Grey shading in the FTIR pies represents uncertainty (see Section 3.5.2.1). For the HR-ToF-AMS pies, the lighter shading shows the CE_{IC} that was applied, grey shading is the uncertainty (see Section 3.5.2.2), and the dark grey is the percent difference between the FTIR and HR-ToF-AMS OM. In the LS-ToF-AMS pies, the light grey area is the number based CE_{LS}. The individual circles that make up the STXM-NEXAFS pies represent the small number of particles measured by the technique, and the numbers of particles are written in each section of the pie. The light grey shading represents the overall lower particle statistics and higher uncertainty for the STXM-NEXAFS measurements. For the HR-ToF-AMS and FTIR spectroscopy pies, the percent of the total OM that is high and low O/C are included, and for the LS-ToF-AMS, the percent of total organic particles that are high and low O/C are included.

3.3 Comparison of Measurement Techniques

The OM composition of ambient atmospheric and generated marine aerosol was measured by four complementary techniques and classified into two types of OM: high O/C OM which is highly oxidized and low O/C OM which has little or no oxidization. For the four techniques, OM was separated by: (i) functional groups with high and low O/C (FTIR spectroscopy), (ii) mass fragments with $C_XH_YO_{>1}$, $C_XH_YO_1$, and C_XH_Y (HR-ToF-AMS), (iii) single particles with high m/z 44 or C_XH_Y signatures (LS-ToF-AMS), and (iv) single particles that were alkyl-like or oxidized (STXM-NEXAFS). The high and low O/C classification of OM provides a basis to compare the four measurement techniques (Figure 3.2). While the techniques have different capabilities for sampling the high and low O/C OM compositions, the composition of the particles measured by HR-ToF-AMS and FTIR spectroscopy are generally consistent. The larger differences in the generated marine particle composition can be explained by the influence of the high fraction of larger diameter sea salt containing particles that were missed by the AMS techniques and by the uncertainties of both the FTIR and AMS techniques.

STXM-NEXAFS measurements provide examples of single-particle morphology for two generated marine particle types: high O/C OM on sea salt particles (similar to particles identified previously as saccharides on sea salt [*Hawkins and Russell*, 2010]) and low O/C OM particles (Figure 3.1l and 3.1p). Of the ambient particles, 13 of 17 of the high O/C particles were also similar to saccharides on sea salt (Figure 3.1l). This morphology of a small fraction of saccharide-like organic components compared to sea salt (for particles with d_a of 0.47 to 6.4 μm that the STXM-NEXAFS sees), results in

particles that are largely refractory at 650°C and, hence, may bounce off the vaporizer. The alkyl-like (low O/C OM) particle type has a more uniform morphology with OM throughout the particle and no evidence of sea salt (Figure 3.1p), consistent with these particles being vaporized more efficiently at 650°C than the high O/C OM on sea salt. The less than 100 particles analyzed with this technique were selected manually based on the carbon content detected and do not represent the entire OM particle population. However, the identification of both high and low O/C particle types provides consistency with the FTIR and AMS techniques, in addition to showing that the high O/C OM is typically present on the sea salt-containing particles, especially in the generated marine aerosol.

The HR-ToF-AMS and FTIR measured compositions are similar for ambient particles both with approximately 50% high O/C OM, but there is a larger difference in the generated OM with a HR-ToF-AMS high O/C fraction of 35% and an FTIR high O/C fraction of 46% (Figure 3.2). This larger difference is due to the high (89%) sea salt fraction of these particles (see Section 3.5.2.5). The HR-ToF-AMS measures non-refractory particles only and is influenced by particle bounce effects. Even at 650°C, sea salt is inefficiently vaporized in the AMS. Any OM present on sea salt particles, as observed in the STXM-NEXAFS morphology, is also inefficiently vaporized in the HR-ToF-AMS. The larger fraction of low O/C OM measured by HR-ToF-AMS, compared to FTIR is a result of the high O/C OM that is associated with sea salt and low transmission efficiency of the larger sea salt particles.

The OM composition as determined by FTIR spectroscopy and HR-ToF-AMS are more similar for the ambient particles (within 10%, Figure 3.2b), due to the smaller

fraction of sea salt in the ambient particles. If all of the sea salt (3% of the particle mass) is from sea spray and the same ratio of OM to sea salt as the generated particles (11:89, Table 3.3), only 0.37% of the particle mass is associated with sea salt, which is less than 1% of the total OM. The OM that is not associated with sea salt is non-refractory and less influenced by bounce effects and is sampled efficiently by both the FTIR and CE-corrected AMS techniques.

The LS-ToF-AMS measurements demonstrate that a large number (93%) of generated marine particles are not vaporized in the AMS and are refractory or bounce off the vaporizer, even though they are optically detected by light scattering. The large fraction of LS-only particles observed during sampling generated marine particles is consistent with a large fraction of sea salt in those particles, compared to the lower fraction of sea salt in the ambient particles. The submicron generated particles were 89% sea salt (Table 3.3), consistent with an LS-only fraction of 93%. Additionally, the ratio of LS+MS particles to total particles observed by light scattering is negatively correlated with sea salt concentrations ($r = -0.60$). This result implies that the sea salt particles detected by LS are not vaporized (no mass spectrum with total S/N exceeding 3 is obtained), consistent with the refractory nature of sea salt (which contributes to particle bounce) and the morphology measured by STXM-NEXAFS.

The composition of the LS-ToF-AMS particles includes a much higher low O/C fraction than the other techniques, for both generated and ambient particles (Figure 3.2). This is the result of a disproportionately low representation of the high O/C OM associated with refractory sea salt. Additionally, the LS-ToF-AMS measures single particles in a limited size range, which may not be directly comparable to the other

techniques that include larger (STXM-NEXAFS and FTIR) and smaller (HR-ToF-AMS) particles (Table 3.1 and Figure 3.3). See Section 3.5 for more discussion.

3.4 Implications for Marine Organic Aerosol Composition

The results of the HR-ToF-AMS and FTIR measurement techniques show consistent OM concentrations and comparable high and low O/C fractions for ambient atmospheric aerosol. The discrepancy in the results was greater for the generated OM, consistent with the larger fraction of refractory particles. The sea salt particles and associated OM do not vaporize at 650°C and are more prone to particle bounce. For both aerosol types, the high O/C OM consists of hydroxyl and carboxylic acid functional groups measured by FTIR spectroscopy and STXM-NEXAFS and mass fragments of the $C_XH_YO_1$ and $C_XH_YO_{>1}$ groups measured by LS-ToF-AMS and HR-ToF-AMS. The low O/C OM consists of alkane and alkyl functional groups measured by FTIR spectroscopy and STXM-NEXAFS and C_XH_Y mass fragments measured by LS-ToF-AMS and HR-ToF-AMS.

The FTIR spectroscopy and HR-ToF-AMS high and low O/C fractional composition show good agreement for the ambient marine measurements, with O/C approximately 50% of the total OM. The generated marine OM fractions measured by the HR-ToF-AMS and FTIR spectroscopy have differences up to 31%. This is consistent with the larger fraction of sea salt particles in the generated marine OM, compared to the ambient marine OM and the larger fraction of high O/C OM associated with the sea salt particles. With CE_{IC} correction applied, the average ratio of HR-ToF-AMS to FTIR spectroscopy OM is 0.86, which is within the 20% uncertainty for these measurements.

STXM-NEXAFS measurements show both high O/C and low O/C particles are present in the generated marine OM, which is similar to the FTIR spectroscopy and HR-ToF-AMS measured compositions. The difference in the generated and ambient marine particle composition compared to FTIR spectroscopy and HR-ToF-AMS is likely the result of the low counting statistics and the selection of particles for analysis. The LS-ToF-AMS measurements demonstrate that a large number of the optically detected marine generated particles are not vaporized in the AMS. The result is a disproportionately high representation of the low O/C particles in the mass spectra for the LS-ToF-AMS (see Section 3.5.8).

3.5 Appendix

3.5.1 Marine OM Measurement Techniques

The composition of the organic component of both ambient and generated marine aerosol particles differ substantially in recently reported results [*Rinaldi et al.*, 2010; *Bates et al.*, 2012]. The cause of the difference, attributed to either different OM measurement approaches or differences in seawater properties that produce the marine particles, is still unresolved [*Rinaldi et al.*, 2010]. The purpose of this study is to resolve the discrepancy in OM composition of generated marine aerosol as observed by Fourier transform infrared (FTIR) spectroscopy and high resolution time of flight aerosol mass spectrometry (HR-ToF-AMS) measurements through the use of multiple measurement techniques including FTIR spectroscopy, HR-ToF-AMS, evolved gas analysis (EGA), scanning transmission X-ray microscopy near edge absorption fine structure (STXM-NEXAFS), and a light scattering module of the HR-ToF-AMS (LS-ToF-AMS).

Given the complexity of the organic composition of marine aerosol particles, characteristics can be determined through the combination of techniques that provide complementary information. The measurement techniques vary in the fraction of OM they can quantify and in the degree to which the organics can be speciated. Spectroscopy techniques (FTIR, Raman, and nuclear magnetic resonance) can be used to determine the functional group composition, while mass spectrometry techniques (gas chromatography mass spectrometry and aerosol mass spectrometry) can be used to determine mass fragments. These techniques and others have been utilized to measure the organic composition of ambient and generated marine aerosol particles. The multiple techniques used and the general organic compositions of marine aerosol determined by each are shown in Table 3.2.

3.5.2 Marine Aerosol Measurements during WACS

During the WACS cruise, the R/V *Ronald H. Brown* traveled from Boston, MA, to Bermuda, stopping in the colder, eutrophic seawater of George's Bank and the warmer, oligotrophic seawater of the Sargasso Sea. The nascent (or newly generated) SSA particles, referred to as generated marine aerosol particles, were generated with the Sea Sweep. These particles were free of influence from ambient air and were transported from the sea surface to the research vessel for sampling through a humidity and temperature-controlled inlet.

Table 3.2: Organic composition of generated and ambient marine aerosol particles measured using different techniques.

Technique Used[a]	OM Composition	Reference
Ambient		
FT-ICR MS; H-NMR	Biomolecules with high aliphaticity	[*Schmitt-Kopplin et al.*, 2012]
FTIR spectroscopy and STXM-NEXAFS	Polysaccharides	[*Russell et al.*, 2010]
GC-MS	Oxo-, mono-, and di-carboxylic acids	[*Kawamura and Gagosian*, 1987]
GC-MS	Low molecular weight saturated fatty acids	[*Mochida et al.*, 2002]
GC-MS	Low molecular weight fatty acids, fatty alcohols, and sterols	[*Fu et al.*, 2011]
GC-MS; EGA	Saccharides; isoprene products	[*Fu et al.*, 2013]
H-NMR	WIOM; WSOM	[*Facchini et al.*, 2008]
H-NMR	Diethyl and dimethyl amine salts	[*Facchini et al.*, 2010]
H-NMR; LC-MS	Lipids, fatty acids, short chain aliphatics; WSOC	[*Decesari et al.*, 2011]
HPLC	Proteins, amino acids, and polysaccharides in gels	[*Kuznetsova et al.*, 2005]
HPLC	Free amino acids in WSOC	[*Matsumoto and Uematsu*, 2005]
HR-ToF-AMS	Hydrocarbons; oxygenated hydrocarbons	[*Ovadnevaite et al.*, 2011]
HR-ToF-AMS	N/A	[*Shank et al.*, 2012]
IC; EGA	WSOC and TOC	[*Yoon et al.*, 2007]
IC; IC-EIT-MS; EGA	WIOM; levoglucosan, glucose	[*Kaku et al.*, 2006]
IC; solid/liquid phase elemental analysis	WSOC: methanesulfonic acid, alkylammonium salts, dicarboxylic acids	[*Rinaldi et al.*, 2010]
IC; TOC liquid analysis; EGA	WIOC; WSOC aliphatic and partially oxidized humic-like substances	[*Cavalli et al.*, 2004]
IC; TOC liquid analysis; EGA	Enriched in WIOC with high molecular weight; Enriched in WSOC (partly oxidized species with extended aliphatic moieties)	[*O'Dowd et al.*, 2004]
IC; TOC liquid analysis; EGA; Eddy covariance	WIOC; WSOC	[*Ceburnis et al.*, 2008]
IC-EIT-MS	Dicarboxylic acids, carbohydrates	[*Crahan et al.*, 2004]

Table 3.2 (Continued): Organic composition of generated and ambient marine aerosol particles measured using different techniques.

STXM-NEXAFS	Polysaccharides, proteins, and phytoplankton fragments	[*Hawkins and Russell*, 2010]
TEM	Marine microorganisms; microcolloidal aggregates	[*Leck and Bigg*, 2005]
TEM	WIOC aggregates; exopolymeric gels	[*Bigg*, 2007]
TEM	Exopolymers	[*Bigg and Leck*, 2008]
TOC Analyzer	WSOC, WIOC, TOC	[*Sciare et al.*, 2009]
Generated		
FTIR spectroscopy and HR-ToF-AMS	Polysaccharide-like, alkyl-like, pattern of CH-fragments	[*Bates et al.*, 2012]
H-NMR	WIOM: colloids	[*Facchini et al.*, 2008]
H-NMR	WIOM: lipo-polysaccharides	[*Facchini et al.*, 2010]
Raman microspectroscopy	Aliphatic hydrocarbons	[*Ault et al.*, 2013]
TOC Analyzer	WSOC	[*Keene et al.*, 2007]

[a]Relevant acronyms: Fourier transform ion cyclotron resonance mass spectrometry (FT-ICR MS); Fourier transform infrared (FTIR); gas chromatography mass spectrometry (GC-MS); proton nuclear magnetic resonance (H-NMR); liquid chromatography mass spectrometry (LC-MS); high performance liquid chromatography (HPLC); high resolution time of flight aerosol mass spectrometer (HR-ToF-AMS); ion chromatography (IC); evolved gas analysis (EGA); ion chromatography electrospray ion trap mass spectroscopy (IC-EIT-MS); scanning transmission X-ray microscopy with near-edge X-ray absorption fine structure (STXM-NEXAFS); transmission electron microscopy (TEM); total organic carbon (TOC); water insoluble organic mass/carbon (WIOM/C); water soluble organic mass/carbon (WSOM/C).

3.5.2.1 FTIR spectroscopy

Ambient and generated marine particles were collected on pre-scanned 37 mm Teflon filters (Pall Inc., 1 μm pore size) for 1 to 8 hours, after passing through a diffusion drier filled with silica gel and a 1 μm cut cyclone. The cyclone has a 100% particle transmission efficiency for particles with aerodynamic diameters (d_a) less than 750 nm [*Gussman et al.*, 2002], shown in Figure 3.3. Five ambient and sixteen generated samples were collected. The filters were analyzed aboard the R/V *Ronald H. Brown* using Fourier transform infrared (FTIR) spectroscopy (Tensor 27 spectrometer, Bruker, Billerica, MA).

The filters were then frozen and transported back to San Diego, CA, for further analysis. The generated marine samples were dehydrated using the method outlined by *Frossard and Russell* [2012] to remove interference of sea salt hydrate bound water with the organic signal in the FTIR spectra.

The FTIR spectrum from each filter was baselined and integrated at specific peak locations to determine the peak areas of the organic functional groups using an automated algorithm outlined by *Maria et al.* [2002] and revised by *Russell et al.* [2009] and *Takahama et al.* [2012]. The absorptivity and molar masses were used to convert peak area to mass for each functional group including: organic hydroxyl (C-O-H), alkane (C-C-H), amine (C-N-H), carboxylic acid (COOH), and non-acid carbonyl (C=O). Alkene (C=C-H) and aromatic functional groups were below the detection limit in all of the samples. The total OM for each sample was calculated as the sum of the organic functional groups. 20% uncertainty is shown in Figure 3.2, based on *Maria et al.* [2002].

3.5.2.2 HR-ToF-AMS

A high resolution time of flight aerosol mass spectrometer (HR-ToF-AMS) (Aerodyne, Billerica, MA) was used to measure the non-refractory submicron particle composition of the ambient and generated marine particles including ammonium, sulfate, nitrate, sea salt, and OM concentrations [*Canagaratna et al.*, 2007; *DeCarlo et al.*, 2006]. Ambient and generated particles passed through a diffusion drier filled with silica gel and a 1 μm cut cyclone before sampling. The AMS lens has 100% particle transmission efficiency for particles with d_a from 90 to 700 nm (Figure 3.3) and 30% transmission efficiency for 1 μm particles (d_a) [*Williams et al.*, 2013]. The HR-ToF-AMS alternated

between sampling in V-mode (both pToF and mass spectrum modes), W-mode, and LS-mode, which is discussed in the next section, on a 2-minute cycle for each mode. The V and W-mode data was analyzed using the ToF-AMS HR Analysis 1.10H program (Pika, D. Sueper, available at http://cires.colorado.edu/jimenez-group/ToFAMSResources/ToFSoftware/index.html). However, only V-mode data were used in this study. pCO2 concentrations were measured during the cruise [*Wanninkhof et al.*, 2013] and used in the ToF-AMS HR analysis program to correct for CO_2 gas phase influence. The ionization efficiency (IE) was obtained using the method described by *Jimenez et al.* [2003]. 20% uncertainty in the HR-ToF-AMS measurements are shown in Figure 3.2 [*Drewnick et al.*, 2005].

3.5.2.3 LS-ToF-AMS

A light scattering (LS) module on the HR-ToF-AMS (LS-ToF-AMS) was used to optically detect single particles before characterizing with the mass spectrometer, as described by *Liu et al.* [2013]. The LS-ToF-AMS has the lens efficiency of the HR-ToF-AMS, but the smallest particles with significant optical signal are d_a = 180 nm (Figure 3.3). Using the LS data processing software Sparrow 1.04D (available at http://cires.colorado.edu/jimenez-group/ToFAMSResources/ToFSoftware/index.html #Sparrow), single particles were observed and classified based on their vaporization behavior. Briefly, in order to determine a sufficient chemical signal, ten high intensity ion fragments (m/z 36, 41, 43, 44, 48, 55, 57, 58, 64, 81) were selected to make up the mass intensity profile for each particle [*Liu et al.*, 2013]. Based on the intensity profiles, particles were separated by those that had light scattering and mass spectral signals

(LS+MS) and those that only had light scattering signals (LS-only). The LS-only particles were optically detected but not sufficiently vaporized with total mass spectral signal to noise less than 3.

In addition to the optically detected particles, more triggers were saved but did not have detectable optical signals, as described by *Liu et al.* [2013] as an additional duty cycle due to an unusual noise spike in the LS channel. During sampling, the coincident particles (e.g., more than one particle is optically detected in one cycle) were less than 0.5% of the total particles and are not included in this analysis, consistent with *Liu et al.* [2013].

3.5.2.4 STXM-NEXAFS

Ambient and generated particles were collected on silicon nitride windows (Si_3N_4, Silson Ltd, Northampton, England) using a Streaker (PIXE International Corp., Tallahassee, FL) for impaction. The windows were frozen after collection to prevent evaporation. Generated particles were collected from 22:00 to 01:00 UTC starting on 21 August 2012. Ambient particles were collected from 19:00 to 00:00 UTC starting on 23 August 2012. The windows were analyzed at the Advanced Light Source at Lawrence Berkeley National Laboratory using scanning transmission X-ray microscopy with near-edge X-ray absorption fine structure (STXM-NEXAFS) at atmospheric temperature and under dry He at 1 atm [*Hawkins and Russell*, 2010; *Kilcoyne et al.*, 2003; *Takahama et al.*, 2007; *Takahama et al.*, 2010]. Scans of selected single particles were done from 278 to 320 eV to determine the X-ray absorption spectra of the carbon K-edge, and functional groups were identified by their absorption [*Hawkins and Russell*, 2010]. Image scans of

the particles were used to determine the diameter, morphology, and organic composition of the single particles. Due to instrument and analysis constraints, the number of single particles analyzed by STXM-NEXAFS is limited [*Bahadur et al.*, 2010]. From the particles impacted on the silicon nitride windows, 26 generated and 18 ambient particles were analyzed.

The generated particle diameters (d_p) ranged from 0.65 to 3.1μm, and the ambient particle diameters (d_p) ranged from 0.39 to 2.59 μm. Using a density of 1.1 g cm^{-3} for the low O/C particles and 2.05 g cm^{-3} for the high O/C particles (based on a sea salt density of 2.165 g cm^{-3} and an average sea salt fraction of 89%), the aerodynamic particle diameters ranged from 0.72 to 6.4 μm and 0.47 to 5.3 μm for generated and ambient marine particles, respectively (Figure 3.3).

3.5.2.5 OC and IC measurements

Ambient and generated particles (<1.1 μm at 60% relative humidity) were collected on pre-combusted quartz fiber filters using a two stage impactor downstream of a charcoal denuder [*Bates et al.*, 2004]. They were analyzed with a Sunset Laboratory thermal/optical analyzer to determine the concentrations of organic carbon (OC) with evolved gas analysis, hereafter referred to as EGA OC. Particles (<1.1 μm) were also collected on Millipore Fluoropore filters with a Berner-type multijet cascade impactor. The substrates were extracted and analyzed using ion chromatography (IC) to quantify inorganic ions including Na^+, Cl^-, sulfate, nitrate, and ammonium [*Quinn et al.*, 1998].

Sea salt concentrations for the generated marine particles were calculated as 3.26*Na^+ concentrations measured by IC, based on the calculation by *Quinn et al.*

[Accepted] and the ratio of ions in seawater [*Holland*, 1978]. Ambient sea salt concentrations were calculated using measured Cl^- plus $1.47*Na^+$ concentrations to account for the depletion of Cl^- in the atmosphere [*Holland*, 1978]. As described by *Quinn et al.* [Accepted] using these measurements, the generated marine particle mass was 89% sea salt and 11% OM. The ambient particle mass was 3% sea salt, 59% OM, and 38% other mass (Table 3.3).

Table 3.3: Mass fractions of OM, non-sea salt sulfate, ammonium, methanesulfonic acid (MSA), and sea salt in ambient and generated marine particles (based on *Quinn et al.* [Accepted]).

	Ambient	**Generated**
OM (FTIR)	0.59	0.11
Non-sea salt sulfate	0.25	
Ammonium	0.11	
MSA	0.02	
Sea salt	0.03	0.89

3.5.2.6 Aerosol physical measurements

Ambient and generated marine aerosol size distributions were measured using differential mobility particle sizers (DMPS, Aitken and Accumulation) and an aerodynamic particle sizer (APS, TSI model 3321) as described by *Bates et al.* [2012]. The number and mass size distributions for the generated and ambient marine particles are shown in Figure 3.3.

The 100% transmission efficiency aerodynamic diameter (d_a) ranges for FTIR spectroscopy, HR-ToF-AMS, and LS-ToF-AMS, in addition to the range of particles analyzed by STXM-NEXAFS, are included in Figure 3.3 and listed in Table 3.1. Figure 3.3 shows the overlap of the d_a ranges with the maximum concentration ranges for the LS-ToF-AMS, HR-ToF-AMS, and FTIR measurements. The STXM-NEXAFS technique

measured particles with larger d_a but overlaps with the other techniques at their largest d_a values.

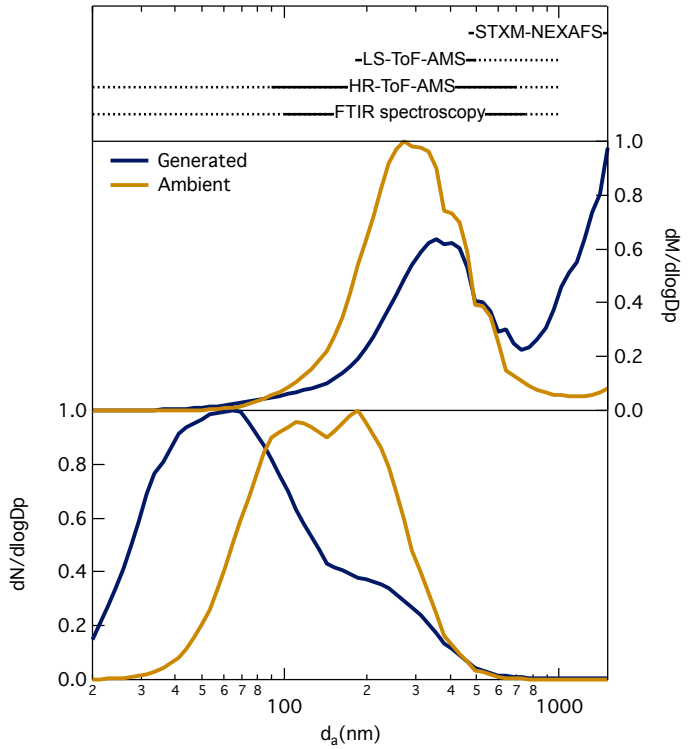

Figure 3.3: Normalized (bottom) number and (middle) mass size distributions of generated and ambient marine aerosol particles. (top) Ranges of aerodynamic diameters of particles measured with the different techniques, based on Table 3.1. The solid lines represent 100% particle transmission efficiency for HR-ToF-AMS and FTIR, the lowest detectable diameters to diameters with 100% transmission efficiency for LS-ToF-AMS, and the diameters of particles measured for STXM-NEXAFS. Dashed lines show the reduced collection on filters and reduced sensitivity for FTIR and 50% transmission efficiency for HR-ToF-AMS and LS-ToF-AMS. At 1 µm, the HR-ToF-AMS and LS-ToF-AMS have particle transmission efficiencies of 30%.

3.5.3 Comparison of HR-ToF-AMS and FTIR OC with EGA OC

The OC mass measured by FTIR spectroscopy was calculated from the total moles of carbon in each sample. On average, the total OC mass measured by FTIR spectroscopy was a factor of 1.06 greater than that measured with the Sunset EGA (r = 0.61) with an average overall percent difference of 3% (Figure 3.4a). HR-ToF-AMS OC

was calculated using the ratio of OM/OC and OM. Overall, comparison with EGA OC gave a slope of 0.31 and a correlation of r = 0.67 (Figure 3.4b). The HR-ToF-AMS and FTIR OM have similar masses after the CE_{IC} is applied (Figure 3.4c), and the ambient samples correlate well (r = 0.88). Table 3.4 shows a summary of OM, OC, and O/C from FTIR, HR-ToF-AMS, and EGA measurements, and Figure 3.5 shows the variation of sea salt, OM, and O/C with time.

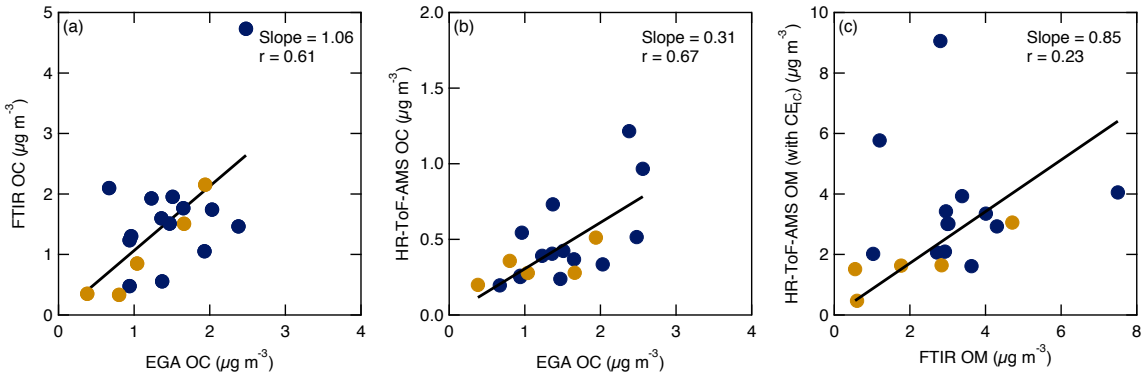

Figure 3.4: Correlations of (a) FTIR OC with EGA OC; (b) HR-ToF-AMS OC with EGA OC; and (c) HR-ToF-AMS OM (using CE_{IC}) with FTIR OM. Markers are colored as generated (dark blue) and ambient (bronze). The overall (ambient and generated together) slopes and correlations are given. Two samples were not included in the correlations due to filter sampling problems and high humidity.

Table 3.4: Ambient and generated marine particle OM, OC, and O/C values measured with FTIR spectroscopy, HR-ToF-AMS, and EGA (OC only). HR-ToF-AMS OC was calculated with HR-ToF-AMS OM/OC elemental ratios. HR-ToF-AMS values do not have a CE applied.

	Ambient	**Generated**
OM (μg m^{-3})		
FTIR	2.09 ± 1.74	3.23 ± 1.52
HR-ToF-AMS	0.58 ± 0.32	0.65 ± 0.36
OC (μg m^{-3})		
EGA	1.16 ± 0.63	1.68 ± 0.75
FTIR	1.04 ± 0.79	1.67 ± 1.01
HR-ToF-AMS	0.33 ± 0.12	0.49 ± 0.30
O/C		
FTIR	0.55 ± 0.17	0.51 ± 0.22
HR-ToF-AMS	0.63 ± 0.11	0.20 ± 0.08

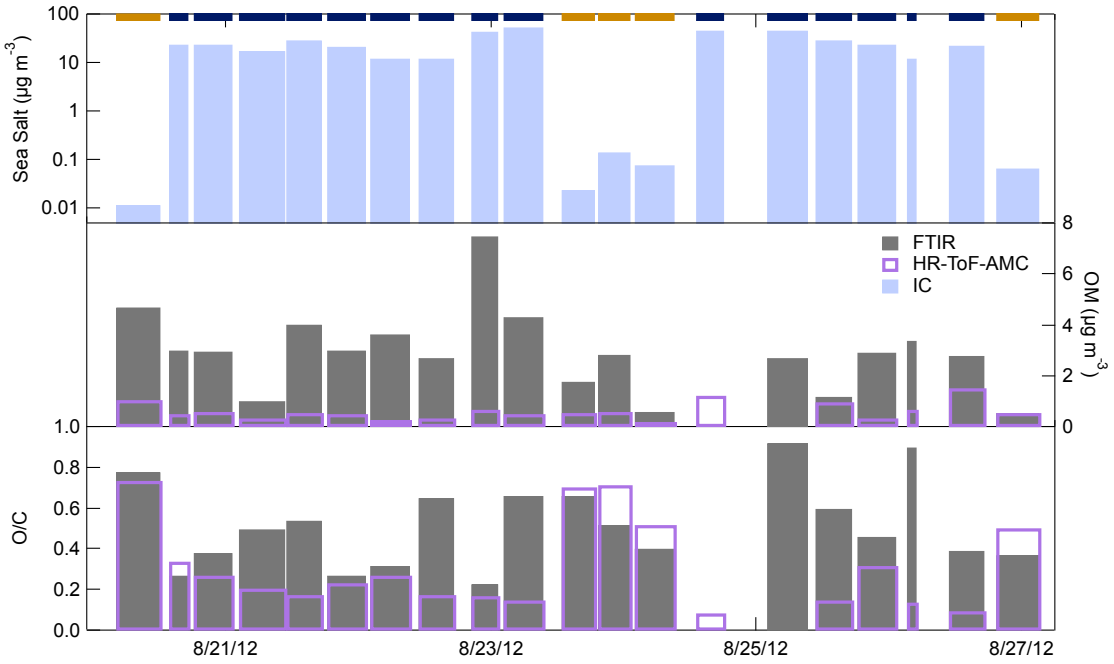

Figure 3.5: Time series of (top) IC sea salt concentration, (middle) FTIR spectroscopy and HR-ToF-AMS (no CE applied) OM concentrations, and (bottom) FTIR and HR-ToF-AMS O/C ratios. The bars at the top represent the type of sample: ambient (bronze) and generated (dark blue) marine aerosol.

3.5.4 HR-ToF-AMS Sea Salt

The heater temperature of the HR-ToF-AMS was set to 650°C to vaporize more of the sea salt components [*Ovadnevaite et al.*, 2012]. The HR-ToF-AMS measurements were used to calculate the mass of sea salt by identifying and scaling specific sea salt ions based on the method outlined by *Ovadnevaite et al.* [2012]. The concentrations of four different combinations of the sea salt ions, outlined in Table 3.5, were averaged over the impactor sampling times. A least squares fit was used to fit the concentrations from the ion groups in Table 3.5 to the IC measured sea salt to determine a HR-ToF-AMS sea salt scaling factor, which is the inverse of the sea salt collection efficiency (CE_{SS}). The combination of sea salt ions Cl^+, HCl^+, $NaCl^+$, Na_2Cl^+, KCl^+, $MgCl^+$ and their isotopes

were used to calculate the final scaling factor based on the correlation to IC sea salt and the combined ion signal. The ambient scaling factor is 12, and the generated marine particle scaling factor is 79, which are similar to those used by *Ovadnevaite et al.* [2012] of 2.5 and 51, respectively, calculated for laboratory generated sea salt. The larger sea salt scaling factors measured here may be due to a decreased lens transmission efficiency of larger sea salt particles, compared to the monodisperse 300 nm particles used by *Ovadnevaite et al.* [2012]. Increasing the number of HR-ToF-AMS sea salt ions in the comparison to IC sea salt decreases the resulting scaling factor. While $NaCl^+$ compared well to the IC sea salt ($r > 0.70$), the scaling factor was very high for both ambient (1302) and generated (1729) marine particles making the corresponding CE_{SS} values very low and indicating that additional ions are needed for the scaling. The concentration of Na^+ is unreliable as a sea salt ion due to its persistence in the HR-ToF-AMS system and was therefore not used to calculate the scaling factor [*Ovadnevaite et al.*, 2012]. The moderate correlations of the HR-ToF-AMS ions and the IC sea salt suggest that the sea salt collection efficiency may also have a size dependence. A more accurate CE could be determined using variations in size and lens transmission efficiency.

3.5.5 HR-ToF-AMS CE Calculations

The HR-ToF-AMS collection efficiency (CE) was calculated by comparing the concentration of HR-ToF-AMS sulfate and the concentration of sulfate from filters measured with IC, as discussed by *Canagaratna et al.* [2007] and calculated by *Bates et al.* [2012] for similar measurements. The sulfate based CE (CE_{IC}) was calculated separately for the ambient and generated marine particles to allow for the differences in

Table 3.5: Comparison of sea salt scaling factors ($1/CE_{SS}$) used to scale HR-ToF-AMS sea salt to IC measured sea salt. The correlation coefficient is shown in parentheses for each case. The average of un-scaled and scaled sea salt is shown for each set of ions.

		Scaling factor (correlation coefficient, r)		Average of HR-ToF-AMS sea salt (μg m^{-3})			
				Un-scaled		Scaled[b]	
HR-ToF-AMS ions used to calculate sea salt	Previous Values	Ambient	Gen.	Ambient	Gen.	Ambient	Gen.
$NaCl^+$	51[a]	1302 (0.98)	1729 (0.71)	9.5e-5	0.015	0.12	25.2
Na^+, Cl^+, HCl^+, $NaCl^+$, $^{37}Cl^+$, $H^{37}Cl^+$, $Na^{37}Cl^+$	2.5[a]	0.216 (0.65)	27 (0.55)	0.43	1.0	0.09	28.2
$NaCl^+$, Na_2Cl, KCl^+, $MgCl^+$, $Na^{37}Cl^+$, $Na_2{}^{37}Cl$, $K^{37}Cl^+$, $^{41}KCl^+$, $^{41}K^{37}Cl^+$, $Mg^{37}Cl^+$	N/A	126 (0.20)	707 (0.67)	9.1e-4	0.037	0.12	25.8
Cl^+, HCl^+, $NaCl^+$, Na_2Cl^+, KCl^+, $MgCl^+$, $^{37}Cl^+$, $H^{37}Cl^+$, $Na^{37}Cl^+$, $Na_2{}^{37}Cl^+$, $K^{37}Cl^+$, $^{41}KCl^+$, $^{41}K^{37}Cl^+$, $Mg^{37}Cl^+$	N/A	12 (0.52)	79 (0.59)	9.9e-3	0.35	0.12	27.6

[a][*Ovadnevaite et al.*, 2012]; laboratory generated sea salt (300 nm, relative humidity = 65%) and vaporizer temperature of 650°C

[b]Average IC sea salt values: ambient = 0.10 μg m^{-3} and generated = 26.7 μg m^{-3}

CE values based on particle type. With the direct comparison to independently measured sulfate, other factors contributing to the CE, such as particle shape, phase, and acidity are taken into account but not directly calculated [*Huffman et al.*, 2005; *Matthew et al.*, 2008; *Middlebrook et al.*, 2012]. This method also includes lens transmission efficiency, which affects the larger particles, such as the OM associated with sea salt. When comparing the HR-ToF-AMS sulfate loadings to IC sulfate only, we obtained a CE_{IC} of 0.35 for

ambient, and a CE_{IC} of 0.17 for the generated particles. The different CE_{IC} values for ambient and generated marine particles indicate that the CE_{IC} incorporates variations in detection efficiency as a function of particle size. The CE_{IC} values were used to scale the OM for comparison with FTIR measured OM.

The CE_{IC} values for generated particles are less than typical AMS CE values of 0.5 [*Canagaratna et al.*, 2007] because a large fraction of the generated particle mass (89%) is sea salt, which does not vaporize efficiently at 650°C (due to its refractory nature and tendency to bounce off the vaporizer) and therefore has a much lower CE (CE_{SS}). For this reason, and to compare directly to LS-ToF-AMS that produces a total CE for all particles through optical detection, a total CE (CE_{total}) for the HR-ToF-AMS was calculated separately for the ambient (CE_{totalA}) and generated (CE_{totalG}) particles using: $CE_{total} = CE_{SS}*X_{SS} + CE_{other}*X_{other.}$ The value of CE_{other} is assumed to be 0.5 [*Canagaratna et al.*, 2007], and X is the fraction of the respective mass measured by IC and/or EGA. The calculated CE_{totalG} (0.07) is less than CE_{totalA} (0.49), indicating that only a small fraction of the total mass is vaporized by the HR-ToF-AMS under the standard operational conditions due to the presence of sea salt. The standard comparison of total particle mass to integrated particle mass size distributions was not included due to differences in sampling conditions between the HR-ToF-AMS and the particle sizing instruments.

3.5.6 STXM-NEXAFS Particle Morphologies

The particle morphologies associated with these spectral types were unique to the OM types. The low O/C particle type mainly had round or irregular shaped particles with

uniformly distributed carbon absorbance. A large fraction of the high O/C particles have the shapes characteristic of polysaccharides on sea salt, with a cuboidal inner-structure surrounded by a high O/C organic [*Hawkins and Russell*, 2010; *Russell et al.*, 2010]. Four of the 17 ambient high O/C particles were round and did not have characteristics of organics on sea salt. These particles may be from oxidization of alkyl-like particles or secondary formation in the atmosphere. Their spectra are similar to secondary organic aerosol particles identified by *Takahama et al.* [2007]. STXM-NEXAFS measurements are too limited (in size range and sample number) to be quantitatively representative of the OM particle.

3.5.7 LS-ToF-AMS and HR-ToF-AMS

The composition of the LS-ToF-AMS particles has a much larger fraction of low O/C OM than the HR-ToF-AMS for both the generated and ambient marine particles. This difference may be attributed to a number of factors. (i) The high and low O/C separation for the LS-ToF-AMS was based on a single particle clustering, where the HR-ToF-AMS OM separation was based on the mass fragment groups of the overall average mass spectra. (ii) Additionally, spectra with less than 6 organic ions were not used in the LS-ToF-AMS clustering as their composition was not representative of the particle. However, those spectra are included in the overall HR-ToF-AMS OM due to the overall mass averaging during sampling. The same idea applies to the spectra that were saved by the light scattering mode. If a significant mass spectrum was not observed, then that spectrum was not used. For the HR-ToF-AMS, all of the mass spectra are averaged, so the lack of ions in an individual spectrum does not affect the total. The low OM signal

from the generated particles is better included in the bulk averaged HR-ToF-AMS than in the individual particles detected by LS-ToF-AMS. (iii) The LS-ToF-AMS has a smaller range of measured particles than the HR-ToF-AMS. The smallest particle with significant optically detected signal is 180 nm (d_a). This is a higher cutoff than the HR-ToF-AMS, which has a particle transmission efficiency of 100% at 90 nm (d_a). The LS-ToF-AMS particle size detection range falls within the size range of the maximum in particle mass concentration but does not have much overlap with the maximum in number concentration for the generated marine particles. (iv) Particles that contain less volatile species, such as sea salt, can bounce off of the vaporizer [*Huffman et al.*, 2005].

3.6 Acknowledgements

The authors gratefully acknowledge Leah Williams, William Brooks, Timothy Onasch, Donna Sueper, and Shang Liu for their assistance in preparing the HR-ToF-AMS and LS-ToF-AMS for deployment and for guidance with the LS-ToF-AMS analysis. They thank the captain, crew, and scientists aboard *Ronald H. Brown* for their support. The authors thank Derek Coffman, Drew Hamilton, and Janin Guzman-Morales for assistance with sample collection. They acknowledge David Kilcoyne at the Lawrence Berkeley National Laboratory Advanced Light Source and Satoshi Takahama for assistance with STXM-NEXAFS and beamline operation.

Chapter 3, in full, is a reprint of the material as it appears in *Aerosol Science and Technology* 2014 with slight modifications. Frossard, A.A., L.M. Russell, P. Massoli, T.S. Bates, and P.K. Quinn (2014), "Side-by-Side Comparison of Four Techniques Explains the Apparent Differences in the Organic Composition of Generated and

Ambient Marine Aerosol Particles." *Aerosol Science and Technology* 48:3, v-x, doi: 10.1080/02786826.2013.879979. The dissertation author was the primary investigator and author of this paper.

References

Ault, A. P., D. F. Zhao, C. J. Ebben, M. J. Tauber, F. M. Geiger, K. A. Prather, and V. H. Grassian (2013), Raman microspectroscopy and vibrational sum frequency generation spectroscopy as probes of the bulk and surface compositions of size-resolved sea spray particles, *Physical Chemistry - Chemical Physics*, *15*(17), 6206-6214, doi: 10.1039/c3cp43899f.

Bahadur, R., L. M. Russell, and K. Prather (2010), composition and morphology of individual combustion, biomass burning, and secondary organic particle types obtained using urban and coastal ATOFMS and STXM-NEXAFS measurements, *Aerosol Science and Technology*, *44*(7), 551-562, doi:10.1080/02786821003786048.

Bates, T. S., D. J. Coffman, D. S. Covert, and P. K. Quinn (2002), Regional marine boundary layer aerosol size distributions in the Indian, Atlantic, and Pacific Oceans: A comparison of INDOEX measurements with ACE-1, ACE-2, and Aerosols99, *Journal of Geophysical Research - Atmospheres*, 107(D19), doi:10.1029/2001jd001174.

Bates, T. S., P. K. Quinn, D. J. Coffman, D. S. Covert, T. L. Miller, J. E. Johnson, G. R. Carmichael, I. Uno, S. A. Guazzotti, D. A. Sodeman, K. A. Prather, M. Rivera, L. M. Russell, J. T. Merrill (2004), Marine boundary layer dust and pollutant transport associated with the passage of a frontal system over eastern Asia, *Journal of Geophysical Research*, *109*(D19), 18 pp., doi:10.1029/2003jd004094.

Bates, T. S., P. K. Quinn, A. A. Frossard, L. M. Russell, J. Hakala, T. Petäjä, M. Kulmala, D. S. Covert, C. D. Cappa, S.-M. Li, K. Hayden, I. Nuaaman, R. McLaren, P. Massoli, M. R. Canagaratna, T. B. Onasch, D. Sueper, D. R. Worsnop, W. C. Keene (2012), Measurements of ocean derived aerosol off the coast of California, *Journal of Geophysical Research - Atmospheres*, *117*(D00V15), doi:10.1029/2012JD017588.

Bigg, E. K. (2007), Sources, nature and influence on climate of marine airborne particles, *Environmental Chemistry*, *4*(3), 155-161, doi:10.1071/en07001.

Bigg, E. K., and C. Leck (2008), The composition of fragments of bubbles bursting at the ocean surface, *Journal of Geophysical Research - Atmospheres*, *113*(D11), doi:10.1029/2007jd009078.

Canagaratna, M. R., J. T. Jayne, D. A. Ghertner, S. Herndon, Q. Shi, J. L. Jimenez, P. J. Silva, P. Williams, T. Lanni, F. Drewnick, K. L. Demerjian, C. E. Kolb and D. R. Worsnop (2007), Chemical and microphysical characterization of ambient aerosols with the aerodyne aerosol mass spectrometer, *Mass Spectrometry Reviews*, *26*(2), 185-222, doi:10.1002/mas.20115.

Cavalli, F., M. C. Facchini, S. Decesari, M. Mircea, L. Emblico, S. Fuzzi, D. Ceburnis, Y. J. Yoon, C. D. O'Dowd, J. P. Putaud, A. Dell'Acqua (2004), Advances in characterization of size-resolved organic matter in marine aerosol over the North

Atlantic, *Journal of Geophysical Research - Atmospheres*, *109*(D24215), doi:10.1029/2004jd005137.

Ceburnis, D., C. D. O'Dowd, G. S. Jennings, M. C. Facchini, L. Emblico, S. Decesari, S. Fuzzi, and J. Sakalys (2008), Marine aerosol chemistry gradients: Elucidating primary and secondary processes and fluxes, *Geophysical Research Letters*, *35*(7), doi:10.1029/2008gl033462.

Crahan, K. K., D. A. Hegg, D. S. Covert, H. Jonsson, J. S. Reid, D. Khelif, and B. J. Brooks (2004), Speciation of organic aerosols in the tropical mid-pacific and their relationship to light scattering, *Journal of the Atmospheric Sciences*, *61*(21), 2544-2558, doi: 10.1175/JAS3284.1

de Leeuw, G., E. L. Andreas, M. D. Anguelova, C. W. Fairall, E. R. Lewis, C. O'Dowd, M. Schulz, and S. E. Schwartz (2011), Production Flux of Sea Spray Aerosol, *Reviews of Geophysics*, 49, doi:10.1029/2010rg000349.

DeCarlo, P. F., J. R. Kimmel, A. Trimborn, M. J. Northway, J. T. Jayne, A. C. Aiken, M. Gonin, K. Fuhrer, T. Horvath, K. S. Docherty, D. R. Worsnop and J. L. Jimenez (2006), Field-deployable, high-resolution, time-of-flight aerosol mass spectrometer, *Analytical Chemistry*, *78*(24), 8281-8289, doi:10.1021/ac061249n.

Decesari, S., Finessi, E., Rinaldi, M., Paglione, M., Fuzzi, S., Stephanou, E. G., Tziaras, T., Spyros, A., Ceburnis, D., O'Dowd, C., Dall'Osto, M., Harrison, R. M., Allan, J., Coe, H. and Facchini, M. C. (2011), Primary and secondary marine organic aerosols over the North Atlantic Ocean during the MAP experiment, *Journal of Geophysical Research - Atmospheres*, *116*, 21, doi:10.1029/2011jd016204.

Drewnick, F., S. S. Hings, P. DeCarlo, J. T. Jayne, M. Gonin, K. Fuhrer, S. Weimer, J. L. Jimenez, K. L. Demerjian, S. Borrmann, D. R. Worsnop (2005), A new time-of-flight aerosol mass spectrometer (TOF-AMS) - Instrument description and first field deployment, *Aerosol Science and Technology*, *39*(7), 637-658, doi: 10.1080/02786820500182040.

Facchini, M. C., M. Rinaldi, S. Decesari, C. Carbone, E. Finessi, M. Mircea, S. Fuzzi, D. Ceburnis, R. Flanagan, E. D. Nilsson, G. de Leeuw, M. Martino, J. Woeltjen, C. D. O'Dowd (2008), Primary submicron marine aerosol dominated by insoluble organic colloids and aggregates, *Geophysical Research Letters*, L17814 (17815 pp.), doi:10.1029/2008gl034210.

Facchini, M. C., M. Rinaldi, S. Decesari, and S. Fuzzi (2010), Marine organic aerosol and biological oceanic activity, *Chemical Engineering*, *22*, 107-112, doi: 10.3303/CET1022017.

Frossard, A. A., and L. M. Russell (2012), Removal of sea salt hydrate water from seawater-derived samples by dehydration, *Environmental Science and Technology*, *46*(24), 13326-13333, doi:10.1021/es3032083.

Fu, P. Q., K. Kawamura, J. Chen, B. Charriere, and R. Sempere (2013), Organic molecular composition of marine aerosols over the Arctic Ocean in summer: contributions of primary emission and secondary aerosol formation, *Biogeosciences*, *10*(2), 653-667, doi:10.5194/bg-10-653-2013.

Fu, P. Q., K. Kawamura, and K. Miura (2011), Molecular characterization of marine organic aerosols collected during a round-the-world cruise, *Journal of Geophysical Research - Atmospheres*, *116*, doi:10.1029/2011jd015604.

Gussman, R. A., L. C. Kenny, M. Labickas, and P. Norton (2002), Design, calibration, and field test of a cyclone for PM1 ambient air sampling, *Aerosol Science and Technology*, *36*(3), 361-365, doi:10.1080/027868202753504461.

Hawkins, L. N., and L. M. Russell (2010), Polysaccharides, Proteins, and Phytoplankton Fragments: Four Chemically Distinct Types of Marine Primary Organic Aerosol Classified by Single Particle Spectromicroscopy, *Advances in Meteorology*, *2010*(Article ID 612132), 14, doi:10.1155/2010/612132.

Hawkins, L. N., L. M. Russell, D. S. Covert, P. K. Quinn, and T. S. Bates (2010), Carboxylic acids, sulfates, and organosulfates in processed continental organic aerosol over the southeast Pacific Ocean during VOCALS-REx 2008, *Journal of Geophysical Research - Atmospheres*, 115 (D13201), doi:10.1029/2009jd013276.

Holland, H. D. (1978), *The Chemistry of the Atmosphere and Oceans*, edited, p. 154, Jon Wiley, New York.

Huffman, J. A., J. T. Jayne, F. Drewnick, A. C. Aiken, T. Onasch, D. R. Worsnop, and J. L. Jimenez (2005), Design, modeling, optimization, and experimental tests of a particle beam width probe for the aerodyne aerosol mass spectrometer, *Aerosol Science and Technology*, *39*(12), 1143-1163, doi:10.1080/02786820500423782.

Jayne, J. T., D. C. Leard, X. F. Zhang, P. Davidovits, K. A. Smith, C. E. Kolb, and D. R. Worsnop (2000), Development of an aerosol mass spectrometer for size and composition analysis of submicron particles, *Aerosol Science and Technology*, 33(1-2), 49-70.

Jimenez, J. L., J. T. Jayne, Q. Shi, C. E. Kolb, D. R. Worsnop, I. Yourshaw, J. H. Seinfeld, R. C. Flagan, X. F. Zhang, K. A. Smith, J. W. Morris, P. Davidovits (2003), Ambient aerosol sampling using the Aerodyne Aerosol Mass Spectrometer, *Journal of Geophysical Research - Atmospheres*, *108*(D7), doi:10.1029/2001jd001213.

Kaku, K. C., D. A. Hegg, D. S. Covert, J. L. Santarpia, H. Jonsson, G. Buzorius, and D. R. Collins (2006), Organics in the Northeastern Pacific and their impacts on aerosol

hygroscopicity in the subsaturated and supersaturated regimes, *Atmospheric Chemistry and Physics*, *6*, 4101-4115.

Kawamura, K., and R. B. Gagosian (1987), Implications of omega-oxocarboxylic acids in the remote marine atmosphere for photooxidation of unsaturated fatty-acids, *Nature*, *325*(6102), 330-332, doi:10.1038/325330a0.

Keene, W. C., H. Maring, J. R. Maben, D. J. Kieber, A. A. P. Pszenny, E. E. Dahl, M. A. Izaguirre, A. J. Davis, M. S. Long, X. L. Zhou, L. Smoydzin, R. Sander (2007), Chemical and physical characteristics of nascent aerosols produced by bursting bubbles at a model air-sea interface, *Journal of Geophysical Research - Atmospheres*, *112*(D21), doi:10.1029/2007jd008464.

Kilcoyne, A. L. D., T. Tyliszczak, W. F. Steele, S. Fakra, P. Hitchcock, K. Franck, E. Anderson, B. Harteneck, E. G. Rightor, G. E. Mitchell, A. P. Hitchcock, L. Yang, T. Warwick, H. Ade (2003), Interferometer-controlled scanning transmission X-ray microscopes at the Advanced Light Source, *Journal of Synchrotron Radiation*, *10*, 125.

Kuznetsova, M., C. Lee, and J. Aller (2005), Characterization of the proteinaceous matter in marine aerosols, *Marine Chemistry*, *96*(3-4), 359-377, doi:10.1016/j.marchem.2005.03.007.

Leck, C., and E. K. Bigg (2005), Source and evolution of the marine aerosol - A new perspective, *Geophysical Research Letters*, *32*(L19803), doi:10.1029/2005gl023651.

Liu, S., L. M. Russell, D. T. Sueper, and T. B. Onasch (2013), Organic particle types by single-particle measurements using a time-of-flight aerosol mass spectrometer coupled with a light scattering module, *Atmospheric Measurement Techniques*, *6*(2), 187-197, doi:10.5194/amt-6-187-2013.

Maria, S. F., L. M. Russell, B. J. Turpin, and R. J. Porcja (2002), FTIR measurements of functional groups and organic mass in aerosol samples over the Caribbean, *Atmospheric Environment*, *36*(33), 5185-5196.

Matsumoto, K., and M. Uematsu (2005), Free amino acids in marine aerosols over the western North Pacific Ocean, *Atmospheric Environment*, *39*(11), 2163-2170, doi:10.1016/j.atmosenv.2004.12.022.

Matthew, B. M., A. M. Middlebrook, and T. B. Onasch (2008), Collection efficiencies in an Aerodyne Aerosol Mass Spectrometer as a function of particle phase for laboratory generated aerosols, *Aerosol Science and Technology*, *42*(11), 884-898, doi:10.1080/02786820802356797.

Middlebrook, A. M., R. Bahreini, J. L. Jimenez, and M. R. Canagaratna (2012), Evaluation of Composition-Dependent Collection Efficiencies for the Aerodyne Aerosol

Mass Spectrometer using Field Data, *Aerosol Science and Technology*, *46*(3), doi:10.1080/02786826.2011.620041.

Mochida, M., Y. Kitamori, K. Kawamura, Y. Nojiri, and K. Suzuki (2002), Fatty acids in the marine atmosphere: Factors governing their concentrations and evaluation of organic films on sea-salt particles, *Journal of Geophysical Research - Atmospheres*, *107*(D17), 10.1029/2001JD001278.

O'Dowd, C. D., M. C. Facchini, F. Cavalli, D. Ceburnis, M. Mircea, S. Decesari, S. Fuzzi, Y. J. Yoon, and J. P. Putaud (2004), Biogenically driven organic contribution to marine aerosol, *Nature*, *431*(7009), 676-680, doi:10.1038/nature02959.

Ovadnevaite, J., D. Ceburnis, M. Canagaratna, H. Berresheim, J. Bialek, G. Martucci, D. R. Worsnop, and C. O'Dowd (2012), On the effect of wind speed on submicron sea salt mass concentrations and source fluxes, *Journal of Geophysical Research - Atmospheres*, *117*, doi:10.1029/2011jd017379.

Ovadnevaite, J., C. O'Dowd, M. Dall'Osto, D. Ceburnis, D. R. Worsnop, and H. Berresheim (2011), Detecting high contributions of primary organic matter to marine aerosol: A case study, *Geophysical Research Letters*, *38*, doi:10.1029/2010gl046083.

Quinn, P. K., T. S. Bates, K. S. Schultz, D. C. Coffman, A. A. Frossard, L. M. Russell, W. C. Keene, and D. J. Kieber (2014), Empirical Constraints on Modeling the Organic Matter Enrichment in Nascent Sea Spray Aerosol, *Nature Geoscience*.

Quinn, P. K., D. J. Coffman, V. N. Kapustin, T. S. Bates, and D. S. Covert (1998), Aerosol optical properties in the marine boundary layer during the First Aerosol Characterization Experiment (ACE 1) and the underlying chemical and physical aerosol properties, *Journal of Geophysical Research - Atmospheres*, *103*(D13), 16547-16563.

Rinaldi, M., S. Decesari, E. Finessi, L. Giulianelli, C. Carbone, S. Fuzzi, C. D. O'Dowd, D. Ceburnis, and M. C. Facchini (2010), Primary and secondary organic marine aerosol and oceanic biological activity: recent results and new perspectives for future studies, *Advances in Meteorology*, *2010* (Arctic ID 310682), 10, doi: 10.1155/2010/310682.

Russell, L. M., L. N. Hawkins, A. A. Frossard, P. K. Quinn, and T. S. Bates (2010), Carbohydrate-like composition of submicron atmospheric particles and their production from ocean bubble bursting, *Proceedings of the National Academy of Sciences of the United States of America*, *107*(15), 6652-6657, doi:10.1073/pnas.0908905107.

Russell, L. M., S. Takahama, S. Liu, L. N. Hawkins, D. S. Covert, P. K. Quinn, and T. S. Bates (2009), Oxygenated fraction and mass of organic aerosol from direct emission and atmospheric processing measured on the R/V Ronald Brown during TEXAQS/GoMACCS 2006, *Journal of Geophysical Research - Atmospheres*, *114*, doi:10.1029/2008jd011275.

Schmitt-Kopplin, P., G. Liger-Belair, B. P. Koch, R. Flerus, G. Kattner, M. Harir, B. Kanawati, M. Lucio, D. Tziotis, N. Hertkorn, I. Gebefuegi (2012), Dissolved organic matter in sea spray: a transfer study from marine surface water to aerosols, *Biogeosciences*, *9*(4), doi:10.5194/bg-9-1571-2012.

Sciare, J., O. Favez, R. Sarda-Esteve, K. Oikonomou, H. Cachier, and V. Kazan (2009), Long-term observations of carbonaceous aerosols in the Austral Ocean atmosphere: Evidence of a biogenic marine organic source, *Journal of Geophysical Research - Atmospheres*, *114*, doi:10.1029/2009jd011998.

Shank, L. M., S. Howell, A. D. Clarke, S. Freitag, V. Brekhovskikh, V. Kapustin, C. McNaughton, T. Campos, and R. Wood (2012), Organic matter and non-refractory aerosol over the remote Southeast Pacific: oceanic and combustion sources, *Atmospheric Chemistry and Physics*, *12*(1), doi:10.5194/acp-12-557-2012.

Takahama, S., S. Gilardoni, L. M. Russell, and A. L. D. Kilcoyne (2007), Classification of multiple types of organic carbon composition in atmospheric particles by scanning transmission X-ray microscopy analysis, *Atmospheric Environment*, *41*(40), 9435-9451, doi:10.1016/j.atmosenv.2007.08.051.

Takahama, S., A. Johnson, and L. M. Russell (2012), Quantification of carboxylic and carbonyl functional groups in organic aerosol infrared absorbance spectra, *Aerosol Science and Technology*, doi:10.1080/02786826.2012.752065.

Takahama, S., S. Liu, and L. M. Russell (2010), Coatings and clusters of carboxylic acids in carbon-containing atmospheric particles from spectromicroscopy and their implications for cloud-nucleating and optical properties, *Journal of Geophysical Research - Atmospheres*, *115*, 21, doi:10.1029/2009jd012622.

Wanninkhof, R., R. D. Castle, and J. Shannahoff (2013), Underway pCO2 measurements aboard the R/V Ronald H. Brown during the 2012 cruises, *http://cdiac.ornl.gov/ftp/oceans/VOS_Ronal_Brown/RB2012/. Carbon Dioxide Information Analysis Center, Oak Ridge National Laboratory, US Department of Energy, Oak Ridge, Tennessee*, doi:10.3334/CDIAC/OTG.VOS_RB_2012.

Williams. L. R., L. A. Gonzalez, J. Peck, D. Trimborn, J. McInnis, M. R. Farrar, K. D. Moore, J. T. Jayne, W. A. Robinson, D. K. Lewis, T. B. Onasch, M. R. Canagaratna, A. Trimborn, M. T. Timko, G. Magoon, R. Deng, D. Tang, E. de La Rosa Blanco, A. S. H. Prevot, K. A. Smith, D. R. Worsnop (2013), Characterization of an aerodynamic lens for transmitting particles greater than 1 micrometer in diameter into the Aerodyne aerosol mass spectrometer, *Atmospheric Measurement Techniques*, 6, 3271-3280, doi:10.5194/amt-6-3271-2013.

Yoon, Y. J., D. Ceburnis, F. Cavalli, O. Jourdan, J. P. Putaud, M. C. Facchini, S. Decesari, S. Fuzzi, K. Sellegri, S. G. Jennings, and C. D. O'Dowd (2007), Seasonal characteristics of the physicochemical properties of North Atlantic marine atmospheric

aerosols, *Journal of Geophysical Research - Atmospheres*, *112*(D04206), doi: 10.1029/2005jd007044.

Chapter 4

Sources and Composition of Submicron Organic Mass in Marine Aerosol Particles

The sources and composition of atmospheric marine aerosol particles (aMAP) have been investigated with a range of physical and chemical measurements from open-ocean research cruises. This study uses the characteristic functional group composition (from Fourier transform infrared, or FTIR, spectroscopy) of aMAP from five ocean regions to show that: (i) The organic functional group composition of aMAP that can be identified as mainly atmospheric primary marine (ocean-derived) aerosol (aPMA) is 65 ± 12% hydroxyl, 21 ± 9% alkane, 6 ± 6% amine, and 7 ± 8% carboxylic acid functional groups. Contributions from photochemical reactions add carboxylic acid groups (15% - 25%), shipping effluent in seawater and ship emissions add additional alkane groups (up

to 70%), and coastal or continental emissions mix in alkane and carboxylic acid groups. (ii) The organic composition of aPMA is nearly identical to model generated primary marine aerosol particles from bubbled seawater (gPMA, which has 55 ± 14% hydroxyl, 32 ± 14% alkane, and 13 ± 3% amine functional groups), indicating that its overall functional group composition is the direct consequence of the organic constituents of the seawater source. (iii) While the seawater organic functional group composition was nearly invariant across all three ocean regions studied and the ratio of organic carbon to sodium (OC/Na) in the gPMA remained nearly constant over a broad range of chlorophyll-*a* concentrations, the gPMA alkane group fraction appeared to increase with chlorophyll-*a* concentrations ($r = 0.66$). gPMA from productive seawater had a larger fraction of alkane functional groups (42 ± 9%) compared to gPMA from non-productive seawater (22 ± 10%), perhaps due to the presence of surfactants in productive seawater that stabilize the bubble film and lead to preferential drainage of the more soluble (lower alkane group fraction) organic components. gPMA has a hydroxyl group absorption peak location characteristic of monosaccharides and disaccharides, where the seawater OM hydroxyl group peak location is closer to that of polysaccharides. This may result from the larger saccharides preferentially remaining in the seawater during gPMA and aPMA production.

4.1 Introduction

Atmospheric marine aerosol particles (aMAP) influence cloud microphysical processes in marine regions [*de Leeuw et al.*, 2011], in addition to scattering and absorbing solar radiation [*Erlick et al.*, 2001] in the marine boundary layer (MBL). aMAP directly scatter incoming solar radiation contributing to a cooling of the surface. Organic constituents mixed with sea salts in aMAP can reduce this cooling effect [*Randles et al.*, 2004]. aMAP also provide cloud condensation nuclei (CCN) over the open ocean [*Clarke et al.*, 2006]. Determining the composition and the sources of the organic fraction of aMAP is important for understanding the degree to which aMAP contributes to the current and future aerosol climate forcing [*Randles et al.*, 2004].

Primary marine aerosol (PMA) particles, also referred to as nascent sea spray aerosol (Table 4.1), are defined as those produced directly at the ocean surface, prior to undergoing chemical reactions or condensational growth in the atmosphere. Breaking waves at the sea surface trap air that then rises as bubbles. At the sea surface, these bubbles burst and their film produces submicron aerosol particles [*Blanchard and Woodcock*, 1980] that contain organic components, in addition to sea salt [*Blanchard*, 1964]. The organic mass (OM) fraction of aMAP has been investigated by numerous analytical methods, each of which has provided an incomplete characterization of aMAP OM composition and its sources (Table 4.2). For example, some studies have focused on the water soluble or water insoluble organic carbon (WSOC and WIOC, respectively) content of submicron aerosol particles. An enrichment in WIOC relative to WSOC has

Table 4.1: Definitions of marine aerosol and relevant seawater terminology.

Term	Definition	Previous Related Usage	Additional Information
Marine Aerosol			
aMAP	atmospheric marine aerosol particles	This Study	See references in Table 4.2
PMA	primary marine aerosol; particles emitted directly from the sea surface	[*O'Dowd and De Leeuw*, 2007; *Long et al.,* 2014]	Sea Spray Aerosol (SSA) [*Quinn et al.,* 2014; and elsewhere]
gPMA	model-generated primary marine aerosol	This Study	nascent SSA [*Quinn et al.,* 2014]; Bubble-mediated marine primary organic aerosol [*Facchini et al.*, 2008]; model-generated PMA (mPMA) [*Long et al.,* 2014]
Four aMAP OM Types[a]			
aPMA	atmospheric PMA particles	This Study	Contains > 70% PMA from seawater and < 30% of other sources.
AMA	aPMA with secondary carboxylic Acid Marine Aerosol particles	This Study	Includes 50-70% aPMA; contains > 10% carboxylic acid groups by mass.
SMA	Shipping influenced Marine Aerosol particles	This Study	Includes > 30% fuel combustion sources in addition < 70% aPMA.
MMA	Mixed and anthropogenic Marine Aerosol particles	This Study	Includes 20-40% each of aPMA, SMA, and AMA.
Seawater			
Productive	Biologically productive seawater in eutrophic conditions	[*Quinn et al.,* 2014]	high biological activity (HBA) [*O'Dowd et al.*, 2004]
Non-productive	Biologically non-productive seawater in oligotrophic conditions	[*Quinn et al.,* 2014] (Oligotrophic)	low biological activity (LBA) [*O'Dowd et al.*, 2004]

[a]Can contain contribution of < 30% from other OM types.

been associated with PMA OM, which was separated from non-marine aerosol based on surface wind direction and speed and black carbon and particle number concentrations at a coastal ground site in Ireland influenced by aerosol from the northeastern Atlantic [*O'Dowd et al.*, 2004]. Measurements of vertical concentration gradients of submicron WIOC at this site were used to infer that measured WIOC was PMA [*Ceburnis et al.*,

2008]. At that same site, *Ovadnevaite et al.* [2011] measured the mass spectral signature of non-refractory aMAP from the North Atlantic and classified the hydrocarbon-like components as PMA, based on their similarity to water insoluble organic mass (WIOM) [*O'Dowd et al.*, 2004]. In addition, collection and extraction of filter samples has enabled quantification of low molecular weight (LMW) saturated fatty acids in aMAP from the North Pacific, which, based on correlations with sea salt, were found to be associated with PMA [*Mochida et al.*, 2002]. Other studies have characterized PMA OM by its functional group composition: in the North Atlantic and Arctic oceans, submicron aMAP OM was identified as largely PMA based on correlation to submicron Na^+ and wind speeds, as well as back trajectories, and was observed to contain carbohydrate-like (saccharide) content [*Hawkins and Russell*, 2010; *Russell et al.*, 2010].

In addition to PMA generated from seawater, aMAP has contributions from (i) photochemical products of atmospheric reactions, (ii) ship effluents in seawater, and (iii) transported coastal and continental emissions from fossil fuel combustion, biogenic, and biomass burning sources. PMA also quickly evolve in the atmosphere due to incorporation and loss of gas phase species. Several studies have focused on characterizing the secondary fraction of organic aerosol particles (SOA) formed through photochemical atmospheric reactions [*O'Dowd et al.*, 2002; *Rinaldi et al.*, 2010; *Facchini et al.*, 2010] (Table 4.2), but more than 22% of the WSOC fraction of aMAP (identified as marine SOA) remains uncharacterized [*Rinaldi et al.*, 2010]. However, the fact that increases in seawater biological activity or phytoplankton productivity (identified by chlorophyll-*a,* chl-*a,* concentration) have been linked to increases in the concentration of both PMA (identified as WIOC) and marine-derived SOA (identified as WSOC)

submicron particles [*Ceburnis et al.*, 2008; *O'Dowd et al.*, 2004] has confounded attempts to clearly distinguish between primary and secondary organic components in aMAP.

Contributions from both (ii) seawater pollution and (iii) air pollution from shipping and continental sources are also challenging to characterize since the marine atmosphere mixes rapidly with non-ocean-derived sources, which then also react with solar radiation and trace gases [*Erickson et al.*, 1999]. Even in the relatively pristine southeastern Pacific, aMAP has been found to have much larger contributions from continental emissions than from PMA OM, the latter of which was frequently below detection [*Hawkins et al.*, 2010; *Shank et al.*, 2012]. Some measurements that met several criteria for being considered "clean marine" at Mace Head, Ireland (including particle concentrations less than 700 cm^{-3}, black carbon less than 50 ng m^{-3}, and surface wind from the North Atlantic Ocean) still contained carbon that isotopic analysis indicated was 21% from non-ocean sources [*Ceburnis et al.*, 2011]. Such results are not surprising given the ubiquity of shipping emissions in many ocean regions [*Coggon et al.*, 2012], as well as continental influences. It is exceedingly difficult to reliably exclude shipping and other anthropogenic influences using criteria that consider only wind direction, trajectory classification, black carbon concentration, or particle concentration. Comprehensive criteria are needed to exclude non-marine sources in order to accurately resolve the PMA portion of aMAP.

An alternative approach to study PMA is to create models of the ocean system in which primary marine aerosol particles are produced by artificially generating bubbles in seawater thereby mimicking sea spray production from wave breaking under controlled conditions [*Bates et al.*, 2012; *Collins et al.*, 2013; *Facchini et al.*, 2008; *Fuentes et al.*,

2010; *Hultin et al.*, 2010; *Keene et al.*, 2007; *King et al.*, 2012; *Martensson et al.*, 2003; *Sellegri et al.*, 2006]. These model-generated primary marine aerosol particles are hereafter referred to as gPMA. The advantage of this approach is that the PMA composition can be studied before it (i) accumulates secondary components or (iii) mixes with shipping or continental emissions. These models have been used to study the organic composition of gPMA for different ocean regions (Table 4.2), providing insight on the size-dependent composition of gPMA. In the northeastern Atlantic, gPMA contained WIOC with lipopolysaccharides [*Facchini et al.*, 2008; *Facchini et al.*, 2010]. Also, the water-extractable OM fraction of gPMA from Sargasso seawater [*Keene et al.*, 2007] and the WIOC fraction of gPMA from northeastern Atlantic seawater [*Facchini et al.*, 2008] increased with decreasing particle size. gPMA from northeastern Pacific seawater were identified to be similar in organic content to polysaccharides and contained a hydrocarbon-like component [*Bates et al.*, 2012]. Using seawater from Scripps pier in a wave flume apparatus, *Ault et al.* [2013] observed a change in the structure of hydrocarbon molecules in the gPMA produced from seawater before and after the addition of a culture of bacteria and phytoplankton.

However, none of these studies have measured the extent to which the observed gPMA composition was controlled by the bulk seawater composition or by the potential OM partitioning that occurs during bubble formation, processing, and bursting that produces PMA. A large fraction of dissolved organic carbon (DOC) in the surface ocean is recalcitrant (less biologically available). In addition, the distribution of much of the DOC is controlled by circulation of deep ocean waters [*Hansell*, 2013; *Druffel et al.*, 1992]. Still, while seawater is generally known to include saccharides that contribute up

Table 4.2: Selected references investigating the organic composition and concentration of PMA, gPMA, secondary, and general aMAP measured in different ocean regions.

Reference	Ocean Region[a]	OM Composition	Particle Size (OM, μg m^{-3})
PMA			
Fu et al., 2013	Arctic	Saccharides	Bulk
Russell et al., 2010	Arctic and N Atlantic	Polysaccharides	Submicron
Hawkins and Russell, 2010	Arctic and SE Pacific	Polysaccharides, proteins, and phytoplankton fragments	Submicron and Supermicron
O'Dowd et al., 2004	NE Atlantic (Ireland)	Enriched in WIOC with high molecular weight	Submicron
Ceburnis et al., 2008	NE Atlantic (Ireland)	WIOC	Submicron
Facchini et al., 2008	NE Atlantic (Ireland)	WIOM	Submicron
Bigg and Leck, 2008	NE Atlantic (Ireland)	Exopolymers	Submicron, < 200 nm
Ovadnevaite et al., 2011	NE Atlantic (Ireland)	Hydrocarbon	Submicron
Mochida et al., 2002	N Pacific	LMW saturated fatty acids	Bulk
Sciare et al., 2009	Austral Ocean	WIOC	Bulk
gPMA			
Facchini et al., 2008	NE Atlantic (Ireland)	WIOM: colloids	Submicron
Facchini et al., 2010	NE Atlantic (Ireland)	WIOM: lipo-polysaccharides	Submicron
Keene et al., 2007	NW Atlantic (Sargasso Sea)	WSOC	Submicron and Supermicron
Schmitt-Kopplin et al., 2012	SE Atlantic	Biomolecules with high aliphaticity	< 10 μm
Bates et al., 2012	NE Pacific (Coastal)	Polysaccharide-like, Alkyl-like, pattern of CH-fragments	Submicron
Ault et al., 2013	NE Pacific (Coastal)	Aliphatic hydrocarbons	0.15-10 μm
Quinn et al., 2014	NE Pacific (Coastal) and NW Atlantic	Saccharide-like	Submicron
Secondary			
Fu et al., 2013	Arctic	Isoprene product	Bulk
O'Dowd et al., 2004	NE Atlantic (Ireland)	Enriched in WSOC (partly oxidized species with extended aliphatic moieties)	Submicron
Ceburnis et al., 2008	NE Atlantic (Ireland)	WSOC	Submicron
Facchini et al., 2008	NE Atlantic (Ireland)	WSOM	Submicron
Facchini et al., 2010	NE Atlantic (Ireland)	Diethyl and dimethyl amine salts	Submicron

Table 4.2 (continued): Selected references investigating the organic composition and concentration of PMA, gPMA, secondary, and general aMAP measured in different ocean regions.

Rinaldi et al., 2010	NE Atlantic (Ireland)	WSOC: MSA, alkylammonium salts, dicarboxylic acids	Submicron
Meskhidze and Nenes, 2006	Southern Ocean	Isoprene product	Bulk
Turekian et al., 2003	NW Atlantic (Sargasso Sea)	Oxalate	Submicron and Supermicron
aMAP[b]			
Cavalli et al., 2004	NE Atlantic (Ireland)	WIOC; aliphatic and partially oxidized humic-like substances	Submicron OC (0.66); Supermicron OC (0.26)
Cavalli et al., 2004	NE Atlantic (Ireland)	WSOC	Submicron 0.25
Kawamura and Gagosian, 1987	N Pacific	Oxo-, mono-, and di-carboxylic acids	Bulk
Matsumoto and Uematsu, 2005	N Pacific	Free amino acids in WSOC	< 2.5 μm
O'Dowd et al., 2004	NE Atlantic (Ireland)	WIOC and WSOC	Total OC (0.07, LBA; 0.62, HBA)
Yoon et al., 2007	NE Atlantic (Ireland)		Total OC (1.2, spring; 0.1, winter) Submicron OC (0.2, spring; 0.05, winter)
Ovadnevaite et al., 2011	NE Atlantic (Ireland)		Submicron (3.8)
Schmitt-Kopplin et al., 2012	SE Atlantic	Biomolecules with high aliphaticity	< 10 μm
Crahan et al., 2004	Tropical Mid-Pacific	Dicarboxylic acids, carbohydrates	< 3.5 μm
Bigg, 2007	SW Pacific (Tasmania)	WIOC aggregates; exopolymeric gels	Submicron, < 200 nm
Shank et al., 2012	SE Pacific	N/A	Submicron (0.01)
Kuznetsova et al., 2005	NW Mediterranean	Proteins, amino acids, and polysaccharide gels	Bulk
Fu et al., 2011	N Pacific, N Atlantic, Indian, South China	LMW fatty acids, fatty alcohols, and sterols	Bulk

[a]The specific stationary sampling locations are in parentheses.
[b]The OM in the studies in this category were not identified as PMA or secondary and are thus included as general atmospheric marine aerosol particles (aMAP).

to 80% of the high molecular weight DOC in seawater [*Aluwihare and Repeta*, 1999; *Aluwihare et al.*, 1997; *Benner et al.*, 1992], the organic composition of the labile and semilabile (more biologically available) DOC will vary with the phytoplankton populations that are present and their metabolic processes that consume and produce organic components [*Hansell*, 2013]. *Hoffman and Duce* [1976] used the ratio of organic carbon (OC) to Na (OC/Na) as a metric for comparing the composition of gPMA and seawater, observing an increase in OC/Na in gPMA from biologically productive seawater. This led them to assert that the chemical form of the organic material could be critical in determining the OC/Na ratio of PMA. Changes in the sea surface biological activity have been shown to alter the surface-active properties of organics and to influence bubble bursting [*Sellegri et al.*, 2006]. But are these changes in seawater organic composition reflected in changes in gPMA (and PMA components of aMAP) or do other factors have a stronger influence?

In this study, we compare the organic composition of gPMA produced by two different model ocean systems with the organic composition of seawater from three ocean regions that were selected to reflect a range of open ocean seawater types: (i) Coastal California in the northeastern Pacific, which is influenced by wind-driven, large-scale upwelling leading to productive or eutrophic (nutrient-rich) seawater and high chl-*a* concentrations (5 ± 4 μg L^{-1}), (ii) George's Bank in the northwestern Atlantic, which is also influenced by nutrient upwelling and eutrophic seawater with phytoplankton productivity and high chl-*a* concentrations (7 ± 2 μg L^{-1}), and (iii) the Sargasso Sea in the subtropical western Atlantic, which is oligotrophic and nutrient-limited, reflected in low phytoplankton productivity and low chl-*a* concentrations (0.03 ± 0.05 μg L^{-1}) (Table 4.1).

In order to provide as complete as possible characterizations of the organic fraction of aMAP, here we use Fourier transform infrared (FTIR) spectroscopy because it provides information about the functional group composition that is characteristic of aMAP [*Russell et al.*, 2010] and represents the marine organic fraction more completely than is possible with techniques that measure non-refractory mass (vaporizable at 650°C) [*Frossard et al.,* 2014]. The three questions that are addressed in this work are: (i) What is the organic functional group composition of ocean-derived aMAP? (ii) How much of aMAP composition can be explained by generating primary marine aerosol (gPMA) from bubbled seawater? and (iii) What are the differences between the organic compositions of gPMA and seawater?

4.2 Methods

The organic functional group composition of submicron aMAP was measured during five shipboard campaigns (Table 4.3). During two of the cruises, gPMA and seawater OM compositions were also measured. The tracks for each campaign are overlaid in Figure 4.1. In this study we use aMAP measurements from all five cruises to provide context, and then we focus on the two campaigns during which aMAP, gPMA, and seawater OM were characterized simultaneously, in regions representing broad ranges in seawater productivity (and chl-*a* concentrations), sea surface temperature, and other air-sea conditions.

4.2.1 Shipboard Campaigns that Sampled Open-Ocean aMAP

aMAP were characterized in the MBL during (i) the International Chemistry Experiment in the Arctic Lower Troposphere (ICEALOT) project in March and April

2008 on board the R/V *Knorr* in the North Atlantic and Arctic Oceans; (ii) the VAMOS Ocean-Cloud-Atmosphere-Land Study Regional Experiment (VOCALS) in October 2008 on board the R/V *Ronald H. Brown* in the southeastern Pacific; (iii) the California research at the Nexus of Air Quality and Climate Change study (CalNex) in May and June 2010 on board the R/V *Atlantis* which traveled from San Diego to Sacramento, CA; (iv) the Eastern Pacific Emitted Aerosol Cloud Experiment (EPEACE) in July 2011 on board the R/V *Point Sur* off the coast of Moss Landing, CA; and (v) the Western Atlantic Climate Study (WACS) in August 2012 on board the R/V *Ronald H. Brown* that traveled from Boston, MA, sampling first at George's Bank (Station 1) and then in the Sargasso Sea (Station 2) before continuing on to St. George's, Bermuda. During ICEALOT, VOCALS, CalNex, and WACS, aMAP were sampled through a humidity and temperature controlled isokinetic, wind-pointing inlet, similar to that described by *Bates et al.* [2002], at ~18 m above sea level; EPEACE used a simple vertical-tube inlet with a lower flow rate for submicron particles [*Russell et al.*, 2013; *Wonaschutz et al.*, 2013]. Additional sampling conditions during each campaign are given in Table 4.3, including average sea surface temperature (SST), seawater chl-*a* concentrations, salinity, air temperature, wind speed, and atmospheric radon concentrations, which is a decay product of crustal material and can be used as a measure of the continental influence of the sampled air masses.

4.2.2 Model Ocean Systems Used for Producing gPMA

During CalNex and WACS, two marine aerosol generators were used to model bubble bursting at the ocean surface: the Sea Sweep and the Bubbler. gPMA were

generated in the biologically productive seawater at WACS Station 1 and CalNex and the non-productive, oligotrophic seawater at WACS Station 2 [*Quinn et al.*, 2014] in order to determine the influence of the phytoplankton productivity on the OM composition of the gPMA.

The Sea Sweep generator consists of a stainless steel frame attached to a small raft that was deployed alongside the R/V *Atlantis* and R/V *Ronald H. Brown* [*Bates et al.*, 2012]. Stainless steel frits were positioned at 0.75 m below the sea surface. While on station and steaming slowly forward to maintain continuous renewal of sea surface water, zero air was pumped through the frits to create bubbles that burst at the seawater surface. The resulting gPMA in sample air were directly transported to the instruments for analysis. A curtain of particle-free air prevented ambient air from mixing with the bubbling seawater.

The Bubbler models the ocean system using a 20-cm-diameter 40 L Pyrex cylinder, into the base of which fresh seawater was pumped at 4 L min^{-1} from the bow of the ship at 5 m below the sea surface [*Keene et al.*, 2007]. Seawater drained to waste evenly over the top annular rim, continuously replacing surface seawater and minimizing the formation of standing bubble rafts [*Long et al.*, 2014]. Bubbles were produced at a mean depth of 84 cm below the model sea surface using zero air pumped through fine or coarse sintered glass frits at varying flow rates (1.5 to 6 L min^{-1}). The Bubbler was also equipped with glass tubes that could be configured to generate gPMA by impinging jets of fresh seawater onto the model sea surface. Purified zero (sweep) air hydrated to 80 (± 2)% relative humidity transferred gPMA under laminar flow to instruments for characterization of number size distributions and size-resolved and bulk chemical

composition. The number size distributions and average compositions of gPMA generated using different production configurations are compared in Figure 4.12 of Section 4.6.

Table 4.3: The seawater and ambient atmospheric sampling conditions during the collection of the marine samples during the five projects given as the average and standard deviation of the marine samples. Salinity, temperature, and wind speed are abbreviated as Sal., T, and WS, respectively.

			Submicron aMAP		Seawater Characteristics			Atmospheric Conditions		
Project (Sample Numbers)	Sampling Period	Ocean	OM ($\mu g\ m^{-3}$)	O/C	SST (°C)	Chl-*a* ($\mu g\ L^{-1}$)	Sal.	T (°C)	WS ($m\ s^{-1}$)	Radon ($mBq\ m^{-3}$)
ICEALOT (13)	19 Mar. - 24 Apr. 2008	N Atl., Arctic	0.44 ± 0.21	0.96 ± 0.26	6 ± 3	N/A	34.7 ± 0.5	1 ± 7	11 ± 4	315 ± 108
VOCALS (12)	20 Oct. - 30 Nov. 2008	SE Pacific	0.40 ± 0.17	0.56 ± 0.11	19 ± 1	N/A	35.0 ± 0.1	13 ± 1	7 ± 2	106 ± 75
CalNex (8)	15 May - 7 Jun. 2010	NE Pacific	0.71 ± 0.36	0.52 ± 0.22	14 ± 1	5.0 ± 4.0	33.2 ± 0.2	13 ± 1	5 ± 2	811 ± 664
EPEACE (38)	12 Jul. - 24 Jul. 2011	NE Pacific	0.62 ± 0.48	0.61 ± 0.38	14 ± 1	0.4 ± 0.6	33.5 ± 0.2	14 ± 1	13 ± 5	N/A
WACS (11)	19 Aug. - 28 Aug. 2012	NW Atl.	1.23 ± 1.29	0.60 ± 0.34	27 ± 4	0.8 ± 2.3	35.4 ± 1.5	26 ± 4	4 ± 2	301 ± 365
(3)		St 1	1.81 ± 1.79	0.87 ± 0.30	19 ± 3	3.6 ± 2.7	32.4 ± 0.4	19 ± 2	2 ± 1	725 ± 88
(8)		St 2	1.14 ± 1.04	0.50 ± 0.31	28 ± 1	0.1 ± 0.1	35.9 ± 0.4	27 ± 1	5 ± 2	233 ± 322

4.2.3 Aerosol and Related Measurements

4.2.3.1 Chemical Analysis of Particles Collected on Filters

Submicron aMAP and gPMA were dried by a diffusion dryer filled with silica gel on EPEACE and WACS and by a temperature and humidity controlled inlet on ICEALOT, VOCALS, and CalNex before collection on 37 mm Teflon filters (Pall Inc., 1 μm pore size) at a flow rate of 8 L min^{-1} for 1 to 20 hrs. The filters were frozen and

transported to San Diego for analysis by Fourier transform infrared (FTIR) spectroscopy (Bruker Tensor 27 spectrometer) [*Frossard et al.*, 2011; *Hawkins et al.*, 2010]. The Bubbler gPMA from CalNex were not size selected before collection and were dried after collection (before analysis). During WACS and EPEACE, FTIR scans were carried out on board the research vessel prior to freezing, to evaluate possible effects of transport and storage; no artifacts from storage were identified in either the OM composition or concentration.

During CalNex and WACS, unfiltered seawater was collected from the sampling regions in sterile glass mason jars, atomized (TSI constant output atomizer 3076), and then collected on Teflon filters without a cyclone. The gPMA samples and atomized seawater samples were dehydrated using the procedure outlined by *Frossard and Russell* [2012] to remove interference of sea salt hydrate bound water with the organic signal in the FTIR spectra.

The FTIR spectrum from each filter was baselined and integrated at specific peak locations to determine the peak areas of the organic functional groups using an automated algorithm [*Maria et al.*, 2002; *Russell et al.*, 2009; *Takahama et al.*, 2012]. The absorptivity and molar mass were used to convert peak area to mass for each organic functional group including: organic hydroxyl (C-O-H), alkane (C-C-H), amine (C-N-H), carboxylic acid (COOH), and non-acid carbonyl (C=O). Alkene (C=C-H) and aromatic functional groups were below the detection limit in all of the samples and are excluded from this discussion. The total OM analyzed in each sample was calculated as the sum of the concentrations of the organic functional groups. The OM measured by this technique has an uncertainty of 20% [*Maria et al.*, 2002; *Takahama et al.*, 2013], indicating that up

to 20% of the OM may not have been characterized. This 20% could consist of functional groups that were below detection by FTIR spectroscopy but have been previously observed in marine regions, such as amide and carboxylic acid groups. The molar ratio of oxygen to carbon (O/C) was calculated by summing the moles of oxygen in oxygen-containing functional groups (hydroxyl, carboxylic acid, and non-acid carbonyl) and dividing by the total moles of carbon in all observed functional groups for each sample [*Russell et al.*, 2009]. Converting the total moles of carbon to mass gives the total organ carbon (OC) mass of the samples. After non-destructive FTIR analysis, X-ray fluorescence (XRF; Chester LabNet, Tigard, OR) was used to quantify the elemental masses for elements Na and heavier on the filters [*Maria et al.*, 2003] sampled during ICEALOT, VOCALS, and EPEACE.

Submicron aMAP and Sea Sweep gPMA were also collected with a Berner-type multijet cascade impactor during ICEALOT, VOCALS, CalNex, and WACS. Particles were impacted on Millipore Fluoropore filters and the substrates from these filters were extracted and analyzed using ion chromatography to quantify inorganic ions including Na^+, Cl^-, SO_4^{2-}, NO_3^-, and NH_4^+ [*Quinn et al.*, 1998].

Sea salt concentrations were calculated using IC measurements for ICEALOT, VOCALS, CalNex, and WACS and XRF measurements for EPEACE. For the gPMA, sea salt concentration equals 3.26 times the Na^+ mass, based on the calculation by the ratio of ($Na^+ + Mg^{2+} + Ca^{2+} + K^+ + Cl^- + SO_4^{2-} + HCO_3^-$) / Na^+ in seawater [*Holland*, 1978]. Atmospheric ambient sea salt concentrations were calculated using measured Cl^- and 1.47*Na^+ concentrations, to account for the possible depletion of Cl^- in the atmosphere, where 1.47 is the ratio of ($Na^+ + Mg^{2+} + Ca^{2+} + K^+ + SO_4^{2-} + HCO_3^-$)/ Na^+ in seawater

[*Holland*, 1978]. This sea salt calculation represents an upper limit for sea salt mass because the HCO_3^- would have been titrated before Cl^- was depleted significantly via acid displacement reactions. HCO_3^- is 0.3% of the total mass of sea salt. Excluding HCO_3^- from the ratio, as a lower limit, the ratio of $(Na^+ + Mg^{2+} + Ca^{2+} + K^+ + SO_4^{2-} + HCO_3^-)/ Na^+$ is 1.45, instead of 1.47, making the salt mass calculated < 2% lower than calculated here.

4.2.3.2 Single Particle Measurements

During CalNex and WACS, aMAP (0.39 – 2.6 μm) and gPMA (0.65 – 3.1 μm) were collected on silicon nitride windows (Si_3N_4, Silson Ltd, Northampton, England) using a Streaker impactor (PIXE International Corp., Tallahassee, FL). The windows were frozen after collection to prevent evaporation. Particles were collected for 30 to 90 min, depending on the particle number concentrations. The windows were analyzed at the Advanced Light Source at Lawrence Berkeley National Laboratory using Scanning Transmission X-ray Microscopy with Near Edge X-ray Absorption Fine Structure (STXM-NEXAFS) to determine the morphology and organic composition of the single particles [*Hawkins and Russell*, 2010; *Takahama et al.*, 2007; *Takahama et al.*, 2010].

4.2.3.3 Other Measurements

Meteorological parameters that were measured include temperature, wind speed, wind direction, and solar radiation. Measured seawater parameters include salinity, sea surface temperature (SST), and fluorescence (relative chl-*a* concentrations). The continuous fluorescence signal for each cruise was calibrated for chl-*a* concentration

using discrete samples of seawater collected during the cruise and a commercially available chl-*a* standard [*Bates et al.*, 2012].

4.3 Results

This study focuses on "marine" aerosol particles, where we use "marine" to mean ocean sources that meet the three criteria discussed in Section **4.**3.1. In this sense, "marine" includes both natural emissions from the pristine open-ocean as well as man-made emissions from ocean-based activities, such as shipping, and some coastal (or other continental) anthropogenic emissions. This section summarizes and classifies the measured composition of the samples that meet this definition of aMAP and compares the composition of gPMA and seawater OM.

4.3.1 Classification of aMAP

Three criteria were used to distinguish aMAP from non-marine aerosol particles. First, aMAP samples collected within 1 km of a port or land were excluded. Second, sampling was controlled using automated valves to suspend sampling during periods when particle concentrations (generally greater than 1000 cm^{-3}) indicated the presence of ship exhaust. This conditioned sampling excluded sampling of direct emissions of nearby ships and of the research vessel itself. Third, only samples with air mass back trajectories, calculated using the isentropic Hybrid Single Particle Lagrangian Integrated Trajectory (HYSPLIT) model [*Draxler and Rolph*, 2003], of predominantly marine origin (3-day back trajectories that originated from over the ocean and spent more than 75% of the sampling time over the ocean) were considered to be "marine" for this analysis.

Additional project-specific criteria used in the aMAP sample selection are included in Section 4.6.1. All of the aMAP samples discussed here met all three of these criteria.

4.3.2 Comparison of aMAP OM From Five Marine Regions

The mean organic compositions of submicron aMAP measured by FTIR spectroscopy during five research cruises are shown in Figure 4.1b. During CalNex the submicron aMAP OM concentrations ranged from 0.13 to 1.45 μg m^{-3} and averaged 0.71 (± 0.36) μg m^{-3} (Table 4.3). The aMAP OM had an average functional group composition of 23 (± 15)% hydroxyl, 48 (± 12)% alkane, 3 (± 3)% amine, and 26 (± 11)% carboxylic acid (Figure 4.1b). The CalNex samples have higher alkane and carboxylic acid functional group fractions than previous measurements of OM identified as PMA (10-15% and less than 10%, respectively) [*Russell et al.*, 2010] and have the highest average fraction of alkane functional groups compared to the other projects analyzed in this study (Figure 4.1b). The average ratio of O/C for the submicron aMAP OM during CalNex was 0.52, indicating that the marine OM was also highly oxygenated.

During EPEACE, the concentration of submicron aMAP OM ranged from 0.06 to 1.09 μg m^{-3} with an average of 0.62 (± 0.48) μg m^{-3} (Table 4.3). The mean OM composition was 41 (± 15)% hydroxyl, 43 (± 23)% alkane, 3 (± 6)% amine, and 13 (± 15)% carboxylic acid functional groups, but the composition varied substantially in the FTIR spectra of the EPEACE samples (Figure 4.1b). The wind speed during sampling ranged from 5 to 24 m s^{-1} with an average of 13 (± 5) m s^{-1}, which is sufficiently high enough for wave breaking and active production of PMA. The chl-*a* concentration varied from 0.4 μg L^{-1} to 2.6 μg L^{-1}. The seawater salinity was relatively constant (with an

average and standard deviation of 33.5 ± 0.2), as was the air temperature (14 ± 1 °C) and the SST (14 ± 1 °C) (Table 4.3).

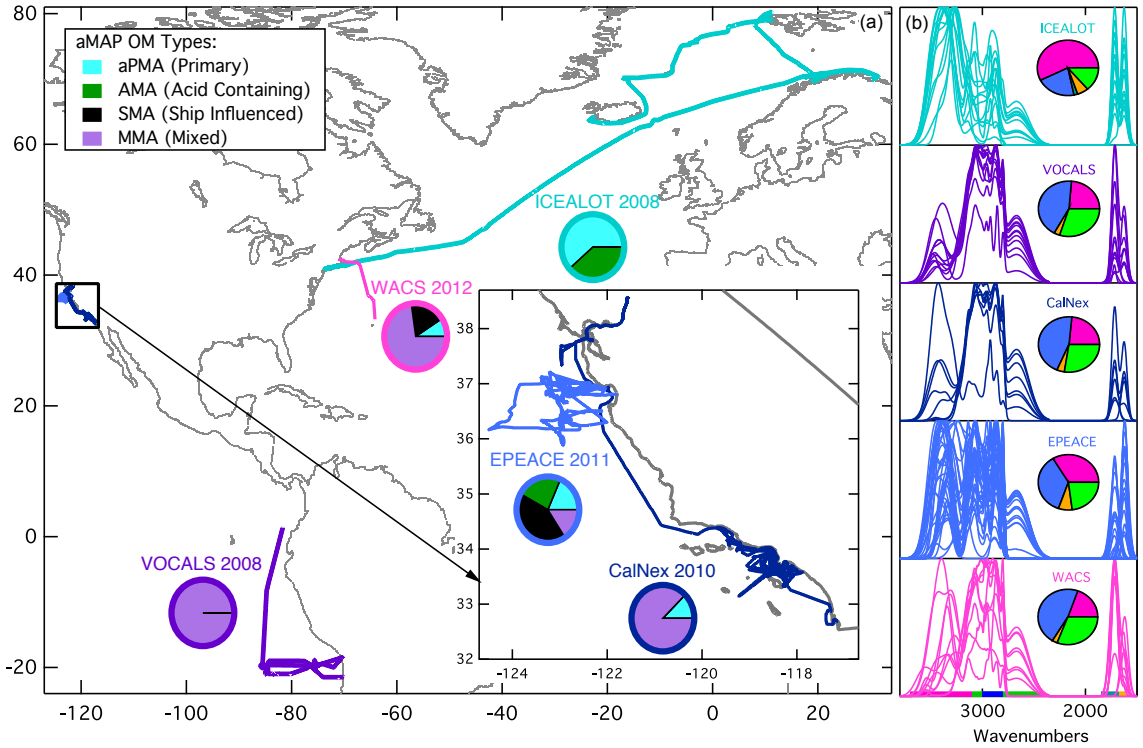

Figure 4.1: (a) Map of the cruise tracks for ICEALOT, VOCALS, CalNex, EPEACE, and WACS. The pie charts at each location represent the fraction of samples associated with each aMAP OM type shown in the legend. (b) Comparison of the normalized organic FTIR spectra of the marine samples from the five projects. The pie charts represent the corresponding mean organic functional group compositions with hydroxyl (pink), alkane (blue), carboxylic COH (green), carbonyl (teal), and amine (orange).

During the WACS cruise (Figure 4.1a), submicron aMAP OM was 1.23 (± 1.29) µg m^{-3} with a mean composition of 21 (± 16)% hydroxyl, 50 (± 20)% alkane, 3 (± 2)% amine, and 26 (± 21)% carboxylic acid functional groups (Figure 4.1). Submicron aMAP OM was sampled during two periods with distinct atmospheric and seawater properties (Table 4.3). The more biologically productive seawater of Station 1 had higher average chl-*a* concentrations (3.6 ± 2.7 µg L^{-1}), which were variable but stayed well above

oligotrophic seawater concentrations (0.1 μg L^{-1}). The air temperature (19 ± 2 °C), SST (19 ± 3 °C), and salinity (32.4 ± 0.4) were lower than Station 2. The average OM was higher at Station 1 (1.81 ± 1.79 μg m^{-3}), and the average composition was 17 (± 4)% hydroxyl, 35 (± 12)% alkane, 3 (± 3)% amine, and 48 (± 8)% carboxylic acid functional groups. The oligotrophic, non-productive seawater at Station 2 is warmer (28 ± 1 °C) and saltier (35.9 ± 0.4). The air temperature was also higher (27 ± 1 °C), and the region was non-productive with little variability in the low average chl-*a* concentration of 0.06 (± 0.08) μg m^{-3}. The average OM was 1.14 (± 1.04) μg m^{-3} with a mean composition of 22 (± 19)% hydroxyl, 53 (± 19)% alkane, 3 (± 3)% amine, and 23 (± 19)% carboxylic acid functional groups.

During VOCALS, aMAP were collected in the southeastern Pacific (Figure 4.1a). The average submicron aMAP OM was 0.40 (± 0.17) μg m^{-3} (Table 4.3). The average OM composition was 24 (± 7)% hydroxyl, 43 (± 7)% alkane, 2 (± 2)% amine, and 30 (± 5)% carboxylic acid functional groups (Figure 4.1b).

Submicron aMAP OM was sampled during ICEALOT in the North Atlantic and Arctic oceans (Figure 4.1a). The average aMAP OM was 0.44 (± 0.21) μg m^{-3} (Table 4.3), and the average composition included 58 (± 13)% hydroxyl, 21 (± 9)% alkane, 2% carbonyl, 6 (± 3)% amine, and 14 (± 8)% carboxylic acid functional groups (Figure 4.1b). The average SST during ICEALOT was 6 (± 3) °C, lower than CalNex, EPEACE, VOCALS, or WACS.

4.3.3 Source Identification of atmospheric Marine Aerosol Particles (aMAP) OM

Ward cluster analysis [*Ward*, 1963] was used to classify the individual FTIR spectra of submicron aMAP OM collected during all of the projects. Results yielded four clusters of samples (Figure 4.2), each of which differs from the others in that the cosine similarities of the characteristic spectra to each other are lower (by 0.1) than the cosine similarity of the spectra within each cluster (additional details in Section 4.6.2). Based on the atmospheric and seawater conditions, locations during sampling, and spectral features, these aMAP OM types were characterized as: (i) atmospheric primary marine aerosol particles (aPMA); (ii) carboxylic acid-containing primary marine aerosol particles (AMA); (iii) shipping-influenced marine aerosol particles (SMA); and (iv) mixed and other anthropogenically-influenced marine aerosol particles (MMA). Of these four aMAP types, only aPMA and AMA are considered "clean" in the sense of being derived from the natural ocean (with AMA also including atmospheric contributions that may be from ocean-derived biogenic volatile organic compounds, such as the photochemical products of isoprene, but may also include photochemical products of man-made volatile organic compounds). While all four aMAP OM types are marine, based on the selection criteria in Section 4.3.1, SMA and MMA have compositions and OM spectral signatures indicative of anthropogenic sources (typically incomplete fossil fuel combustion), as described in later sections. Since individual atmospheric samples generally include contributions from more than one source, this classification categorizes samples based on the source that contributes the majority of the OM and denotes as MMA samples for

which multiple OM types each contributed, as summarized in Table 4.1. For example, aPMA contained an average of 65% by mass of hydroxyl functional groups, which are likely to be entirely primary OM from biogenic ocean sources [*Russell et al.*, 2010]. AMA, SMA, and MMA OM types all have some aPMA contribution, and, in addition, they contain OM contributions from carboxylic acid, shipping, or mixed sources. Consequently, each of these four aMAP OM sample types contains one or more source contributions, and the clustering identifies either the lack of substantial contributions (<30%) from anything but ocean-derived biogenic sources in the case of aPMA, or the mixture of aPMA sources with carboxylic acid (AMA), shipping (SMA), or multiple other mixed sources (MMA). The fraction of organic mass associated with these source types was tested by creating artificial mixtures with varying quantities of the aMAP OM types and re-executing the clustering algorithm. The four aMAP OM types and their production processes are shown in Figure 4.3, in addition to their relation to gPMA. A description of each OM type and the basis for each classification are given in the following paragraphs.

The atmospheric primary marine aerosol particles (aPMA) have an average OM of 0.45 μg m^{-3} and a functional group composition of 65 (± 12)% hydroxyl, 21 (± 9)% alkane, 6 (± 6)% amine, and 7 (± 8)% carboxylic acid (Figure 4.2a), where the variability is indicated as one standard deviation (Table 4.4). This OM type was present during 23% (17 samples) of the total sampling time included in this study and was observed during ICEALOT, EPEACE, CalNex, and WACS but not during VOCALS (Figure 4.1a). aPMA was more frequently identified during high wind speeds, typically 5 to 24 m s^{-1} with an average of 13 m s^{-1}. All but two of the samples had average wind speeds greater than 7.3

m s^{-1}, and all of the samples contained periods with wind speeds greater than 10 m s^{-1}, which allowed for sufficient wave breaking (wind speeds greater than 8 m s^{-1}) and bubble bursting [*Gantt et al.*, 2011]. The wind speed correlates with submicron Na concentrations (r = 0.70), consistent with a wind-driven source such as aPMA production. This is also consistent with previous studies that have shown a correlation between wind speed and PMA production in the open ocean [*Nilsson et al.*, 2001]. Eight of the 17 aPMA samples were collected at high latitude during ICEALOT at relatively high wind speeds, low temperatures, and low solar radiation, supporting the primary nature of this OM.

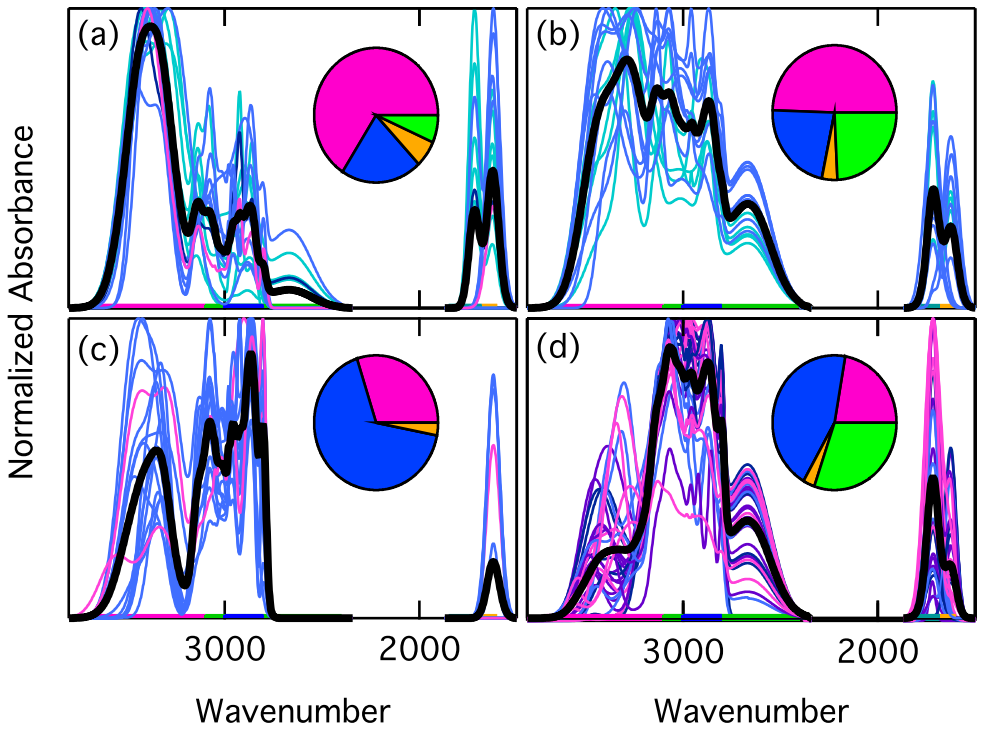

Figure 4.2: Normalized FTIR spectra of submicron aMAP separated into four marine OM types: (a) aPMA, (b) AMA, (c) SMA, and (d) MMA. Thick black lines are the average spectra of each OM type. Individual spectra are colored by project including ICEALOT (teal), VOCALS (purple), CalNex (dark blue), EPEACE (light blue), and WACS (pink). Pies represent the average functional group composition of each OM type with hydroxyl (pink), alkane (blue), carboxylic COH (green), and amine (orange) functional groups.

The average Na/Cl ratio for samples in the aPMA OM type is 0.74 (± 0.15), which is higher than the Na/Cl mass ratio of seawater (0.56) [*Lewis and Schwartz*, 2004], likely due to Cl depletion by acid displacement [*Buseck and Posfai*, 1999; *Keene et al.*, 1998; *Lewis and Schwartz*, 2004; *Pszenny et al.*, 1993]. The aPMA Na/Cl ratio is within 25% of the Na/Cl ratio of seawater, and the lower values fall close to the ratio for seawater, consistent with this OM being classified as largely primary from a seawater source. The similarity of the Na/Cl ratio in the aPMA to that of seawater indicates that little Cl has been depleted since emission into the atmosphere.

The second clean marine OM type was identified as carboxylic acid-containing primary marine aerosol particles (AMA), namely marine OM that includes more than 10% carboxylic acid functional groups by mass. AMA has an average composition of 49 (± 6)% hydroxyl, 24 (± 7)% alkane, 4 (± 4)% amine, and 22 (± 6)% carboxylic acid functional groups (Figure 4.2b), and the ranges represent the variability as one standard deviation (Table 4.4). This OM type was observed during 14% of the total sampling time (14 of the samples) in this study, and only during ICEALOT and EPEACE (Figure 4.1a), both of which had frequent boundary layer clouds. The sampling conditions were similar to the aPMA OM type conditions but had slightly lower average wind speeds (11 m s^{-1}) that were still sufficient for local wave breaking and hence for PMA production. The Na/Cl ratio is similar to the aPMA (0.80 ± 0.20), consistent with aerosol particles that have not been depleted in Cl.

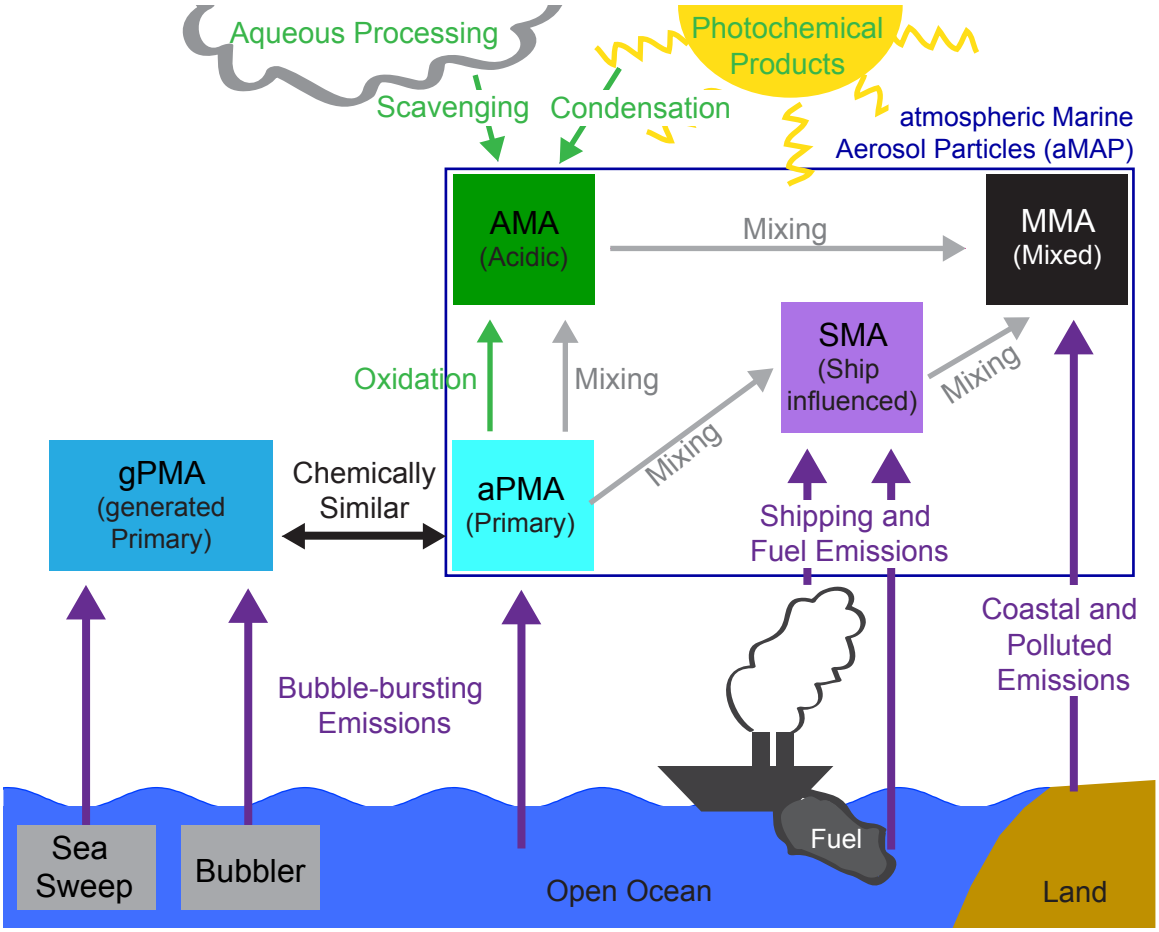

Figure 4.3: Diagram illustrating the categories of marine aerosol types used in this paper: generated marine aerosol particles (gPMA), atmospheric primary marine aerosol particles (aPMA), aPMA with secondary carboxylic acid marine aerosol particles (AMA), shipping influenced marine aerosol particles (SMA), and mixed and anthropogenic marine aerosol particles (MMA). aPMA, AMA, SMA, and MMA are the four aMAP OM types. These mixing arrows show the contribution of aPMA to the other three OM types. Additionally, aPMA may contain up to 30% of other sources.

The third OM type was identified as shipping influenced marine aerosol particles (SMA) OM and contains 31 (± 5)% hydroxyl, 66 (± 6)% alkane, and 3 (± 6)% amine functional groups (Figure 4.2c, Table 4.4). This SMA was observed during 11% of the total sampling time (18 samples), mainly as part of EPEACE and WACS (Figure 4.1a). During WACS, one of the two SMA samples was collected near (approximately 100 km) the port of Bermuda. The spectra of the SMA OM type have features indicative of a long

chain alkane-type species with absorption peaks at 2981, 2956, 2923, 2865, 2804 cm^{-1}. The peaks at 2923 and 2865 cm^{-1} represent repeating unsaturated CH_2 groups [*Pavia et al.*, 2001]. These signatures have been observed in FTIR spectra of ship diesel and other fuels prior to combustion [*Guzman-Morales et al.*, 2013] and direct ship stack emissions [*Wonaschutz et al.*, 2013]. The similarity between the SMA spectrum and a spectrum of gPMA added to a ship diesel spectrum illustrates the likely contribution of alkane-rich fuel and shipping emissions to the SMA OM (Figure 4.4a). The SMA OM has the highest average fraction of alkane functional groups (66% ± 6%) compared to the other marine OM types (Table 4.4) and has a significantly larger alkane functional group fraction than aPMA (21 ± 9%) and AMA (24 ± 7%). SMA also contains no carboxylic acid functional groups (Figure 4.2), which indicates that these particles did not have detectable contributions from aqueous or photochemical processing. Also, the fuel signatures could originate from incorporation of ship effluent in surface seawater, which is then transferred to the aerosol particles via PMA production. The average fractions of hydroxyl and amine functional groups, 30% and 3%, respectively, likely indicate a contribution from organic aPMA. The corresponding wind speeds during these sampling times had an average of 11 m s^{-1}, which is fast enough to produce PMA from ambient bubble bursting.

The last type of aMAP OM was identified as mixed and other anthropogenically-influenced marine aerosol particles (MMA) due to the evidence for contributions of aPMA, AMA, and SMA, as well as continental sources, in varying amounts (Figure 4.4b). MMA composition was 23 (± 7)% hydroxyl, 45 (± 13)% alkane, 2 (± 2)% amine, and 30 (± 11)% carboxylic acid functional groups, with an average OM of 0.53 μg m^{-3}

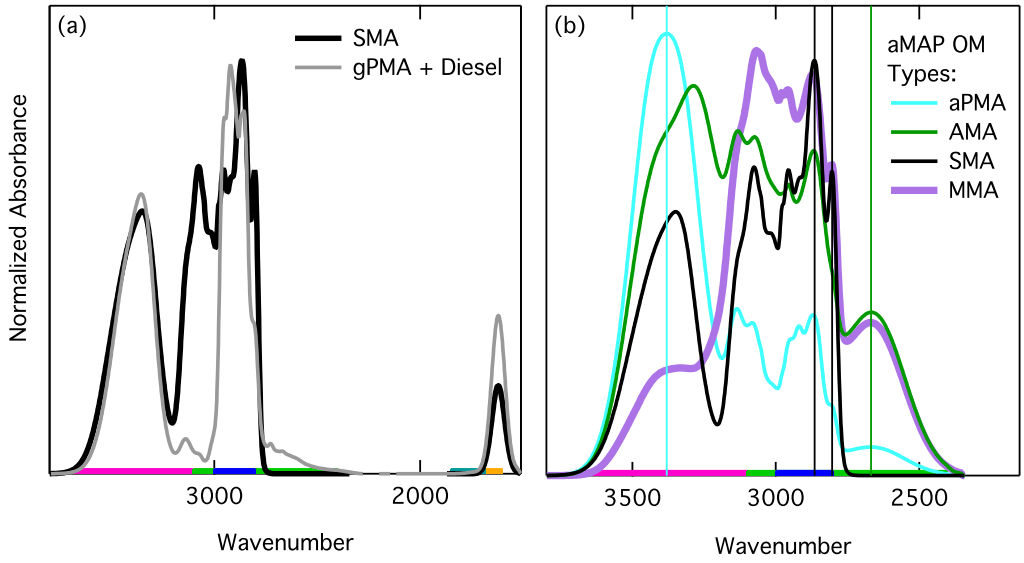

Figure 4.4: Normalized FTIR spectra of (a) SMA and gPMA with ship diesel and (b) the four aMAP OM types. The spectral similarities are shown with vertical lines in (b) at the aPMA max hydroxyl group peak location (3380 cm^{-1}), the SMA alkane group signatures (2865 and 2804 cm^{-1}), and the AMA carboxylic acid group peak (2668 cm^{-1}).

(Figure 4.2d, Table 4.4). Thirty-three of the aMAP samples are MMA, which corresponds to 51% of the total sampling time in this study. MMA was observed during VOCALS, CalNex, EPEACE, and WACS (Figure 4.1a). The composition and spectrum of this OM type have features of the other three aMAP OM groups, including: (i) a similar average hydroxyl group peak location (3380 cm^{-1}) to aPMA (3377 cm^{-1}), within the method uncertainty of ± 6 cm^{-1} for hydroxyl group peak location (measured with replicates of atomized ribose standards [*Takahama et al.*, 2013]), (ii) alkane functional group double peaks at 2957 and 2806 cm^{-1} similar to SMA (2956 and 2804 cm^{-1}), within the method uncertainty of ± 3 cm^{-1} for alkane group peak location, and (iii) a carboxylic acid functional group fraction (30 ± 11%) within the measured variability of the carboxylic acid functional group fraction of AMA (22 ± 6%) (Figure 4.4b). The MMA OM includes VOCALS samples that were previously identified as "polluted marine"

[*Hawkins et al.*, 2010]. In addition, the CalNex samples in this type were sampled close to the California coast, consistent with the possible contribution of continental sources. These samples were collected during the lowest average wind speed periods (7 m s^{-1}), suggesting that there was little local production that contributed to aPMA from bubble bursting (consistent with the lower sea salt concentration of less than 0.1 μg m^{-3}, compared to aPMA which had more than 1 μg m^{-3}). The high Na/Cl ratio (2.6 ± 1.3), in the absence of crustal sources of Na, is likely the result of Cl depletion by acid substitution in seawater-derived NaCl. The high level of depletion of Cl in the MMA (relative to aPMA or AMA) is consistent with atmospheric reactions in particles that have more inorganic acid present (relative to aPMA or AMA), which is more likely associated with anthropogenic sources of NO_3^- (such as NO_x from combustion) associated with either shipping or other continental fossil fuel burning sources (consistent with the presence of multiple source types in MMA). The average spectrum of MMA OM is similar to spectra observed from continental and anthropogenic sources, such as the oxidized fossil fuel combustion source identified by *Guzman-Morales et al.* [2013] using positive matrix factorization (PMF) during CalNex. The 7 CalNex samples in this OM type all have characteristic absorption similar to that of oxidized combustion sources, indicating one contribution to MMA in CalNex is oxidized fossil fuel combustion emissions.

The number of samples of each aMAP OM type for the individual projects is shown in Figure 4.1a. During CalNex, of the 8 aMAP samples, only 1 was determined to be aPMA, while the other 7 were MMA, indicating that during the CalNex sampling, close to the coast of California, there was very limited time in which polluted marine

(continental or ship) emissions did not impact the OM composition. The EPEACE aMAP OM included 7, 9, and 6 of the samples in the aPMA, AMA, and MMA OM types, respectively, as well as 16 samples identified as SMA. This large number of SMA samples is consistent with the large contribution of shipping emissions to the aMAP OM in the northeastern Pacific [*Coggon et al.*, 2012]. During WACS, 1 of the 11 samples was determined to be the aPMA OM type, while 2 were SMA, and 8 were MMA OM. All of the 12 aMAP samples from VOCALS were determined to be MMA OM, with no clean marine OM observed during this sampling period. The ICEALOT sampling region contained only samples identified as clean aMAP OM with 8 aPMA and 5 AMA samples.

4.3.4 Organic Composition of gPMA

Sea Sweep and Bubbler gPMA generated during CalNex and WACS were similar in composition with large fractions of hydroxyl, some alkane, and small fractions of amine functional groups, with an overall average composition of 55 (± 14)% hydroxyl, 32 (± 14)% alkane, and 13 (± 3)% amine functional groups (where the ranges represent the observed variability as one standard deviation, as shown in Table 4.4). No detectable carboxylic acid functional group mass was observed in any of the gPMA samples. The Sea Sweep flow rates were not comparable to the Bubbler, so the comparison between the two model ocean systems is based on the relative fractions of organic components in the gPMA rather than the absolute concentrations. During WACS, the Sea Sweep gPMA showed a higher average OC/Na ratio produced at Station 1 (productive) than at Station 2 (non-productive) with 0.28 (± 0.13) and 0.17 (± 0.13), respectively, but the difference

between the two stations (0.09) is smaller than the variability within each station (0.13), as reported by *Quinn et al.* [2014]. The Bubbler used a controlled air flow rate that was varied from 1.5 to 6 lpm (see Section 4.6.4). At the same flowrate (4 lpm), the Bubbler gPMA had an OC/Na of 0.51 (± 0.06) in productive (Station 1) seawater and 0.19 (± 0.06) in oligotrophic (Station 2) seawater. While the station-to-station difference of 0.32 for the Bubbler gPMA samples is larger than for the Sea Sweep, the limited number of samples collected at 4 lpm (N = 4; 2 at each station) constrains the resolution with which this result can be generalized.

At WACS Station 1, the Sea Sweep gPMA (N = 8) had a mean composition and standard deviation of 43 (± 11)% hydroxyl, 43 (± 10)% alkane, and 14 (± 4)% amine functional groups. At WACS Station 2 (N = 4), the hydroxyl group fraction increased to 58 (± 11)%, the alkane group fraction decreased to 29 (± 11)%, and the amine fraction was quite similar at 12 (± 1)%. A similar difference in composition was observed in the Bubbler gPMA for the two sampling regions, with a composition of 51 (± 2)% hydroxyl, 39 (± 3)% alkane, and 10 (± 2)% amine groups at WACS Station 1 (N = 2) and 70 (± 7)% hydroxyl, 18 (± 8)% alkane, and 12 (± 4)% amine at Station 2 (N = 6). During CalNex, the Sea Sweep gPMA (N = 6) had an average composition of 47 (± 14)% hydroxyl, 38 (± 13)% alkane, and 15 (± 3)% amine functional groups, while the Bubbler gPMA (N = 8) had a composition of 42 (± 9)% hydroxyl, 44 (± 8)% alkane, and 14 (± 3)% amine functional groups.

Bubbler and Sea Sweep gPMA samples that overlapped in time and location are compared for the two projects in Figure 4.8 (see Section 4.6.3 for the samples selected). Using these collocated samples, at WACS Station 1, the Sea Sweep gPMA (N = 3) had a

mean composition and standard deviation of 54 (± 4)% hydroxyl, 34 (± 3)% alkane, and 12 (± 1)% amine functional groups. At WACS Station 2 (N = 2), the hydroxyl group fraction increased to 67 (± 8)%, the alkane group fraction decreased to 21 (± 7)%, and the amine fraction was quite similar at 12 (± 1)%. The same difference in composition was observed in the Bubbler gPMA for the two sampling regions, with a composition of 51 (± 2)% hydroxyl, 39 (± 3)% alkane, and 10 (± 2)% amine groups at WACS Station 1 (N = 2) and 73 (± 6)% hydroxyl, 14 (± 2)% alkane, and 14 (± 4)% amine at Station 2 (N = 3). During CalNex, the Sea Sweep gPMA (N = 5) had an average composition of 51 (± 10)% hydroxyl, 34 (± 8)% alkane, and 14 (± 3)% amine functional groups, while the Bubbler gPMA (N = 4) had a composition of 47 (± 7)% hydroxyl, 39 (± 7)% alkane, and 14 (± 1)% amine functional groups.

The difference (42% versus 22%) in alkane group fraction of the combined Sea Sweep and Bubbler gPMA measured at WACS Station 1 and Station 2 is comparable to the variability (± 9% and ± 13%) at each station; the difference (35% versus 16%) is more significant when only the collocated samples at each station are compared as the variability for those samples is less (± 6% and ± 4%). The collocated samples may reflect local, short-term trends that are masked by averaging over the longer times and wider regions that were sampled during the entire cruise. Hence, it is also true that for the wider range of seawater sampled by the entire 9-day cruise, the average Sea Sweep gPMA OM alkane fraction for the two stations were closer to each other than the variability that was sampled, as noted by *Quinn et al.* [2014]. Nonetheless, this investigation should be considered exploratory, as only 3 days of sampling at each site is not sufficient to

establish whether these local differences are characteristic of broader temporal and spatial scales.

4.3.5 aMAP and gPMA Single Particle Composition

STXM-NEXAFS spectra of aMAP and gPMA single particles collected during WACS and CalNex were sorted into two OM types with those spectra containing oxidized groups (i.e. carboxylic carbonyl and alcohol) as a high O/C particle type and those containing only absorption in the alkyl region in the low O/C particle type (following the classification of *Frossard et al.,* [2014]). The high O/C particles were further separated into those that contained spectral features and morphology similar to the polysaccharides on sea salt particles observed by *Russell et al.* [2010] and *Hawkins and Russell* [2010] and those that were uniformly organic throughout the particle. The WACS aMAP studied by STXM-NEXAFS consisted of 13 high O/C particles each associated with sea salt, 4 high O/C particles (without sea salt contributions in the individual particles), and 1 low O/C particle (without sea salt). These particles had geometric diameters that ranged from 0.39 to 2.6 μm [*Frossard et al.,* 2014]. Together, the Sea Sweep and Bubbler gPMA during WACS was made up of 29 high O/C particles and 25 low O/C particles.

4.3.6 Seawater OM Functional Group Composition

Seawater OM measured during CalNex (N = 4) and WACS Station 1 (N = 3) and Station 2 (N = 3) had similar mean compositions with 70 (± 1)%, 72 (± 6)%, and 74 (± 2)% hydroxyl, 17 (± 7)%, 18 (± 3)%, and 15 (± 2)% alkane, and 12 (± 7)%, 10 (± 7)%, and 11 (± 1)% amine functional groups, respectively. The seawater OM samples

collected during WACS Station 1 at 27.2 m (N = 1) and Station 2 at 2500 m (N = 1) are also similar in composition to the near-surface seawater (5 m), both with 69% hydroxyl, 16% alkane, and 15% amine functional groups. However, the limited number of deep seawater samples is insufficient to characterize the variability of seawater with depth.

4.4 Discussion

The aMAP and gPMA measurements made in multiple ocean regions are used to determine the factors that contribute to the organic composition of aMAP, including the influence of PMA. Three main questions are addressed: (i) What is the organic functional group composition of ocean-derived aMAP? (ii) How much of aMAP composition can be explained by generating primary marine aerosol (gPMA) from bubbled seawater? and (iii) What are the differences between the organic compositions of gPMA and seawater?

4.4.1 Chemical Composition of Ocean-derived aMAP: aPMA and AMA

The organic composition of aMAP contains two ocean-derived or "clean" marine OM types measured in four of the five sampling regions: aPMA and AMA (Table 4.1). aPMA and AMA are considered clean marine based on the aMAP classification in Section 4.3.1 and the lack of fossil-fuel-related alkane functional group signatures. aPMA OM has a composition (and observed variability, indicated as one standard deviation of the mean) of 65 (± 12)% hydroxyl, 21 (± 9)% alkane, 6 (± 6)% amine, and 7 (± 8)% carboxylic acid functional groups, which is similar to the composition of saccharides, as shown in Figure 4.5. In general, the organic composition of the aPMA samples and saccharides all have hydroxyl functional group fractions greater than 55% and alkane

functional group fractions less than 45% (with the specific ranges of saccharide alkane functional group fractions in Table 4.8). The average FTIR spectrum of the aPMA OM samples has high average cosine similarities (all greater than 0.80) with saccharide spectra (Table 4.8), indicating that aPMA composition is consistent with any of the saccharide standards or a mixture thereof, since the specific molecular mixture cannot be identified by FTIR. The aPMA OM type spectra have a similar hydroxyl functional group peak location (3377 ± 44 cm^{-1}) to the monosaccharides (3373 ± 4 cm^{-1}) and disaccharides (3383 ± 4 cm^{-1}). While the average aPMA peak locations are more similar to those of the smaller (mono and di) saccharides, the range of hydroxyl group peak locations for individual samples are also within the range of the polysaccharides (3425 ± 24 cm^{-1}), as shown in Table 4.5, indicating that the variability sampled during the five projects is too large to identify the composition as either monosaccharides or disaccharides rather than polysaccharides. Likely it is a complex mixture of multiple compounds of both classes. This hydroxyl group peak location and overall composition is consistent with the previously identified polysaccharide-like composition of PMA OM [*Russell et al.*, 2010]. However, the larger fraction of alkane functional groups in this aPMA OM type (21 ± 9%) is likely more accurate than the 10-15% alkane group associated with the "marine factor" obtained by positive matrix factorization (PMF) [*Russell et al.*, 2010], since the PMF results rely on the statistical separation of non-covarying factors in a time series that includes a sufficient number of unmixed aPMA samples.

The general composition, including the presence of amine functional groups, and the average spectrum of the aPMA OM is also similar to that of the polysaccharide chitosan which is derived from the deacetylation of chitin, a constituent of the high

molecular weight fraction of OM in seawater [*Aluwihare et al.*, 2005]. Chitosan has a broad IR absorbance (peak at 3410 cm^{-1}) in the hydroxyl functional group region and IR absorbance at 1630 cm^{-1} in the amine functional group region, similar to the average aPMA OM spectrum, with absorption at 3377 and 1623 cm^{-1} (shown in Figure 4.13 and Table 4.8). The functional group composition calculated from the molecular structure of chitosan contains 59% hydroxyl, 27% alkane, and 14% amine functional groups, similar to the aPMA OM composition (65 ± 12% hydroxyl, 21 ± 9% alkane, 6 ± 6% amine, and 7 ± 8% carboxylic acid functional groups).

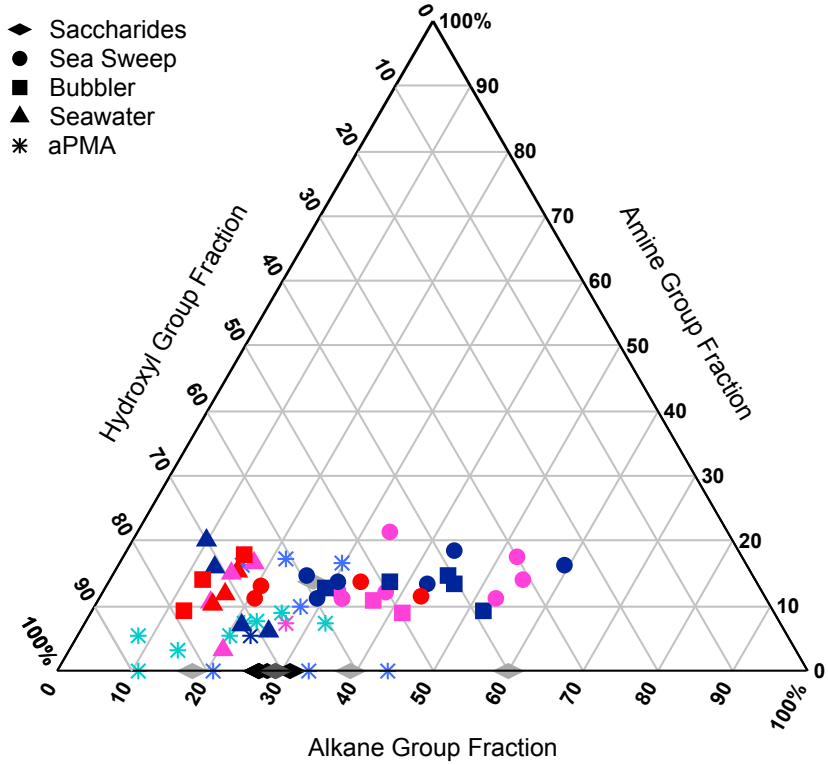

Figure 4.5: The hydroxyl, alkane, and amine functional group fractional composition of gPMA, aPMA, seawater, and saccharide OM. Each marker represents an individual sample. Markers are colored based on the sample project and location for WACS Station 1 (pink), WACS Station 2 (red), EPEACE (light blue), CalNex (dark blue), and ICEALOT (teal). Saccharides are shown in grey diamonds as polysaccharides (light grey), disaccharides (grey), and monosaccharides (dark grey). For the aPMA particles, the hydroxyl group fraction includes carboxylic acid.

Additional amino sugars (monosaccharides) such as glucosamine and galactosamine have been observed in both seawater particulate organic matter (POM) and ultra-filtered seawater dissolved organic matter (DOM) [*Benner and Kaiser*, 2003]. Another constituent of seawater OM is peptidoglycan, which has absorbance at 3300 and 1657 cm^{-1}, is a major component of bacteria cell walls, and contains one base compound (N-acetyl-glucosamine) in common with chitosan [*Naumann et al.*, 1982]. The amine functional group fraction observed in the aPMA OM may also indicate the presence of amino acids. For example, the spectrum of the amino acid asparagine has an IR absorption bend of NH_2 at 1620 cm^{-1} [*Venyaminov and Kalnin*, 1990]. *Aminot and Kerouel* [2006] also measured dissolved free primary amines and amino acids in seawater, and amine carbons were observed in DOM by *Benner et al.* [1992]. Additionally, the molar ratios of C/N (Table 4.4) in the aPMA (9.8), gPMA (6.9), and seawater (8.0) OM are similar to the range of measured C/N in the cellular material of phytoplankton (8.8) [*Biersmith and Benner*, 1998] and slightly larger than that measured for samples of marine plankton and bacteria (6.3) [*Emerson and Hedges*, 2008] and demonstrated by the Redfield Ratio (6.6). The similarity of the amine functional group fraction in gPMA and seawater is also consistent with recent measurements of seawater and gPMA that found that nitrogen-containing organic compounds were present in similar, but slightly lower, proportions in gPMA compared to seawater [*Schmitt-Kopplin et al.*, 2012]. It is also worth noting that the measured amine functional groups may reflect the contributions of amide-containing molecules, since mild acid hydrolysis (as might occur during sample drying) can destroy the amide functional group bond linkage

in seawater proteins and release amino acids, resulting in amine functional groups [*Aluwihare et al.*, 2005].

Table 4.4: Mean molar ratios, mass ratios, and functional group mass compositions of aMAP OM, gPMA OM, and seawater OM.

	Molar Ratios		Mass Ratio	Functional Group Mass Composition			
	O/C	C/N[a]	OC/Na	Hydroxyl	Alkane	Amine	Carboxylic Acid
aMAP OM Types							
aPMA	1.03	9.8	0.45	65 ± 12	21 ± 9	6 ± 6	7 ± 8
AMA	0.93	17.4	1.07	49 ± 6	24 ± 7	4 ± 4	22 ± 6
SMA	0.25	24.9	7.3	31 ± 5	66 ± 6	3 ± 6	0
MMA	0.54	68.1	5.9	23 ± 7	45 ± 13	2 ± 2	30 ± 11
gPMA OM[b,c]	0.68	6.9	0.27 ± 0.15	55 ± 14	32 ± 14	13 ± 3	0
Productive	0.50	7.4	0.30 ± 0.15	45 ± 10	42 ± 9	13 ± 4	0
Non-productive	0.90	6.9	0.18 ± 0.11	65 ± 10	22 ± 10	12 ± 3	0
Seawater OM[c]	1.0	8.0	NA	71 ± 4	17 ± 5	11 ± 6	0

[a]Typical Redfield ratio for seawater C/N is 6.6 (*Redfield*, 1934); aPMA, AMA, SMA, and MMA averages only include samples that contain non-zero moles of N.
[b]Includes all Sea Sweep and Bubbler samples.
[c]WACS only.

The other clean aMAP OM is AMA, which has an average composition (and variability indicated as one standard deviation) of 49 (± 6)% hydroxyl, 24 (± 7)% alkane, 4 (± 4)% amine, and 22 (± 6)% carboxylic acid groups. Compared to the average aPMA OM spectrum, the average AMA OM spectrum has a hydroxyl functional group maximum absorbance at lower wavenumbers (3288 cm^{-1}) indicating that there is a difference in the bond structure of the two OM types (Figure 4.2). The shoulder in the AMA spectrum at higher wavenumbers (around 3385 cm^{-1}) is consistent with the hydroxyl group peak absorbance of the aPMA OM type (3377 ± 44 cm^{-1}), within the

measurement variability, and is consistent with a substantial contribution of aPMA in AMA OM.

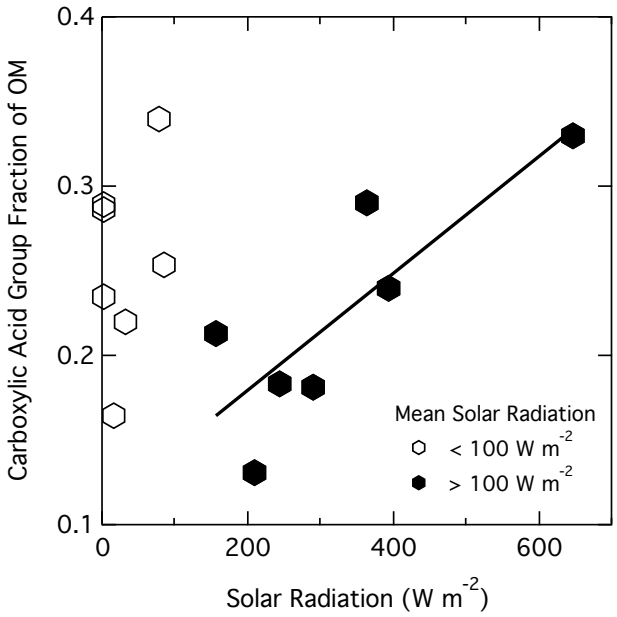

Figure 4.6: Correlation of the carboxylic acid functional group fraction of AMA OM (observed during EPEACE and ICEALOT) with solar radiation. A threshold of 100 W m^{-2} was used to exclude the samples in low-light that were not likely to have OM dominated by local or recent photochemical production.

Carboxylic acid groups in AMA likely originate from the condensation of photochemical reaction products of volatile organic compounds (VOCs), which may be marine in origin, although oxidation or precursors in the particle phase can also contribute. *Turekian et al.* [2003] observed that both of these pathways were sources of oxalic acid in marine aerosol particles. *Zhou et al.* [2008] observed photolysis of gPMA OM which produced OH and hydroperoxides when exposed to solar radiation. Other studies have identified carboxylic acid functional groups as SOA based on correlation with solar radiation [*Rogge et al.*, 1993] and correlation with ozone [*Liu et al.*, 2011; *Satsumabayashi et al.*, 1990]. The carboxylic acid functional group fraction of the AMA

OM is strongly correlated (r = 0.82) with solar radiation, for the samples with mean solar radiation (averaged over the sampling interval) greater than 100 W m^{-2} (Figure 4.6). The samples with mean values less than 100 W m^{-2} were excluded from the correlation because such low-light exposures during sampling meant that those samples were unlikely to have been influenced by local photochemical production and instead likely contained OM formed during prior sunlight exposure. This correlation is consistent with a photochemical source of the carboxylic acid group mass in AMA, providing a "secondary" contribution that is chemically distinct from the hydroxyl-alkane-amine group mixture associated with the primary components of aPMA.

The OC/Na ratio of the aPMA OM type (0.45) is consistent with previously measured submicron PMA particles with OC/Na ranging from 0.1 to 2 [*Russell et al.*, 2010]. The higher ratio of OC/Na (1.07) in AMA compared to the aPMA OM (0.45) can be interpreted as an indicator of secondary contributions of the photochemical products of VOCs to particles in the atmosphere.

The O/C ratio for the aPMA OM type is 1.03 (± 0.21). The O/C ratio of organic aerosol has been observed to increase over time after particles are emitted due to photochemical processing and secondary formation of organic components [*Aiken et al.*, 2008; *Zhang et al.*, 2005]. Generally, an O/C value higher than 0.4 is considered to be highly oxidized [*DeCarlo et al.*, 2008]. In marine conditions, the interpretation of high O/C as secondary is not appropriate since the large fraction of hydroxyl groups in saccharides means that even primary components have high O/C. The calculated O/C value for the monosaccharide reference standard glucose is 1.33, which is more than 3 times higher than O/C values attributed in non-marine conditions as secondary (0.4).

Nonetheless, the increase in the O/C ratio between the aPMA OM samples (0.80 ± 0.18) and the AMA OM (1.09 ± 0.17) samples in EPEACE is consistent with a larger secondary component in AMA relative to aPMA. This observed increase in the fraction of carboxylic acid functional groups is consistent with the accumulation of LMW products such as dicarboxylic acids [*Kawamura and Sakaguchi*, 1999; *Zhou et al.*, 2008], but it is possible that the VOC precursors of these acids may be either marine or continental in origin. More discussion of the presence of marine carboxylic acids is included in the Section 4.6.6.

STXM-NEXAFS single particle measurements of aMAP also show the presence of carboxylic acid and oxidized functional groups in the atmosphere during WACS. Of the 18 aMAP particles measured, 17 were classified as high O/C. This high fraction of more oxidized particles is consistent with the high carboxylic acid functional group fraction identified by FTIR in these samples.

4.4.2 Chemical Similarities between gPMA and aPMA and Differences between gPMA and other aMAP

The similarities of the organic composition of gPMA and aMAP provide direct evidence for the sources of aMAP and, specifically, for the contribution of PMA to aMAP. The similarities between aPMA and gPMA spectra and composition show the extent to which this type of aMAP is natural and ocean-derived. The differences between gPMA and non-ocean derived aMAP (SMA and MMA) provide clear evidence for the contribution non-marine sources to particle OM over the ocean. These contributions are provided to both marine air and marine seawater, since human activities also affect the

composition of breaking waves. One striking example of the effect of shipping effluent on seawater is the observed increase in the alkane group fraction of gPMA while sampling in the San Francisco Bay.

4.4.2.1 Similarities Between gPMA and aPMA

Comparison of the aPMA and gPMA (Figure 4.5) OM shows the similarities in the functional group compositions of OM of these two types. The average aPMA OM spectrum has cosine similarities of greater than 0.90 with the gPMA OM spectra. The gPMA OM spectra have similar hydroxyl group peak locations (3369 ± 10 cm^{-1}) to the aPMA spectra (3377 ± 44 cm^{-1}), as shown in Table 4.5. The average gPMA OM composition (and sample variability as one standard deviation) is 55 (± 14)% hydroxyl, 32 (± 14) % alkane, and 13 (± 3)% amine functional groups, which is very similar to the aPMA composition with 65 (± 12)% hydroxyl, 21 (± 9)% alkane, 6 (± 6)% amine, and 7 (± 8)% carboxylic acid functional groups. Additionally, the OC/Na ratio of the aPMA (0.45) falls within the range of gPMA (0.06 - 0.6) measured during WACS. This similarity in organic composition between aPMA and gPMA provides evidence that the aPMA is ocean-derived, likely produced through a bubble-bursting mechanism similar to that of gPMA, supporting both the assertion that most aPMA OM is directly emitted in the particle phase from the ocean to the atmosphere and the utility of the Sea Sweep and Bubbler in generating gPMA that is, in key respects, similar to aPMA. Also, as discussed earlier for aPMA, the average functional group composition of gPMA (55% hydroxyl, 32% alkane, and 13% amine functional groups) is quite similar to that of the amino sugar

chitosan (59% hydroxyl, 27% alkane, and 14% amine functional groups), a seawater constituent.

Table 4.5: The location of the maximum hydroxyl group peak (cm^{-1}) for seawater, gPMA, aPMA, and saccharides.

OM Type	**Hydroxyl Group Peak Location (cm^{-1})**
Seawater	3401 ± 14
gPMA	3369 ± 10
Productive	3362 ± 7
Non-productive	3376 ± 9
aPMA	3377 ± 44
Monosaccharides[a]	3373 ± 4
Disaccharides[b]	3383 ± 4
Polysaccharides[c]	3425 ± 24

[a]glucose, fructose, xylose, galactose
[b]lactose, cellobiose
[c]pectin, carboxymethyl cellulose, Chitosan

4.4.2.2 Differences between gPMA and Non-ocean-derived OM in aMAP

Some of the marine samples selected by back trajectories and the other criteria identified in Section 4.3.1 to exclude coastal and continental sources still retain the chemical signatures of shipping and other marine pollution in their FTIR spectra. This is evident in the SMA (Figure 4.2c) and MMA (Figure 4.2d) OM types, in which the alkane peak absorption is similar to that of fossil fuel emissions [*Guzman-Morales et al.,* 2013]. These two OM types make up 63% of the total measured aMAP OM concentration, consistent with the near ubiquity of black carbon (BC) measured in the southeastern Pacific [*Shank et al.*, 2012]. Even though these types show chemical components characteristic of anthropogenic sources, the quantitative contributions are sufficiently dilute that the average SMA and MMA OM concentration is only 0.55 $\mu g\ m^{-3}$ (with more than 80% of the sample concentrations less than 1 $\mu g\ m^{-3}$), concentrations that many

classification schemes would consider “clean.” In addition, these low concentrations are not excluded by filters triggered by the high particle counts (e.g. >1000 cm^{-3}) that are associated with nearby sources, since the emissions have been diluted by mixing with cleaner air in the boundary layer.

Cloud droplet composition measurements off the coast of central California, where 16 of the 18 SMA OM samples were collected, show that 72% of the cloud droplets in that area are at least moderately perturbed by shipping emissions [*Coggon et al.*, 2012]. Additionally, a major shipping lane between the port of San Francisco and the southern California ports transits through the area sampled during EPEACE. The factor of 2-3 higher alkane functional group mass fraction (66 ± 6%) in SMA OM, compared to the clean aMAP (aPMA with 21 ± 9% and AMA with 24 ± 7%), is likely due to shipping emissions.

The MMA OM type has a high ratio of OC/Na (greater than 5) suggesting that a substantial fraction of the OC is not primary OC from seawater. These samples also have the highest average corresponding solar radiation, which could increase the contribution of photochemical products of VOCs to the OC. The fraction of carboxylic acid functional groups is consistent with this result [*Liu et al.*, 2011], but there is no strong correlation of the carboxylic acid fraction with solar radiation, indicating that the carboxylic acid functional groups may have been transported from elsewhere rather than forming recently. The MMA OM type was observed in all of the sampling regions, except the North Atlantic and Arctic during ICEALOT. It is interesting that the composition of MMA is quite similar in multiple ocean regions, reflecting the general chemical

similarity of both shipping fuel and ocean components across very different parts of the world.

4.4.2.3 Shipping Effluent Signatures in gPMA

A striking example of how gPMA can also incorporate non-natural seawater components was identified during CalNex in seawater that contained increasing amounts of fuels as the R/V *Atlantis* entered the increasingly dense shipping lanes in the San Francisco Bay. The alkane functional group fraction of the gPMA OM increased as the R/V *Atlantis* proceeded into the higher-traffic shipping lanes and into the bay (Figure 4.7b). The gPMA OM in the bay had a much higher fraction of alkane functional groups (62%) than the gPMA furthest outside of the bay (37%). Since the gPMA do not have any contributions from atmospheric processes, the observed change in the alkane functional group fraction results from changes in the seawater organic composition. A likely explanation is that the higher-traffic shipping lanes contribute more fuel waste to the bay, resulting in seawater with a higher alkane group fraction and corresponding higher fractions in the bubbled gPMA. Additional sources of hydrocarbons, such as coastal runoff into the bay, may also increase the seawater hydrocarbon content. Also, increased surfactants in the seawater in the bay may contribute to the larger alkane fraction of the gPMA, consistent with the mechanism discussed in Section 4.4.3.3.

This link between changes in seawater composition and PMA has also been seen in the associated aMAP. *Bahadur et al.* [2010] reported a unique link between the high lignin waterways of the St. Lawrence and the aMAP measured in the western north Atlantic. A study in Leghorn harbor showed evidence for ship fuel signatures in aMAP

measured in that region [*Cincinelli et al.*, 2001]. However, in those studies the influence of atmospheric processing could not be ruled out. By analyzing the composition of gPMA, the increasing alkane group fraction can be directly linked to the seawater composition changes rather than airborne sources of OM. We also note that the alkane functional group peaks of the FTIR spectra for the fuel and ship influenced marine type (Figure 4.2c) are very similar to those for the San Francisco Bay gPMA (Figure 4.7a), both with peaks at 2923 and 2804 cm^{-1}. This similarity means that seawater and atmospheric contributions to the alkane group components cannot be separated in aMAP, except by comparison to gPMA.

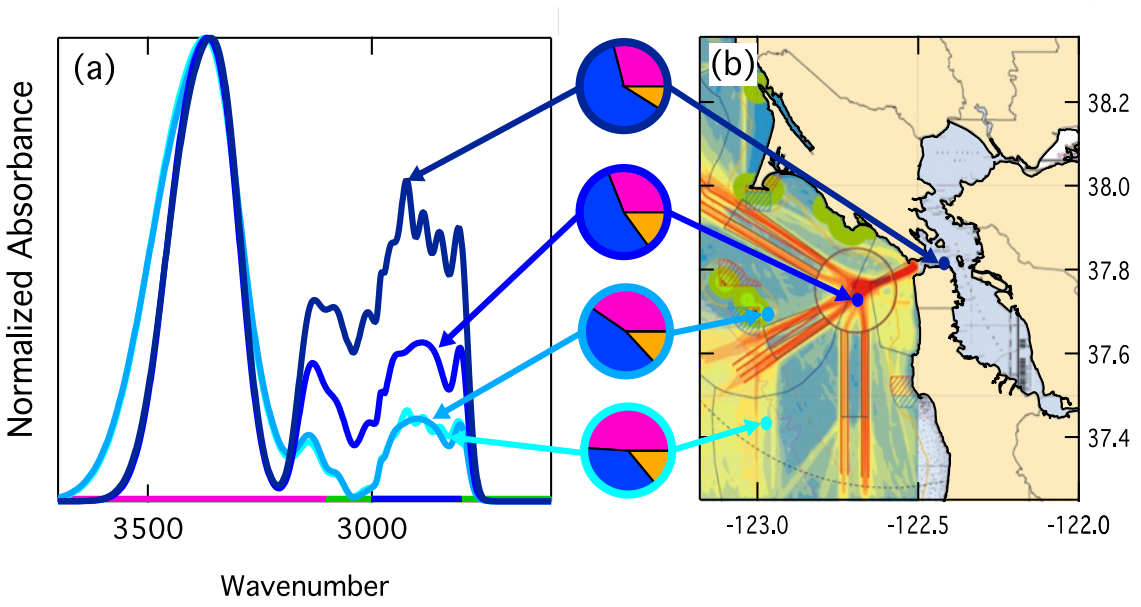

Figure 4.7: (a) Normalized FTIR spectra of Bubbler gPMA generated at 4.2 lpm at four locations starting outside (light blue) and ending in (dark blue) the San Francisco Bay. (b) Map of locations where gPMA were generated overlaid on a map of shipping lanes (red) into the San Francisco Bay (source: http://www.calacademy.org/sciencetoday/shipping-lane-changes/5511420/). The pies represent the functional group composition of the gPMA OM at the four locations with alkane (blue), hydroxyl (pink), and amine (orange) functional groups.

4.4.3 Influence of Seawater OM on gPMA OM

Collecting seawater and gPMA in the same areas reveals a very strong relationship between the composition of seawater and the gPMA produced from it across three very different ocean regions. In general, gPMA OM composition is similar to seawater OM composition, but there are two main differences. The first observed difference between seawater and gPMA is the type of saccharide associated with the measured hydroxyl group absorbance, which we suggest is attributed to the larger saccharides preferentially remaining in the seawater during PMA formation. Second, there is an enhancement of the alkane group fraction of gPMA in the productive seawater, and we suggest this difference may be attributed to the preferential drainage of hydroxyl-containing molecules during the film bursting process.

4.4.3.1 Spectral Similarities and Differences between gPMA and Seawater

Seawater OM and gPMA particle OM have similar FTIR spectra and functional group compositions (Figure 4.5), both with large fractions (50-75%) of hydroxyl functional groups and smaller contributions from alkane groups (15-40%) and amine groups (5-20%). The OM spectra of the collocated gPMA and seawater samples are shown in Figure 4.8, and the range of hydroxyl group and alkane group fractions of all the gPMA samples and seawater are shown in Figure 4.5. This graph also illustrates that the hydroxyl and alkane group fractions of the measured seawater and gPMA are within the ranges expected for saccharides identified in seawater (polysaccharides 18-60% alkane groups; monosaccharides and disaccharides 19-31% alkane groups). The samples with smaller than expected mass fractions of alkane functional groups (10-15%) are

samples for which the alkane mass was above the limit of detection but below the limit of quantification (for which method uncertainty is >50% rather than 20% applicable to the other samples).

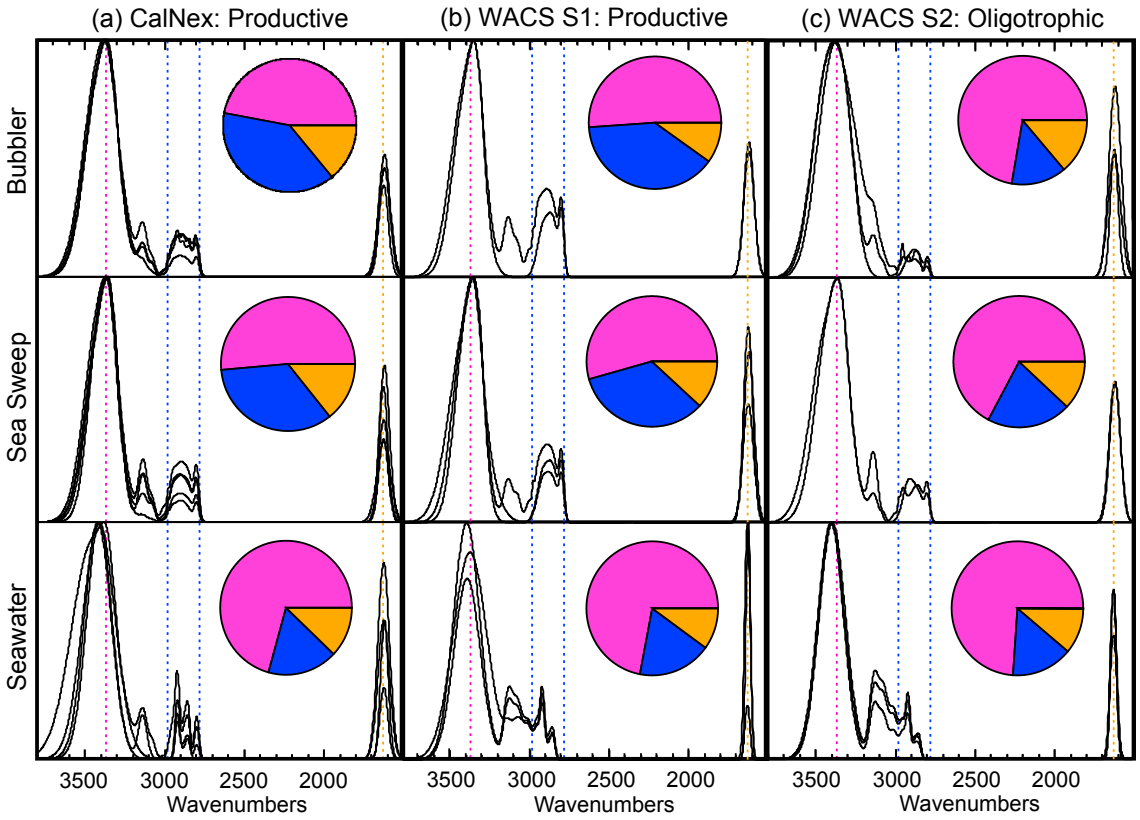

Figure 4.8: Comparison of the selected normalized organic FTIR spectra and average functional group composition measured at (a) CalNex, (b) WACS Station 1, and (c) WACS Station 2 in the gPMA generated with (top panel) the Bubbler and (middle panel) the Sea Sweep and (bottom panel) the corresponding composition of OM in surface seawater. Pies represent the organic functional group composition as hydroxyl (pink), alkane (blue), and amine (orange). Dashed vertical lines indicate hydroxyl functional group peak absorption at 3369 cm^{-1} (pink), and amine functional group peak absorption at 1630 cm^{-1} (orange). The range of alkane functional group absorption from 2980 to 2780 cm^{-1} (blue dashed lines) is also shown. The higher wavenumber peak absorption of the hydroxyl functional groups is evident in the seawater panel. The functional group compositions and spectra are from the subset of collocated samples.

One subtle but interesting difference between seawater and gPMA is shown in the average hydroxyl functional group peak location listed in Table 4.5, which are also evident in the spectra in Figure 4.8. The broad seawater hydroxyl functional group

absorption region overlaps that of the gPMA OM spectra (Figure 4.8). This similarity in hydroxyl group absorbance between seawater OM and gPMA OM is consistent with seawater being the source of gPMA. The general location of the hydroxyl group peak is consistent with known seawater saccharides, such as chitosan (see Section 4.6.5 and Figure 4.13). However, the hydroxyl functional group peak locations differ between the gPMA and seawater OM, with gPMA peaking at 3369 and seawater peaking at 3401 cm^{-1} (Table 4.5). This 32 cm^{-1} average difference in peak location is larger than the measured variability (± 10 for gPMA and ± 14 for seawater) and the method error (which was measured to be ± 6 cm^{-1} for the hydroxyl group peak location using atomized ribose standards [*Takahama et al.*, 2013]). Consequently the difference in peak location could indicate a systematic difference in the molecular structure and in the mixture of the saccharides in the seawater and the gPMA, since peak location shifts to higher wavenumbers for larger saccharides [*Mathlouthi and Koenig*, 1986; *Kuhn* 1950]. The hydroxyl group peak location of the gPMA (3369 ± 10 cm^{-1}) is more characteristic of monosaccharide (3373 ± 4 cm^{-1}) and disaccharide (3383 ± 4 cm^{-1}) molecules, than the seawater hydroxyl group peak location (3401 ± 14 cm^{-1}), which is more characteristic of polysaccharide (3425 ± 24 cm^{-1}) molecules (Figure 4.9a). While the complexity of the mixture of saccharides that are present in both seawater and gPMA clearly prevents a specific molecular identification, this shift in peak location likely reveals differences in the relative contributions from different saccharide types.

The hydroxyl functional group peak locations measured in these samples are not correlated ($r < 0.4$) to SST, salinity, chl-*a* concentration, or insolation and also are not region specific. The one factor that seems related to the hydroxyl functional group peak

location in gPMA is the functional group composition of the OM, with a negative correlation to the alkane functional group fraction (r = -0.65) and a complementary positive correlation with the hydroxyl functional group fraction (r = 0.63) (Figure 4.9). The hydroxyl functional group peak location decreases as the hydroxyl group fraction decreases and the alkane group fraction increases.

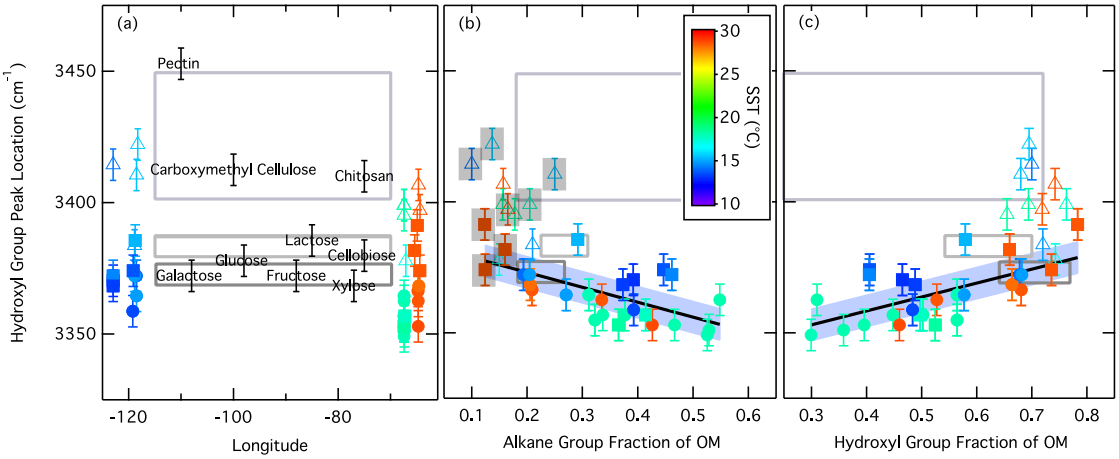

Figure 4.9: Comparison of maximum hydroxyl functional group peak location with (a) sample longitude, (b) alkane functional group fraction of OM, and (c) hydroxyl functional group fraction of OM for the gPMA and seawater. Marker shapes indicate the sample type including Sea Sweep (circles), Bubbler (squares), and seawater (open triangles). The saccharides are plotted at different longitudes for comparison in (a) and at their corresponding molecular alkane and hydroxyl functional group fractions in (b) and (c), respectively. Large open grey boxes represent the average range of hydroxyl group peak absorption (average ± standard deviation) for polysaccharides (light grey), disaccharides (grey), and monosaccharides (dark grey). Error bars of ± 6 cm^{-1} are shown for the hydroxyl group peak location on each marker to represent the method error. The uncertainty in the alkane and hydroxyl functional group mass is 20% [*Russell*, 2003]. The shaded boxes around individual markers (3 Bubbler and 5 seawater samples) are samples where the alkane functional group mass is above the detection limit but below the limit of quantification (twice the standard deviation), making the alkane mass fraction have uncertainty of >50% rather than 20%. gPMA hydroxyl group peak location correlates with the alkane functional group fraction (r = -0.65) and the hydroxyl functional group fraction (r = 0.63).

4.4.3.2 Chlorophyll-a Dependent Enhancement of Alkane Group Fraction in gPMA

Chl-*a* concentration is used as a measure of biological activity (phytoplankton productivity) in the surface ocean, and high biological activity, as observed in productive regions with high concentrations of chl-*a*, may affect the organic composition of aMAP [*O'Dowd et al.*, 2004]. The alkane group fraction of the OM in gPMA particles is correlated with the chl-*a* concentration (r = 0.66) over the range of chl-*a* concentrations measured in this study (Figure 4.10a). Consequently, the hydroxyl functional group fraction of gPMA is negatively correlated with the chl-*a* concentration (r = -0.67, Figure 4.10b). Together, the Sea Sweep and Bubbler generated gPMA suggest a difference between the OM composition of gPMA from productive and non-productive seawater (Table 4.4), indicated by high and low seawater chl-*a* concentrations, respectively. There is a consistently higher fraction of alkane functional groups in the gPMA from the productive seawater of CalNex and WACS Station 1 (42 ± 9%) than from the non-productive seawater at WACS Station 2 (22 ± 10%). As discussed above, more data are needed to confirm this result.

The seawater has an average composition (and variability indicated as one standard deviation) of 71 (± 4)% hydroxyl, 17 (± 5)% alkane, and 11 (± 6)% amine functional groups in all samples (Figure 4.8). The average composition of the surface seawater OM in the productive and non-productive seawater is fairly similar, which is consistent with measurements that found no significant differences in seawater film composition (including inorganic and organic components) in eutrophic and oligotrophic seawater [*Williams et al.*, 1986]. At WACS Station 1, seawater was also collected at a depth of 27.2 m, and at WACS Station 2, seawater was collected at a depth of 2500 m.

The OM in these samples is similar to the surface seawater composition, with a variation of less than 5%.

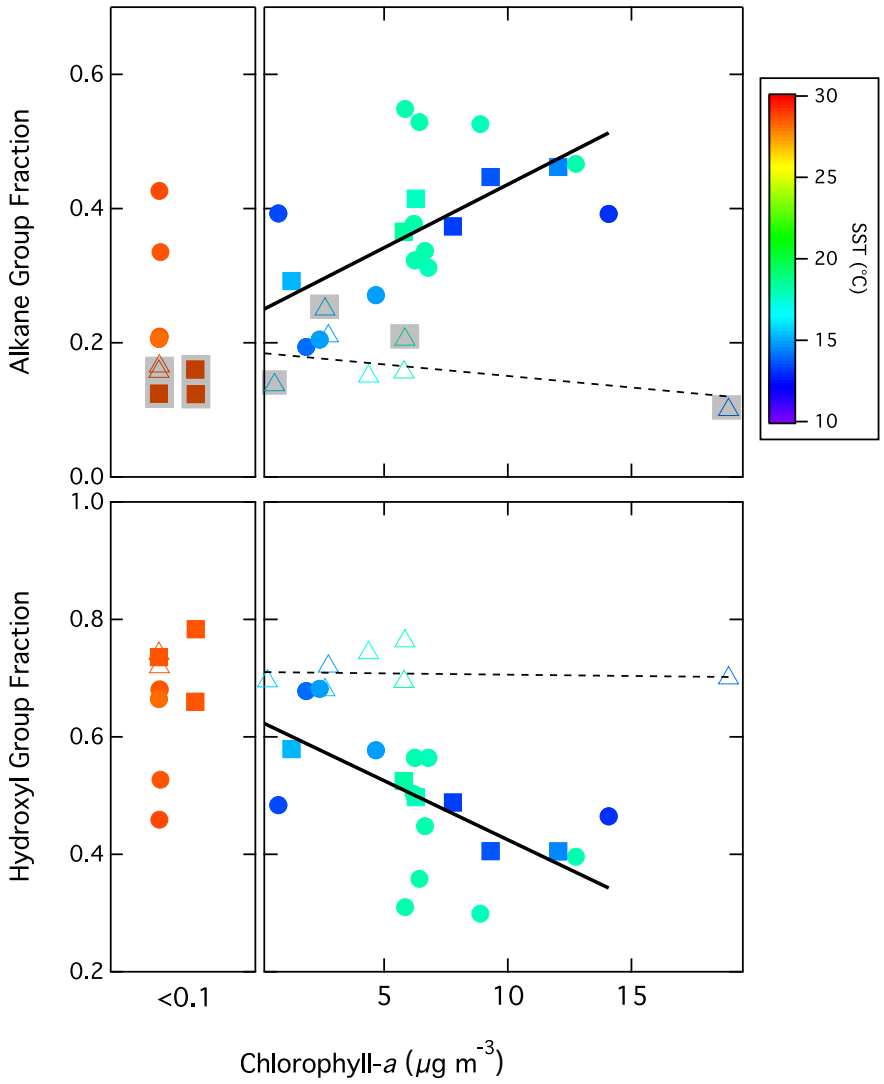

Figure 4.10: (a) Correlation of alkane functional group fraction of gPMA OM with seawater chl-*a* concentrations (r = 0.66) and (b) negative correlation of hydroxyl functional group fraction of gPMA OM with seawater chl-*a* concentrations (r = -0.67) during WACS and CalNex (over the range of chl-*a* concentrations measured in this study). Markers represent sample types as Sea Sweep (circles), Bubbler (squares), and seawater (open triangles). Seawater alkane and hydroxyl functional group OM fractions do not correlate with chl-*a* concentrations, indicated with the dashed lines. The shaded boxes around individual markers (3 Bubbler and 5 seawater samples) are samples where the alkane functional group mass is above the detection limit but below the limit of quantification (twice the standard deviation), making the alkane mass fraction have uncertainty of >50% rather than 20%.

These differences in gPMA OM composition between the productive and non-productive seawater during WACS are also observed in the single particle types measured by STXM-NEXAFS. In the productive seawater, there were 6 high O/C particles and 9 low O/C particles with diameters 0.65 to 1.5 μm, while in the non-productive seawater, there were 12 high O/C and 7 low O/C particles measured with diameters less than 1.5 μm. While the small number of particles analyzed by STXM-NEXAFS were selected based on carbon content and may not be representative of the entire OM particle population, these measurements indicate that there may be a higher fraction of low O/C particles in the gPMA from the productive seawater. This is in agreement with the larger fraction of alkane functional groups measured by FTIR in the gPMA generated in the productive seawater compared to the oligotrophic seawater.

Additionally, the alkane group fraction of PMA calculated using a classical Langmuir theory model, combined with estimates of ocean distributions of several classes of chemical compounds [*Burrows et al.*, 2014], correlates with chl-*a* concentration. The model posits that a group of primarily aliphatic, lipid-like compounds is present in concentrations that are correlated with chl-*a* and that this group outcompetes other molecules for inclusion in the bubble film due to its strong surface affinity. The direction of the model-predicted chl-*a* to alkane group fraction relationship is the same as observed in this study, even though the model does not fully reflect the scale of the observed values. The same model also predicts a lack of correlation between the predicted seawater OM alkane group fraction and the seawater chl-*a* concentration, similar to this study. These similar trends suggest consistency between the measurements and the classical Langmuir theory model.

4.4.3.3 Proposed Explanations for the Retention of Polysaccharide-like OM in Seawater and the Enhancement of Alkane Groups in gPMA

Here we consider the process by which the OM composition from seawater changes as particles form from bubbles bursting in seawater. Two processes are needed to explain the observations of (i) the similarity of gPMA to monosaccharide and disaccharide OM and (ii) the relative enhancement of alkane functional groups in gPMA. The retention of polysaccharides in seawater is likely caused by the failure of these compounds to be incorporated in bubble films due to the colloidal formation that is likely associated with their large molecular weight and possible gel-forming tendencies. The enhancement of alkane groups may result from a difference in the surfactants and the preferential drainage of more soluble (lower alkane group fraction) organics back into the seawater before the film bursts. These processes are summarized in Figure 4.11 and are discussed below.

The retention of polysaccharide-like OM in the seawater, resulting in its depletion relative to monosaccharide and disaccharide-like OM in gPMA, is likely the result of the polysaccharide-like OM not being incorporated into the bubble films that produce particles. One possible explanation for this preferential partitioning is that polysaccharides can form transparent exopolymer gels in the surface microlayer [*Wurl and Holmes*, 2008; *Verdugo et al.*, 2004], and such colloidal structures could prevent their inclusion in the bubble films and consequently their partitioning in the aerosol phase. Another possible explanation is that polysaccharides could be cleaved by ultraviolet radiation at the sea surface [*Orellana and Verdugo*, 2003], reducing the

abundance of polysaccharides available at the sea surface to contribute to the films that make aerosol particles.

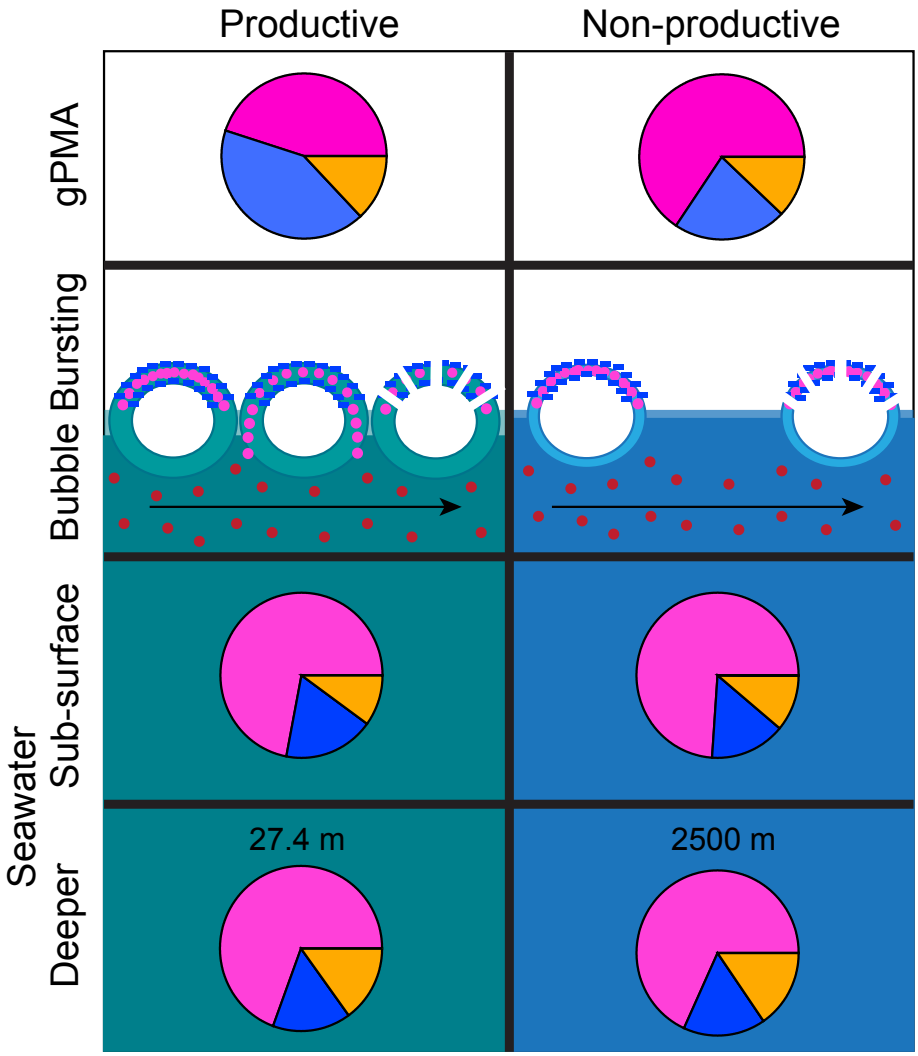

Figure 4.11: Average functional group composition of OM in (top panel) gPMA generated with the Sea Sweep and Bubbler, (middle panel) surface seawater, and (bottom panel) deep seawater at 27.4 m and 2500 m measured in productive (left) and non-productive (right) seawater during WACS. Colors in the pies represent the organic functional group fractions for hydroxyl (pink), alkane (blue), and amine (orange). The bubbles show the bubble draining process in both seawater types, with more surfactant in the productive seawater. The OM is shown as hydrophobic (blue squares), hydrophilic (pink circles), and polysaccharides (red circles).

The samples taken in productive seawater have higher concentrations of chl-*a* (Table 4.3), indicative of higher phytoplankton concentrations and productivity, which

have been associated with increased surfactant concentrations [*Zutic et al.*, 1981; *Sellegri et al.*, 2006; *Wurl et al.*, 2011]. This connection provides the opportunity to use chl-*a* as a proxy for surfactant concentrations. Even though the organic functional group composition of seawater is the same in productive and non-productive seawater, the chl-*a* concentrations are different, and that small (below detection limit) change in organic composition is sufficient to account for substantial changes in surfactant properties of the seawater [*Modini et al.*, 2013]. Higher concentrations of surfactants increase bubble persistence at the seawater surface before bursting [*Sellegri et al.*, 2006], as observed with individual bubbles in the laboratory [*Modini et al.*, 2013]. The longer bubbles persist, the more the bubble films are allowed to drain [*Blanchard*, 1963], so an increase in persistence time leads to additional drainage from the films. Since the more soluble constituents of the bubble film drain more than the less soluble ones, the compounds with higher fractions of hydroxyl groups preferentially drain from the bubble film leaving the more insoluble organic compounds (including molecules with higher fractions of alkane groups) [*Oppo et al.*, 1999; *Russell et al.*, 2010]. The result is that the bubble films that form in productive seawater have a larger fraction of alkane groups by the time the bubble film ruptures, which then forms PMA particles that are enriched in alkane groups. Figure 4.11 illustrates this process of preferential draining of the more soluble molecules and the resulting enrichment of the alkane group fraction in the gPMA OM generated from productive seawater. This process is similar to the draining proposed by *Facchini et al.* [2010], in support of their finding that water-insoluble organic components were enhanced in gPMA.

4.5 Conclusions

The organic functional group composition of aMAP (defined as particles collected more than 1 km from land and sampled in air masses with 3-day back trajectories originating over the open ocean) in five ocean regions including the northern Atlantic, Arctic, southeastern Pacific, and northeastern Pacific, both coastal and remote, was determined by FTIR spectroscopy and independent variables (sea salt, solar radiation, etc.) to have contributions from both clean and polluted sources. Ocean-derived organic aMAP included atmospheric primary marine aerosol particles (aPMA) and carboxylic acid containing primary marine aerosol particles (AMA), which had average OM concentrations of 0.45 and 0.68 μg m^{-3} and represented 23% and 14% of the total sampling time, respectively. Shipping influenced marine aerosol particles (SMA) and mixed and other anthropogenically-influenced marine aerosol particles (MMA) OM accounted for 63% of the sampling time with a total aMAP average OM of 0.55 μg m^{-3} observed in four of the five sampling regions, confirming the ubiquitous contribution of non-natural sources to aerosol particles in the MBL.

The average (and variability indicated as one standard deviation) functional group composition of aPMA OM is 65 (± 12)% hydroxyl, 21 (± 9)% alkane, 6 (± 6)% amine, and 7 (± 8)% carboxylic acid functional groups, similar to an overall molecular composition of marine saccharides and amino sugars, such as chitosan and glucosamine, which contain 59% hydroxyl, 27% alkane, and 14% amine functional groups. aPMA was measured during high wind speeds, had a high corresponding concentration of sea salt (OC/Na of 0.45), and showed a correlation between corresponding Na concentration and

wind speed (r = 0.70), all indicative of a primary, ocean-derived source of OM. The aPMA OM is similar in composition to the gPMA OM generated from the Bubbler and the Sea Sweep (55 ± 14% hydroxyl, 32 ± 14% alkane, and 13 ± 3% amine functional groups). This shows that aPMA is dominated by direct, primary emissions from seawater, making primary emissions from seawater an important source of organics to the MBL, with aPMA measured during 23% of the sampling time.

The other ocean-derived OM type, AMA, contains 49 (± 6)% hydroxyl, 24 (± 7)% alkane, 4 (± 4)% amine, and 22 (± 6)% carboxylic acid functional groups. The relative increase in the carboxylic acid functional group fraction, compared to the aPMA (7 ± 8%), is likely the result of contributions from photochemical oxidation in the atmosphere to form secondary products with carboxylic acid functional groups. This is shown by the correlation (r = 0.73) of the carboxylic acid functional group fraction of AMA OM with solar radiation for samples with solar radiation greater than 100 W m^{-2}.

The organic functional group composition of gPMA directly follows changes in seawater organic composition. One example of this was observed in the increase in the alkane functional group fraction of gPMA generated in the San Francisco Bay and shipping lanes (62%) compared to the gPMA furthest outside of the bay (37%). The higher-traffic shipping lanes contribute fuel waste to the bay, which results in a higher alkane functional group fraction in the seawater OM and corresponding gPMA.

Even though the organic composition of the seawater OM and gPMA contain the same functional groups (hydroxyl, alkane, and amine) in nearly the same proportions, there is a difference in the saccharide compositions of the gPMA and seawater OM, which is evident in the differences in the hydroxyl group peak locations of their spectra.

The hydroxyl group peak location of the gPMA (3369 ± 10 cm^{-1}) is similar to monosaccharide and disaccharide molecules (3373 ± 4 and 3383 ± 4 cm^{-1}, respectively), within the measured variability (4 - 10 cm^{-1}) and the method error (± 6 cm^{-1}). The seawater OM hydroxyl group peak location is at higher wavenumbers (3401 ± 14 cm^{-1}) and is consistent with having more polysaccharide contributions (hydroxyl group peak location of 3425 ± 24 cm^{-1}). The difference between the seawater and gPMA OM, demonstrated by the differences in their hydroxyl group peak locations (3401 ± 14 cm^{-1} and 3369 ± 10 cm^{-1}, respectively), results from the more polysaccharide-like OM remaining in the seawater during gPMA production. However, given the variability in the peak locations, a larger number of samples would be needed to identify the extent of the chemical difference between seawater and gPMA.

One other chemical difference is that the gPMA OM composition had a larger fraction of alkane functional groups when generated in eutrophic, productive seawater (42 ± 9%) compared to oligotrophic, non-productive seawater (22 ± 10%). gPMA organic functional group composition variation was not the result of a seawater organic functional group change, since the seawater alkane functional group fraction was consistently around 17% in both the productive and non-productive regions. The difference in the gPMA from productive and non-productive seawater may be the result of a change in the seawater surfactant concentration, identified by the difference in chl-*a* concentrations. The correlation (r = 0.66) between the gPMA alkane functional group fraction of OM and chl-*a* concentration suggests that the alkane functional group fraction of gPMA may be directly related to the chl-*a* concentration, suggesting a link between the ocean ecosystem biotic population and the aerosol composition. The difference may be a result of the

higher concentration of surfactants (and chl-*a*) in the productive seawater, which could increase the persistence time of the bubbles and allow for more draining of the soluble organics, including those with hydroxyl functional groups, from the bubble film before bursting. This process could result in a larger fraction of alkane functional groups in the bursting bubble film OM and the resulting gPMA from productive seawater than from non-productive seawater. Further measurements are needed to test this hypothesis.

4.6 Appendix

4.6.1 Air Mass Identification

In order to identify which atmospheric aerosol particle samples could be considered "marine," three criteria were applied. The first was the simple metric that the ship's distance from land must be at least 1 km. Then meteorological models constrained by reanalysis data were used to identify the recent history of the air that was sampled. Third, radon concentrations and particle number were used as tracers to exclude air masses with coastal influences.

Since CalNex was largely a coastal air quality study, the criteria of distance from land and ports excluded 32 of the 40 samples collected. The samples collected while the R/V *Atlantis* was sitting in the Ports of Long Beach or Los Angeles and the Sacramento River were all strongly influenced by local sources in the ports and major cities, excluding them from consideration as "marine" in this study.

To obtain air mass back trajectories for each project, the isentropic Hybrid Single Particle Lagrangian Integrated Trajectory (HYSPLIT) model [*Draxler and Rolph*, 2003] was used. For CalNex, EPEACE, and WACS, up to 7-day back trajectories were

calculated arriving at 30, 100, 500, and 1000 m above sea level, every hour. The general trend was similar between the back trajectories arriving at different altitudes. Samples were initially selected if their corresponding 3-day air mass back trajectories originated from over the ocean and spent more than 75% of the time over the ocean. For example, all of the air masses sampled during EPEACE were predominately marine, resulting in 39 samples. While some back trajectories passed over areas that were close to the coast, no air masses originated from or spent significant time over land, as discussed by *Wonaschutz et al.* [2013]. The WACS project has 11 of 14 ambient samples classified as having marine origin. The ICEALOT and VOCALS marine sample selection is described by *Frossard et al.* [2011] and *Hawkins et al.* [2010], and the projects have 13 and 12 samples classified as marine in this study, respectively.

During CalNex and WACS, the selected aMAP samples had low average radon concentrations of 805 mBq m^{-3} and 355 mBq m^{-3}, respectively, which are consistent with lower radon concentrations in marine regions, further from continental influence. The marine samples during ICEALOT and VOCALS had similarly low radon concentrations [*Frossard et al.*, 2011; *Hawkins et al.*, 2010]. During EPEACE, marine particles were also selected in real time using automated valves to turn off particle sampling when total particle counts (CPC, TSI model 3010) were higher than approximately 500 cm^{-3} at low wind speeds and 1000 cm^{-3} at high wind speeds. (The higher cutoff was used for high wind speeds to accommodate the higher expected production of sea spray particles.)

4.6.2 Cluster Analysis of FTIR Spectra and Identification of Clusters

In order to complete the cluster analysis reported here, the FTIR spectra of all aMAP samples were first normalized to maximum absorbance. The absorbance region between 3800 and 1500 cm^{-1}, excluding 2340-1870 cm^{-1}, was used in the cluster analysis because this region represents the absorbance region of functional groups quantified in this study and excludes the region of interference from Teflon absorption. In order to determine the number of clusters that best represented the combined marine aerosol spectra, solutions with two through nine clusters were tested. Cosine similarity [*Stein and Scott*, 1994] was used to determine the similarity between spectra within a cluster and to compare that to the similarity between the averages of each cluster. The eight-cluster solution had the lowest similarity between the average spectra of each cluster (0.78), compared to the other solutions. In addition, the similarity of the spectra within each cluster was highest for the eight-cluster solution (0.92 average). This result suggests that there is adequate separation of the spectra into unique clusters.

While these eight clusters met the minimum criteria for uniqueness (overall cosine similarity between the clusters of less than 0.80), some pairs of cluster averages had high cosine similarity (greater than 0.90) and very similar average spectra (and functional group compositions), which suggested that a smaller number of clusters could be used to represent the spectra with comparable accuracy. Clusters 1 and 3, Clusters 4, 5, and 6, and Clusters 7 and 8 were combined into three larger clusters, resulting in four "recombined clusters" of spectra that still retained the low cosine similarity between their average spectra (0.81). Cluster 7 had only 4 spectra and was not considered to be

meaningful on its own. The cosine similarities of the spectra within each recombined cluster are 0.88, 0.93, 0.86, and 0.91.

Based on the atmospheric and seawater conditions, locations during sampling, and spectral features, these clusters were identified as: (i) atmospheric primary marine aerosol particles (aPMA); (ii) carboxylic acid-containing marine aerosol particles (AMA); (iii) shipping-influenced marine aerosol particles (SMA); and (iv) mixed and other anthropogenically-influenced marine aerosol particles (MMA). aPMA was identified by the high corresponding wind speeds (periods with wind greater than 10 m s^{-1}), correlation of wind speed with submicron Na concentrations ($r = 0.70$), and an Na/Cl ratio (0.74 ± 0.15) within 25% of the Na/Cl ratio of seawater (0.56). AMA was identified by the large fraction of carboxylic acid functional groups, similar sampling conditions to aPMA, and correlation of the carboxylic acid functional group fraction of OM with solar radiation greater than 100 W m^{-2} (see also Section 4.6.6). SMA was identified through its similar spectral features to ship diesel spectra. Figure 4.4a shows the similarity of the SMA average spectrum to a spectrum of generated marine aerosol particles (gPMA) added to a spectrum of ship diesel. MMA OM was identified by its similarity to the other OM types and low corresponding wind speed. MMA has spectral features of the aPMA, AMA, and SMA, as shown in Figure 4.4b. The MMA spectrum includes: (i) a similar average hydroxyl group peak location (3380 cm^{-1}) to aPMA (3377 cm^{-1}), (ii) alkane functional group structural features (i.e. 2957 and 2806 cm^{-1}) similar to SMA (2956 and 2804 cm^{-1}), and (iii) a carboxylic acid functional group fraction similar to AMA (Figure 4.4b).

4.6.3 Samples Selected for gPMA Comparison

The comparisons of aMAP chemical composition in this paper included all samples collected on the five cruises: ICEALOT, VOCALS, CalNEX, EPEACE, and WACS. However, in order to compare gPMA with seawater, we were limited to the CalNex and WACS cruises since gPMA was not sampled on the other cruises. Since the Bubbler and Sea Sweep and seawater collection operations were not synchronized (and true synchronization would be quite difficult), direct comparisons were not possible. To compare the spectral features of gPMA OM (Figure 4.8), we selected those gPMA and seawater samples that overlapped most closely in time and location so that the range and variability within the average compositions could be compared. This selection excluded a couple samples at each location that had a slightly larger range of variability but did not change the average differences between the locations. The samples included in the spectra comparison in Figure 4.8 are shown in Table 4.7.

The Bubbler gPMA samples include a range of bubbled air flowrates (from 1.5 to 6 lpm during WACS and CalNex), as well as both coarse and fine frits (see also Section 4.6.4), since there was no evidence for systematic differences in organic functional group composition for these conditions. The compositional difference between the particles produced with the fine and coarse frits and varying flowrates in this study is within the measurement variability, as shown in Table 4.6 and discussed in Section 4.6.4.

The average Sea Sweep gPMA OM functional group fractions reported by *Quinn et al.* [2014] during WACS are slightly different (40 (± 11)% hydroxyl, 47 (± 11)% alkane and 13 (± 4)% amine functional groups from the productive seawater and 52 (±12)% hydroxyl, 35 (±12)% alkane, and 13 (± 3)% amine functional groups from the

non-productive seawater) than those reported here (Table 4.6) because four of the samples used in that study were excluded in this study due to uncertainties in instrument performance (Table 4.7).

Table 4.6: The average organic functional group composition, number of samples, and hydroxyl functional group peak location for the gPMA samples. The Bubbler gPMA samples are separated by gPMA frit production type: fine and coarse.

	Bubbler			Sea Sweep
Functional Group Fraction (%)	Total (Frits)	Fine Frits	Coarse Frits	Total[a]
CalNex				
Hydroxyl Group	42 ± 9	45 ± 8	36 ± 6	47 ± 14
Alkane Group	44 ± 8	40 ± 7	50 ± 5	38 ± 13
Amine Group	14 ± 3	14 ± 1	15 ± 5	15 ± 3
Samples (n)	8	5	3	6
Hydroxyl Group Peak Location (cm^{-1})	3372 ± 6	3373 ± 8	3370 ± 4	3366 ± 6
WACS S1				
Hydroxyl Group	51 ± 2	52	50	43 ± 11
Alkane Group	39 ± 3	37	41	43 ± 10
Amine Group	10 ± 2	11	9	14 ± 4
Samples (n)	2	1	1	8
Hydroxyl Group Peak Location (cm^{-1})	3355 ± 3	3353	3356	3356 ± 5
WACS S2				
Hydroxyl Group	70 ± 7	73 ± 6	68 ± 8	58 ± 11
Alkane Group	18 ± 8	14 ± 2	22 ± 10	29 ± 11
Amine Group	12 ± 4	14 ± 4	10 ± 3	12 ± 1
Samples (n)	6	3	3	4
Hydroxyl Group Peak Location (cm^{-1})	3377 ± 8	3382 ± 9	3371 ± 2	3363 ± 7

[a]Excluding the 4 WACS Sea Sweep samples removed based on uncertainty in instrument performance.

Table 4.7: Table of gPMA and seawater samples during WACS and CalNex.

Sea Sweep	Bubbler	Seawater
WACS		
8/20/12 13:38 - 8/20/12 17:00[a] 8/20/12 18:09 - 8/21/12 0:59[a] 8/21/12 2:13 - 8/21/12 10:28[a]		
8/21/12 10:54 - 8/21/12 16:59		8/21/12 13:42 8/21/12 13:42
8/21/12 18:11 - 8/22/12 0:58[a] 8/22/12 1:57 - 8/22/12 9:00[a]		
8/22/12 10:46 - 8/22/12 9:00 8/22/12 20:21 - 8/23/12 1:00[b] 8/23/12 2:06 - 8/23/12 9:10	8/22/12 17:09 - 8/22/12 19:08	8/22/12 23:20
	8/23/12 12:40 - 8/23/12 14:01	8/23/12 14:44
8/24/12 13:00 - 8/24/12 17:57[b] 8/24/12 20:13 - 8/25/12 1:00[b] 8/25/12 1:46 - 8/25/12 9:00	8/24/12 12:09 - 8/24/12 13:17 8/24/12 22:26 - 8/24/12 23:48	
8/25/12 10:35 - 8/25/12 17:00[a] 8/25/12 18:11 - 8/26/12 1:00[a]		
	8/25/12 18:30 - 8/25/12 20:32[a]	
8/26/12 3:12 - 8/26/12 4:38	8/26/12 1:32 - 8/26/12 2:59[a]	8/26/12 0:45
8/26/12 10:43 - 8/26/12 16:59[b]	8/26/12 15:21 - 8/26/12 17:04	8/26/12 18:30 8/26/12 18:40
CalNex		
5/15/10 22:50 - 5/16/10 1:16 5/24/10 14:49 - 5/24/10 20:53		5/29/10 22:41 5/23/10 20:15
5/25/10 19:41 - 5/26/10 1:15	5/30/10 16:23 - 5/30/10 17:32	5/26/10 1:10
5/27/10 20:45 - 5/28/10 1:19[a]	5/28/10 22:35 - 5/28/10 23:33[a] 5/30/10 4:00 - 5/30/10 5:00[a]	
5/18/10 17:41 - 5/18/10 21:58	5/31/10 4:08 - 5/31/10 5:02	
	5/31/10 17:26 - 5/31/10 18:24[a] 6/1/10 3:42 - 6/1/10 4:42[a] 6/2/10 4:06 - 6/2/10 4:54[a] 6/2/10 16:12 6/2/10 17:06[a]	
6/6/10 21:18 - 6/7/10 2:08	6/6/10 20:24 - 6/6/10 21:24 6/7/10 3:45 - 6/7/10 4:44	6/6/10 20:53
	6/7/10 18:18 - 6/7/10 19:17[c] 6/7/10 20:13 - 6/7/10 20:31[c]	

[a]Excluded from the spectra comparison in Figure 4.8 due to lack of collocated samples (in time and/or location).
[b]Excluded from this study based on uncertainty in instrument performance.
[c]Excluded from the composition averages because of sampling in the San Francisco Bay.

4.6.4 Comparison of gPMA Number Size Distributions and Composition for Bubbler

During CalNex and WACS, the organic compositions and number size distributions of gPMA generated in the Bubbler using multiple production configurations, including fine and coarse frits (Ace glass pore sizes D and A, respectively) with varying bubble flow rates were measured. During CalNex, jets of seawater impinged on the model ocean surface were also used for a limited amount of time in Monterey Bay. Since the range of size distributions and the average organic composition were very similar for the different configurations (Figure 4.12), consistent with the results of previous studies [*Keene et al.*, 2007; *Bates et al.*, 2012] likely indicating that the generators produced particles by similar mechanisms, we have included samples from both configurations in assessing the variability and trends of Bubbler gPMA for different regions.

Figure 4.12 shows the normalized number size distribution and average organic functional group composition of gPMA generated in different frit production configurations (fine and coarse) during CalNex. Dry size distributions of the gPMA were measured using a Scanning Mobility Particle Sizer (SMPS, Brechtel Manufacturing Inc.) and an Aerodynamic Particle Sizer (APS, TSI Inc.) [*Long et al.*, 2014]. The fine and coarse frits produce particles with very similar submicron particle size distributions, with the coarse frits producing slightly larger particles (modes at 70 and 83 nm, respectively). The organic compositions of the gPMA produced with the fine and coarse frits are similar within the variability of the measurements with 45 ± 8% hydroxyl, 40 ± 7% alkane, and 14 ± 1% amine functional group composition with the fine frits and 36 ± 6% hydroxyl,

50 ± 5% alkane, and 15 ± 5% amine functional groups with the coarse frits (Table 4.6). *Bates et al.* [2012] shows the similarity of the number distributions of the gPMA from the Sea Sweep and the Bubbler in the fine frit configuration. Since the limited scope of these studies allowed only two particle samples to be collected with the jets (during sampling in Monterey Bay), a comparison of the representative organic composition for the jets compared to frits is not available. The two jet gPMA sample compositions (69% hydroxyl group) were within the variability of the seawater and sampling conditions, providing no evidence for a systematic difference in the submicron organic composition of jet and frit produced particles despite a small difference in their size distribution (shown in Figure 4.12).

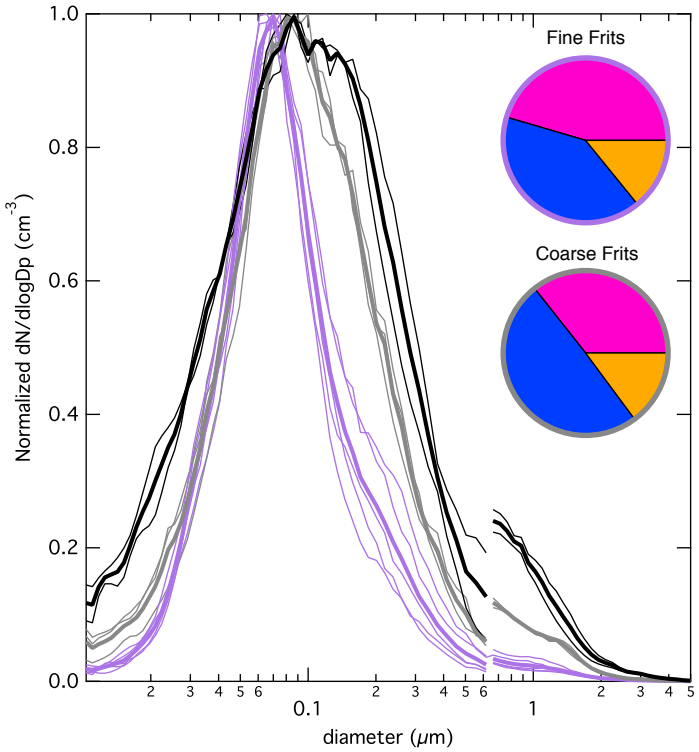

Figure 4.12: Normalized number size distribution of gPMA during CalNex produced with fine frits (purple), coarse frits (grey), and jets (black). The thin lines are individual filter samples, and the thick lines are averages. Pies represent the organic composition of the gPMA, with hydroxyl (pink), alkane (blue), and amine (orange) functional groups.

4.6.5 Marine Reference Saccharides

Saccharide standards were used for comparison to the aPMA OM. The standards were created by atomizing solutions of the saccharides in water or acetone (xanthan gum and carboxymethyl cellulose only). The atomized particles were collected on Teflon filters and analyzed using the same procedures described in the Methods. The saccharide spectra were reported previously [*Russell et al.*, 2010] and their relevant FTIR spectral values are listed in Table 4.8. The spectrum of the amino sugar (and polysaccharide) chitosan is shown in Figure 4.13.

Table 4.8: Comparison of the aPMA OM spectrum with saccharide spectra. Hydroxyl functional group peak location, ratio of alkane to hydroxyl functional group absorption peak heights, and calculated alkane group mass fractions are shown for the saccharides and the aPMA OM type. The cosine similarities of each saccharide spectrum with the aPMA OM are shown.

Name	Hydroxyl Group Peak Location (cm^{-1})	Alkane to Hydroxyl Group Peak Heights	Cosine Similarity with aPMA Spectrum	Calculated Alkane Group Mass Fraction
aPMA OM	3380	0.36	--	
Mono-saccharides				**19-27%**
Galactose	3372	0.36	0.93	
Mannitol	3284	0.21	0.81	
Fructose	3372	0.35	0.92	
Xylose	3368	0.32	0.90	
Glucose	3378	0.24	0.92	
Glucosamine			N/A	
Galactosamine			N/A	
Di-saccharides				**23-31%**
Sucrose	3267	0.68	0.81	
Lactose	3386	0.26	0.93	
Cellobiose	3380	0.33	0.94	
Poly-saccharides				**18-60%**
Xanthan Gum	3382	1.34	0.88	
Carboxymethyl Cellulose	3412	0.66	0.94	
Pectin	3453	0.37	0.97	
Chitosan	3410	0.11	0.94	

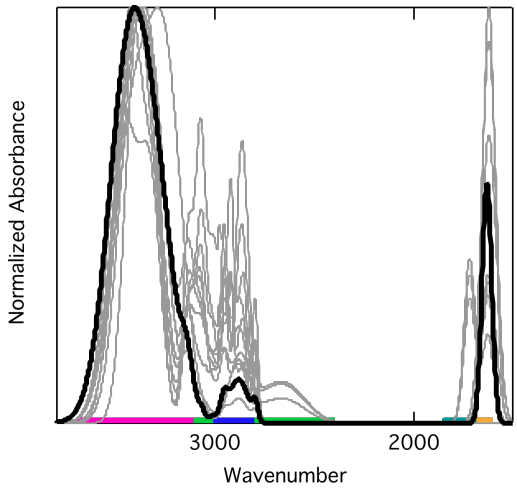

Figure 4.13: Normalized FTIR spectra of aPMA (grey) and chitosan (black). Functional group absorption regions are shown as bars with hydroxyl (pink), alkane (blue), carboxylic acid (green), carbonyl (teal), and amine (orange).

4.6.6 Carboxylic Acid Functional Groups

The carboxylic acid and amide functional groups were not observed in the seawater OM or the gPMA particles from the Bubbler and the Sea Sweep in CalNex or WACS. Previous studies have shown photochemical production of low molecular weight (LMW) carbonyl [*Mopper and Stahovec*, 1986; *Zhou and Mopper*, 1997] and carboxylic acid [*Kieber and Mopper*, 1987] functional groups in seawater. Studies have also shown a contribution of amide functional groups to seawater OM [i.e. *McCarthy et al.*, 1997]. Even though carboxylic acids and amides have been previously measured in seawater, all organic acids are below detection limit (BDL, and contribute to < 20% of the OM) for the seawater samples. A fraction of amide functional groups may be identified in this study as amine functional groups due to sample drying procedures. Mild acid hydrolysis of seawater proteins, which may occur during seawater sample drying, can destroy the amide functional group bond linkage. This results in amino acids, which contain amine

functional groups [*Aluwihare et al.*, 2005]. Organic acids can also bind to Na^+ making them R-(C=O)-ONa instead of R-(C=O)-OH which absorb as carboxylate salts. This leads to a shift in the C=O peak from 1712 to 1552 (± 16) cm^{-1} [*Max and Chapados*, 2004]. There was no detectable absorption in either of these two C=O stretching regions in the samples reported here, indicating that both acids and carboxylates were BDL in the seawater samples. Additionally, primary amides (R-C=O-NH_2) and secondary amides (R-C=O-NH-R') have broad C=O absorption at 1680-1630 cm^{-1}. This overlaps with the N-H bend (1640 to 1620 cm^{-1}) making the band appear as a doublet [*Pavia et al.*, 2001]. In the seawater OM spectra measured in this study, there is a primary amine N-H absorption at 1630 cm^{-1}, which is present as only one narrow peak suggesting that amide functional groups are not present.

Carboxylic acid and amide groups were also BDL in the gPMA samples. Since the acids that have been identified in DOM in seawater are mainly LMW, it is possible that they would not form particles during the bubble bursting processes even if they had been present in the seawater. The LMW carbonyls and acids, being LMW and water soluble, may stay in the dissolved form and drain out as the bubble film drains. *Mochida et al.* [2002] found that the LMW saturated fatty acids they analyzed only accounted for up to 4% of the OM in marine aerosol films, supporting the lack of LMW acids in the aerosol.

4.7 Acknowledgements

This work was funded by NSF grants AGS-1013423, OCE-1129580, and AGS-1360645. PNNL acknowledges additional support from the Office of Science Biological

and Environmental Research Program of the U.S. Department of Energy as part of the Earth System Modelling Program. The authors thank William Keene at the University of Virginia and David Kieber at the State University of New York at Syracuse for deploying the Bubbler during CalNex and WACS and for the use of the data collected with the Bubbler. The authors thank the captains, crews, and scientists on board the R/V *Knorr*, *Ronald H. Brown*, *Atlantis*, and *Point Sur* for their support in the field. The authors also thank Derek Coffman, Drew Hamilton, John Maben, Lelia Hawkins, Janin Guzman-Morales, Anita Johnson, and Robin Modini for assistance with sample collection. The authors acknowledge Grace Weissner, Randelle Bundy, and Katherine Barbeau for running, providing training on, and lending the fluorometer for chl-*a* concentration measurements for the EPEACE samples. They also acknowledge David Kilcoyne at the Lawrence Berkeley National Laboratory Advanced Light Source and Satoshi Takahama for assistance with STXM-NEXAFS and beamline operation. To obtain the data used in this study, please contact the corresponding author (lmrussell@ucsd.edu) or visit http://aerosol.ucsd.edu/publications and http://saga.pmel.noaa.gov/data.

Chapter 4, in full, has been submitted for publication to the *Journal of Geophysical Research – Atmospheres*. Frossard, A.A., L.M. Russell, M.S. Long, S.M. Burrows, S.M. Elliot, T.S. Bates, P.K. Quinn (2014), "Sources and Composition of Submicron Organic Mass in Marine Aerosol Particles." The dissertation author was the primary investigator and author of this paper.

References

Aiken, A. C., P. F. Decarlo, J. H. Kroll, D. R. Worsnop, J. A. Huffman, K. S. Docherty, I. M. Ulbrich, C. Mohr, J. R. Kimmel, D. Sueper, Y. Sun, Q. Zhang, A. Trimborn, M. Northway, P. J. Ziemann, M. R. Canagaratna, T. B. Onasch, M. R. Alfarra, A. S. H. Prevot, J. Dommen, J. Duplissy, A. Metzger, U. Baltensperger and J. L. Jimenez (2008), O/C and OM/OC ratios of primary, secondary, and ambient organic aerosols with high-resolution time-of-flight aerosol mass spectrometry, *Environmental Science & Technology*, *42*(12), 4478-4485, doi:10.1021/es703009q.

Aluwihare, L. I., and D. J. Repeta (1999), A comparison of the chemical characteristics of oceanic DOM and extracellular DOM produced by marine algae, *Marine Ecology-Progress Series*, *186*, 105-117.

Aluwihare, L. I., D. J. Repeta, and R. F. Chen (1997), A major biopolymeric component to dissolved organic carbon in surface sea water, *Nature*, *387*(6629), 166-169.

Aluwihare, L. I., D. J. Repeta, S. Pantoja, and C. G. Johnson (2005), Two chemically distinct pools of organic nitrogen accumulate in the ocean, *Science*, *308*(5724), 1007-1010, doi:10.1126/science.1108925.

Aminot, A., and R. Kerouel (2006), The determination of total dissolved free primary amines in seawater: Critical factors, optimized procedure and artefact correction, *Marine Chemistry*, *98*(2-4), 223-240, doi:10.1016/j.marchem.2005.07.005.

Ault, A. P., D. F. Zhao, C. J. Ebben, M. J. Tauber, F. M. Geiger, K. A. Prather, and V. H. Grassian (2013), Raman microscpectroscopy and vibrational sum frequency generation spectroscopy as probles of the bulk and surface compositions of size-resolved sea spray particles, *Physical Chemistry - Chemical Physics*, *15*(17), 6206-6214.

Bahadur, R., T. Uplinger, L. M. Russell, B. C. Sive, S. S. Cliff, D. B. Millet, A. Goldstein, and T. S. Bates (2010), Phenol Groups in Northeastern US Submicrometer Aerosol Particles Produced from Seawater Sources, *Environmental Science & Technology*, *44*(7), 2542-2548, doi:10.1021/es9032277.

Bates, T. S., D. J. Coffman, D. S. Covert, and P. K. Quinn (2002), Regional marine boundary layer aerosol size distributions in the Indian, Atlantic, and Pacific Oceans: A comparison of INDOEX measurements with ACE-1, ACE-2, and Aerosols99, *Journal of Geophysical Research-Atmospheres*, *107*(D19), doi:10.1029/2001jd001174.

Bates, T. S., P. K. Quinn, A. A. Frossard, L. M. Russell, J. Hakala, T. Petäjä, M. Kulmala, D. S. Covert, C. D. Cappa, S.-M. Li, K. Hayden, I. Nuaaman, R. McLaren, P. Massoli, M. R. Canagaratna, T. B. Onasch, D. Sueper, D. R. Worsnop, W. C. Keene (2012), Measurements of Ocean Derived Aerosol off the Coast of California, *Journal of Geophysical Research - Atmospheres*, *117*(D00V15), doi:10.1029/2012JD017588.

Benner, R., and K. Kaiser (2003), Abundance of amino sugars and peptidoglycan in marine particulate and dissolved organic matter, *Limnology and Oceanography*, *48*(1), 118-128.

Benner, R., J. D. Pakulski, M. McCarthy, J. I. Hedges, and P. G. Hatcher (1992), Bulk chemical characteristics of dissolved organic-matter in the ocean, *Science*, *255*(5051), 1561-1564.

Biersmith, A., and R. Benner (1998), Carbohydrates in phytoplankton and freshly produced dissolved organic matter, *Marine Chemistry*, *63*(1-2), 131-144.

Bigg, E. K. (2007), Sources, nature and influence on climate of marine airborne particles, *Environmental Chemistry*, *4*(3), 155-161, doi:10.1071/en07001.

Bigg, E. K., and C. Leck (2008), The composition of fragments of bubbles bursting at the ocean surface, *Journal of Geophysical Research-Atmospheres*, *113*(D11), doi:10.1029/2007jd009078.

Blanchard, D. C. (1963), The electrification of the atmosphere by particles from bubbles in the sea, *Progress in Oceanography*, *1*(48), 16-16.

Blanchard, D. C. (1964), Sea-to-air transport of surface active material, *Science*, *146*(364), 396-397.

Blanchard, D. C. (1975), Bubble scavenging and water-to-air transfer of organic material in sea, *Advances in Chemistry Series*(145), 360-387.

Blanchard, D. C., and A. H. Woodcock (1980), The production, concentration, and vertical distribution of the sea-salt aerosol, *Annals of the New York Academy of Sciences*, *338*(1), 330-347.

Burrows, S.M., O. Ogunro, A.A. Frossard, L.M. Russell, P.J. Rasch, and S. Elliott (2014). "A Physically-based Framework for Modelling the Organic Fractionation of Sea Spray Aerosol from Bubble Film Langmuir Equilibria." *Atmospheric Chemistry and Physics Discussions*.

Buseck, P. R., and M. Posfai (1999), Airborne minerals and related aerosol particles: Effects on climate and the environment, *Proceedings of the National Academy of Sciences of the United States of America*, *96*(7), 3372-3379, doi:10.1073/pnas.96.7.3372.

Cavalli, F., M. C. Facchini, S. Decesari, M. Mircea, L. Emblico, S. Fuzzi, D. Ceburnis, Y. J. Yoon, C. D. O'Dowd, J. P. Putaud, A. Dell'Acqua (2004), Advances in characterization of size-resolved organic matter in marine aerosol over the North Atlantic, *Journal of Geophysical Research - Atmospheres*, *109*(D24215), doi:10.1029/2004jd005137.

Ceburnis, D., A. Garbaras, S. Szidat, M. Rinaldi, S. Fahrni, N. Perron[5], L. Wacker, S. Leinert, V. Remeikis, M. C. Facchini, A. S. H. Prevot, S. G. Jennings, M. Ramonet, and C. D. O'Dowd (2011), Quantification of the carbonaceous matter origin in submicron marine aerosol by C-13 and C-14 isotope analysis, *Atmospheric Chemistry and Physics*, *11*(16), 8593-8606, doi:10.5194/acp-11-8593-2011.

Ceburnis, D., C. D. O'Dowd, G. S. Jennings, M. C. Facchini, L. Emblico, S. Decesari, S. Fuzzi, and J. Sakalys (2008), Marine aerosol chemistry gradients: Elucidating primary and secondary processes and fluxes, *Geophysical Research Letters*, *35*(7), doi:10.1029/2008gl033462.

Cincinelli, A., A. M. Stortini, M. Perugini, L. Checchini, and L. Lepri (2001), Organic pollutants in sea-surface microlayer and aerosol in the coastal environment of Leghorn - (Tyrrhenian Sea), *Marine Chemistry*, *76*(1-2), 77-98, doi:10.1016/s0304-4203(01)00049-4.

Clarke, A. D., S. R. Owens, and J. C. Zhou (2006), An ultrafine sea-salt flux from breaking waves: Implications for cloud condensation nuclei in the remote marine atmosphere, *Journal of Geophysical Research-Atmospheres*, *111*(D6), doi:10.1029/2005jd006565.

Coggon, M. M., A. Sorooshian, Z. Wang, A.R. Metcalf, A.A. Frossard, J.J. Lin, J.S. Craven, A. Nenes, H.H. Jonsson, L.M. Russell, R.C. Flagan, and J.H. Seinfeld (2012), Ship impacts on the marine atmosphere: insights into the contribution of shipping emissions to the properties of marine aerosol and clouds, *Atmospheric Chemistry and Physics*, *12*(18), doi:10.5194/acp-12-8439-2012.

Collins, D. B., D. Zhao, M. J. Ruppel, G. B. Deane, M. D. Stokes, P. J. DeMott, C. Lee, R. L. Modini, L. M. Russell, and K. A. Prather (2013), Evaluating the properties of sea spray aerosols produced in the laboratory: Comparisons with controlled breaking waves, *AIP Conference Proceedings*, *1527*, 551-554, doi:10.1063/1.4803330.

Crahan, K. K., D. A. Hegg, D. S. Covert, H. Jonsson, J. S. Reid, D. Khelif, and B. J. Brooks (2004), Speciation of organic aerosols in the tropical mid-pacific and their relationship to light scattering, *Journal of the Atmospheric Sciences*, *61*(21), 2544-2558.

de Leeuw, G., E. L. Andreas, M. D. Anguelova, C. W. Fairall, E. R. Lewis, C. O'Dowd, M. Schulz, and S. E. Schwartz (2011), Production Flux of Sea Spray Aerosol, *Reviews of Geophysics*, *49*, doi:10.1029/2010rg000349.

DeCarlo, P. F., E. J. Dunlea, J. R. Kimmel, A. C. Aiken, D. Sueper, J. Crounse, P. O. Wennberg, L. Emmons, Y. Shinozuka, A. Clarke, J. Zhou, J. Tomlinson, D. R. Collins, D. Knapp, A. J. Weinheimer, D. D. Montzka, T. Campos, and J. L. Jimenez (2008), Fast airborne aerosol size and chemistry measurements above Mexico City and Central Mexico during the MILAGRO campaign, *Atmospheric Chemistry and Physics*, *8*(14), 4027-4048.

Draxler, R. R., and G. D. Rolph (2003), HYSPLIT (HYbrid Single-Particle Lagrangian Integrated Trajectory), Air Resources Laboratory, NOAA, Silver Spring, MD, (Model access via NOAA ARL READY Website http://www.arl.noaa.gov/readyhysplit4.html).

Druffel, E. R. M., P. M. Williams, J. E. Bauer, and J. R. Ertel (1992), Cycling of dissolved and particulate organic-matter in the open ocean, *Journal of Geophysical Research-Oceans*, *97*(C10), 15639-15659.

Emerson, S., and J. Hedges (2008), *Chemical Oceanography and the Marine Carbon Cycle*, Cambridge University Press.

Erickson, D. J., C. Seuzaret, W. C. Keene, and S. L. Gong (1999), A general circulation model based calculation of HCl and ClNO2 production from sea salt dechlorination: Reactive Chlorine Emissions Inventory, *Journal of Geophysical Research-Atmospheres*, *104*(D7), 8347-8372, doi:10.1029/98jd01384.

Erlick, C., L. M. Russell, and V. Ramaswamy (2001), A microphysics-based investigation of the radiative effects of aerosol-cloud interactions for two MAST Experiment case studies, *Journal of Geophysical Research-Atmospheres*, *106*(D1), 1249-1269.

Facchini, M. C., M. Rinaldi, S. Decesari, C. Carbone, E. Finessi, M. Mircea, S. Fuzzi, D. Ceburnis, R. Flanagan, E. D. Nilsson, G. de Leeuw, M. Martino, J. Woeltjen, C. D. O'Dowd (2008), Primary submicron marine aerosol dominated by insoluble organic colloids and aggregates, *Geophysical Research Letters*, L17814 (17815 pp.), doi:10.1029/2008gl034210.

Facchini, M. C., M. Rinaldi, S. Decesari, and S. Fuzzi (2010), Marine organic aerosol and biological oceanic activity, *Chemical Engineering*, *22*.

Frossard, A.A., L.M. Russell, P. Massoli, T.S. Bates, and P.K. Quinn (2014) "Side-by-side comparison of four techniques explains the apparent differences in the organic composition of generated and ambient marine aerosol particles." *Aerosol Science and Technology*. 48:3, v-x, doi:10.1080/02786826.2013.879979.

Frossard, A. A., and L. M. Russell (2012), Removal of Sea Salt Hydrate Water from Seawater-Derived Samples by Dehydration, *Environmental Science & Technology*, *46*(24), 13326-13333, doi:10.1021/es3032083.

Frossard, A. A., P. M. Shaw, L. M. Russell, J. H. Kroll, M. R. Canagaratna, D. R. Worsnop, P. K. Quinn, and T. S. Bates (2011), Springtime Arctic haze contributions of submicron organic particles from European and Asian combustion sources, *Journal of Geophysical Research-Atmospheres*, *116*, doi:10.1029/2010jd015178.

Fu, P. Q., K. Kawamura, J. Chen, B. Charriere, and R. Sempere (2013), Organic molecular composition of marine aerosols over the Arctic Ocean in summer:

contributions of primary emission and secondary aerosol formation, *Biogeosciences*, *10*(2), 653-667, doi:10.5194/bg-10-653-2013.

Fu, P. Q., K. Kawamura, and K. Miura (2011), Molecular characterization of marine organic aerosols collected during a round-the-world cruise, *Journal of Geophysical Research-Atmospheres*, *116*, doi:10.1029/2011jd015604.

Fuentes, E., H. Coe, D. Green, G. de Leeuw, and G. McFiggans (2010), Laboratory-generated primary marine aerosol via bubble-bursting and atomization, *Atmospheric Measurement Techniques*, *3*(1), 141-162.

Gantt, B., N. Meskhidze, M. C. Facchini, M. Rinaldi, D. Ceburnis, and C. D. O'Dowd (2011), Wind speed dependent size-resolved parameterization for the organic mass fraction of sea spray aerosol, *Atmospheric Chemistry and Physics*, *11*(16), 8777-8790.

Guzman-Morales, J., A.A. Frossard, A.L. Corrigan, L.M. Russell, S. Liu, S. Takahama; J.W. Taylor, J. Allan, H. Coe, Y. Zhao, and A.H. Goldstein., (2013), Estimated Contributions of Primary and Secondary Organic Aerosol from Fossil Fuel Combustion during the CalNex and Cal-Mex Campaigns, *Atmospheric Environment*.

Hansell, D. A. (2013), Recalcitrant Dissolved Organic Carbon Fractions, *Annual Review of Marine Science, Vol 5*, *5*, 421-445, doi:10.1146/annurev-marine-120710-100757.

Hawkins, L. N., and L. M. Russell (2010), Polysaccharides, Proteins, and Phytoplankton Fragments: Four Chemically Distinct Types of Marine Primary Organic Aerosol Classified by Single Particle Spectromicroscopy, *Advances in Meteorology*, *2010*(Article ID 612132), 14, doi:10.1155/2010/612132.

Hawkins, L. N., L. M. Russell, D. S. Covert, P. K. Quinn, and T. S. Bates (2010), Carboxylic acids, sulfates, and organosulfates in processed continental organic aerosol over the southeast Pacific Ocean during VOCALS-REx 2008, *Journal of Geophysical Research-Atmospheres*, *115*(D13201), doi:10.1029/2009jd013276.

Hoffman, E. J., and R. A. Duce (1976), Factors influencing organic-carbon content of marine aerosols - laboratory study, *Journal of Geophysical Research-Oceans and Atmospheres*, *81*(21), 3667-3670.

Holland, H. D. (1978), *The Chemistry of the Atmosphere and Oceans*, edited, p. 154, Jon Wiley, New York.

Hultin, K. A. H., E. D. Nilsson, R. Krejci, E. M. Martensson, M. Ehn, A. Hagstrom, and G. de Leeuw (2010), In situ laboratory sea spray production during the Marine Aerosol Production 2006 cruise on the northeastern Atlantic Ocean, *Journal of Geophysical Research-Atmospheres*, *115*(D06201), doi:10.1029/2009jd012522.

Kawamura, K., and R. B. Gagosian (1987), Implications of omega-oxocarboxylic acids in the remote marine atmosphere for photooxidation of unsaturated fatty-acids, *Nature*, *325*(6102), 330-332, doi:10.1038/325330a0.

Kawamura, K., and F. Sakaguchi (1999), Molecular distributions of water soluble dicarboxylic acids in marine aerosols over the Pacific Ocean including tropics, *Journal of Geophysical Research-Atmospheres*, *104*(D3), 3501-3509.

Keene, W. C., H. Maring, J. R. Maben, D. J. Kieber, A. A. P. Pszenny, E. E. Dahl, M. A. Izaguirre, A. J. Davis, M. S. Long, X. L. Zhou, L. Smoydzin, R. Sander (2007), Chemical and physical characteristics of nascent aerosols produced by bursting bubbles at a model air-sea interface, *Journal of Geophysical Research-Atmospheres*, *112*(D21), doi:10.1029/2007jd008464.

Keene, W. C., R. Sander, A. A. P. Pszenny, R. Vogt, P. J. Crutzen, and J. N. Galloway (1998), Aerosol pH in the marine boundary layer: A review and model evaluation, *Journal of Aerosol Science*, *29*(3), 339-356, doi:10.1016/s0021-8502(97)10011-8.

Kieber, D. J., and K. Mopper (1987), Photochemical formation of glyoxylic and pyruvic acids in seawater, *Marine Chemistry*, *21*(2), 135-149, doi:10.1016/0304-4203(87)90034-x.

King, S. M., A. C. Butcher, T. Rosenoern, E. Coz, K. I. Lieke, G. de Leeuw, E. D. Nilsson, and M. Bilde (2012), Investigating Primary Marine Aerosol Properties: CCN Activity of Sea Salt and Mixed Inorganic-Organic Particles, *Environmental Science & Technology*, *46*(19), doi:10.1021/es300574u.

Kuhn, L. P. (1950), Infrared spectra of carbohydrates, *Analytical Chemistry*, *22*(2), 276-283, doi:10.1021/ac60038a015.

Kuznetsova, M., C. Lee, and J. Aller (2005), Characterization of the proteinaceous matter in marine aerosols, *Marine Chemistry*, *96*(3-4), 359-377, doi:10.1016/j.marchem.2005.03.007.

Lewis, E. R., and S. E. Schwartz (2004), *Sea salt aerosol production: mechanisms, methods, measurements, and models - a critical review*, American Geophysical Union, Washington.

Liu, S., D. A. Day, J. E. Shields, and L. M. Russell (2011), Ozone-driven daytime formation of secondary organic aerosol containing carboxylic acid groups and alkane groups, *Atmospheric Chemistry and Physics*, *11*(16), 8321-8341, doi:10.5194/acp-11-8321-2011.

Long, M.S., W.C. Keene, D.J. Kieber, A.A. Frossard, L.M. Russell, J.R. Maben, J. D. Kinsey, P.K. Quinn, and T. S. Bates (2014). “Light-enhanced primary marine aerosol

production from biologically productive seawater." *Geophysical Research Letters*. doi: 10.1002/2014GL059436.

Maria, S. F., L. M. Russell, B. J. Turpin, and R. J. Porcja (2002), FTIR measurements of functional groups and organic mass in aerosol samples over the Caribbean, *Atmospheric Environment*, *36*(33), 5185-5196.

Maria, S. F., L. M. Russell, B. J. Turpin, R. J. Porcja, T. L. Campos, R. J. Weber, and B. J. Huebert (2003), Source signatures of carbon monoxide and organic functional groups in Asian Pacific Regional Aerosol Characterization Experiment (ACE-Asia) submicron aerosol types, *Journal of Geophysical Research-Atmospheres*, *108*(D23), doi:10.1029/2003jd003703.

Martensson, E. M., E. D. Nilsson, G. de Leeuw, L. H. Cohen, and H. C. Hansson (2003), Laboratory simulations and parameterization of the primary marine aerosol production, *Journal of Geophysical Research-Atmospheres*, *108*(D9), doi:10.1029/2002jd002263.

Mathlouthi, M., and J. L. Koenig (1986), Vibrational-spectra of carbohydrates, *Advances in Carbohydrate Chemistry and Biochemistry*, *44*, 7-89.

Matsumoto, K., and M. Uematsu (2005), Free amino acids in marine aerosols over the western North Pacific Ocean, *Atmospheric Environment*, *39*(11), 2163-2170, doi:10.1016/j.atmosenv.2004.12.022.

Max, J. J., and C. Chapados (2004), Infrared spectroscopy of aqueous carboxylic acids: Comparison between different acids and their salts, *Journal of Physical Chemistry A*, *108*(16), 3324-3337, doi:10.1021/jp036401t.

McCarthy, M., T. Pratum, J. Hedges, and R. Benner (1997), Chemical composition of dissolved organic nitrogen in the ocean, *Nature*, *390*(6656), 150-154, doi:10.1038/36535.

Meskhidze, N., and A. Nenes (2006), Phytoplankton and cloudiness in the Southern Ocean, *Science*, *314*(5804), 1419-1423, doi:10.1126/science.1131779.

Mochida, M., Y. Kitamori, K. Kawamura, Y. Nojiri, and K. Suzuki (2002), Fatty acids in the marine atmosphere: Factors governing their concentrations and evaluation of organic films on sea-salt particles, *Journal of Geophysical Research-Atmospheres*, *107*(D17).

Modini, R. L., L. M. Russell, G. B. Deane, and M. D. Stokes (2013), Effect of soluble surfactant on bubble persistence and bubble-produced aerosol particles, *Journal of Geophysical Research-Atmospheres*, *118*(3), 1388-1400, doi:10.1002/jgrd.50186.

Mopper, K., and W. L. Stahovec (1986), Sources and sinks of low-molecular-weight organic carbonyl-compounds in seawater, *Marine Chemistry*, *19*(4), 305-321, doi:10.1016/0304-4203(86)90052-6.

Naumann, D., G. Barnickel, H. Bradaczek, H. Labischinski, and P. Giesbrecht (1982), Infrared-spectroscopy, a tool for probing bacterial peptidoglycan - potentialities of infrared-spectroscopy for cell-wall analytical studies and rejection of models based on crystalline chitin, *European Journal of Biochemistry*, *125*(3), 505-515, doi:10.1111/j.1432-1033.1982.tb06711.x.

Nilsson, E. D., U. Rannik, E. Swietlicki, C. Leck, P. P. Aalto, J. Zhou, and M. Norman (2001), Turbulent aerosol fluxes over the Arctic Ocean 2. Wind-driven sources from the sea, *Journal of Geophysical Research-Atmospheres*, *106*(D23), 32139-32154.

O'Dowd, C. D., and G. De Leeuw (2007), Marine aerosol production: a review of the current knowledge, *Philosophical Transactions of the Royal Society a-Mathematical Physical and Engineering Sciences*, *365*(1856), 1753-1774, doi:10.1098/rsta.2007.2043.

O'Dowd, C. D., M. C. Facchini, F. Cavalli, D. Ceburnis, M. Mircea, S. Decesari, S. Fuzzi, Y. J. Yoon, and J. P. Putaud (2004), Biogenically driven organic contribution to marine aerosol, *Nature*, *431*(7009), 676-680, doi:10.1038/nature02959.

O'Dowd, C. D., K. Hameri, J. M. Makela, L. Pirjola, M. Kulmala, S. G. Jennings, H. Berresheim, H.-C. Hansson, G. de Leeuw, G. J. Kunz, A. G. Allen, C. N. Hewitt, A. Jackson, Y. Viisanen, and T. Hoffman (2002), A dedicated study of New Particle Formation and Fate in the Coastal Environment (PARFORCE): Overview of objectives and achievements, *Journal of Geophysical Research-Atmospheres*, *107*(D19), doi:10.1029/2001jd000555.

Oppo, C., S. Bellandi, N. D. Innocenti, A. M. Stortini, G. Loglio, E. Schiavuta, and R. Cini (1999), Surfactant components of marine organic matter as agents for biogeochemical fractionation and pollutant transport via marine aerosols, *Marine Chemistry*, *63*(3-4), 235-253, doi:10.1016/s0304-4203(98)00065-6.

Orellana, M. V., and P. Verdugo (2003), Ultraviolet radiation blocks the organic carbon exchange between the dissolved phase and the gel phase in the ocean, *Limnology and Oceanography*, *48*(4), 1618-1623.

Ovadnevaite, J., C. O'Dowd, M. Dall'Osto, D. Ceburnis, D. R. Worsnop, and H. Berresheim (2011), Detecting high contributions of primary organic matter to marine aerosol: A case study, *Geophysical Research Letters*, *38*, doi:10.1029/2010gl046083.

Pavia, D. L., G. M. Lapman, and G. S. Kriz (2001), *Introduction to spectroscopy*, Third ed., Brooks/Cole.

Pszenny, A. A. P., W. C. Keene, D. J. Jacob, S. Fan, J. R. Maben, M. P. Zetwo, M. Springeryoung, and J. N. Galloway (1993), Evidence of inorganic chlorine gases other than hydrogen-chloride in marine surface air, *Geophysical Research Letters*, *20*(8), 699-702, doi:10.1029/93gl00047.

Quinn, P. K., D. J. Coffman, V. N. Kapustin, T. S. Bates, and D. S. Covert (1998), Aerosol optical properties in the marine boundary layer during the First Aerosol Characterization Experiment (ACE 1) and the underlying chemical and physical aerosol properties, *Journal of Geophysical Research-Atmospheres*, *103*(D13), 16547-16563.

Quinn, P.K., T.S. Bates, K.S. Schultz, D.C. Coffman, A.A. Frossard, L.M. Russell, W.C. Keene, and D.J. Kieber (2014). "Empirical Constraints on Modeling the Organic Matter Enrichment in Nascent Sea Spray Aerosol." *Nature Geoscience.*

Randles, C. A., L. M. Russell, and V. Ramaswamy (2004), Hygroscopic and optical properties of organic sea salt aerosol and consequences for climate forcing, *Geophysical Research Letters*, *31*(L16108), doi:10.1029/2004gl020628.

Redfield, A. C. (1934), On the proportions of organic derivatives in sea water and their relation to the composition of plankton, *James Johnstone Memorial Volume 1934.*, 176-171.

Rinaldi, M., S. Decesari, E. Finessi, L. Giulianelli, C. Carbone, S. Fuzzi, C. D. O'Dowd, D. Ceburnis, and M. C. Facchini (2010), Primary and secondary organic marine aerosol and oceanic biological activity: recent results and new perspectives for future studies, *Advances in Meteorology*, *2010*(Arctic ID 310682), 10.

Rogge, W. F., M. A. Mazurek, L. M. Hildemann, G. R. Cass, and B. R. T. Simoneit (1993), Quantification of urban organic aerosols at a molecular-level - identification, abundance and seasonal-variation, *Atmospheric Environment Part a-General Topics*, *27*(8), 1309-1330.

Russell, L. M. (2003), Aerosol organic-mass-to-organic-carbon ratio measurements, *Environmental Science & Technology*, *37*(13), 2982-2987, doi:10.1021/es026123w.

Russell, L. M., L. N. Hawkins, A. A. Frossard, P. K. Quinn, and T. S. Bates (2010), Carbohydrate-like composition of submicron atmospheric particles and their production from ocean bubble bursting, *Proceedings of the National Academy of Sciences of the United States of America*, *107*(15), 6652-6657, doi:10.1073/pnas.0908905107.

Russell, L. M., A. Sorooshian, J.H. Seinfeld, B.A. Albrecht, A. Nenes, L. Ahlm, Y.-C. Chen, M. Coggon, J.S. Craven, R.C. Flagan, A.A. Frossard, H. Jonsson, E. Jung, Jack J. Lin, A.R. Metcalf, R.L. Modini, J. Mülmenstädt, G.C. Roberts, T. Shingler, S. Song, Z. Wang, A. Wonaschütz (2013), Eastern Pacific Emitted Aerosol Cloud Experiment, *Bulletin of the American Meteorological Society*, *94*(5), 709-+, doi:10.1175/bams-d-12-00015.1.

Russell, L. M., S. Takahama, S. Liu, L. N. Hawkins, D. S. Covert, P. K. Quinn, and T. S. Bates (2009), Oxygenated fraction and mass of organic aerosol from direct emission and atmospheric processing measured on the R/V Ronald Brown during

TEXAQS/GoMACCS 2006, *Journal of Geophysical Research-Atmospheres*, *114*, doi:10.1029/2008jd011275.

Satsumabayashi, H., H. Kurita, Y. Yokouchi, and H. Ueda (1990), Photochemical formation of particulate dicarboxylic-acids under long-range transport in central Japan, *Atmospheric Environment Part a-General Topics*, *24*(6), 1443-1450, doi:10.1016/0960-1686(90)90053-p.

Schmitt-Kopplin, P., G. Liger-Belair, B. P. Koch, R. Flerus, G. Kattner, M. Harir, B. Kanawati, M. Lucio, D. Tziotis, N. Hertkorn, I. Gebefuegi (2012), Dissolved organic matter in sea spray: a transfer study from marine surface water to aerosols, *Biogeosciences*, *9*(4), doi:10.5194/bg-9-1571-2012.

Sciare, J., O. Favez, R. Sarda-Esteve, K. Oikonomou, H. Cachier, and V. Kazan (2009), Long-term observations of carbonaceous aerosols in the Austral Ocean atmosphere: Evidence of a biogenic marine organic source, *Journal of Geophysical Research-Atmospheres*, *114*, doi:10.1029/2009jd011998.

Sellegri, K., C. D. O'Dowd, Y. J. Yoon, S. G. Jennings, and G. de Leeuw (2006), Surfactants and submicron sea spray generation, *Journal of Geophysical Research-Atmospheres*, *111*(D22), doi:10.1029/2005jd006658.

Shank, L. M., S. Howell, A. D. Clarke, S. Freitag, V. Brekhovskikh, V. Kapustin, C. McNaughton, T. Campos, and R. Wood (2012), Organic matter and non-refractory aerosol over the remote Southeast Pacific: oceanic and combustion sources, *Atmospheric Chemistry and Physics*, *12*(1), doi:10.5194/acp-12-557-2012.

Stein, S. E., and D. R. Scott (1994), Optimization and testing of mass spectral library search algorithms for compound identification, *Journal of the American Society for Mass Spectrometry*, *5*(9), 859-866.

Takahama, S., S. Gilardoni, L. M. Russell, and A. L. D. Kilcoyne (2007), Classification of multiple types of organic carbon composition in atmospheric particles by scanning transmission X-ray microscopy analysis, *Atmospheric Environment*, *41*(40), 9435-9451, doi:10.1016/j.atmosenv.2007.08.051.

Takahama, S., A. Johnson, and L. M. Russell (2012), Quantification of carboxylic and carbonyl functional groups in organic aerosol infrared absorbance spectra, *Aerosol Science and Technology*, doi:10.1080/02786826.2012.752065.

Takahama, S., S. Liu, and L. M. Russell (2010), Coatings and clusters of carboxylic acids in carbon-containing atmospheric particles from spectromicroscopy and their implications for cloud-nucleating and optical properties, *Journal of Geophysical Research-Atmospheres*, *115*, 21, doi:10.1029/2009jd012622.

Turekian, V. C., S. A. Macko, and W. C. Keene (2003), Concentrations, isotopic compositions, and sources of size-resolved, particulate organic carbon and oxalate in near-surface marine air at Bermuda during spring, *Journal of Geophysical Research-Atmospheres*, *108*(D5), doi:10.1029/2002jd002053.

Venyaminov, S. Y., and N. N. Kalnin (1990), Quantitative IR spectrophotometry of peptide compounds in water (H2O) solutions .1. Spectral parameters of amino-acid residue absorption-bands, *Biopolymers*, *30*(13-14), 1243-1257, doi:10.1002/bip.360301309.

Verdugo, P., A. L. Alldredge, F. Azam, D. L. Kirchman, U. Passow, and P. H. Santschi (2004), The oceanic gel phase: a bridge in the DOM-POM continuum, *Marine Chemistry*, *92*(1-4), 67-85, doi:10.1016/j.marchem.2004.06.017.

Ward, J. H. (1963), Hierarchical grouping to optimize an objective function, *Journal of the American Statistical Association*, *58*(301), doi:10.2307/2282967.

Williams, P. M., A. F. Carlucci, S. M. Henrichs, E. S. Vanvleet, S. G. Horrigan, F. M. H. Reid, and K. J. Robertson (1986), Chemical and microbiological studies of sea-surface films in the southern gulf of California and off the west-coast of Baja-California, *Marine Chemistry*, *19*(1), 17-98, doi:10.1016/0304-4203(86)90033-2.

Wonaschutz, A., M. Coggon, A. Sorooshian, R. Modini, A. A. Frossard, L. Ahlm, J. Muelmenstaedt, G. C. Roberts, L. M. Russell, S. Dey, F. J. Brechtel, and J. H. Seinfeld (2013), Hygroscopic properties of smoke-generated organic aerosol particles emitted in the marine atmosphere, *Atmospheric Chemistry and Physics*, *13*, 9819-9835.

Wurl, O., and M. Holmes (2008), The gelatinous nature of the sea-surface microlayer, *Marine Chemistry*, *110*(1-2), 89-97, doi:10.1016/j.marchem.2008.02.009.

Wurl, O., E. Wurl, L. Miller, K. Johnson, and S. Vagle (2011), Formation and global distribution of sea-surface microlayers, *Biogeosciences*, *8*(1), 121-134, doi:10.5194/bg-8-121-2011.

Yoon, Y. J., D. Ceburnis, F. Cavalli, O. Jourdan, J. P. Putaud, M. C. Facchini, S. Decesari, S. Fuzzi, K. Sellegri, S. G. Jennings, and C. D. O'Dowd (2007), Seasonal characteristics of the physicochemical properties of North Atlantic marine atmospheric aerosols, *Journal of Geophysical Research-Atmospheres*, *112*(D04206), doi:10.1029/2005jd007044.

Zhang, Q., D. R. Worsnop, M. R. Canagaratna, and J. L. Jimenez (2005), Hydrocarbon-like and oxygenated organic aerosols in Pittsburgh: insights into sources and processes of organic aerosols, *Atmospheric Chemistry and Physics*, *5*, 3289-3311.

Zhou, X. L., and K. Mopper (1997), Photochemical production of low-molecular-weight carbonyl compounds in seawater and surface microlayer and their air-sea exchange, *Marine Chemistry*, *56*(3-4), 201-213, doi:10.1016/s0304-4203(96)00076-x.

Zhou, X. L., A. J. Davis, D. J. Kieber, W. C. Keene, J. R. Maben, H. Maring, E. E. Dahl, M. A. Izaguirre, R. Sander, and L. Smoydzyn (2008), Photochemical production of hydroxyl radical and hydroperoxides in water extracts of nascent marine aerosols produced by bursting bubbles from Sargasso seawater, *Geophysical Research Letters*, *35*(20), doi:10.1029/2008gl035418.

Zutic, V., B. Cosovic, E. Marcenko, N. Bihari, and F. Krsinic (1981), Surfactant production by marine-phytoplankton, *Marine Chemistry*, *10*(6), 505-520, doi:10.1016/0304-4203(81)90004-9.

Conclusions

Ambient atmospheric and generated marine aerosol particles collected in multiple ocean regions and characterized using complementary measurement techniques were used to determine the sources and composition of aerosol particles in the marine boundary layer (MBL). The following questions were posed in the Introduction, and their answers are summarized below.

(i) What are the sources and composition of the OM in the springtime Arctic MBL? Aerosol particles measured in the Atlantic and Pacific regions of the Arctic MBL were influenced by emissions of European and Asian combustion sources. Based on factor analysis, combustion sources contributed to more than 60% of the total submicron OM in the Arctic MBL. These combustion sources were identified as industrial and other petroleum burning from eastern Europe, measured in the Atlantic Arctic region, and biomass burning and shipping emissions, measured in the Pacific Arctic region. The high emissions of sulfate from coal-burning in northeastern Europe, combined with the high acidity of the aerosol, produced significant concentrations of organosulfate functional groups (10% of the submicron OM in the Atlantic Arctic MBL) through acid-catalyzed aqueous reactions. The overall Atlantic Arctic springtime OM composition was 46% hydroxyl, 23% alkane, 6% amine, 5% carbonyl, 12% carboxylic acid, and 7%

organosulfate functional groups, while the Pacific Arctic springtime OM composition was 30% hydroxyl, 34% alkane, 6% amine, and 30% carboxylic acid functional groups.

(ii) How can seawater-derived particle samples be prepared for analysis by FTIR spectroscopy to avoid interference of sea salt hydrate bound water? A method for removing the sea salt hydrate bound water, which absorbs in the same infrared region as hydroxyl functional groups, from seawater-derived samples, such as those produced by model ocean systems, was developed. Model ocean systems (the Bubbler and the Sea Sweep) were used to generate primary, ocean-derived marine aerosol particles. Low heating (70°C) at atmospheric pressure after freezing removes the sea salt hydrate and its spectral signature (double peak at 3380 and 3235 cm^{-1} and single peak at 1640 cm^{-1}). The difference of spectra before and after dehydration have high cosine similarity values with the spectra of sea salt hydrates confirming that the mass removed during dehydration was hydrate water. This dehydration technique permits the use Fourier transform infrared (FTIR) spectroscopy to measure the organic composition of seawater-derived samples. The spectra of the dehydrated OM resemble spectra of atmospheric particles from clean marine regions.

(iii) What causes the discrepancy between the organic composition of generated primary marine aerosol particles measured with different techniques? Sea Sweep generated and atmospheric marine aerosol particles were analyzed using four techniques to address this discrepancy: FTIR spectroscopy, high resolution time of flight aerosol mass spectrometry (HR-ToF-AMS), HR-ToF-AMS with a light scattering module (LS-ToF-AMS), and scanning transmission X-ray microscopy with near-edge absorption fine structure (STXM-NEXAFS). The organic compositions were separated into low and high

oxygen to carbon (O/C) fractions. The FTIR spectroscopy and HR-ToF-AMS measurements show good agreement for the atmospheric marine organic composition, both with approximately 50% high O/C OM. However, the generated marine aerosol OM fractions have differences up to 31%. This is consistent with the larger fraction of sea salt particles in the generated marine OM and the larger fraction of high O/C OM associated with the sea salt particles (observed by STXM-NEXAFS). The sea salt particles and associated OM do not vaporize at the HR-ToF-AMS heater temperature of 650°C and are more prone to particle bounce, which reduces the fraction of high O/C OM observed by the HR-ToF-AMS.

(iv) What is the organic composition of ocean-derived atmospheric marine aerosol particles? The organic functional group composition of marine aerosol particles measured in the MBL of five ocean regions was determined to have contributions from both clean and polluted sources. Ocean-derived organic marine particles included atmospheric primary marine aerosol particles (aPMA) and carboxylic acid containing marine aerosol particles (AMA), which have average OM concentrations of 0.45 and 0.68 μg m^{-3} and represented 23% and 14% of the total sampling time, respectively. The average aPMA OM contains 65% hydroxyl, 21% alkane, 6% amine, and 7% carboxylic acid functional groups, suggesting an overall molecular composition similar to marine saccharides and amino sugars. This composition is similar to the generated primary marine aerosol particles OM (55% hydroxyl, 32% alkane, and 13% amine functional groups), indicating it is dominated by direct emission from seawater. The AMA OM type contains 49% hydroxyl, 22% alkane, 4% amine, and 24% carboxylic acid functional groups. The large fraction of carboxylic acid functional groups is likely the result of contributions from

photochemical oxidation in the atmosphere forming secondary products with carboxylic acid groups. Shipping influenced marine aerosol particles (SMA) and mixed marine aerosol particles (MMA) OM together accounted for 62% of the sampling time (average OM of 0.55 μg m^{-3}) and were observed in four of the five sampling regions, confirming the ubiquitous contribution of non-marine derived OM to aerosol particles in the MBL.

(v) How much of the atmospheric marine aerosol particle organic composition can be explained by generating primary marine aerosol (gPMA) from bubbled seawater? The OM composition of the generated primary marine aerosol particles reflects changes in seawater organics, demonstrated by the increase in the alkane functional group fraction measured in the San Francisco Bay and shipping lanes (62%) compared to the open ocean (37%). The similarity between the organic functional group composition of the gPMA and the aPMA suggests that aPMA OM is a direct result of ocean bubble bursting and can be well represented by gPMA OM. This shows that aPMA OM is similar to gPMA OM, making primary emissions from seawater an important source of organics to the MBL, with aPMA measured during 23% of the sampling time. aPMA OM represents 17% of the total OM measured samples classified as marine, with an average OM of 0.45 μg m^{-3}. Additionally, aPMA can contribute up to 58% of the measured OM, much of occurs in mixtures with other sources.

(vi) What are the differences between gPMA and seawater? The seawater organic functional group composition varied little in the open ocean regions sampled, but the generated marine particles OM composition had a larger fraction of alkane functional groups in eutrophic, productive seawater (35%) compared to oligotrophic, non-productive seawater (16%). This is due to the higher concentration of surfactants in the

productive seawater that stabilize the bubbles at the sea surface and allow more draining of the soluble organics (i.e. those containing hydroxyl functional groups) from the bubble films. This causes a relative enrichment of alkane functional groups in the resulting particles. Additionally, the generated marine aerosol has a hydroxyl group absorption peak location (3369 cm^{-1}) characteristic of monosaccharides (3373 cm^{-1}) and disaccharides (3383 cm^{-1}), where the seawater OM hydroxyl group peak location (3401 cm^{-1}) is more consistent with polysaccharides (3425 cm^{-1}). This may result from the larger saccharides preferentially remaining in the seawater during gPMA and aPMA production.

The measurements presented in this dissertation contribute to a better characterization of the contribution of primary, ocean-derived and anthropogenic emissions to the composition and concentration of organic aerosol particles in the MBL. This work provides a characterization of the composition of the organic fraction of marine aerosol particles, which is a prerequisite for determining the overall climate influence of marine aerosol particles. Future work can use the absorption properties of the marine aerosol organic functional group composition to determine the impacts of the organic fraction of marine aerosol on current and future climate. The organic composition of the primary marine aerosol particles presented here can be used in climate models in order to parameterize the contribution of natural marine sources to the total organic mass. A critical component of estimating aerosol effects on climate is correctly attributing the organic mass to natural sources.

In addition, other measurements can be made to address topics raised in this dissertation. One example is side by side measurements of generated marine aerosol

particles using the four measurement techniques presented, but with the HR-ToF-AMS vaporizer temperature increased. This work demonstrated that a fraction of the organic mass associated with sea salt is not efficiently measured by the HR-ToF-AMS due to its refractory nature and tendency to bounce off the vaporizer. Increasing the vaporizer temperature will increase its ability to vaporize the sea salt and associated organics, and varying the humidity of the aerosol will decrease its tendency to bounce. At the same time, changing the humidity will change the particle sizes and thus their transmission efficiency, which is also a consideration for the quantification of the organic fraction of generated marine aerosol. Laboratory experiments with known mixtures of sea salt and organics can be done to quantify the fraction of OM measured by the HR-ToF-AMS at varying heater temperatures, aerosol humidities, and sea salt fractions. This will contribute to a better understanding of the direct impact of the refractory nature of sea salt (and its tendency to bounce) on the quantification of the organic fraction of primary marine aerosol using HR-ToF-AMS. Another example of measurements would be to use model systems such as the Bubbler and the Sea Sweep to study the formation of secondary organic aerosol and atmospheric processing of marine particles. Gases and particles emitted during bubble-bursting could be transported to a smog chamber where the many factors of the marine aerosol system can be controlled, such as solar radiation and anthropogenic emissions. This experiment could demonstrate the processing of primary marine aerosol and the accumulation of secondary components, as observed in this work with the carboxylic acid functional groups on primary marine aerosol.